UNIVERSITY OF SOUTHAMPTON

To: The Academic Registrar
University of Southampton.

Title of thesis . ~~Spatial Variation of Stress.~~ Stress Distributions in Randomly Excited Structures in Structures Subject to Broad Band Random Vibration

The requisite number of copies of the above thesis are now formally submitted for the degree of . Ph.D.
Should the Senate of the University award me either this degree or another higher degree in respect of this thesis I, Stanley M. Steam . . . , hereby agree that from the date of the award the thesis may be made available for inter-library loan or for photocopying.

Signed [redacted] Date . 28. Oct. 1970. .

STRESS DISTRIBUTIONS IN RANDOMLY EXCITED STRUCTURES

by

STUART MALCOLM STEARN

of the

Institute of Sound and Vibration Research,
Faculty of Engineering and Applied Science
University of Southampton

A thesis submitted for the degree

of

Doctor of Philosophy

February, 1970

ABSTRACT

FACULTY OF ENGINEERING AND APPLIED SCIENCE

INSTITUTE OF SOUND AND VIBRATION RESEARCH

Doctor of Philosophy

STRESS DISTRIBUTIONS IN RANDOMLY EXCITED STRUCTURES

by Stuart Malcolm Stearn

The work analyses the distribution of dynamic stress in flat plate and cylindrical shell structures, such as are found in the cooling gas circuits of nuclear reactors, when vibrating in response to broad frequency band excitation. The vibration predominantly takes the form of bending waves.

Two analytical models are considered, namely the normal mode and the travelling wave models. The normal mode model is chosen to examine the distribution of stress in regions away from any boundaries of the structure; the travelling wave model is used to predict variations of stress in the vicinity of a boundary or discontinuity. In order to simplify the analysis of local stress, an idealised model of a diffuse, travelling bending wave field is assumed. Acceleration and strain correlation experiments are used to investigate the conditions necessary to establish a good approximation to such a field. It is found that such an approximation is valid whenever more than ten modes are excited simultaneously. An additional requirement for a cylindrical shell is that the frequency of response must be above the cylinder's ring frequency.

The travelling wave model is used to predict the ratios of mean square stress and strain to mean square velocity averaged over the structure. This ratio is confirmed by experiment. Also, the mean square stress at a weld and a change of section is predicted in terms of the space averaged mean square stress. These results are confirmed by experiment. All these results are found to be applicable even when fewer than ten modes are excited.

The normal mode model is used to predict the standard deviation of mean square stress and acceleration from their space averaged values when more than ten modes are excited. Experimental results show

good agreement with theory, when more than twenty to thirty modes are excited. When less than that number of modes are available, the measured standard deviation is lower than that predicted.

In both sections of the work, the effect of structural damping on the validity of the analyses is found to be small. The total number of normal modes excited is by far the most important consideration.

Finally, it is suggested how the results might form the basis of a relatively straightforward design method, and possible future extensions of this are considered.

LIST OF CONTENTS

		Page
CHAPTER 1	Introduction	1
CHAPTER 2	Bending Waves: A Brief Summary of their Behaviour	8
2.1.	The Low Frequency Bending Wave Equation	10
2.2.	Solution of the Bending Wave Equation	16
2.3.	The Bending Wave at a Boundary	17
CHAPTER 3	The Analysis of the Forced Vibration of Extended Plate and Shell Structures: a Summary of Available Methods	21
3.1.	The Normal Mode	21
3.2.	The Travelling Wave	28
3.3.	The Analysis of Stress Distribution	30
3.3.1.	Normal Mode Analysis	32
3.3.1.1.	Powell's Equation: Accurate Summation of the Effect of Several Known Normal Modes	32
3.3.1.2.	Asymptotic Summation of the Response of Many Normal Modes	35
3.3.1.3.	Statistical Summation of the Response of Many Normal Modes	35
3.3.2.	The Travelling Wave Analysis	36
3.4.	Comparison of the Analyses	40
CHAPTER 4	Formal Tests of the Diffuse Field Model	41
4.1.	Cross-Correlation of Acceleration	41
4.1.1.	Theoretical Value of Cross-Correlation Coefficient	42
4.1.2.	Experimental Procedure	46
4.1.3.	Computational Tests	58
4.1.4.	Discussion of Results	63
4.1.4.1.	Interpretation	63
4.1.4.2.	The Effect of Number of Modes and the Degree of Modal Overlap	67
4.1.4.3.	The Effect of Heavy Damping: The Mechanically Excited Plate	71
4.1.4.4.	The Computed Results	76
4.2.	The Cross-Correlation of Strain	66
4.2.1.	Theoretical Value of Cross-Correlation Coefficient	77
4.2.2.	Experimental Procedure	80
4.2.3.	Discussion of Results of Strain Correlation	82

Page

4.3. Conclusions 83

4.3.1. Conditions for Diffuse Bending Wave Field 83
4.3.2. Comparison of the two Tests 83
4.3.3. Sensitivity of the Tests to Diffuseness of Field 84

CHAPTER 5 The Ratio of Mean Square Stress and Strain to Velocity 85

5.1. Theoretical Analysis based on the Diffuse Field Model 85
5.2. Experimental Tests 88
5.3. Comments on the Results 90
5.4. Conclusions 92

CHAPTER 6 Stress and Strain Concentration at a Weld 93

6.1. The Behaviour of a Bending Wave Incident on a Butt Weld 95

6.1.1. Wave Velocities 97
6.1.2. Boundary Conditions 101

6.2. The Stress in a Plate Generated Normal to a Weld 107

6.2.1. Stress Due to Reflected Waves 107

6.3. Details of Numerical Evaluation of the Integrals 111

6.3.1. Structural Parameters of Weld 112
6.3.2. The Limits of the Integration 114
6.3.3. Modifications for Strain 115

6.4. Experimental Tests 117

6.4.1. Experimental Procedure 117
6.4.2. Computational Procedure 120
6.4.3. Comparison of Computed and Experimental Results 121

6.5. Conclusions 123

CHAPTER 7 Stress and Strain Concentrations at a Change of Section 125

7.1. The Behaviour of a Bending Wave Incident on a Change of Section 125

7.1.1. Wave Velocities 125
7.1.2. The Boundary Conditions: Transmission 132

7.1.2.1. Equality of Lateral Velocity 132
7.1.2.2. Equality of Angular Velocity 132
7.1.2.3. Equality of Bending Moment 132
7.1.2.4. Equality of Shearing Forces 133

Page

7.1.3. The Boundary Conditions: Total Reflection 141

7.2. The Stress Generated Normal to a Change of Section 142

7.2.1. Stress due to Partial Reflection 143
7.2.2. Stress due to Total Reflection 145
7.2.3. Stress due to Partially Transmitted Bending Waves 146
7.2.4. Stress due to Totally Non-Transmitted Bending Waves 149

7.3. Evaluation of Results 151

7.3.1. Computation 151
7.3.2. Discussion of Computed Results 153

7.4. Experimental Tests 157

7.4.1. Experimental Procedure 160
7.4.2. Experimental Results 164
7.4.3. Discussion of Results 169

7.5. Conclusions to Chapters 6 and 7 169

CHAPTER 8 Stress Distribution in the Mid-Structure Regions 172

8.1. Deviation of Mean Square Stress in a Flat Plate with Arbitrary Boundary Conditions 173

8.2. Statistics of Mean Square Stress 180
8.2.1. Determination of Spatial Mean Square Stress 180
8.2.2. Probability Distribution of Mean Square Stress in space 181

8.3. Experimental Tests 187
8.4. Discussion of Results 191
8.5. Conclusions: Extension to Existing Estimates: Effect of Assumptions 196

CHAPTER 9 Conclusions 199

9.1. A Review of the Main Results 199
9.2. Design Criteria 202
9.3. Limitations on Design Method 204
9.4. Future Extensions 204

ACKNOWLEDGMENTS 206

REFERENCES 207

Page

APPENDIX I	Effect of Accelerometer on Measured Response of an Infinite Plate	211
APPENDIX II	Phase Match of Analogue Filter	214
APPENDIX III	Use of Powell's Equation to Compute Cross-Correlation of Acceleration on a Plate	216
APPENDIX IV	The Correlation Coefficient of Acceleration of a Diffuse Bending Wave Field with a Superimposed Unidirectional Travelling Bending Wave	221
APPENDIX V	Ratio of the Reverberant Field to the Radiating Field in the $\frac{1}{4}$ inch Plate Mechanically Excited	226
APPENDIX VI	Tests of Three Channel Strain Gauge Amplifier	228
APPENDIX VII	Stress Concentration in a Plate, Normal to a Solid Boundary	231
APPENDIX VIII	Loss Factor at a Change of Section	236
APPENDIX IX	Variation of Mean Square Acceleration	239
APPENDIX X	Effect of Measurement Error on Variation	241
TABLE 1		20
TABLE 2		164
TABLE 3		186
TABLE 4		196

N O T A T I O N

A_i	amplitude of bending wave i
a	side length of rectangular panel
B	bending stiffness
B_o	bending stiffness of weld (Chapter 7)
b	side length of rectangular panel
C_B	speed of bending waves
C_L	speed of longitudinal waves
D	diameter, amplitude of transmitted travelling wave, compressive stiffness
D'	amplitude of transmitted near field
E	Young's modulus
F_x	lateral force transmitted (Figure 50)
f_r	ring frequency. (page 69)
G	shear modulus
$H(\underline{r},\underline{r}_o';\omega)$	cross impedance of structure between positions $\underline{r}$ and $\underline{r}_o'$ at frequency ω
h	plate thickness
I	second moment of area
Jo(x)	Bessel function of order zero
K	ratio of wavenumbers = k_2/k_i , constant. p.180
$[K]$	stiffness matrix for distributed system
k	wavenumber = $\frac{2\pi}{\lambda}$
$[M]$	mass matrix for distributed system

M_z bending moment about z axis

M_{zz}, M_{xz}, M_{xx} bending moments (see pages 134 et seq)

m mass per unit area, mass per unit length, integer.

N ratio of bending stiffnesses (Chapter 7), number of modes available.

n integer

$P(\underline{r}_o,\underline{r}_o';\omega)$ cross spectral density of exciting force

Q_x shear force (Figure 50)

$\{q\}$ coordinate matrix for distributed system

$R_{x,y}(\tau)$ cross correlation coefficient between x and y at time τ

R amplitude of reflected travelling wave

R' amplitude of reflected near field

r separation

$\underline{r},\underline{r}',\underline{r}_o,\underline{r}_o'$ position vectors

S_a signal a

$S_p(\omega)$ spectral density of exciting force

T time, torsional rigidity

T_c critical angle (Chapter 7)

t time (variable)

V variation = standard deviation/average

V_y lateral velocity

W_z angular velocity of weld (Chapter 6)

$W(\underline{r},\underline{r}';\omega)$ cross spectral density of response

x,y,z Cartesian coordinates

$Y_a(\omega)$ acceptance of mode a at frequency ω

Z_c	characteristic impedance
α	variable
β	variable
γ	variable, transmission loss
γ_a	random phase angle for modal response
ζ	displacement
η	displacement perpendicular to plate
Θ	moment of inertia of weld (Chapter 6)
θ	angle of incidence
κ	constant
λ	wavelength
ν	Poisson's ratio
ξ	strain, displacement
ρ	density
σ	stress
$\overline{\sigma}_a^2$	mean square stress due to partially reflected bending waves
$\overline{\sigma}_b^2$	mean square stress due to transmitted bending waves
$\overline{\sigma}_c^2$	mean square stress due to totally reflected bending waves
$\overline{\sigma}_d^2$	mean square stress due to totally non-transmitted bending waves
τ	time lag
τ_{xz}	shear stress in plane xz
$\psi_a(r)$	displacement at of mode α
ω	angular frequency
ω_z	angular frequency about z axis

ω_a	natural frequency of mode a
ϕ	angle of departure of transmitted wave, argument of vector on wavenumber diagram (p 174 et seq)
$\overline{\quad}$	time average
$< >$	space average

LIST OF FIGURES

Figure Number	Title	Page
1	Typical Gas Cooled Reactor	4
2	Part of one-sixth Scale Model of Dungeness B Reactor	5
3	Comparison of Bending and Compressive Waves	9
4	Rayleigh Surface Waves	11
5	Boundary Conditions for Compressive Waves	12
6	Equilibrium of an Element of a Uniform Beam in Bending	14
7	Infinite Beam Excited in Bending at a Point	19
8	Frequency Response of a Multi-degree of Freedom System with Light and Heavy Damping	27
9	Wave Number Diagram for a Simply Supported Panel showing Two Normal Modes and their Corresponding Vectors	31
10	Wave Number Diagram for a Simply Supported and a Clamped Rectangular Plate	38
11	Experimental Set-Up for Correlation on a Flat Plate	47
12a	The Flat Plate showing Accelerometer Positions	47
12b	The Cylinder showing Accelerometer Positions	47
13	$\frac{1}{4}$ inch Acoustically Excited Correlation Coefficient at 500 H_z	49
14	Do. at 800 H_z	49
15	Do. at 1250 H_z	49
16	Do. at 2500 H_z	49
17	Do. at 3150 H_z	50
18	Do. at 4000 H_z	50
19	$\frac{1}{8}$ inch Plate Acoustically Excited Correlation Coefficient at 2000 H_z	52
20	Do. at 4000 H_z	52
21	Correlation Coefficient Measured on Cylinder at High Frequencies	53
22	Do. Low Frequencies	53
23	Mechanically Excited $\frac{1}{4}$ inch Plate Cross-Correlation at 1600 H_z	54
24	Do. at 2500 H_z	54
25	Do. at 3150 H_z	55
26	Experimental Set-Up	57
27	Computed Correlation Coefficient on $\frac{1}{8}$ inch Plate in $\frac{1}{3}$ Octave at 2000 H_z Acoustically Excited	64
28	Computed Correlation Coefficient on $\frac{1}{8}$ inch Plate in $\frac{1}{3}$ Octave at 1250 H_z Acoustically Excited	64
29	$\frac{1}{4}$ inch Plate Mechanically Excited Cross Correlation Computed at $\frac{1}{3}$ Octave at 1600 H_z	65
30	Computed Correlation Coefficient on $\frac{1}{4}$ inch Plate at $\frac{1}{3}$ Octave at 2000 H_z Mechanically Excited	65

Figure Number	Title	Page
31	$\frac{1}{4}$ inch Plate Mechanically Excited Computed Correlation $\frac{1}{3}$ Octave at 2500 H_z	66
32	Theoretical Number of Modes per $\frac{1}{3}$ Octave Bandwidth for the Steel Plates and Cylinders	68
33	Wave-Number Space for a Cylinder	70
34	Variation of the Total Loss Factor of the $\frac{1}{4}$ inch Plate	72
35	Radius from Shaker on $\frac{1}{4}$ inch Plate at which Reverberant Field is 10/3 dB above the Radiated Field	72
36	Loss Factor Measured on a Typical Industrial Structure	74
37	Cross Correlation of Strain on Acoustically Excited $\frac{1}{8}$ inch Plate	81
38	Acoustically Excited Cylinder Cross-Correlation between Two Strain Gauges at 90° Remote from Boundaries	81
39	Ratio of Mean Square Velocity to Mean Square Strain	89
40	Modes per $\frac{1}{3}$ Octave Bandwidth for the Large Change of Section Specimens	91
41	Forces on Weld	96
42	Trace Wavelength at Weld	98
43	Dimensions of Cross Section of Weld	98
44	Transmission past a Rectangular Rib (a) Low Frequency (b) High Frequency	116
45	The Welded Aluminium Plate	118
46	Theoretical Stress and Strain Concentration at a Weld	122
47	do.	122
48	Strain Normal to Weld, Experimental vs. Predicted Levels	124
49	Equality of Trace Wavelengths at a Change of Section	127
50	Shear Forces in Edge of Plate	134
51	Shear Strain	136
52	Stress Concentration at a Change of Section	152
53	Strain do.	154
54	Stress Concentration vs. Angle of Incidence	158
55	do.	159
56	Large 4:1 Change of Section Specimen	161
57	Small 4:1 do.	162
58	Damping of Small 4:1 Specimen with and without lower section connected. Suspended ($\frac{1}{3}$ O.B. Measurements)	162
59	Small Specimen 4:1 Change of Section 2500/400 H_z $\frac{1}{3}$ O.B. Thick Edge. Good Fit by Least Square Method of Exponential Curve	165
60	4:1 Change of Section. Small Specimen. Good Extrapolation Not Possible	166
61	Strain Measured at a 4:1 Change of Section	167
62	do 2:1 do.	168
63	Wavenumber Space for a Simply Supported Panel showing Possible Shift due to Boundary	175
64	High Order Modes on $\frac{1}{8}$ inch Plate	178
65	Standard Deviation of $\overline{\text{Acceleration}^2}/\langle\overline{\text{Acceleration}^2}\rangle$ over a Series of Structures	188
66	Standard Deviation of $\overline{\text{Strain}^2}$ / $\langle\overline{\text{Strain}^2}\rangle$ over a Series of Structures	189
67	Standard Deviation for a Plate with and without an Added Lump Mass	190

Figure Number	Title	Page
68	Probability Distribution of Mean Square Strain in $\frac{1}{8}$ inch thick Plate Acoustically Excited by $\frac{1}{3}$ Octave Random Noise Centred at 400 H_z	193
69	Probability Distribution of Mean Square Strain in $\frac{1}{8}$ inch thick Plate Acoustically Excited by $\frac{1}{3}$ Octave Random Noise Centred at 1600 H_z	193
70	Effect of Loading Impedance of Accelerometer on Estimation of Mean Square Velocity and Phase	213
71	Phase Match of $\frac{1}{3}$ Octave Band Filters	215
72	Effect of Radiating Field on Diffuse Field Correlogram	225
73	Calibration and Noise of Strain Gauge Amplifier	230
74	Loss Factor at a Change of Section	238

Chapter I

I N T R O D U C T I O N

THE PROBLEM

Gas Cooled Nuclear Power Stations are extremely expensive items. Their cost approaches £100 per kw installed capacity, compared with £40 per kw installed capacity for a conventional coal fired station[1]. It is therefore a critical matter to reduce the capital cost as much as possible in order to reduce the cost per unit of electricity generated to levels competitive with conventional stations, i.e. 0.45d./unit.

To achieve this, the specific output must be raised to the highest possible level. This, in turn, demands that the rate of heat transfer in the core and heat exchanger regions must be as high as possible. It is not difficult to achieve high rates of heat transfer between the fuel and the working fluid in coal fired stations. The coal is incandescent at an extremely high temperature and need retain no mechanical strength; the rate of heat transfer can be very high, without the need for exceptionally high heat transfer coefficients on the gas side of the boiler tubes. However, in the present generation of reactors, nuclear fuels must retain their mechanical properties and cannot run at such high temperatures. At Dungeness B Advanced Gas Cooled Reactor, to be commissioned in 1971, the upper fuel can temperature will be 800°C, the outlet gas temperature 675°C, the steam temperature 565°C. To achieve

the high heat transfer coefficients necessary for adequate rates of heat transfer, a dense gas, carbon dioxide, is used to carry heat from the reactor core to the steam boiler. The gas must be at high pressure, 450 lbf/in^2 abs., and must be circulated at relatively high speed, approximately 30 feet per second. The gas circulators have to be powerful, using as much as 60,000 HP, 8-10% of the total station output. Such big machines cause severe acoustic conditions in the reactor gas circuits; noise levels of up to 180 dB are produced. The high power levels themselves demand that the circulators are designed to the highest efficiency, which tends to increase their noise output. Simultaneously, the need to reduce the capital cost dictates that the least possible material be used in the construction of the plant, consistent with satisfactory mechanical performance.

Meeting this requirement leads to the situation where acoustically induced dynamic stresses in the structures of the cooling gas circuits may be critical.

The problem first became apparent during the commissioning of Hinkeley Point A reactor in 1963. There was a failure of the diffuser when a large portion of it broke out[2]. Correction of this type of failure is very expensive, for even one day's lost output costs approximately £20,000. Clearly, it is desirable to avoid such failures in the design stage.

The design analysis may be divided into three parts:-

(i) Prediction of the intensity, frequency spectrum and pressure field distribution of the acoustic field

(ii) Prediction of the stress distribution caused by the acoustic field in the structure

(iii) Prediction of the fatigue life of the structure under these stresses.

The present work is concerned with the second part of the problem. Broadly, we may divide the reactor gas circuit structures into two types of component; plate and shell, or rod and tube. Figure (1) diagrammatically shows the main components in a typical gas cooled reactor. In this work we shall confine our attention to the vibration of the plate and shell structures of the reactor. Of course, the rods and tubes vibrate and represent a design problem as well, but the approach to this is usually rather different from the problems of shell and plate response and is currently being tackled by other workers.

Ungar[3] describes an analytical method by which it is possible to derive an estimate of the spatial mean square vibration velocity in a structure, in terms of the mean square pressure to which it is subjected, by considering the flow of energy between sets of modes of the structure and the acoustic field. Fahy[4] and Beany et al[5] discuss the specific application of this analysis to the problems of nuclear reactor structures, and it is not discussed any further in this work. We will consider the next step, how we may deduce the likely distribution of stress in a complex structure, given this mean square level of velocity.

In response to an acoustic field, the plate like structures in a reactor will vibrate in bending at frequencies high compared with their fundamental frequencies. The structures are complex. Figure 2 shows a

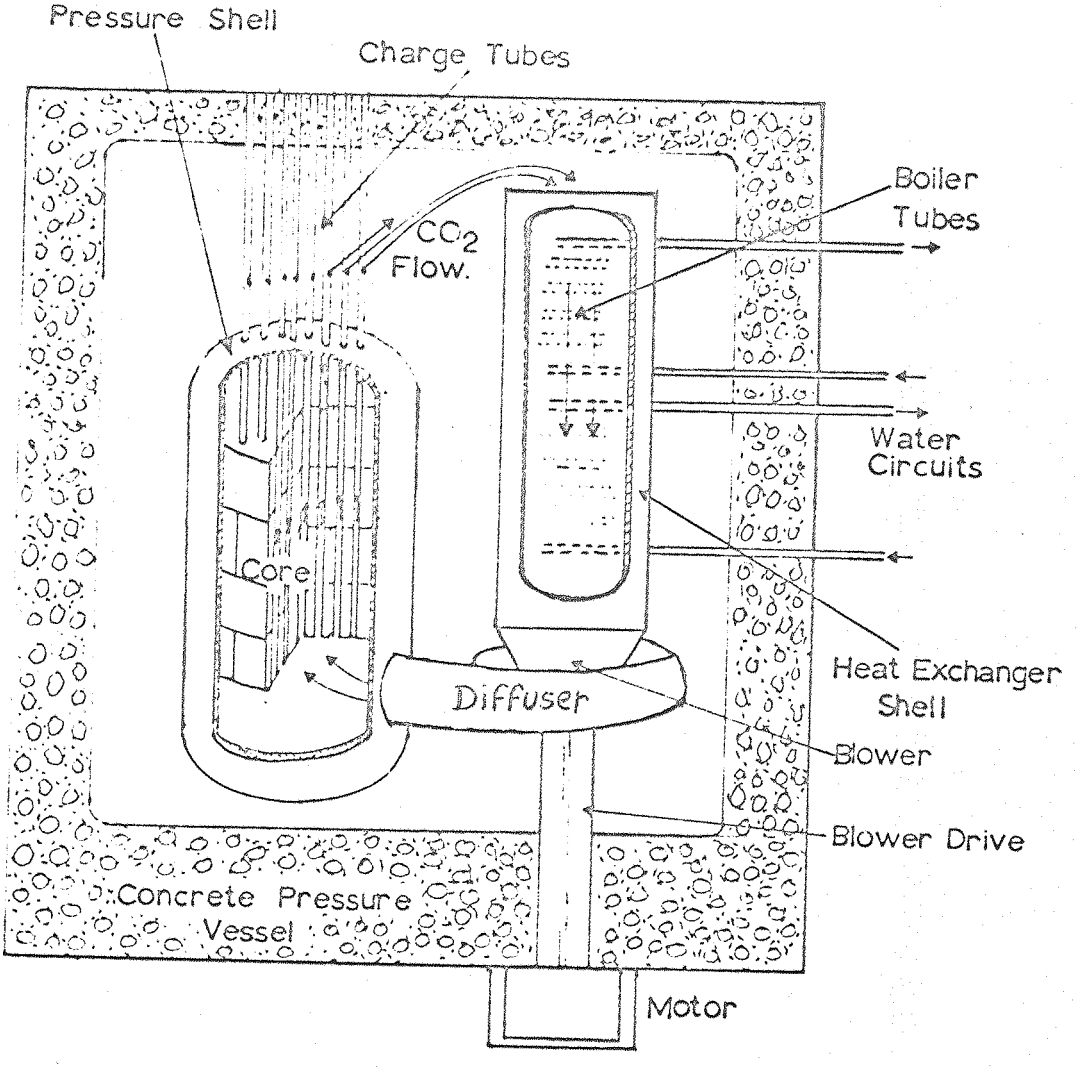

Figure 1 Typical Gas Cooled Reactor

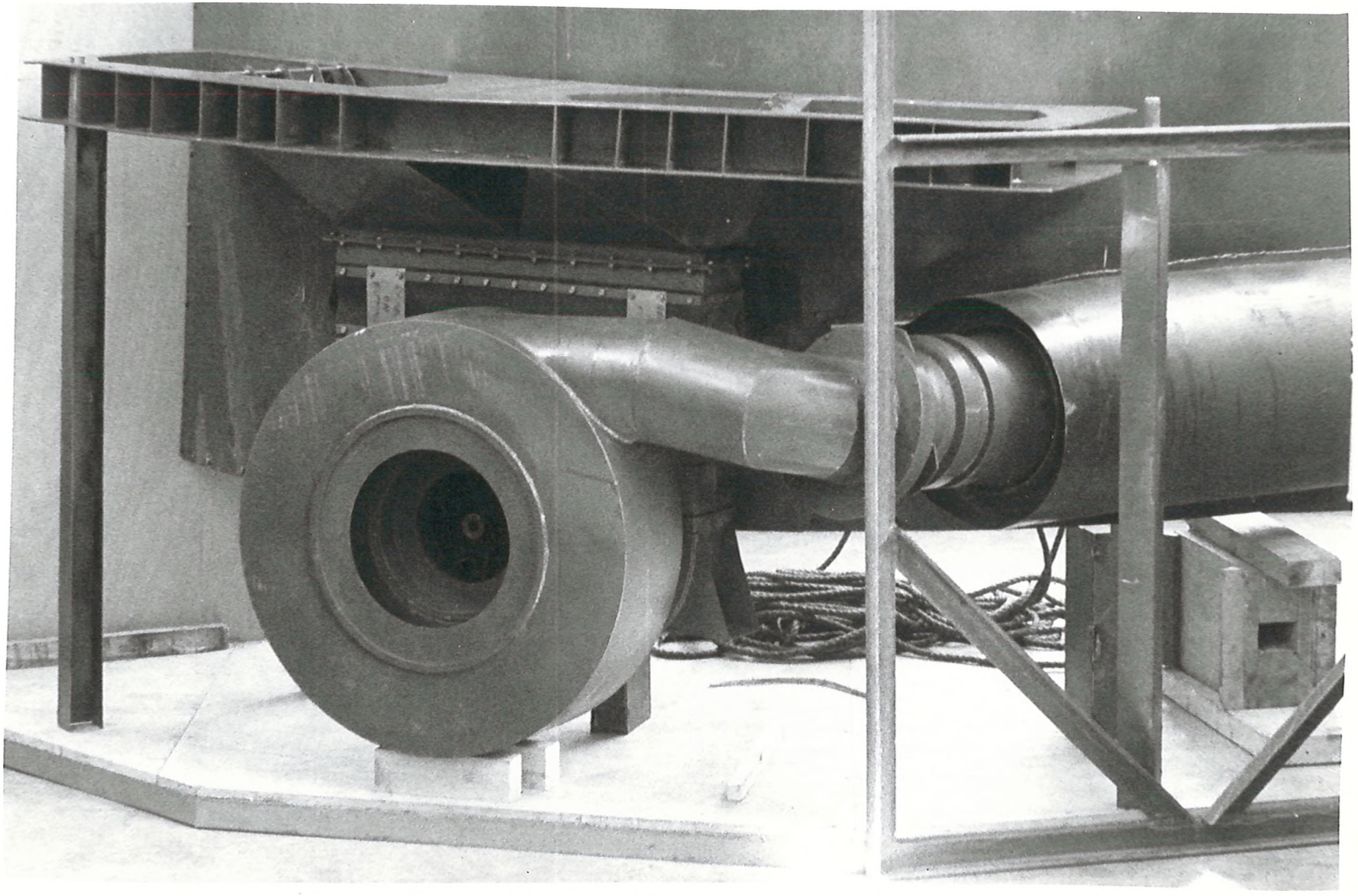

Figure 2 Part of 1/6 Scale Model of Dungeness B Reactor.

model of part of the gas circuitry of Dungeness B reactor, from which one may appreciate the complexity of the many structures bolted and welded together. The frequency bandwidth of the excitation depends on the type of compressor used. Axial blowers, such as were used in earlier designs, produced very narrow band random noise; more recent designs use centrifugal blowers which produce more broad frequency band random noise.

Cracks often start from discontinuities in a structure. A designer needs to know if significant stresses are going to be induced by a particular discontinuity, when these stresses are compared with those that might be expected in the mid structure. Very little work has been done on this problem and the following references are the only known relevant contributions to date. Beany et al[5] derive a value for the ratio of maximum to mean stress in a simply supported plate, vibrating in a single mode. Lyon[6] discusses the ratio of maximum to mean response that is likely to occur when many modes may be excited at once by a single tone. Ungar[7] discusses the concentration of strain at a reinforcing beam when a straight crested bending wave reaches it. There is also an interesting paper by Cheng and Jaharshahiia[8] which describes the concentration of strain set up round a circular obstacle in an infinite plate, excited at a point by a harmonic force. However, none of these papers covers the design problems associated with nuclear gas circuit structures; that is, structures of complex shape, excited at frequencies several times their fundamental by broad frequency band noise.

In Chapter 2 we consider the properties of bending waves in

plates, for this is the most important mode of structural response to sound. In Chapter 3 we compare the two analytical models which might be applied to the behaviour of structures vibrating in bending; these are the normal mode and the travelling wave models. We also consider the use of the diffuse, reverberant field model as a further simplification. Chapter 4 discusses experiments performed on various structures to test the validity of the diffuse, reverberant field model under broad frequency band excitation.

In Chapter 5 this model is used to predict the ratios of mean square strain and stress to mean square velocity; in Chapters 6 and 7 it is used to predict the stress concentrations at a weld and at a change of section.

In Chapter 8 we use the normal mode model to predict the statistics of mean square stress, strain and acceleration about their spatial means, away from the boundaries of a structure.

Finally, in Chapter 9 we discuss the inclusion of the results obtained in a design method, and possible future extensions of the work.

Chapter 2

Bending Waves: A Brief Summary of their Behaviour

There are several ways in which solids may vibrate: they may vibrate in torsion, in shear, in compression or in bending. When acoustically excited, structures in reactor gas circuits vibrate predominantly in bending, for this is the mode of vibration that couples most effectively with the sound field.

Figure 3 shows two different modes of vibration in plates and beams. In bending the plate is displaced laterally, and initially parallel sections are no longer so. An acoustic field is a compressive wave field in a gas, and if energy is to flow from the acoustic field into the structure, then the structure most move laterally. Longitudinal vibrations cause small lateral movements, due to the effect of Poisson's ratio, but these are negligible compared with those caused by bending waves. Further, the speed of bending waves, though dependent on several factors, is often of the same order as the speed of sound in air, and also that in carbon dioxide under reactor service conditions. This also ensures high energy exchange between the acoustic field and the structure. At a typical service frequency, the wave lengths in the structure and in the acoustic field will be comparable. Maidanik[9] described this effect and it is beyond the scope of this work to consider it further here.

At high frequencies, ripples occur on the surface of the

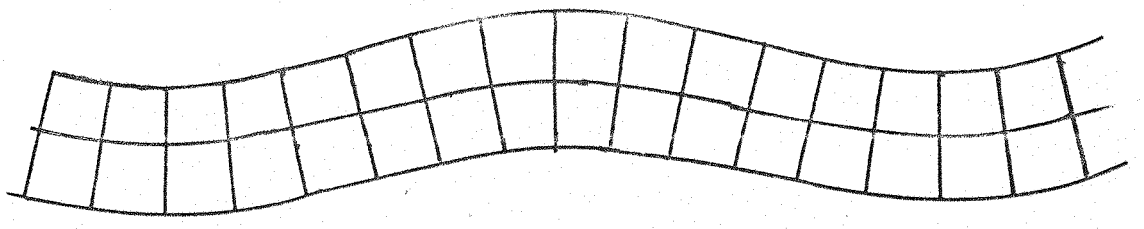

a) Bending Wave.

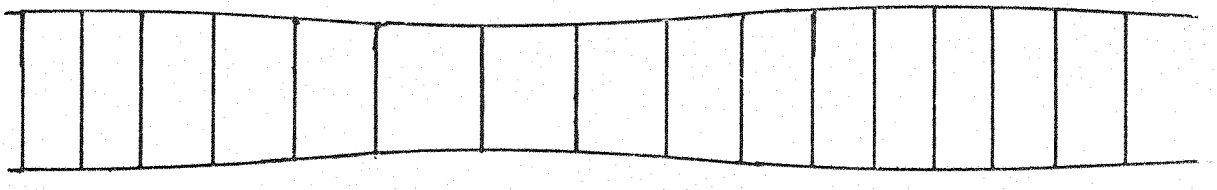

b) Longitudinal or Compressive Wave.

Figure 3 Comparison of Bending and Compressive Waves

material which do not propagate into it, as shown on Figure 4. These are Rayleigh Surface Waves. However, provided that the bending wavelength is more than six times the plate thickness, it is reasonable to ignore any such effect[10]. For a 1 inch thick plate, this condition holds at frequencies below 10,800 Hz, and for a $\frac{1}{4}$ inch thick steel plate below 43,000 Hz. These frequencies are well above those considered in present nuclear design studies. In this work we need only consider the behaviour of the low frequency bending wave.

2.1. The Low Frequency Bending Wave Equation

What follows is well established theory[10]. However it is useful to go over the derivation, for there are important differences between the behaviour of bending waves and the more familiar compressive waves.

To define the state of a compressive wave we need fix only two quantities, say the velocity and the pressure. These are sufficient boundary conditions from which to deduce, for example, the behaviour of a sound wave reaching the boundary between two different acoustic media, say air and carbon dioxide. But to define the state of a bending wave we need four quantities. The most common quantities used are as shown in Figure 5:-

(a) the Lateral Velocity, Vy;

(b) the Angular Velocity, ω_z, about an axis normal to the deflection and in the plane of the structure;

(c) the Bending moment about the z axis, Mz;

(d) the Lateral or Transverse Force, Fy.

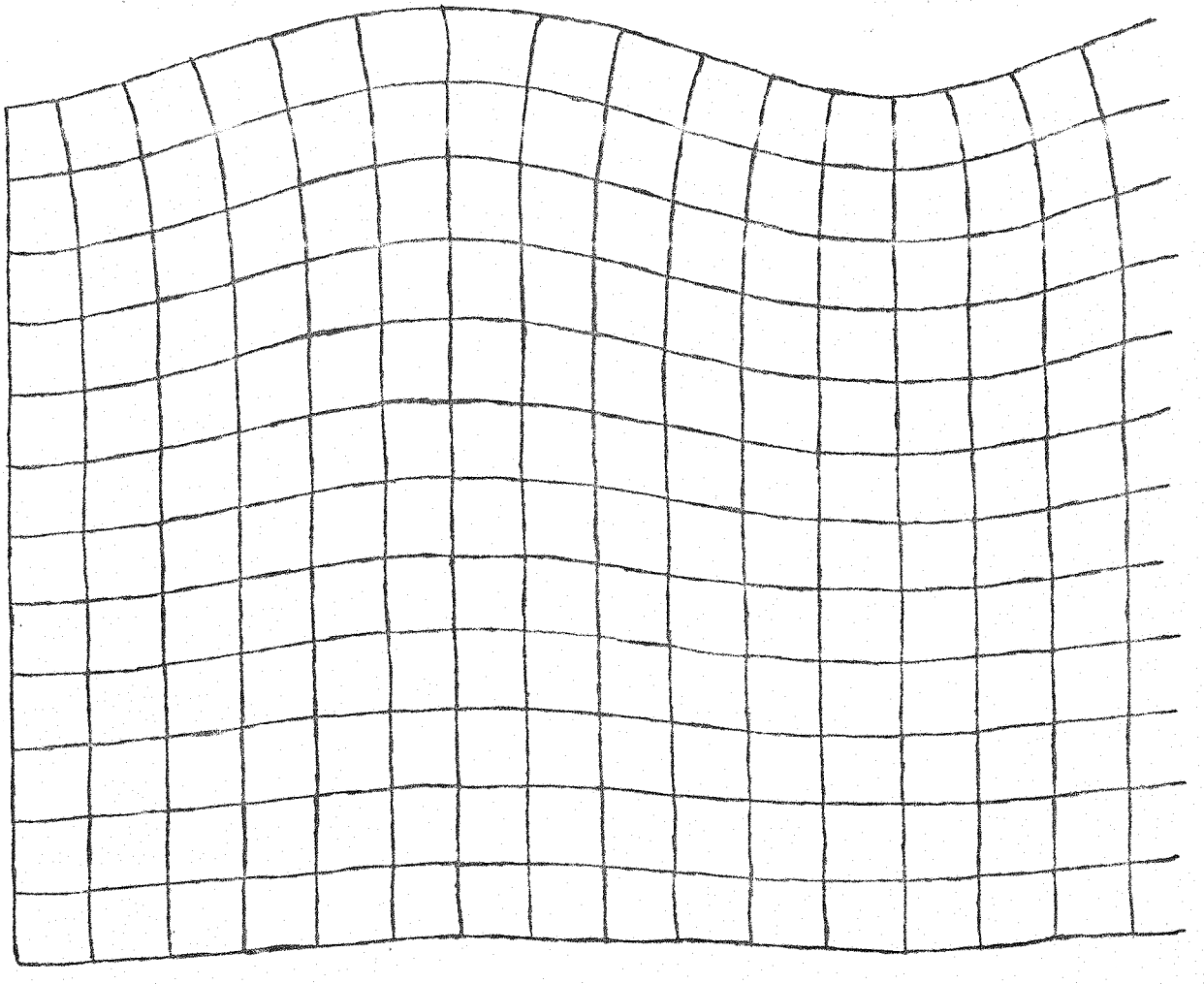

Figure 4 Rayleigh Surface Waves

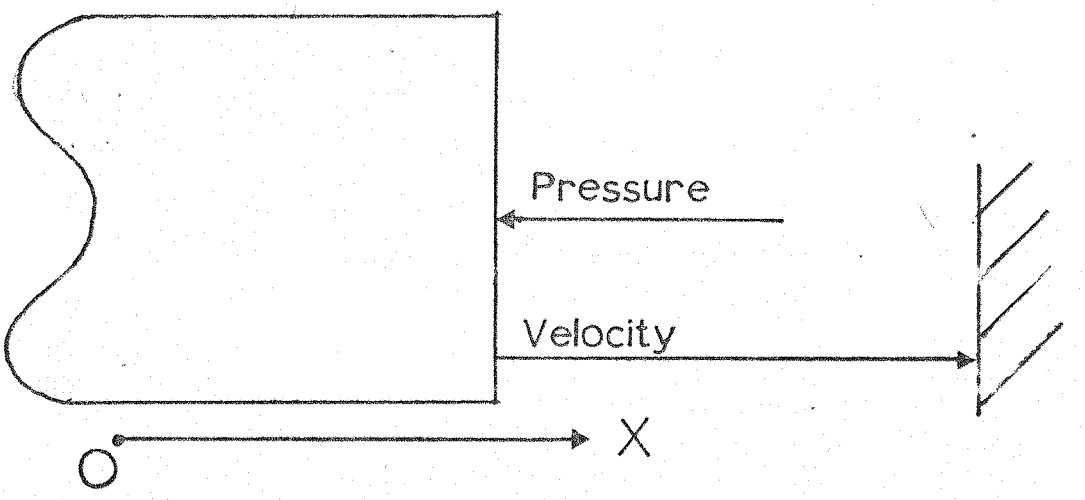

a Compressive

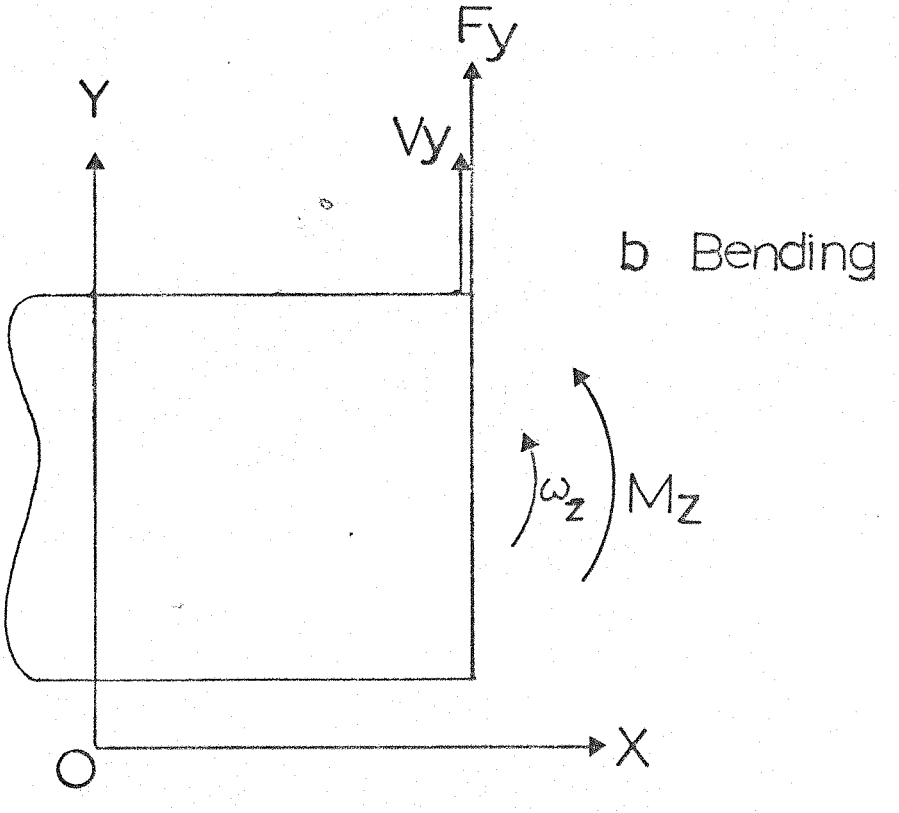

b Bending

Figure 5 Boundary Conditions for Compressive and Bending Waves.

In plates, the bending moment and lateral shear force are referred to a unit width of cross section and denoted as Mz', Fy'.

These quantities are connected by the following equations.

Consider a beam lying in the direction O-x.

Then $$\omega_z = \frac{\partial V_y}{\partial x} \qquad 2.1.$$

Now, from (11), the bending moment may be written as:-

$$M_z = -EI \frac{\partial \eta^2}{\partial x^2} \qquad 2.2.$$

where η = lateral displacement in the y direction, normal to Ox.

E = Young's modulus

I = second moment of area of the cross section of the beam.

Differentiating with respect to time we obtain:

$$\frac{\partial M_z}{\partial t} = -B \frac{\partial \omega_z}{\partial x} \qquad 2.3.$$

where

B = bending stiffness, EI.

A well known result relates the bending moment and the transverse force.

Consider the dynamic equilibrium of a section of a bar, δx, under bending and shear loads, as in Figure 6. Taking moments about one end:

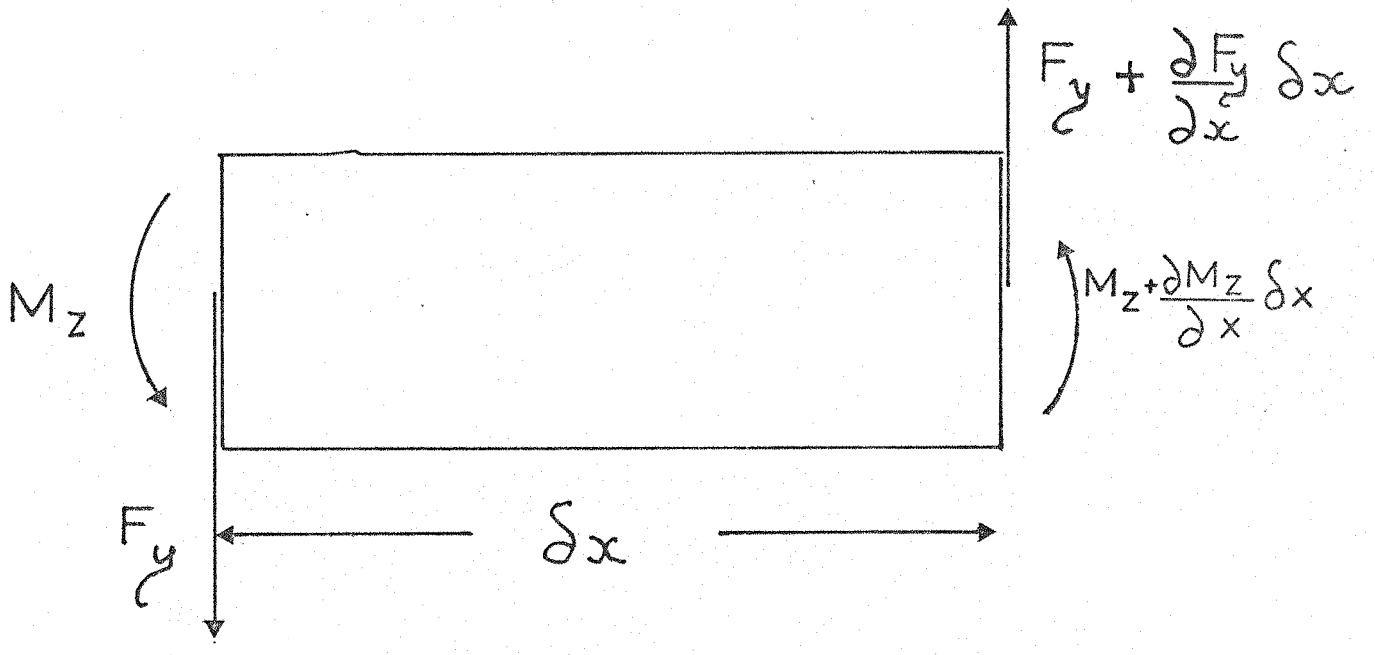

Figure 6 Equilibrum of an element of a Uniform Beam in Bending.

$$M_z - \left(M_z + \left(\frac{\partial M_z}{\partial x}\right)\delta x\right) - F_y.\delta x = 0 \qquad 2.4.$$

Then:

$$\boxed{F_y = -\frac{\partial M_z}{\partial x}} \qquad 2.5.$$

In deriving this, we have not considered the effect of rotary inertia in 2.4. However, Cremer has shown[10] that when the bending wave length is large compared to the thickness of the plate or bar, then the kinetic energy of rotation is negligible compared to the kinetic energy of lateral movement. Since we are restricting our analysis to frequencies where the wavelength is more than six times the thickness, this approximation is reasonable, and we may neglect the effect of rotary inertia.

Finally, if we consider the dynamic vertical equilibrium of the element in Figure 6 we obtain the expression:-

$$F_y - \left(F_y + \left(\frac{\partial F_y}{\partial x}\right)\delta x\right) = m.\delta x.\frac{\partial V_y}{\partial t} \qquad 2.6.$$

where m = mass per unit length, for a bar, or per unit area for a plate.

Then $$\boxed{-\frac{\partial F_y}{\partial x} = m.\frac{\partial V_y}{\partial t}} \qquad 2.7.$$

If we combine the framed equations, 2.1., 2.3., 2.5., 2.7., we obtain the partial differential equation for all field quantities in a one dimensional form:-

$$-\left(\frac{B}{m}\right)\frac{\partial^4}{\partial x^4}\left(V_y, \omega_z, M_z, F_y\right) = \frac{\partial^2}{\partial t^2}\left(V_y, \omega_z, M_z, F_y\right) \qquad 2.8.$$

2.2. Solution of the Bending Wave Equation

The wave equation for a compressive wave is of the form (10):-

$$\left[\frac{D}{\rho}\right]\frac{\partial^2}{\partial x^2}\left(V_x\right) = \frac{\partial^2}{\partial t^2}\left(V_x\right) \qquad 2.9.$$

where ρ = density and D = compressive stiffness.

V_x is the velocity in the O - x direction at X.

Any solution of the form $V_x = F\left(t \pm \sqrt{\frac{D}{\rho}}x\right)$ will satisfy the Equation. The velocity of propagation is independent of frequency and is given by $\sqrt{D/\rho}$. Waves of complex frequency content can propagate without dispersion, and the shape of a given wave will not change as it propagates through free space.

The solution to the Bending Wave Equation cannot take so simple a form. The derivative with respect to space is of a different order from the derivative with respect to time and is of opposite sign.

A possible solution is:-

$$V_y = A_y . \sin\left(\omega t - kx + \alpha\right) \qquad 2.10.$$

provided that $$k^4 = \frac{m\omega^2}{B}$$ 2.11.

where k is the wave number, which equals $\frac{2\pi}{\lambda}$

where λ is the wavelength.

For this solution, a sinusoidal variation with time, the velocity of wave propagation, C_B, is given by:-

$$C_B = \frac{\omega}{k} = \sqrt[4]{B/m}\,\sqrt[2]{\omega}$$ 2.12.

This is no longer independent of frequency; waves of many different frequency harmonics may no longer propagate undistorted in an infinite plate.

The various properties of compressive and bending waves are compared in Table 1 at the end of this chapter. However, the differences that will most concern us are over the behaviour at boundaries, where now four, rather than just two, boundary conditions must be satisfied.

2.3. The Bending Wave at a Boundary

Imagine that a bending wave reaches an arbitrary boundary. In addition to satisfying the boundary conditions, we must satisfy the general solution to the bending wave equation.

We will restrict our considerations to solutions of the form of 2.10., then:-

$$D^2V - k^4V = 0 \quad \text{where} \quad D = \frac{\partial^2}{\partial x^2}$$ 2.13.

Then:

$$(D-k^2)(D+k^2)V=0 \qquad 2.14.$$

thus:

$$D-k^2=0 \qquad 2.15a.$$

$$D+k^2=0 \qquad 2.15b.$$

We have therefore four possible solutions.

From the second equation, 2.15b., we will obtain terms of the form exp.($\pm ikx$), which describes travelling bending waves which may carry energy away from the boundary. From equation 2.15a., we will obtain terms of the form exp.($\pm kx$), which describe decaying near fields that do not propagate away from the boundary, and which do not carry any energy.

Figure 7 shows the near field set up when a long bar is excited in bending at a point. (from Cremer(10)). The solid line represents the shape of the bar; the dashed line shows the travelling wave component on its own.

In later chapters we will deal with the relative magnitude of each of the fields at various discontinuities or boundaries in a plate. For

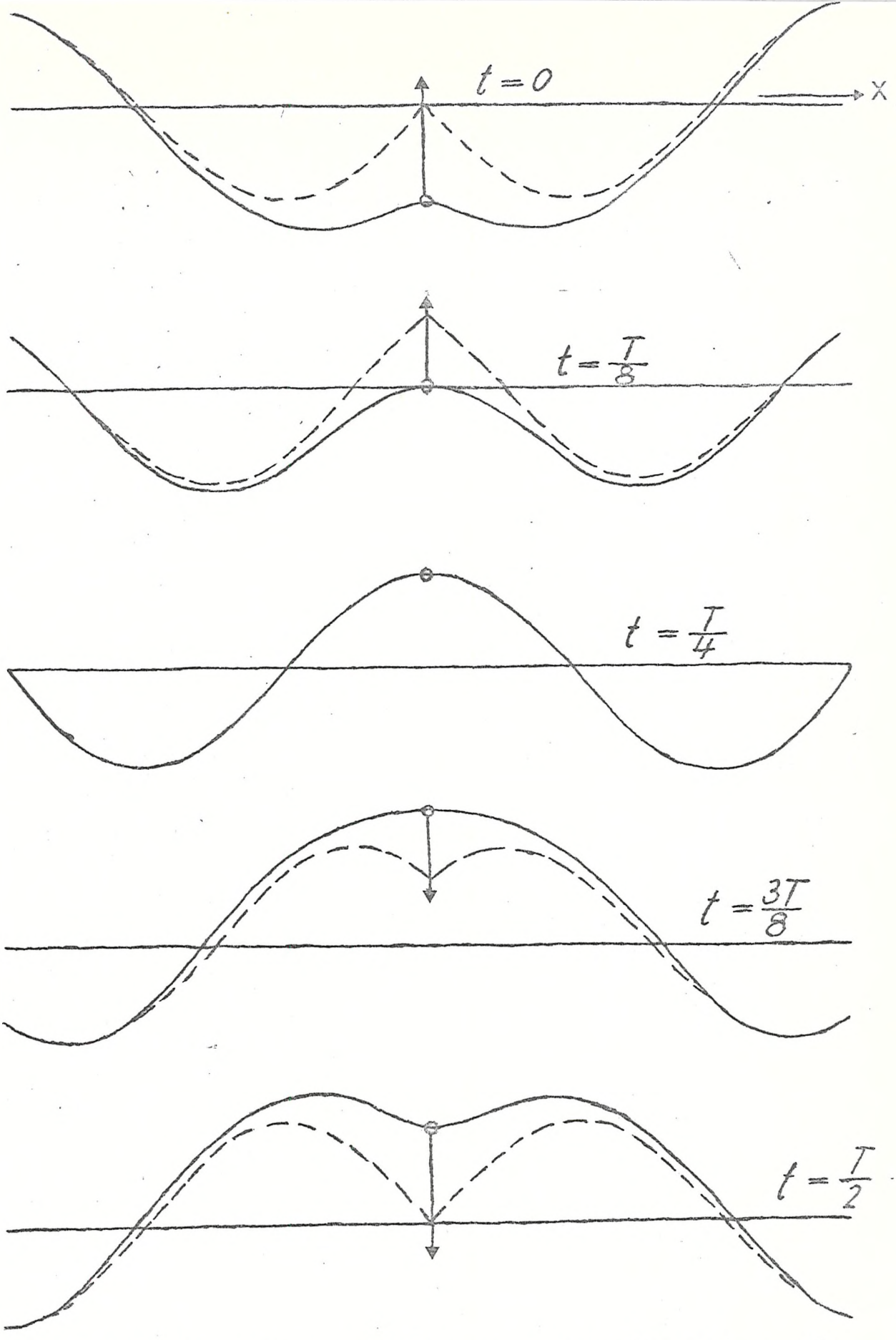

Figure 7 Infinite Beam Excited in Bending at a point.

the moment it is sufficient to appreciate that in addition to the energy carrying waves, a boundary can induce waves that do not carry energy and that decay with distance, even when the plate is of unrestricted area. This is not to be confused with the acoustic near fields set up, for example, near a dipole source in an infinite space. Such near fields are the result of complex interference effects and also occur with bending waves. But the decaying waves induced by a boundary in an unrestricted area are peculiar to bending waves.

TABLE I

Comparison of Some Properties of Compressive and Bending Waves in a Bar

	Compressive	Bending
Velocity of Propagation	$C_L = \sqrt{\frac{D}{\rho}}$ D = Compressive Stiffness ρ = Density (Speed independent of frequency)	$C_B = \sqrt{\frac{B}{m}}\sqrt{\omega}$ B = Bending Stiffness m = mass/unit length ω = frequency (Speed dependent on frequency)
Intensity I	$I = U_{TOT} * C_L$	$I = U_{TOT} * 2C_B$ $2C_B$ = Group Velocity (10)
Energy Density (U_{TOT})	$U_{TOT} = A^2Dk^2.\cos^2.kx$ k = wavenumber A = Amplitude of Compressive Wave x = Distance along bar (Dependent on position)	$U_{TOT} = \frac{B}{2}A^2k^4$ k = wavenumber A = Amplitude of Bending Wave (Independent of position)

Chapter 3

The Analysis of the Forced Vibration of Extended Plate and Shell Structures : a Summary of Available Methods

There are two analytical models that we may use, namely, the Normal Mode and the Travelling Wave models.

First we will consider the derivation of the two models, their properties and limitations in accurately representing the behaviour of vibrating plate and shell structures.

Next we will consider the problems of analysing the stress distribution in a complex structure at high frequency, when many modes may be excited. We will use the two models and compare their value to us.

3.1. The Normal Mode

Let us consider the free vibration of a multi-degree of freedom system that is conservative, i.e. undamped. This analysis is well known and we will only consider its main results.

For n degrees of freedom we may describe the free oscillation about an equilibrium position as:-

$$\left.\begin{aligned} M_{11}\ddot{q}_1 + \cdots\cdots + M_{1n}\ddot{q}_n + K_{11}q_1 + \cdots\cdots + K_{1n}q_n = 0 \\ M_{21}\ddot{q} + \cdots\cdots + M_{2n}\ddot{q}_n + K_{21}q_1 + \cdots\cdots + K_{2n}q_n = 0 \\ M_{n1}\ddot{q}_1 + \cdots\cdots + M_{nn}\ddot{q}_n + K_{n1}q_1 + \cdots\cdots + K_{nn}q_n = 0 \end{aligned}\right\} \quad 3.1$$

where $q_{[1 \to n]}$ are coordinates necessary to define the state of the system and where M_{rs} and K_{rs} are coefficients of mass and stiffness.

More simply, we may write:-

$$[M]\{\ddot{q}\} + [K]\{q\} = 0 \qquad 3.2.$$

where $[M]$, $\{q\}$, $[K]$ are mass, coordinate and stiffness matricies.

We note that $[M]$ and $[K]$ are symmetric matrices.

Let us consider solutions of 3.2. corresponding to pure harmonic motions of the form:-

$$\{q\} = \{A\} \sin(\omega t + \theta)$$

where $\{A\}$ is a matrix of amplitude constants, ω is the angular frequency and θ an arbitrary phase angle. Then:-

$$\left\{[K] - \omega^2 [M]\right\}\{A\} = \{0\} \qquad 3.3.$$

There will be a solution of this equation wherever the determinant of $[K] - \omega^2[M]$ vanishes, i.e., wherever the frequency ω

equals n certain values, ω_r . Thus we may set up our general solution as:-

$$\{q\} = \sum_{r=1}^{r=n} \{A_r\} \sin(\omega_r t + \theta_r) \qquad 3.4.$$

The values of ω_r are set by the stiffness and inertia of the system and are known as natural frequencies of the system. The column matrices $\{A_r\}$ are known as Modal Columns. Having specified the value of one element of $\{A_r\}$ all the other elements are fixed, for this matrix defines the shape of mode r of the vibrating system.

One of the most important properties of modal columns is that they are orthogomal. An elegant proof of this is quoted by Pipes[12].

Briefly, let us consider the r th modal column. It satisfies the equation

$$\omega_r^2 [M]\{A_r\} = [K]\{A_r\} \qquad 3.5.$$

The s th modal column satisfies

$$\omega_s^2 [M]\{A_s\} = [K]\{A_s\} \qquad 3.6.$$

Premultiply 3.5 by $\{A_s\}'$ and 3.6 by $\{A_r\}'$

we have

$$\omega_r^2 \{A_s\}'[M]\{A_r\} = \{A_s\}'[K]\{A_r\} \qquad 3.7$$

and

$$\omega_s^2 \{A_r\}' [M] \{A_s\} = \{A_r\}' [K] \{A_s\} \qquad 3.8.$$

where $\{A\}'$ is the transposed matrix. $\{A\}$.

Now

$$\left([a][b][c]\right)' = [c]'[b]'[a]' \qquad 3.9.$$

where $[a],[b],[c]$ are three conformable matrices

Then, from 3.7.

$$\omega_r^2 \{A_r\}' [M] \{A_r\} = \{A_r\}' [K] \{A_s\} \qquad 3.10.$$

for $[M],[K]$ are symetric matricies.

Then subtracting 3.10. from 3.8.;

$$(\omega_s^2 - \omega_r^2) \{A_r\}' [M] \{A_s\} = 0 \qquad 3.11.$$

If $r \neq s$, then in general it follows that

$$\{A_r\}' [M] \{A_s\} = 0 \qquad 3.12.$$

This is the modal orthogonality condition.

We may call these modes Normal modes.

We now have an alternative sets of axes with which to describe our system. Instead of describing the state of each coordinate, q, we may define instead the amplitude of each column matrix $\{A_r\}$. This we are free to do without interfering with the amplitude of the other normal modes.

Now, a plate has an infinite number of degrees of freedom, and it is much more convenient to describe the normal modes whose natural frequencies lie within a given frequency band than to give the displacement of each point on the structure, which is in principle an infinite task, for within a certain finite bandwidth we find that there are a finite number of normal modes.

For a lightly damped structure with well separated modes, the existence of normal modes may be demonstrated practically. The natural frequencies may be approximately determined by exciting the structure with a discrete tone, and noting the frequencies that cause maximum response. A typical response curve is shown in Figure 8. The response is then almost entirely due to one mode. On a flat plate, the mode shapes may be dramatically demonstrated by scattering sand on the plate and exciting it at a resonance. The sand will indicate the nodal points, or points of rest, in the modal pattern. An example of this is shown later on

in Figure 64.

However, while it is successful for low damping, when the damping is high the model is less satisfactory. The modes may well no longer be orthogonal; they can only be so if the damping, if viscous, is distributed in proportion to the local stiffness or mass[13]. In practice, when structures are highly damped, the damping is often extremely localised; a bolted joint may be responsible for most of it. This may beshown by measuring the damping of a continuous and a bolted structure of the same size and material; the damping in the bolted structure will be much higher. In this situation, the damping will clearly not be distributed according to the local stiffness and the modes will no longer be orthogonal. With high damping it is difficult to interpret the normal mode model physically. As damping is introduced to the system, the bandwidths of the modes become finite; the peaks in the frequency response curve become flattened and we can no longer be sure of finding a natural frequency by simply looking for a local maxima of frequency response. This is shown on Figure 8.

The Anechoic Room, where all acoustic energy that reaches the walls is absorbed, represents the ultimate in highly damped systems. No resonances may be detected in the air space of the room, and it is no longer correct to talk about normal modes.

However, under many service conditions, the damping is not very high, and it is reasonable to use the normal mode model to describe the vibration of many structures. Whether or not it is the best description

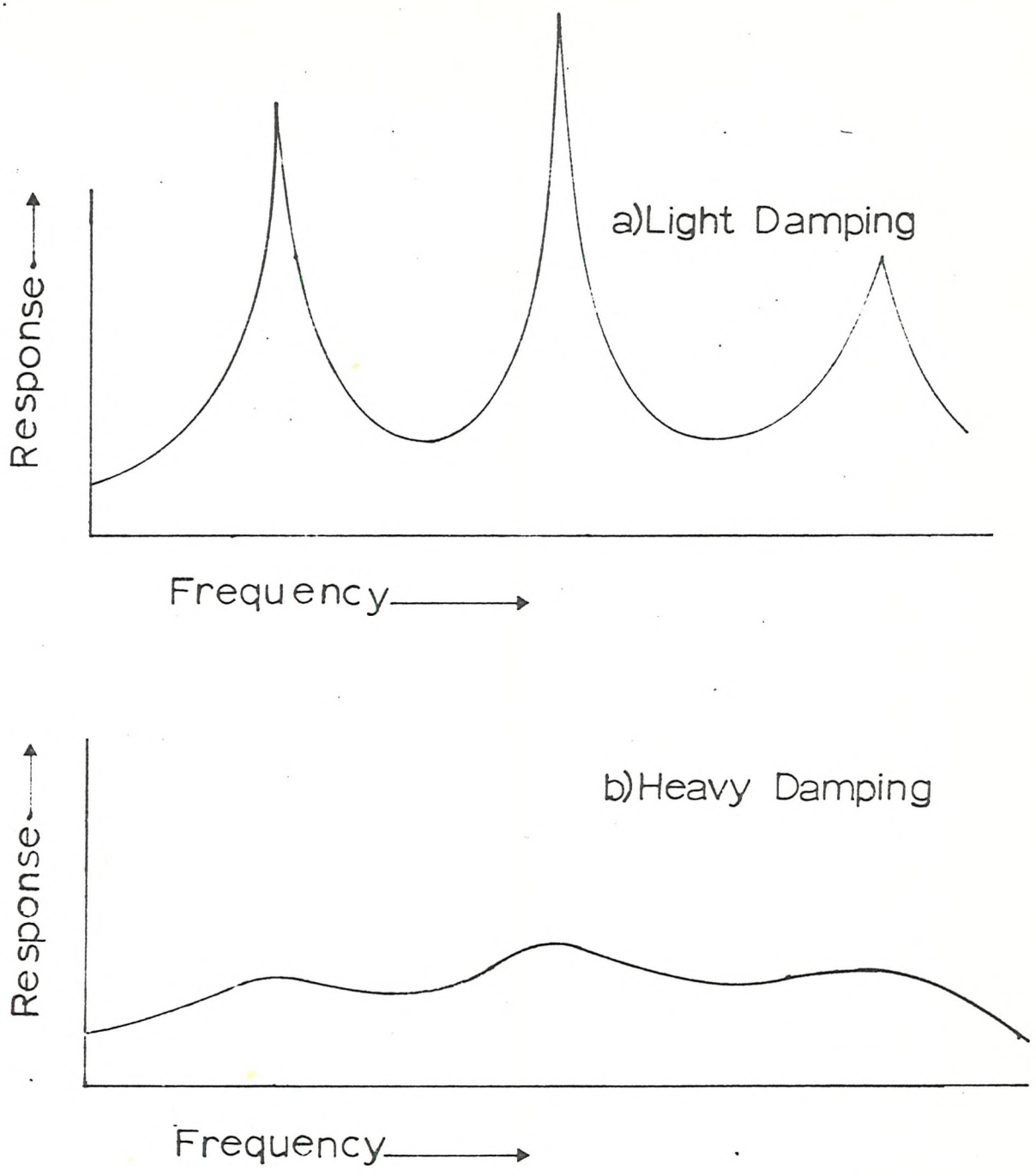

Figure 8 Frequency Response of a Multi-Degree of Freedom System with Light and Heavy Damping.

will be discussed in Section 3.3.1. of this chapter.

3.2. The Travelling Wave

A standing wave, or normal mode, in a room or in a structure, may be regarded as a set of travelling waves which constructively interfere to form nodes and anti-nodes. In solving the wave equation for a bounded region, whether this be for bending waves or acoustic waves, the imposition of the various boundary conditions imposes restrictions on the form of the bending waves. For undamped systems, we find that waves may only travel in a limited number of directions if the frequencies of the waves lie within a certain band. In other directions, and at other frequencies within the band, the boundary conditions cannot be satisfied.

This is, of course, identical to the normal mode situation. The frequency of the "permitted" wave is a normal mode frequency, and the permitted wave direction merely specifies the mode shape. Figure 9 attempts to demonstrate the relationship between two normal mode shapes of a flat, rectangular, simply-supported plate and the direction of the alternative travelling wave as specified on the Wave Number Diagram.

The wavenumber of a particular wave, k, we have already defined as $2\pi/\lambda$ where λ is the wavelength. Each dot on figure 8a represents a normal or a constructively interfering travelling wave. Let us consider wave number vector 1 corresponding to mode 1. The wavenumber in the 0 - x direction is $3\pi/a$ and in the 0 - z is π/b ; i.e. the wavelength in the 0 - x direction is $\frac{2}{3}a$ and $2b$ in the 0 - z direction. Vector 2 is more complex; the wavelength in the 0 - x

direction is a and in the direction O - z is $\frac{2}{3}b$ The resulting angle θ is the direction in space, relative to the O- x axis, in which the travelling wave will propagate.

The wavenumbers are related to frequency by:-

$$\left(\frac{m\pi}{a}\right)^2 + \left(\frac{n\pi}{b}\right)^2 = k_m^2 + k_n^2 = \left(\frac{\omega_\alpha}{c_\beta}\right)^2 \qquad 3.13.$$

for a rectangular, simply supported plate. ω_α is the frequency of the wave α or normal mode α . Other structures have more complicated wavenumber diagrams and we will consider some of these later.

Going to the trouble of expressing normal modes in terms of permitted wave directions can lead to a better understanding of the behaviour of the system when the damping is localised, as it often is in practice. We may talk of bending waves losing energy on a reflection at a boundary. Clearly, for such a system, a pure standing wave cannot be set up. For constructive interference from the reflected waves is impossible as amplitude of the reflected waves will be less than the incident wave.

It is quite easy to discuss the flow of energy in an anechoic room, if we consider waves travelling to the boundaries and not being reflected. It is quite obvious that such a sound field will behave as if it were in an infinite space. As we have seen, we cannot describe this situation using normal modes.

Doak[14] uses a combination of standing and travelling waves to describe the behaviour of sound waves in partially absorbent rooms. Mead[15] has also used the idea of travelling waves to describe how the location of damping materials in a structure can affect the total damping. Using the travelling wave model is particularly appropriate for this, as the effect of position can be more readily appreciated than when the damping is fed in as a generalised modal damping affecting the whole structure. Heckl[16] also discusses the superiority of the travelling wave model when dealing with localised damping, and points out the success with which it has been used in architectural acoustics.

A point of great interest to us later is that alterations in the boundary conditions do not have serious effects on the wave number diagram. Figure 9, from the work of Bolotin[17] shows the wavenumber diagram for a clamped and simply supported plate. The grid of lines has shifted a little on clamping. This implies that although individual modes have been distorted locally and their frequencies altered, the direction associated with them has altered little.

3.3. The Analysis of Stress Distribution

The object of this work is to try and establish a method of predicting the distribution of stress in a complex structure, vibrating at high frequency, from the design stage. We will now consider the details of the analysis, using the models described, to see which will most reasonably allow us to estimate this distribution.

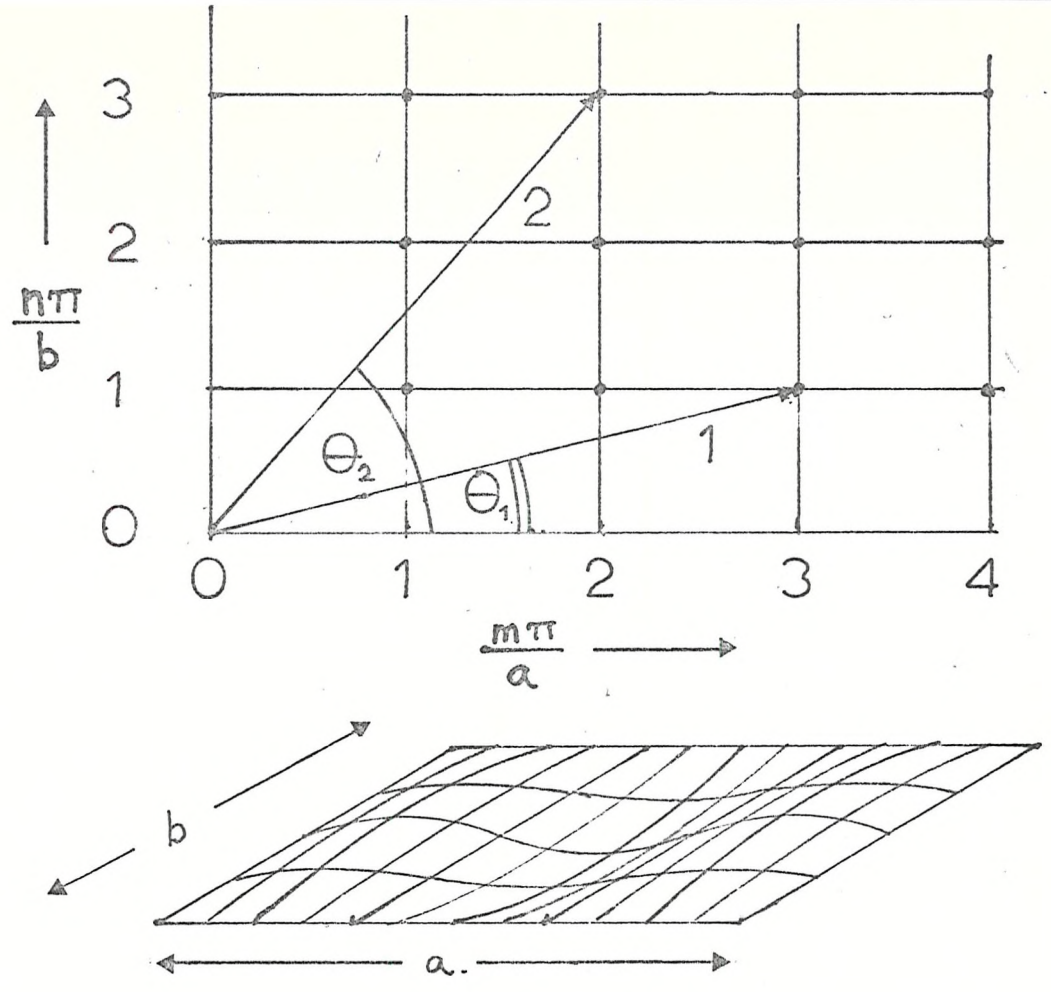

MODE 1

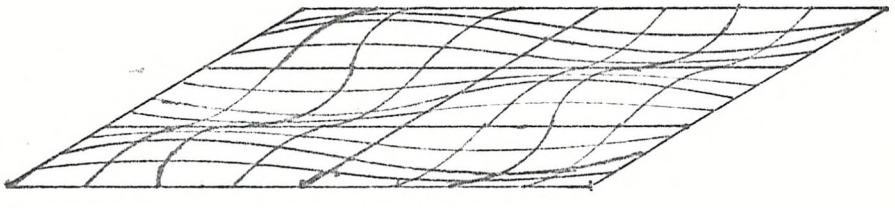

MODE 2

FIGURE 9 WAVE NUMBER DIAGRAM FOR A SIMPLY SUPPORTED PANEL, SHOWING TWO NORMAL MODES AND THEIR CORRESPONDING WAVE VECTORS.

3.3.1. Normal Mode Analysis

3.3.1.1. Powell's Equation:- Accurate Summation of the Effect of Several Known Normal Modes

In principle, all linear shell vibrations are described by Powell's Equation, quoted in (18) as:-

$$W(r,r';\omega)=\iint_A H(r,r_o,\omega)\, H^{\star}(r',r_o';\omega)\, P(r_o,r_o';\omega)\, dr_o\, dr_o' \quad (3.14.)$$

$W(r,r';\omega)$ is the cross spectral density of the response and describes the relative phases and amplitude of the response at different positions at various frequencies: $P(r_o,r_o';\omega)$ is the cross spectral density of the exciting forces. Formally, the cross spectral density is the Fourier Transform from the time domain to the frequency domain of the cross correlation of the quantities, response or force, at r and r', or r_o and r'_o. Estimating the value of $P(r_o,r'_o;\omega)$ is often an extremely uncertain procedure. The only situations in which estimates are reasonable is when the acoustic field is a travelling wave travelling in one direction only, or travelling waves in every direction. A further discussion of this is beyond the scope of this work. Bull et al[19] discuss further ramifications.

$H(r,r'_o;\omega)$ is the cross impedance of the structure; this is the response at r due to a unit exciting force of frequency $\frac{\omega}{2\pi}$ at r'_o.

We may write it as (19):-

$$H(r, r_0'; \omega) = \sum \frac{\psi_a(r)\ \psi_a(r_0')}{Y_a(\omega)} \qquad 3.15.$$

where ψ_a represents the shape of mode a

and $Y_a(\omega)$ is the impedance of mode a at frequency $\frac{\omega}{2\pi}$

If we hope to solve Powell's equation to find the response of a structure, we must find an expression for ψ_a and for $Y_a(\omega)$, even if we do have an expression for the cross spectral density $P(r_0, r_0'; \omega)$ of the exciting forces.

Analytic solutions are only possible for the simplest structures, for example, the simply supported rectangular plate or cylinder. In order to produce solutions for even slight departures from this situation, say a plate, lightly bolted round its edges, we must assume something about the boundary. We might try to get the mode shapes by assuming that the boundary is simply supported, or perhaps rigid. Either way is generally unsatisfactory. We most probably would want to find the stress at the boundary; yet we are obliged to ignore those very details which are most likely to cause the stress concentrations that we seek.

The so-called Finite Element technique is an alternative method by which the form of the normal modes may be determined for complex structures. Briefly, the structure is broken up into a large number of small elements. By matching up the boundary conditions of the complete structure and of the adjacent elements, and knowing the equations of

motion of the elements, it is possible to predict the normal mode shapes and frequencies of the structure. This technique is very successful in predicting the low order modes of complex structures. Ermutlu[20] has used it to study the response of arch dams to earthquakes, and Deb Nath et al[21] have used it to examine the low order modes of curved shells.

Mason[22] has studied the computational requirements for predicting the normal modes of a rectangular plate. Beyond the 12th normal mode over 10^4 store locations are needed in the computer to accurately predict further modes. In general, we are concerned with very high order modes of the gas circuit structure, typically the 100th mode and often higher. Even with the largest available machines it is doubtful if enough information could be included to predict the detailed stress distribution at operating frequencies.

Whether the normal modes are found analytically or numerically, there is a further objection to using this model to investigate detailed local stress distributions. Even a very modest change in boundary condition can produce large changes in natural frequency and mode shape, particularly at high mode order. If a small change is introduced into the structure, either deliberately or by accident during manufacture, then the normal modes are all changed, and our calculations are invalid. In fact, we know this to be an exaggeration, but using a normal mode model we have no grounds for saying so, unless we re-calculate the response for all possible conditions.

3.3.1.2. Asymptotic Summation of the Response of Many Normal Modes

Skudrzyk[23] has developed an approach to the analysis of the impedance of vibrating systems, based on the concepts of electrical network theory. He develops this for low order modes; he then examines the form of the asymptotic solution at high frequencies. He finds that frequency average impedance for high order modes relies on what he terms the structure's basic parameters. These are gross properties of the structure; exactly which properties are to be considered depends on the basic shape of the structure. For example, for flat plates the Characteristic Impedance to a point force is given by:-

$$Z_c = 8\sqrt{B'm'} \qquad 3.16$$

where B' = Bending Stiffness per unit width of plate,

m' = Mass per unit area.

Skudrzyk shows how these impedances, which may easily be determined with little attention to structural details, can be used to predict the flow of energy from one vibrating system to another. He quotes the example of a mass loaded joint to illustrate the use of the method, and compares his results derived theoretically with experimental results.

However, these results cannot help us determine either the stress concentration around a discontinuity, or the excursions of stress that are likely from a given estimated mean value. These are our chief interest.

3.3.1.3. Statistical Summation of the Response of Many Normal Modes

Waterhouse[24] and Lubman[25], among others, have investigated the

statistics of sums of normal modes to predict the variation in sound pressure level about the spatial mean square pressure in reverberant rooms, when many normal modes are excited simultaneously. In general, the more modes excited, the lower is the standard deviation of sound pressure level, measured at various points about the room. These theoretical findings have been borne out by measurements made in reverberant rooms.

A similar analysis could be very useful in deciding the likely variation from the spatial mean square stress in a plate. The spatial mean square stress is, of course, the stress estimated from the statistical energy analysis. Intuitively, one would imagine that given enough modes, then a similar result should hold. In Chapter 8, where this is discussed in detail, we find that this is so. For brevity, the details of the analysis will not be repeated here.

The important point is this: the property we are trying to find is related to the whole plate, and an approach via the normal mode model is thus eminently suitable. However, again, such an approach cannot tell us anything about conditions near a boundary, or, indeed, in any specific location.

3.3.2. The Travelling Wave Analysis : The Diffuse Field Model

First let us consider a single travelling bending wave incident at an arbitrary discontinuity at an angle. θ . Without yet delving into the mathematics, we have already seen from Chapter 2 that this boundary will reflect some of the bending waves and transmit the rest.

The reflected and transmitted wave will give rise to interference fringes near the discontinuity, which will cause local alterations of stress. We may draw a cautious analogy with the behaviour of light passing through a narrow slit. Interference fringes are produced, as shown by local alterations in the intensity of light. As we have seen, the bending wave is further complicated by the extra decaying near fields. However, we can, in principle, predict the bending stress normal to the discontinuity due to a bending wave of given amplitude arriving from a given direction θ.

Using the travelling wave model we can make an important generalisation about the form of the bending wave field, that can make our analysis of the stress at a particular discontinuity general for any structure containing this discontinuity.

If we are to perform design calculations on any unknown structure we must make some assumption as to the actual form of the wavenumber diagram. We might assume that all the waves travel in one direction or that the waves can travel in every direction statistically independent of each other. By statistically independent we mean, for example, that the total mean square stress due to all bending waves is the sum of the mean square stress caused by each bending wave on its own. The actual form of the wavenumber diagram is probably beyond our computational powers. Heckl[16] points out that the second assumption has worked well in architectural acoustics. (See also Morse[26]). Certainly, looking at Figure 10, it would seem that if we are concerned with the behaviour over a band of frequencies, then, indeed, waves will

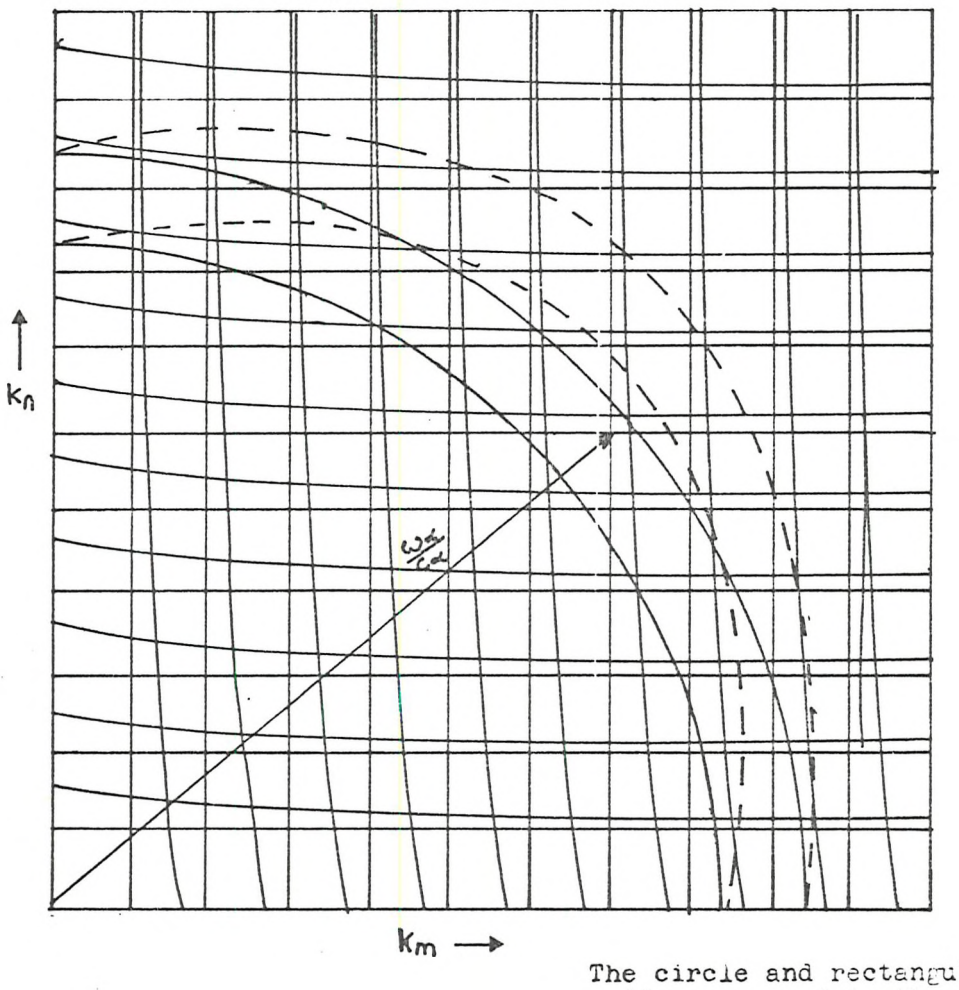

The circle and rectangular grid correspond to the simple supports; the dashed line and offset grid to the clamped plate.

Figure 10 Wavenumber Diagram for a Simply-Supported and a Clamped Rectangular Panel.

arrive from many directions. This assumption makes use of the fact that small changes in boundary condition will alter the direction of individual waves only slightly.

Of course, the approximation that bending waves arrive from every direction can only be exact for a plate of infinite extent. In building acoustics the assumption works well, as mentioned. It works because the modal density, i.e., the number of modes in a bandwidth of one cycle per second, is very high in acoustic spaces. A room 10 ft. x 10 ft. x 10 ft. at 1000 Hz will have a modal density of 9.44 modes/Hz; a steel plate 10 ft. x 10 ft. x 1 inch will have a modal density of 0.12 modes/Hz at all frequencies[27].

One of our tasks will be to see how many structural modes are necessary for this assumption to be adequate. Incidentally, a point that is likely to favour the assumption is that we only have two dimensions to fill. The normal modes available in the acoustic volume have to produce an even energy flux in three dimensions; in the structure they only have to produce an even flux in two dimensions.

A further valuable advantage of the travelling wave model is that it is possible to localise the effect of a boundary. The near field effects do not propagate. This implies that the stress changes are only local. This is in accordance with the findings of Bolotin[28]. He describes the dynamic edge effects close to boundaries of shell structures. The changes from the sinusoidal deflected shape that occur at a boundary do not propagate into the mid-field regions.

Far from a boundary, the bending waves are sinusoidal in shape, as if the plate was simply supported. In short, this approach implies that if we change a particular boundary, say, clamp a hitherto free edge, then the major alterations in stress will be near that particular boundary and the stress elsewhere will be largely unaffected.

In Chapters 6 and 7 we put these ideas into practice.

3.4 Comparison of the Analyses

We may conclude very simply. For investigating the local stress changes near a boundary we will use the model of waves travelling in a diffuse reverberant field; for investigating properties relating to the whole plate, like the statistics of mean square stress, the normal mode model is more appropriate.

Chapter 4

Formal Tests of the Diffuse Field Model

In Chapter 3 we decided that when investigating the variation of stress near a boundary, we should use the analytical model of bending waves, travelling about the structure in a diffuse field. We assume that many bending waves, statistically independent of each other, will travel about the structure in all directions. In this chapter we devise formal tests to see if this is a reasonable representation of what happens in practice.

The parameter that will most affect the accuracy of the assumption is the number of bending wave directions, or modes, excited in the structure. This we will investigate. We will also see if damping has any effect on the reverberance or diffuseness of the field, either by increasing the amount by which adjacent modes overlap in frequency or by creating a radiating field as in an anechoic room.

Two tests have been used; the cross-correlation of accelerations at separated points on a thin plate or shell structure and the cross-correlation of strains at individual points in two orthogonal directions. The acceleration correlation experiments have also been simulated on a digital computer by using Powell's Equation (Section 4.1.3.) to show that the two models, the normal mode and the travelling wave, give consistent results.

4.1. Cross-Correlation of Acceleration

Cook et al[29] describe a series of experiments in which they tested the diffuseness of the acoustic field in a reverberant room. They set up two microphones in the room, separated by a distance r, and

measured the cross-correlation of the outputs when a sinusoidal signal, slowly changing in frequency with time, drove a loudspeaker in the room. They then compared the results with a theoretical prediction of cross-correlation coefficient based on the assumption that the field was diffuse, which they give as $(\sin kr)/kr$ where k is the wavenumber.

The analogous experiment on a structure is to cross-correlate the outputs from two accelerometers, separated by a distance r. Both quantities, acceleration and sound pressure, are independent of the direction of any given wave, unlike, for example, strain. The method is attractive because accelerometers are easy to handle and usually provide good signals for subsequent correlation.

A summary of the following work is given in reference (30).

4.1.1. Theoretical Value of Cross-Correlation Coefficient

Suppose that a bending wave approaches the line 0 - x at an angle θ_1 to 0 - x, then the output S_a from an accelerometer at 0 will be:-

$$S_a = A_i \omega_i^2 \cos(\omega_i t + \alpha_i) \qquad 4.1a.$$

where A_i is the amplitude of the bending wave,

$\frac{\omega_i}{2\pi}$ is the frequency of the wave,

and α_i is some arbitrary phase angle.

The output from the other accelerometer, also on the line 0 - x, but separated from the first by a distance r, will be:-

$$S_b = A_i \omega_i \cos\left(\omega_i t + \alpha_i + k_i r.\cos.\theta_i\right) \qquad 4.1b.$$

where k_i is the wavenumber, given by $\frac{2\pi}{\lambda}$

The phase difference between the two outputs will be $k_i r.\cos.\theta_i$

The phase angle α_i is common to both signals and will not affect the cross-correlation; for convenience it is omitted in the rest of the analysis.

Assuming that many modes are responding in a band of frequencies the outputs will be:-

$$S_a = \sum_{i=1}^{N} A_i \omega_i^2 .\cos.\omega_i t \qquad 4.2.$$

$$S_b = \sum_{i=1}^{N} A_i \omega_i^2 \cos\left(\omega_i t + k_i r.\cos\theta_i\right) \qquad 4.3.$$

The cross-correlation at a time lag τ of two variables X,Y is:-

$$R'_{XY}(\tau) = \lim_{T\to\infty} \left[\frac{1}{2T}\int_{-T}^{T} X(t)\,Y(t+\tau)\,dt\right]$$

and normalised is:-

$$R_{XY}(\tau) = \frac{R'_{XY}(\tau)}{\sqrt{\overline{X^2_{(t)}} \cdot \overline{Y^2_{(t)}}}}$$

where $\overline{\qquad}$ indicates a time average.

We want this cross-correlation coefficient for a time delay = 0 and this will be:-

$$R_o = \frac{\int_{-T}^{T} \sum_{i=1}^{N} A_i \omega_i^2 . \cos \omega_i t . \sum_{i=1}^{N} A_i \omega_i^2 \cos\left(\omega_i t + k_i r . \cos\theta_i . dt\right)}{\sqrt{\sum_{i=1}^{N} A_i^2 \omega_i^4 . \cos^2 \omega_i t \cdot \sum_{i=1}^{N} A_i^2 \omega_i^4 . \cos^2\left(\omega_i t + k_i r . \cos\theta_i\right)}} \quad 4.4.$$

$$= \frac{\sum_{i=1}^{N} A_i \omega_i^2 . \cos\left(k_i r . \cos\theta_i\right)}{\sum_{i=1}^{N} A_i \omega_i^2} \quad 4.5.$$

if we assume that the modes are statistically independent.

To evaluate this expression we must assume that, for a large number of modes, we can reasonably replace the summated terms by a continuous function. For a diffuse field, even over a small angle there would be waves of all frequency and we may write:-

$$R_o = \frac{1}{2\pi} \int_0^{2\pi} \frac{\int_{k_1}^{k_2} A\omega^2 \cos.(kr.\cos.\theta)\, dk}{\int_{k_1}^{k_2} A\omega^2 .dk.} .d\theta \qquad 4.6.$$

$A\omega^2$ is now a function of k_i

If we assume that the spectral density of the generalised force on the structure is constant over, say, a third octave (23%), frequency band, then we may assume that $A\omega^2$ is constant. This assumption is necessary if we are to proceed with the analysis and it will probably be reasonable for small frequency bands of analysis if the structure responds at all frequencies within that band.

We may now simplify our expression to:-

$$R_o = \frac{1}{2\pi} \int_0^{2\pi} \frac{\int_{k_1}^{k_2} \cos.(kr.\cos.\theta)\, dk}{(k_2 - k_1)} .d\theta \qquad 4.7.$$

$$= \frac{1}{2\pi} \int_0^{2\pi} \frac{2.\mathrm{SIN}.\left(\frac{(k_2-k_1)r.\cos\theta}{2}\right) \cos\left(\frac{(k_2+k_1)r.\cos\theta}{2}\right)}{(k_2-k_1)r.\cos.\theta} d\theta \qquad \ldots.$$

If we restrict our analysis to third octave bands, then we may write $\frac{k_2 + k_1}{2}$ as a constant k. If we never consider values of kr greater than 10 this will affect the accuracy by less than 10%. For a mild steel plate of $\frac{1}{4}$ inch thick, at 2500 Hz this implies r < 10 in. and at 5000 Hz, r < 7 in.

We may now write:-

$$R_o = \frac{1}{2\pi} \int_0^{2\pi} \cos(kr.\cos.\theta)\, d\theta \qquad 4.9.$$

$$= J_o(kr) \qquad 4.10.$$

4.1.2. Experimental Procedure

Measurements were made on two flat plates, 2.2 ft. by 2.7 ft., $\frac{1}{4}$ in. and $\frac{1}{8}$ in. thick, clamped rigidly at their edges to a cistern 2 ft. deep packed round with sand. The plate could be excited acoustically by the noise of a jet of compressed air at high pressure escaping into the cistern from a gate valve. The $\frac{1}{4}$ in. thick plate could also be excited mechanically by an electro-mechanical shaker driven through a power amplifier from a white noise generator. Figure (11) shows the complete arrangement.

Measurements were also taken on a mild steel cylinder 3 ft. in

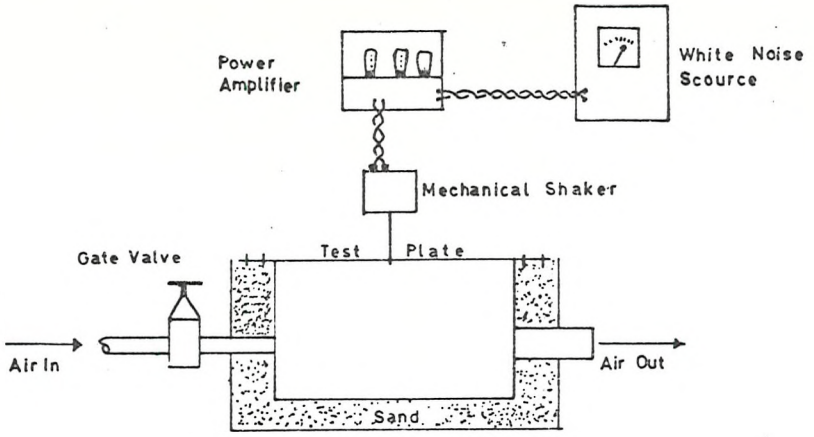

Figure 11 Experimental Set-Up for Correlations on Flat Plate

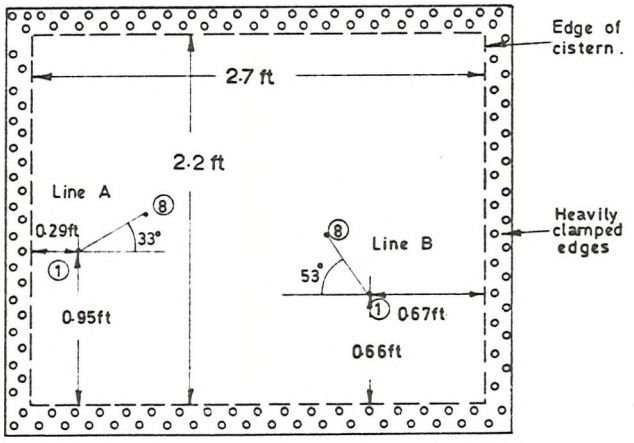

Figure 12a The flat plate showing accelerometer positions.

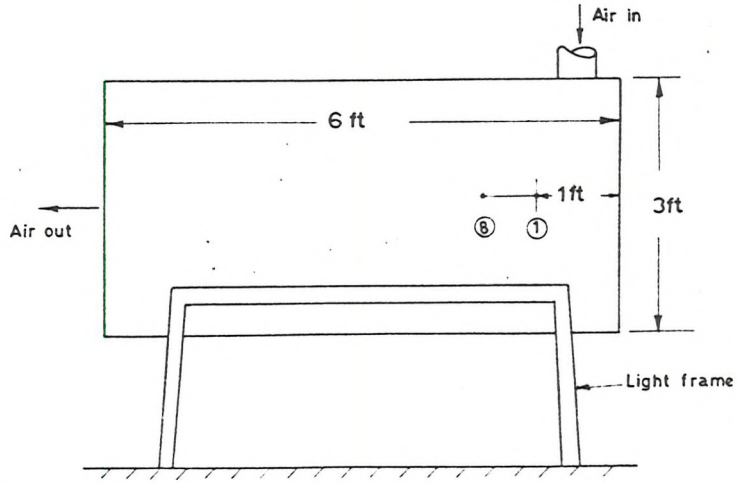

Figure 12b The cylinder showing accelerometer positions.

diameter, 6 ft. long and made of 3/16 in. plate. The cylinder was free standing on a light steel frame and could be excited acoustically by sound generated inside by high pressure air escaping from a gate valve. The cylinder was completely closed at one end and could either by completely open at the other end or partially closed. This was to alter the acoustic conditions inside the tank for another research programme.

The positions of the accelerometers are shown in Figure 12a for the $\frac{1}{4}$ in. plate and on 12b for the cylinder; the positions chosen on the $\frac{1}{8}$ in. plate were similar to those on the $\frac{1}{4}$ in. plate, except that the spacing between each position and the next was smaller. The spacing between each accelerometer on the $\frac{1}{4}$ in. plate was 1 in. and on the $\frac{1}{8}$ in. plate was 0.7 in. On the cylinder, each position was 1 in. apart. During the tests, one accelerometer was held at one end of the chosen line and the position of the other accelerometer was altered to achieve different values of the separation. The cross-correlation was measured along two lines, chosen at random, on the plates and along one axial line chosen at random on the cylinder.

The results for the acoustically excited $\frac{1}{4}$ in. plate are from four different experiments. In Figures 13 to 18 the triangle and circle represent the results from two experiments on line A, the cross and square from experiments on line B. The triangle and cross represent the results obtained when one accelerometer was held at the ends of the lines marked 1, the other being moved up the line to 8; the circle and square marks represent the results when the fixed accelerometer was at 8.

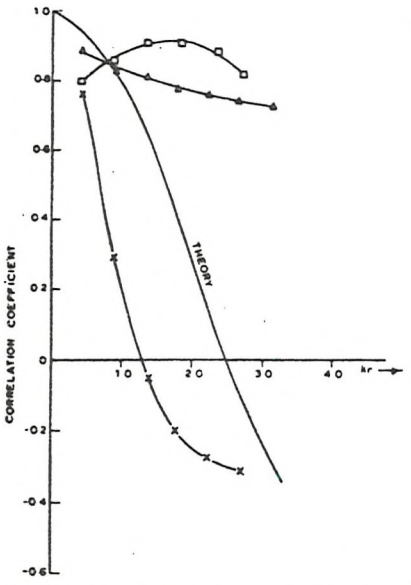

Figure 13 ¼" plate acoustically excited. Correlation coefficient at ⅓ octave at 500 Hz.

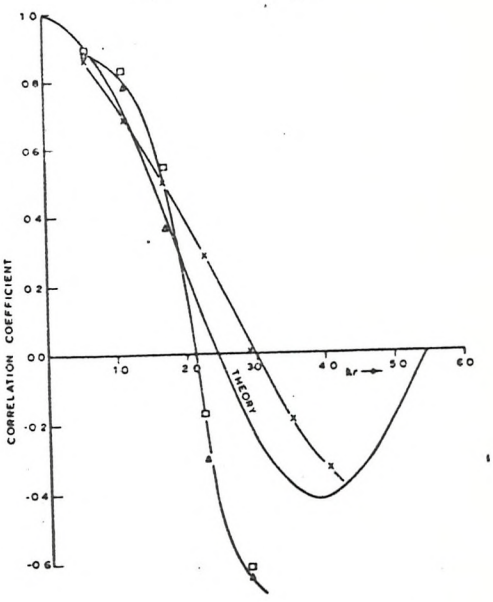

Figure 14 ¼" plate acoustically excited. Correlation coefficient at ⅓ octave at 800 Hz.

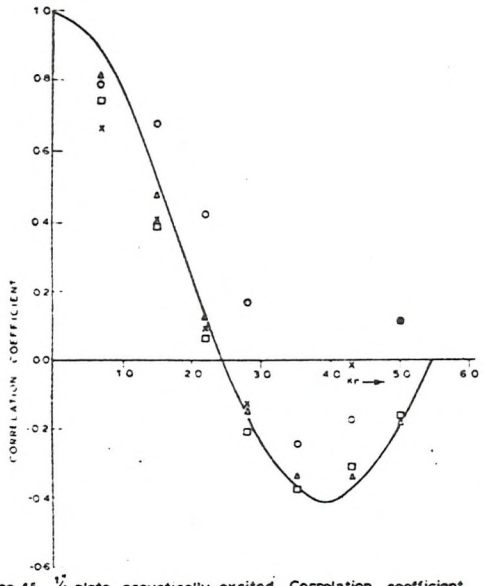

Figure 15 ¼" plate acoustically excited. Correlation coefficient at ⅓ octave at 1250 Hz

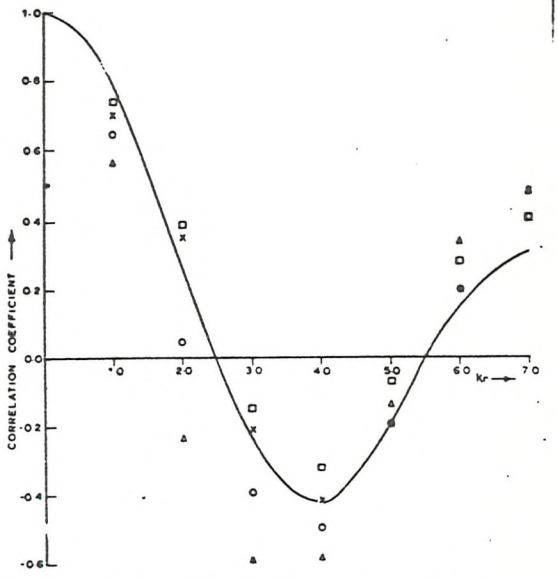

Figure 16 ¼" plate acoustically excited. Correlation coefficient at ⅓ octave at 2500 Hz.

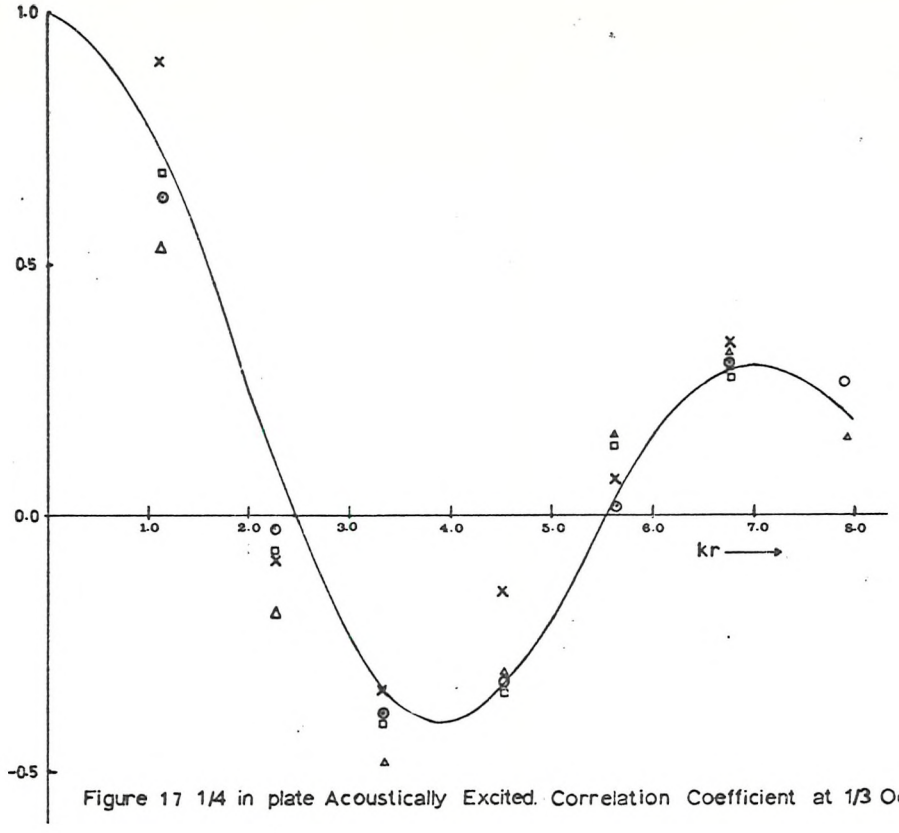

Figure 17 1/4 in plate Acoustically Excited. Correlation Coefficient at 1/3 Octave at 3150 Hz

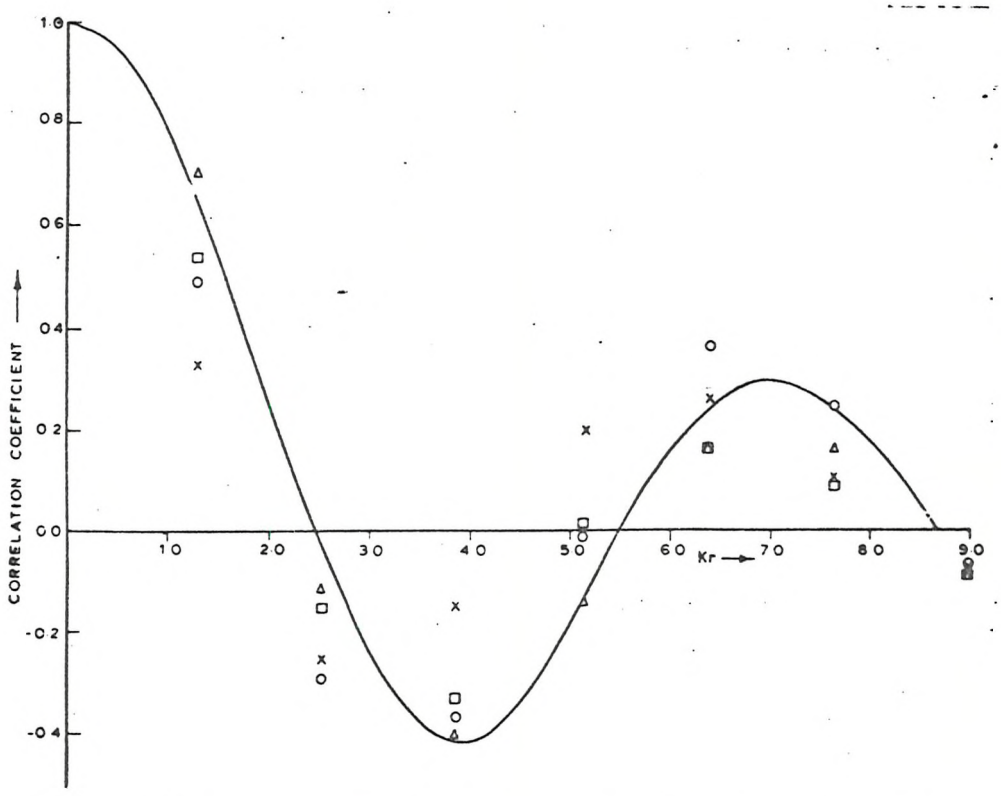

Figure 18. 1/4 plate acoustically excited. Correlation coefficient at 1/3 octave at 4000 Hz.

The results from the $\frac{1}{8}$ in. plate are presented on Figures 19 and 20 and from the cylinder in Figures 21 and 22. The results from the mechanically excited $\frac{1}{4}$ in. plate are presented in Figures 23 to 25 . They are taken from two experiments only, one on line A and one on line B.

Bruel and Kjaer 13 gram accelerometers were used on the $\frac{1}{4}$ in. plate and cylinder and 3 gram accelerometers on the $\frac{1}{8}$ in. plate. In appendix 1 the effect of these accelerometers on the structures is discussed. At the frequencies of interest to us, the effect of the added local mass on the response of the structure was negligible. Accelerometers are usually fixed on with magnets, a thin layer of sticky wax or a small screwed stud. During these tests, the accelerometers were fixed on with studs screwed into holes, drilled and tapped into the structures. Magnets added to the mass of the accelerometers might well have affected the local response. Advice given by experienced field workers at the Berekely Nuclear Research Laboratories of the Central Electricity Generating Board suggested that fixing the accelerometers with wax could not be relied on to give accurate phase measurements at high frequency. Simple experiments, where two accelerometers were fixed to the end of a vibrating cantilever with wax, one on each face, showed that at frequencies of interest the phase relationship between the two transducers was a function of the care with which they were fixed to the base. Only by using studs screwed into the structure could good phase information be preserved. Of course, at frequencies where the

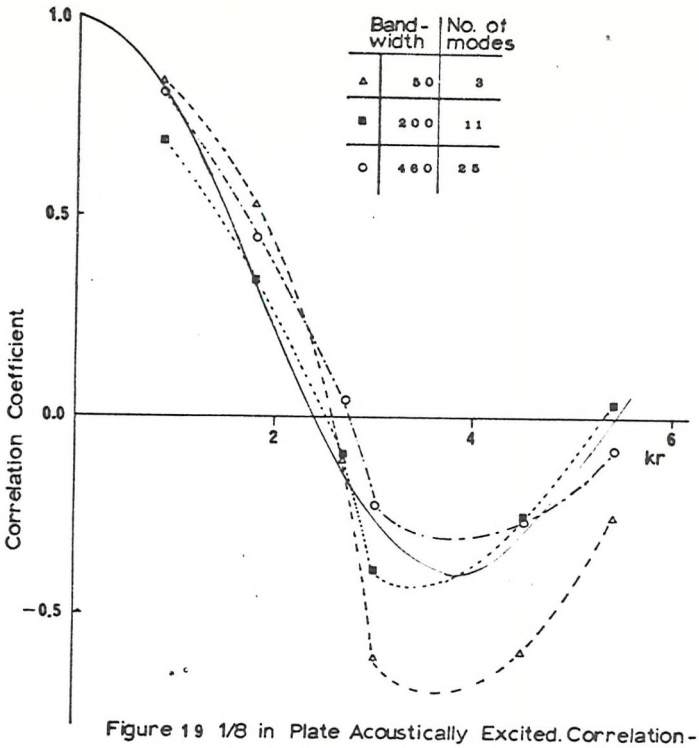

Figure 19 1/8 in Plate Acoustically Excited. Correlation-Coefficient Measured at 2000 Hz Centre Frequency

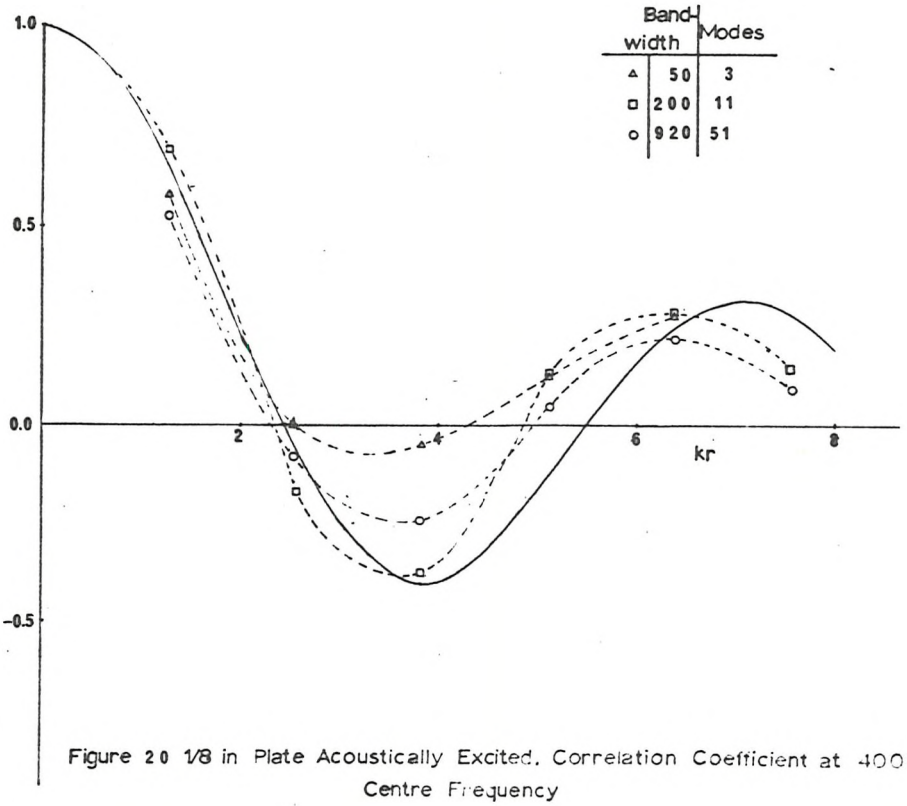

Figure 20 1/8 in Plate Acoustically Excited. Correlation Coefficient at 4000 Hz Centre Frequency

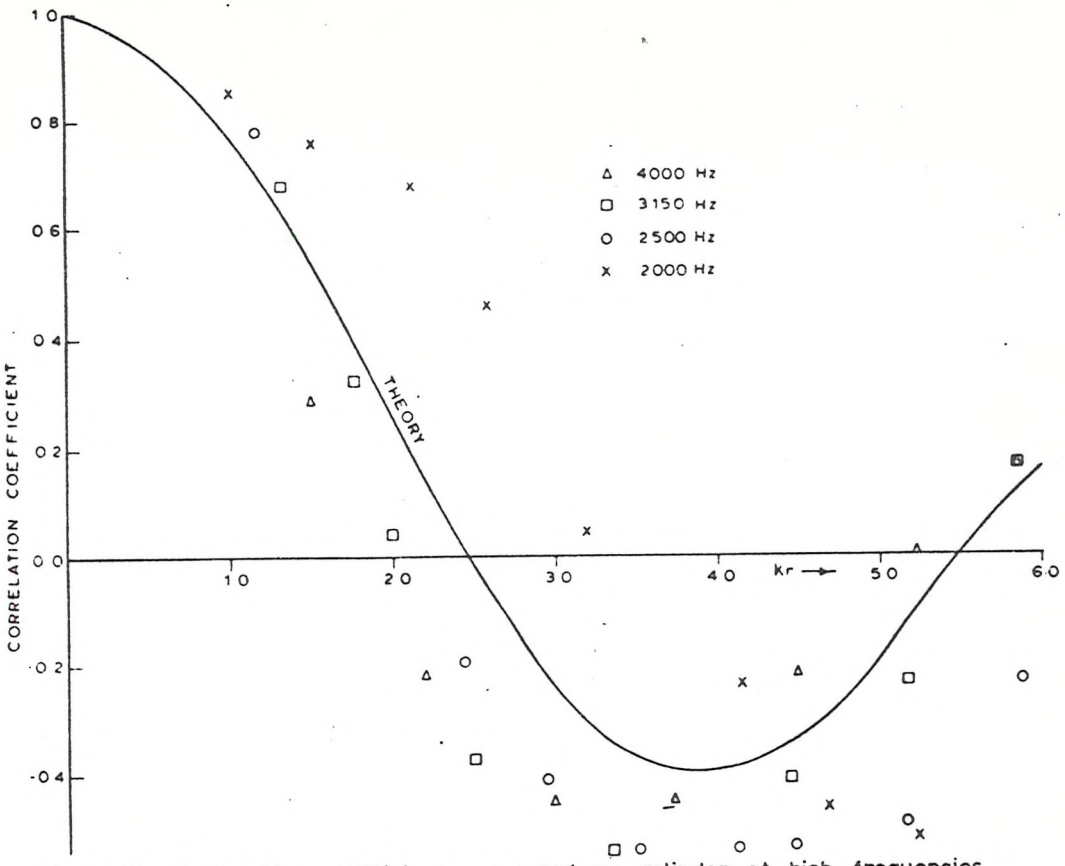

Figure 21 Correlation coefficient measured on cylinder at high frequencies. 1/3 octave bands.

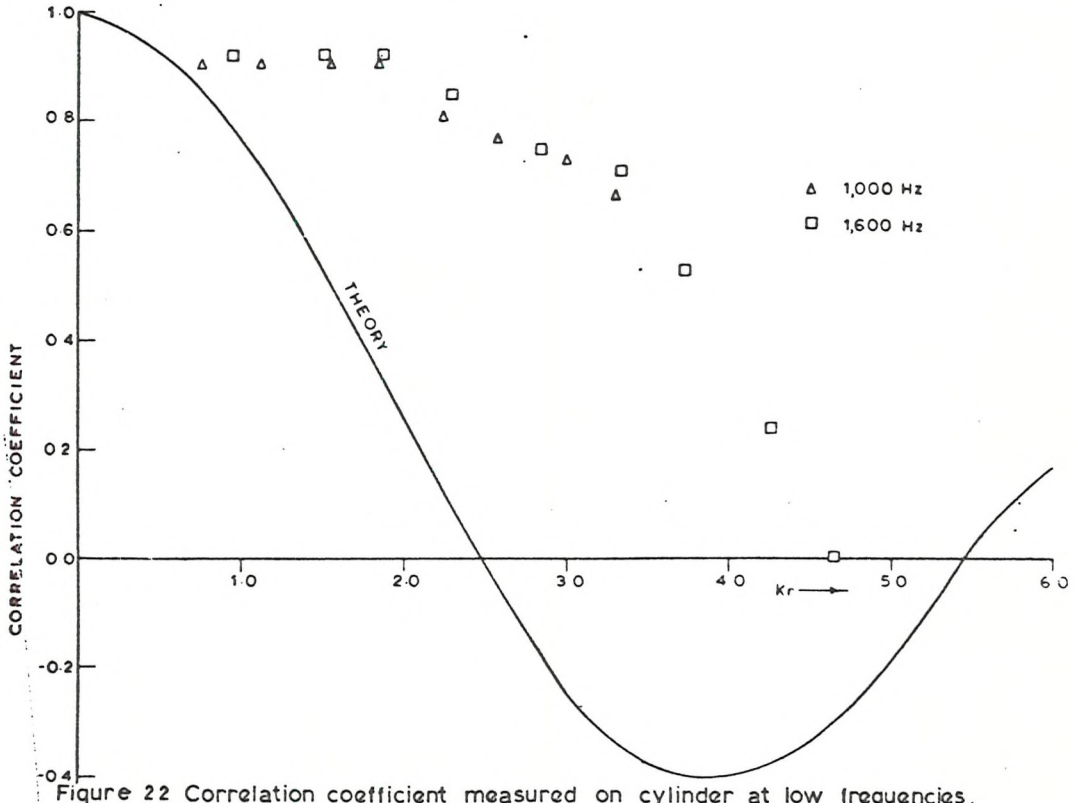

Figure 22 Correlation coefficient measured on cylinder at low frequencies. 1/3 octave band.

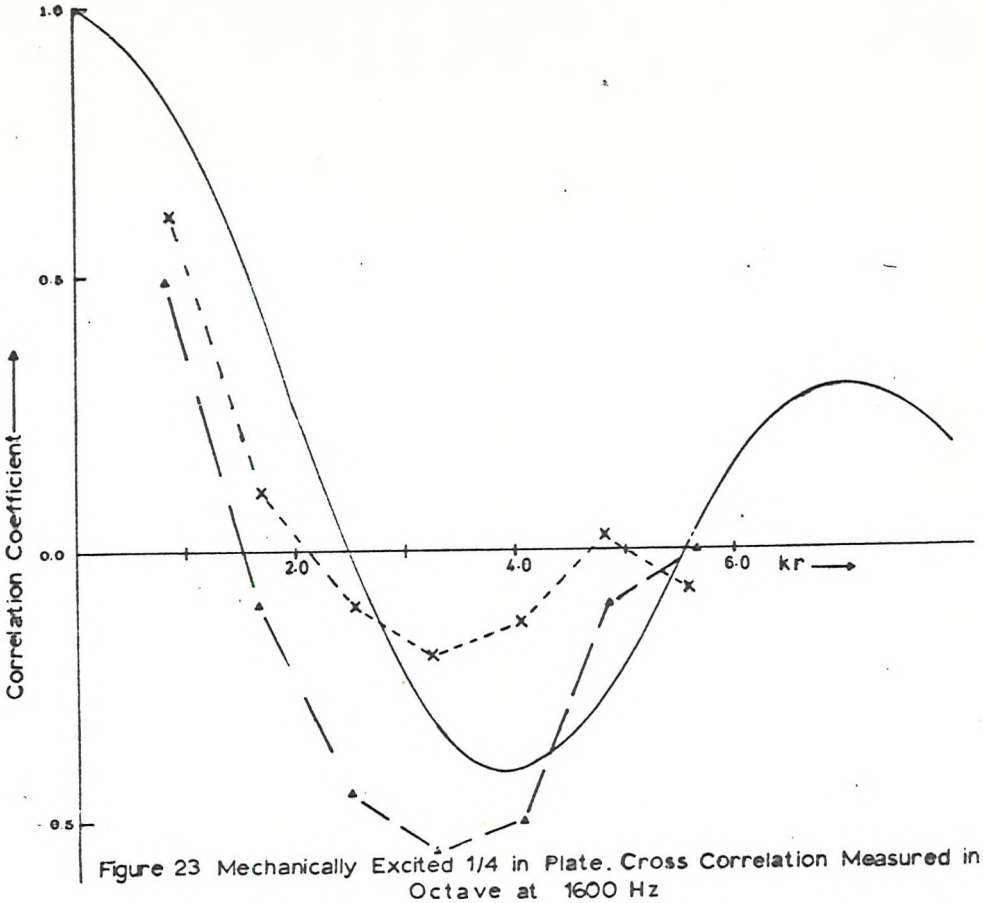

Figure 23 Mechanically Excited 1/4 in Plate. Cross Correlation Measured in 1/3 Octave at 1600 Hz

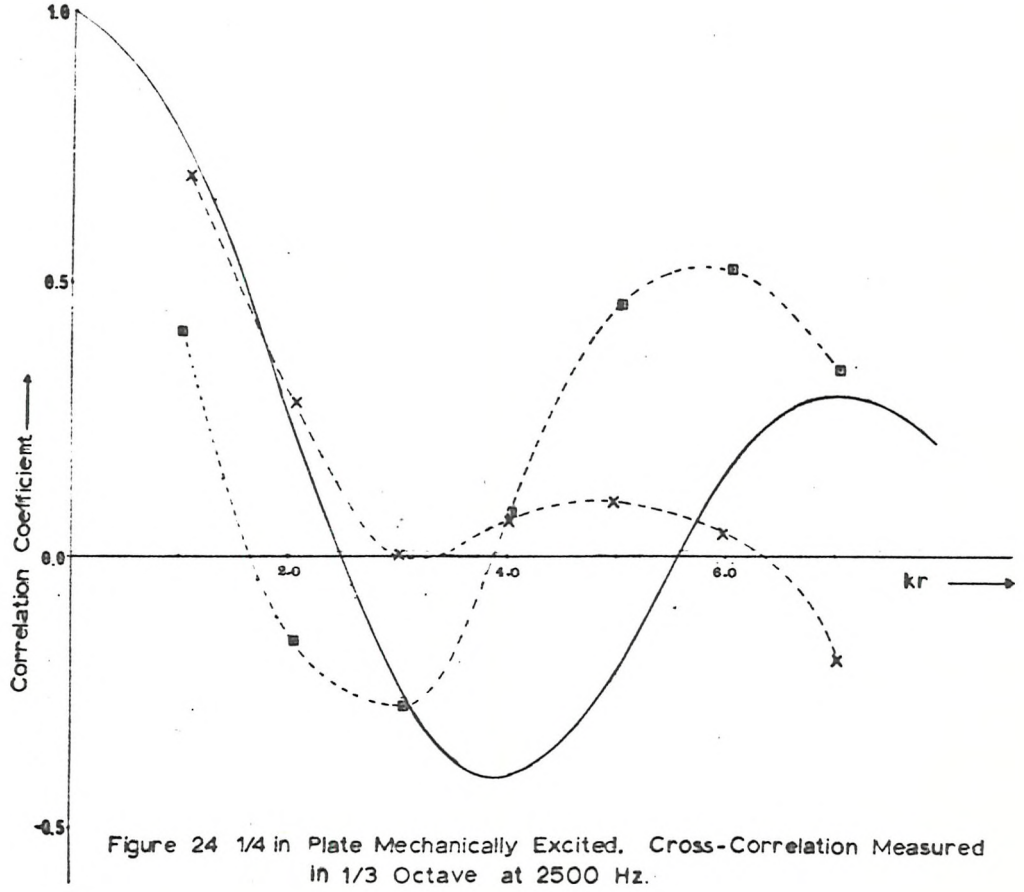

Figure 24 1/4 in Plate Mechanically Excited. Cross-Correlation Measured in 1/3 Octave at 2500 Hz.

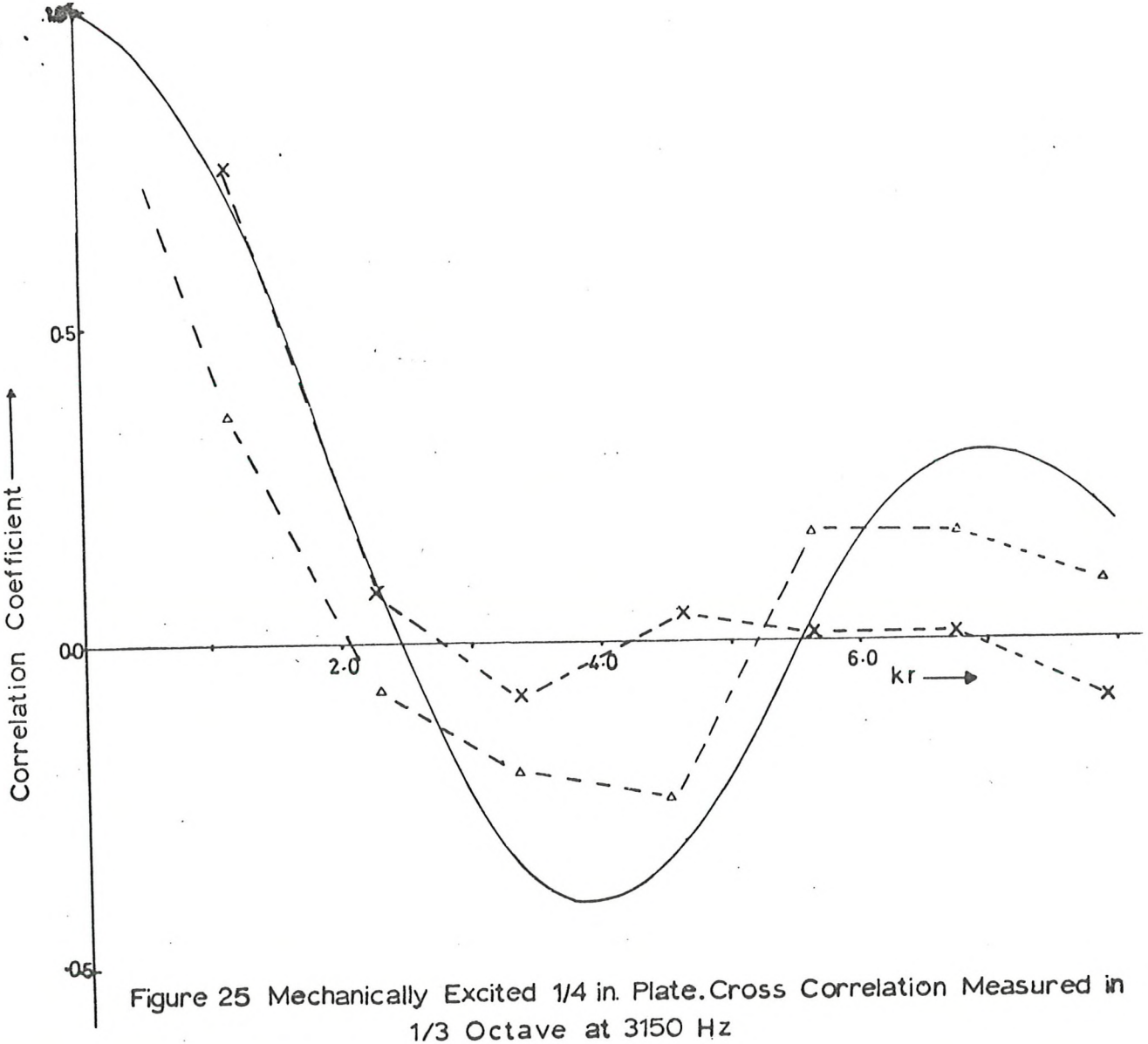

Figure 25 Mechanically Excited 1/4 in. Plate. Cross Correlation Measured in 1/3 Octave at 3150 Hz

accelerometers could vibrate on their studs, even this would not have been satisfactory. Fortunately, these frequencies would have been much higher than those of interest (> 10 kHz)

The signals from the two accelerometers were recorded on a multi-track tape recorder. The signals from the $\frac{1}{4}$ in. plate and the cylinder were analysed on an analogue correlator on playback, filtered before correlation through a pair of third octave filters selected to have good phase matching. The phase match of the filter pair was tested as described in appendix 2 and was good enough to ensure that the results are correct within about 10%. It was not possible to use narrower bandwidth filters as a suitably phase matched pair were not available. A signal flow diagram is given in Figure 26. Since the work was first reported (30) a digital analysis system has been commissioned at the I.S.V.R. at Southampton, in which large quantities of random data may be processed on a digital computer (31). Using this system it has been possible to analyse the signals from the $\frac{1}{8}$ in. plate using a digital filtering routine on the computer before correlation. This ensured that the phase matching was perfect between the two signal channels; there could be no question of one channel suffering an arbitrary phase change with respect to the other except in the recording or playback from the tape recorder. The recorder was a high quality machine, recording frequency modulated signals. Its upper frequency limit 10,000 Hz. The highest frequency considered was 4,000 Hz, and when control signals of white noise recorded on to both channels from the

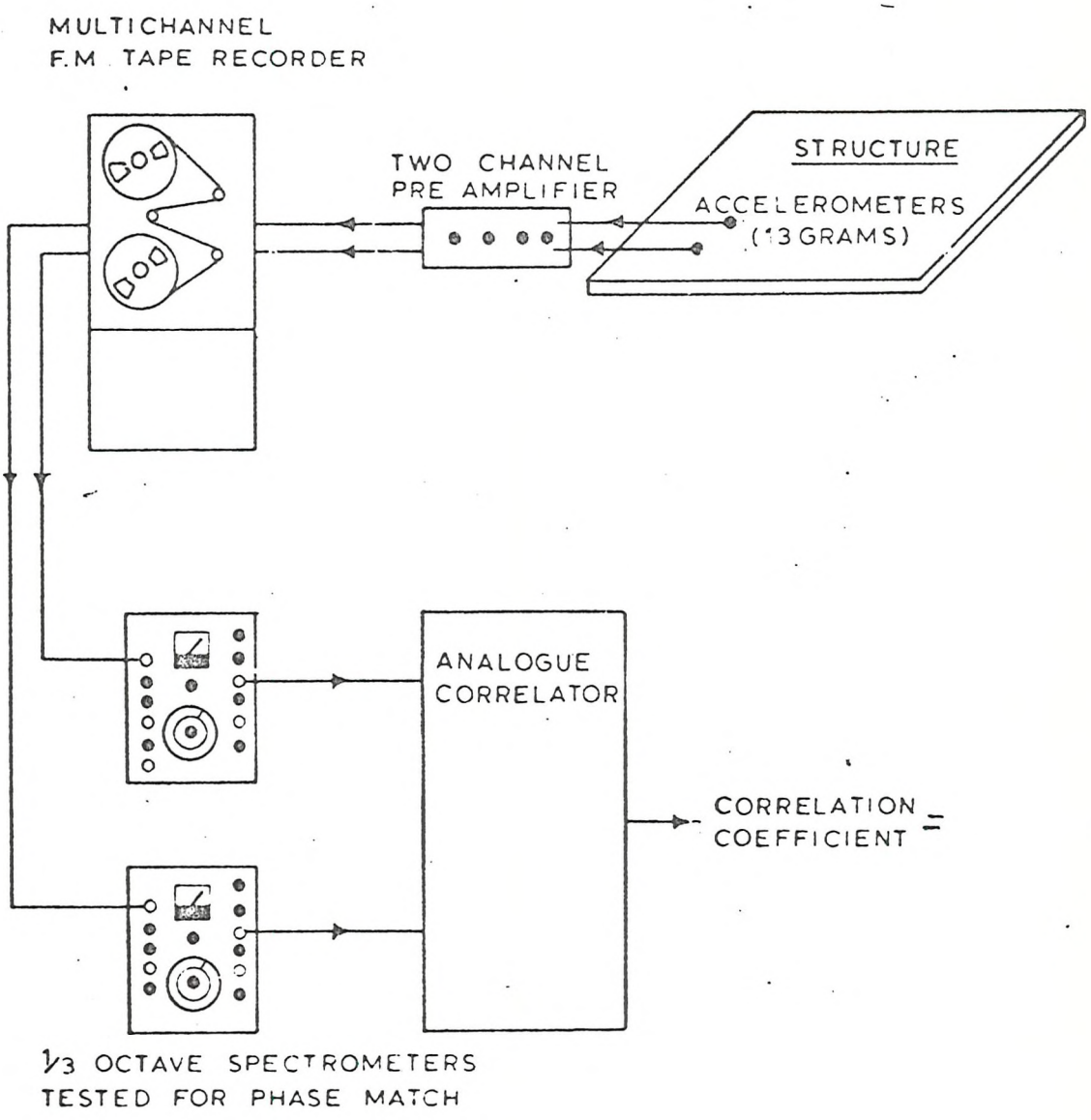

Figure 26 Experimental set up.

same source were played back, no phase shifts could be detected by cross-correlation or any other means.

4.1.3. Computational Tests

In these tests the behaviour of the test panels was simulated by studying the behaviour of a simply supported rectangular panel, using Powell's Equation. The object of these tests was to see that the two models of the vibrating system, the diffuse bending wave model and the normal mode model, were consistent. If an adequate number of normal modes are considered, then the two approaches should predict the same value of cross-correlation coefficient. These tests also reveal some of the practical difficulties of using Powell's Equation.

In fact, Morrows et al[32] have carried out an analytical summation of the effect of an infinite number of normal modes, responding in a room and in a plate and, indeed, the two models give the same answer for the cross-correlation. However, using the computer, it is possible to vary the number of normal modes included to see how sensitive is the result to this number.

Two forms of broad frequency band excitation are considered, point excitation and excitation by a diffuse, reverberant acoustic field.

Consider the equation for the cross-spectral density of displacement, $W\left(\underline{r},\underline{r}',\omega\right)$, in response to a forcing field of cross spectral density (18)

$$W(\underline{r},\underline{r}',\omega) = \iint_{AA} H(\underline{r},\underline{r}_o,\omega)\, H^*(\underline{r}',\underline{r}_o',\omega)\, P(\underline{r}_o,\underline{r}_o',\omega)\, d\underline{r}_o\, d\underline{r}_o' \qquad 4.11.$$

$H(\underline{r},\underline{r_o};\omega)$ is the cross modal acceptance of the structure.

Then the cross-correlation of the response at $\underline{r}$ and $\underline{r'}$ at a time delay τ is:-

$$R_{\underline{r},\underline{r'}}(\tau) = \int_{-\infty}^{\infty}\iint_{AA} H(\underline{r},\underline{r_o};\omega)\, H^*(\underline{r'},\underline{r_o'};\omega)\, P(\underline{r_o},\underline{r_o'};\omega)\, e^{j\omega\tau}\, d\underline{r_o}\, d\underline{r_o'}\, d\omega. \qquad 4.12.$$

Then at zero time delay, to correspond with our experiment,

$$R_{\underline{r},\underline{r'}}(\tau) = \int_{-\infty}^{\infty}\iint_{AA} H(\underline{r},\underline{r_o};\omega)\, H^*(\underline{r'},\underline{r_o'};\omega)\, P(\underline{r_o},\underline{r_o'};\omega)\, d\underline{r_o}\, d\underline{r_o'}\, d\omega \qquad 4.13.$$

We will now consider the problem for the structure driven at a point. Appendix 3 considers the more involved problem of the structure when acoustically excited.

The first problem is to find the value of $P(\underline{r_o},\underline{r_o'};\omega)$

From the Fourier Transform:-

$$P(\underline{r_o},\underline{r_o'};\omega) = \frac{1}{2\pi}\int_{-\infty}^{\infty} R_{F_{\underline{r_o},\underline{r_o'}}}(\tau)\, e^{-j\omega\tau}\, d\tau \qquad 4.14.$$

$$= \frac{1}{2\pi}\int_{-\infty}^{\infty} \overline{F_{\underline{r_o}}(\tau) \times F_{\underline{r_o'}}(t+\tau)}\, e^{-j\omega\tau}\, d\tau \qquad 4.15.$$

where R_F is the cross-correlation of the exciting force and $F_{\underline{r}_o}(t)$ is the exciting force at $\underline{r}_o$ at time t.

Clearly, for a point force, $F_{\underline{r}_o}(t) = F_{\underline{r}_o'}(t) = 0$ unless $\underline{r}_o = \underline{r}_o' = \underline{r}_s$ where $\underline{r}_s$ is the position of the point force.

Then R_F is the auto correlation function of the point force and

$$P(\underline{r}_o, \underline{r}_o'; \omega) = 0 \quad \text{if } \underline{r}_o, \underline{r}_o' \neq \underline{r}_s \qquad 4.16.$$

$$= S_F(\omega) \quad \text{if } \underline{r}_o = \underline{r}_o' = \underline{r}_s$$

where $S_F(\omega)$ is the spectral density of the exciting force

Thus we may write 4.13 as:-

$$R_{(r,r')O} = \int_{-\infty}^{\infty} H(r, \underline{r}_s; \omega)\, H^*(r', \underline{r}_s; \omega) S_F(\omega)\, d\omega \qquad 4.17.$$

Next we must evaluate the value of the cross acceptances.

From (19), $H(r, \underline{r}_s; \omega) . H^*(r', \underline{r}_s; \omega)$ is :-

$$\sum_{\alpha} \frac{\psi_\alpha(\underline{r})\, \psi_\alpha(\underline{r}_s)}{Y_\alpha(\omega)} \quad \sum_{\beta} \frac{\psi_\beta(\underline{r}')\, \psi_\beta(\underline{r}_s)}{Y_\alpha(\omega)} \qquad 4.18.$$

$$= \sum_{\alpha} \frac{\psi_\alpha(\underline{r})\,\psi_\alpha(\underline{r}')\,\psi_\alpha^2(\underline{r}_s)}{|\,Y_\alpha(\omega)\,|^2}$$

$$+ \sum_{\alpha}^{\alpha \neq \beta} \sum_{\beta} \frac{\psi_\alpha(\underline{r})\,\psi_\beta(\underline{r}')\,\psi_\alpha(\underline{r}_s')\,\psi_\beta(\underline{r}_s)}{|\,Y_\alpha(\omega)\,Y_\beta^*(\omega)\,|} \qquad 4.19.$$

If we can ignore the cross terms in comparison to the direct terms in 4.19., then the computational effort required will be reduced by a factor of N, where N is the number of modes considered. As we intend to go up to 20 modes or more, this is a substantial saving of time and therefore cost. It will be fair to make this assumption if the damping of the system is light, for then the product $Y_\alpha(\omega)\,Y_\beta^*(\omega)$ will be large compared to $|Y_\alpha(\omega)|^2$ near the natural frequency of mode α, provided that the modes are well separated in frequency.

This means that for structures with high modal densities the damping must be so light that the half power bandwidth of the modes is smaller than the average frequency gap between them.

If we assume this, we may write 4.13. as:-

$$R_{r,r'}(0) = \int_{-\infty}^{\infty} \sum_{\alpha} \frac{\psi_\alpha(\underline{r})\,\psi_\alpha(\underline{r}')\,\psi_\alpha^2(\underline{r}_s)}{|\,Y_\alpha(\omega)\,|^2} S_F(\omega)\,d\omega. \qquad 4.20.$$

We are now faced with the difficulty of representing the value of $\psi_a(r)$. As we have already discussed in Chapter 3, it would be very difficult for us to find the correct expression for the actual test panels used in the experiments. So we are obliged to make some assumption about boundary conditions. It would be convenient if we were to assume that the plate is simply supported, for this would mean that $\psi_a(r)$ would be a simple sine wave in $\underline{r}$. In fact, this is quite a reasonable assumption to make. Bolotin[28] explains how a change of boundary condition results in only a small change in position of the nodes of a given normal mode. Provided that we are not examining a structure near a boundary of some sort, then the mode shape will not be very different from that of a simply-supported plate no matter what boundary conditions apply to the structure, except that the nodal points will be shifted in space. We must, of course, restrict the analysis to frequencies many times higher than that of the lowest normal mode for this to apply. Now, if we are examining the effect of many normal modes, then these unknown shifts of nodal point from mode to mode will not matter. We are considering the behaviour of several modes, and if one nodal point is shifted considerably in space, then this will doubtless be compensated by the shift of another, provided we are considering several normal modes at once.

Damping has been considered uniform over each frequency bandwidth of analysis. Thus it appears as a constant in the denominator of expression 4.20. When the final result for cross-correlation is normalised the effect of damping is lost, for it affects only the magnitude of

the response.

The computed results are presented on Figures 27 and 28 for the acoustically excited plates and on Figures 29 to 31 for the point excited plate. The plates modelled in these tests had the same area as the practical test samples. The thicknesses are quoted on the Figures. The lines along which correlation was measured were picked at random so as not to be near a boundary. Very many points were considered along each line to provide a continuous picture of the correlogram in space. A theoretical curve, $J_o(kr)$, derived for the diffuse field, is drawn for comparison.

4.1.4. Discussion of Results

4.1.4.1. Interpretation

The correlation coefficient of a diffuse field has its zero at separation distances dependent only on the wavenumber k, not on the absolute position on the structure. If a measured, or simulated field, does not satisfy the conditions, then that field might be said not to be diffuse. For example, if only one mode were excited, the cross-correlation coefficient would be a square wave function with separation. The zero crossing separation would depend on the relative position of the accelerometers and the nodal lines of the mode. On the other hand, if the plate was "anechoic", with all the vibration energy incident on the boundaries absorbed, then the first zero crossing would be at a quarter of a wavelength separation for a narrow band of analysis,

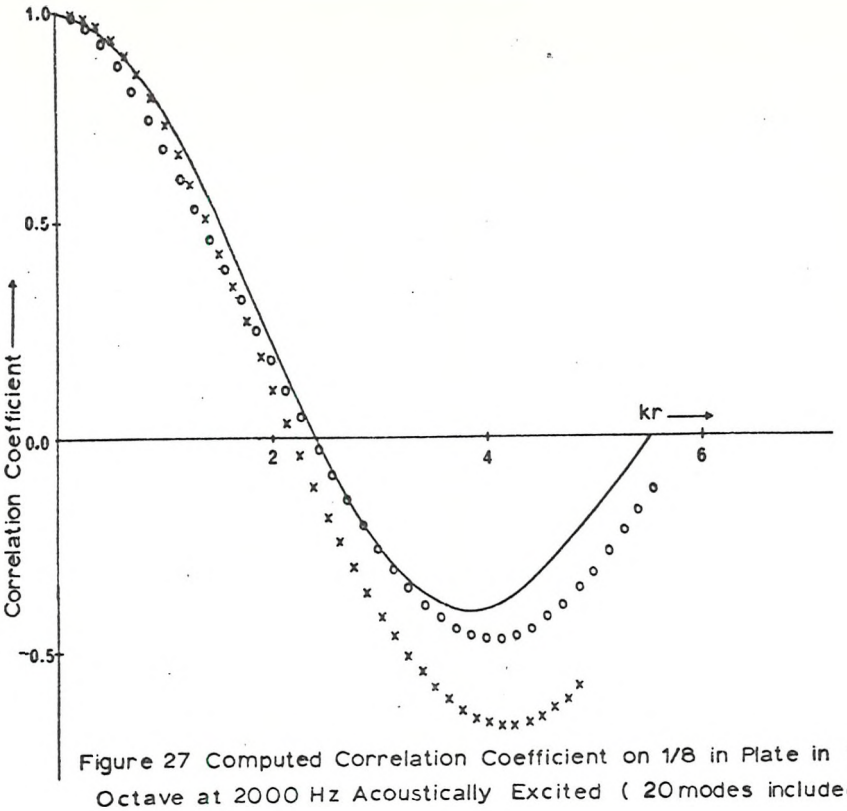

Figure 27 Computed Correlation Coefficient on 1/8 in Plate in 1/3 Octave at 2000 Hz Acoustically Excited (20 modes included)

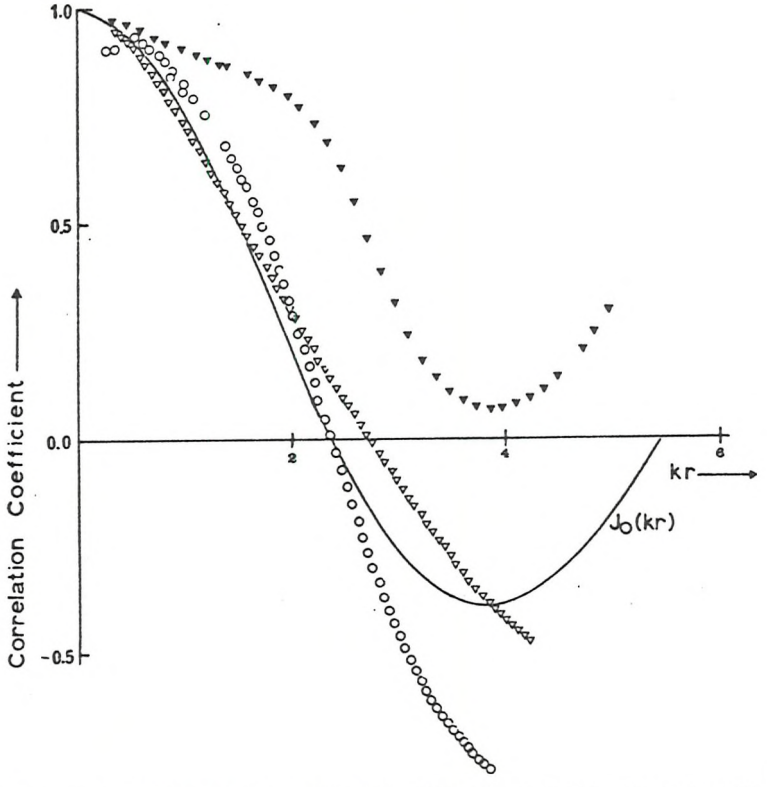

Figure 28 Computed Correlation Coefficient on 1/8 in Plate in 1/3 Octave Acoustically Excited at 1250 Hz (12 modes included)

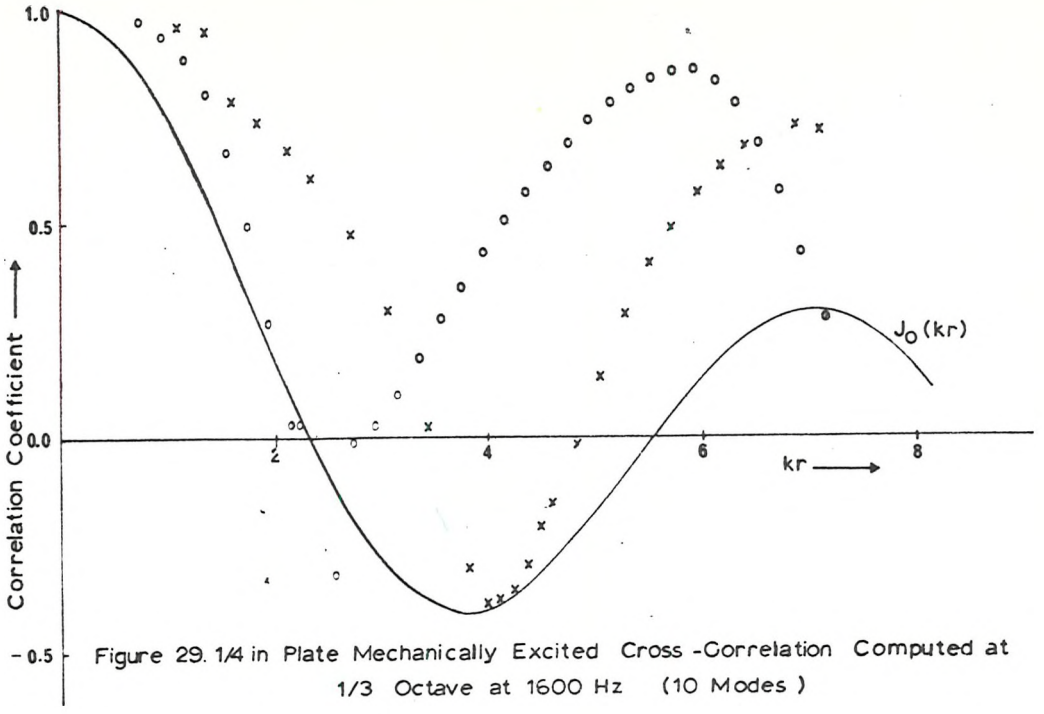

Figure 29. 1/4 in Plate Mechanically Excited Cross-Correlation Computed at 1/3 Octave at 1600 Hz (10 Modes)

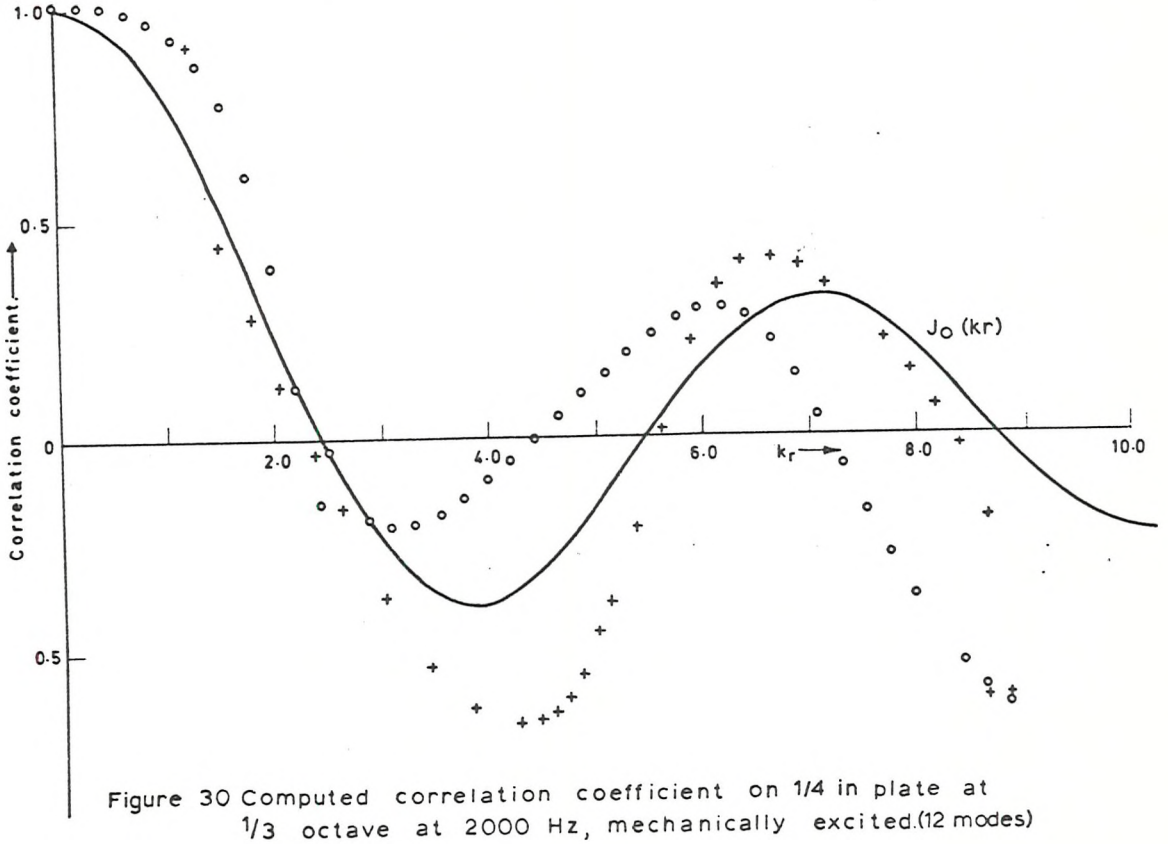

Figure 30 Computed correlation coefficient on 1/4 in plate at 1/3 octave at 2000 Hz, mechanically excited.(12 modes)

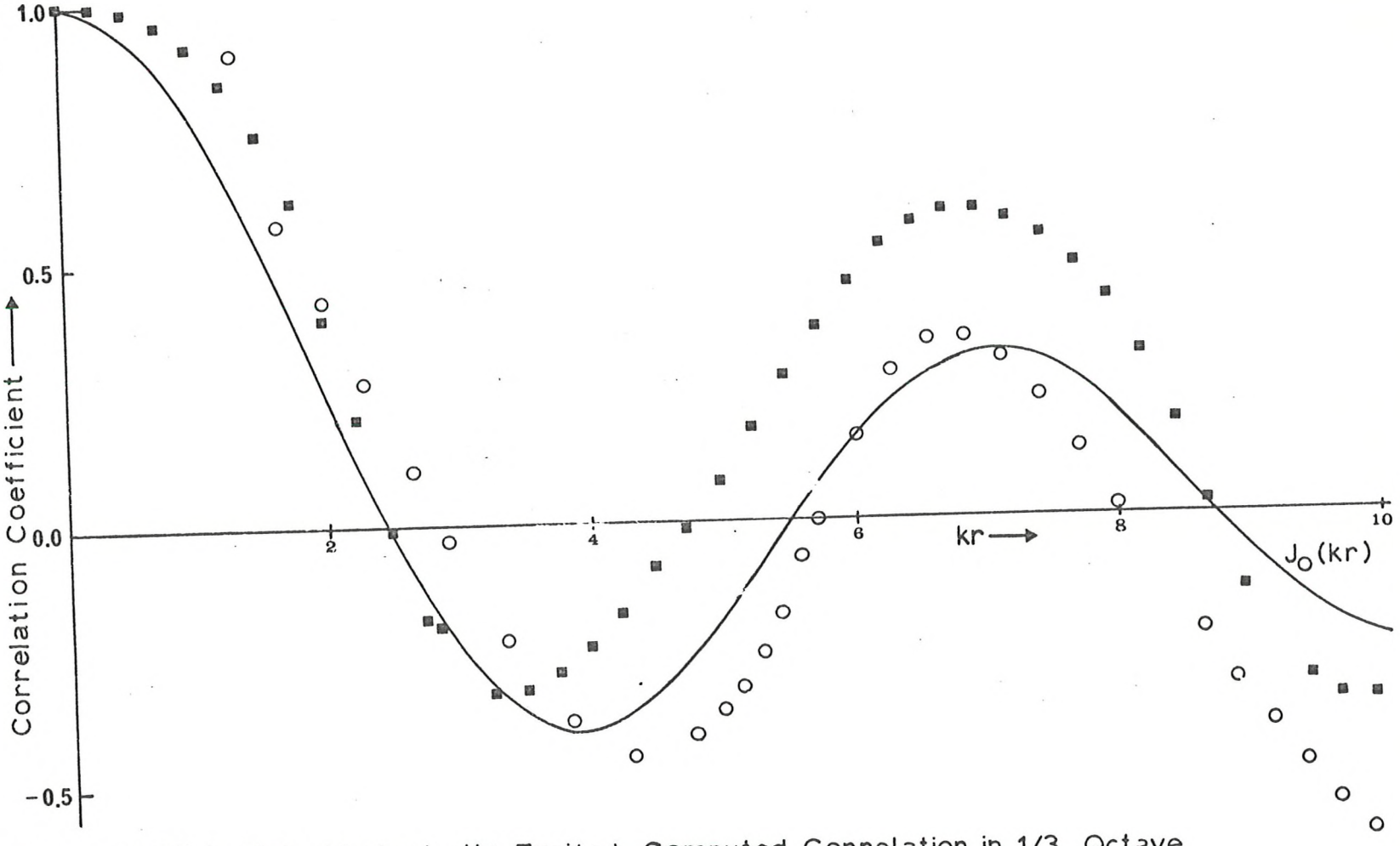

Figure 31 1/4 in Plate Mechanically Excited Computed Correlation in 1/3 Octave at 2500 Hz (20 modes)

independent of the position of the structure. The effect on the correlogram of radiating fields set up by large energy losses (at the boundaries) is discussed further in appendix IV.

4.1.4.2. The Effect of Number of Modes and the Degree of Modal Overlap

In this section we examine the results from the acoustically excited plates and the cylinder.

The signals from the $\frac{1}{4}$ in. plate and the cylinder were analysed in third octave bands. The modal density of a flat plate is independent of frequency and at low frequencies and bandwidths few modes were included in the analysis. Under these conditions the plate did not exhibit a diffuse field, as seen in Figures 12 and 13. The theoretical number of modes in each third octave band is given in Figure 32 as calculated from (27). At higher frequencies, particularly when more than 10 modes were included, the behaviour is more in accordance with that predicted for a diffuse field. See Figures 14 to 17.

The results from the acoustically excited $\frac{1}{8}$ in. plate were analysed on the digital data analysis centre and it was possible to select a greater variety of bandwidths. Thus we are able to see the effect of including very few modes at a high frequency, when the agreement with the derived cross-correlation for many modes in a diffuse field should be bad. From Figures 18 and 19 we may see that, indeed, when there are less than about 10 modes included the field is not diffuse, whether the frequency is 2000 or 4000 Hz.

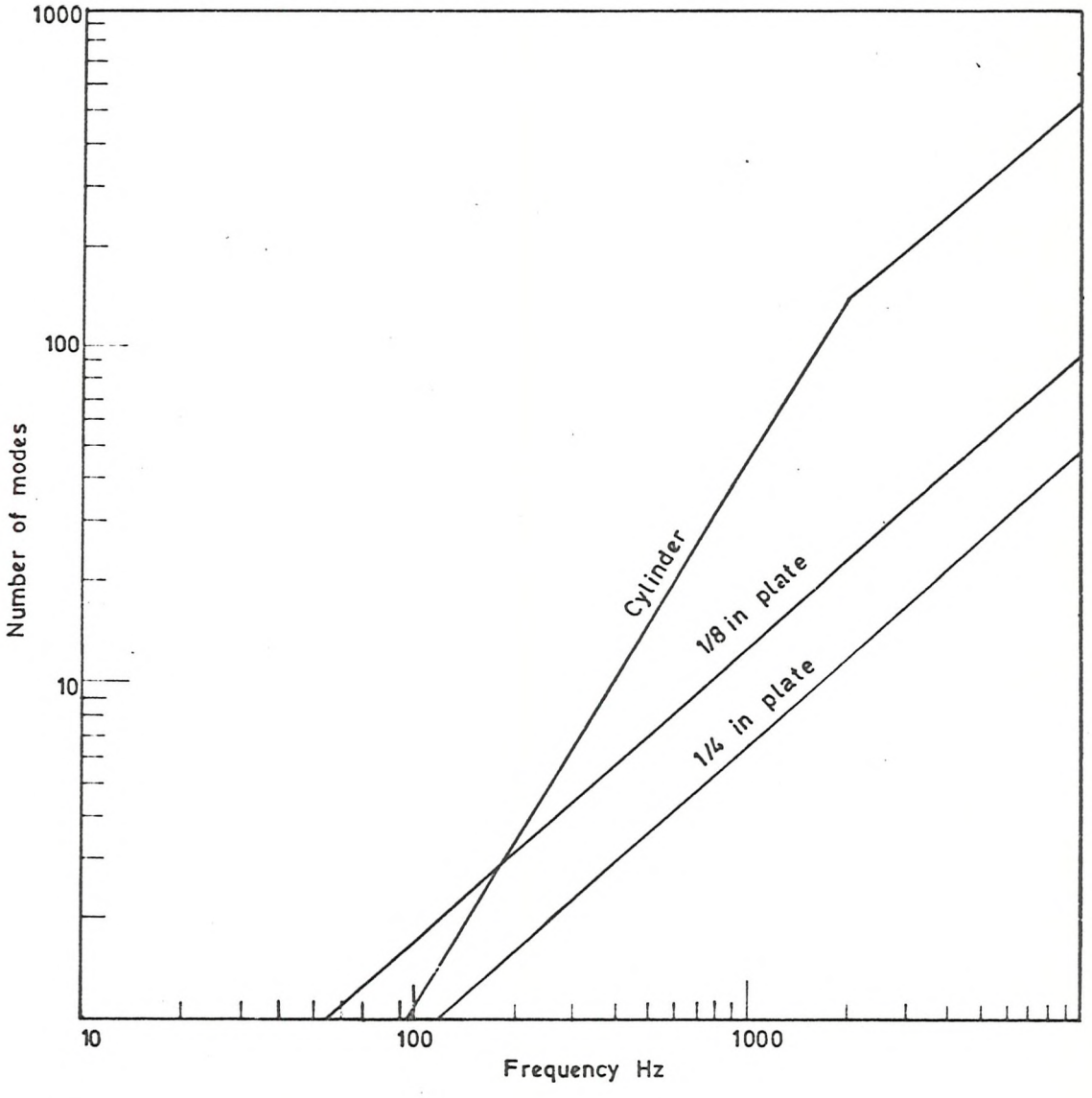

Figure 32 Theoretical number of modes /1/3 Octave Bandwidth for the Steel Plates and the Cylinder.

Now the loss factor, η_{tot} , at 2000 Hz was 0.0063 and at 4000 Hz was 0.010. As the modal density of the $\frac{1}{8}$ in. plate was 0.053 modes/Hz, then the modal overlap factor, the modal density x modal bandwidth is η_{tot} x frequency x 0.053. Thus, at 2000 Hz this factor is 0.67 and at 4000 Hz is 2.12. But, despite this large change in the overlapping of adjacent modes, the agreement with the diffuse field theory correlogram is unaffected for the same number of included modes.

The results for the cylinder, analysed in third octave bands, show a similar trend, agreeing well at high frequence (2500 Hz upwards) as shown in Figure 20. However, the disagreement with the diffuse field cross-correlation becomes marked at 2000 Hz and lower frequencies, as shown on Figure 21. From Figure 32 the total number of modes available was high, over 100 , and by analogy with the behaviour in the plates this should have produced a diffuse field.

Now Manning et al[33] describe the behaviour of a cylinder at various frequencies. Below the ring frequency, bending waves may not propagate in an axial direction down the cylinder. This is shown on the wavenumber diagram for a cylinder, Figure 33, taken from (34). The ring frequency is given by:-

$$f_r = \frac{C_l}{\pi D} \qquad 4.17.$$

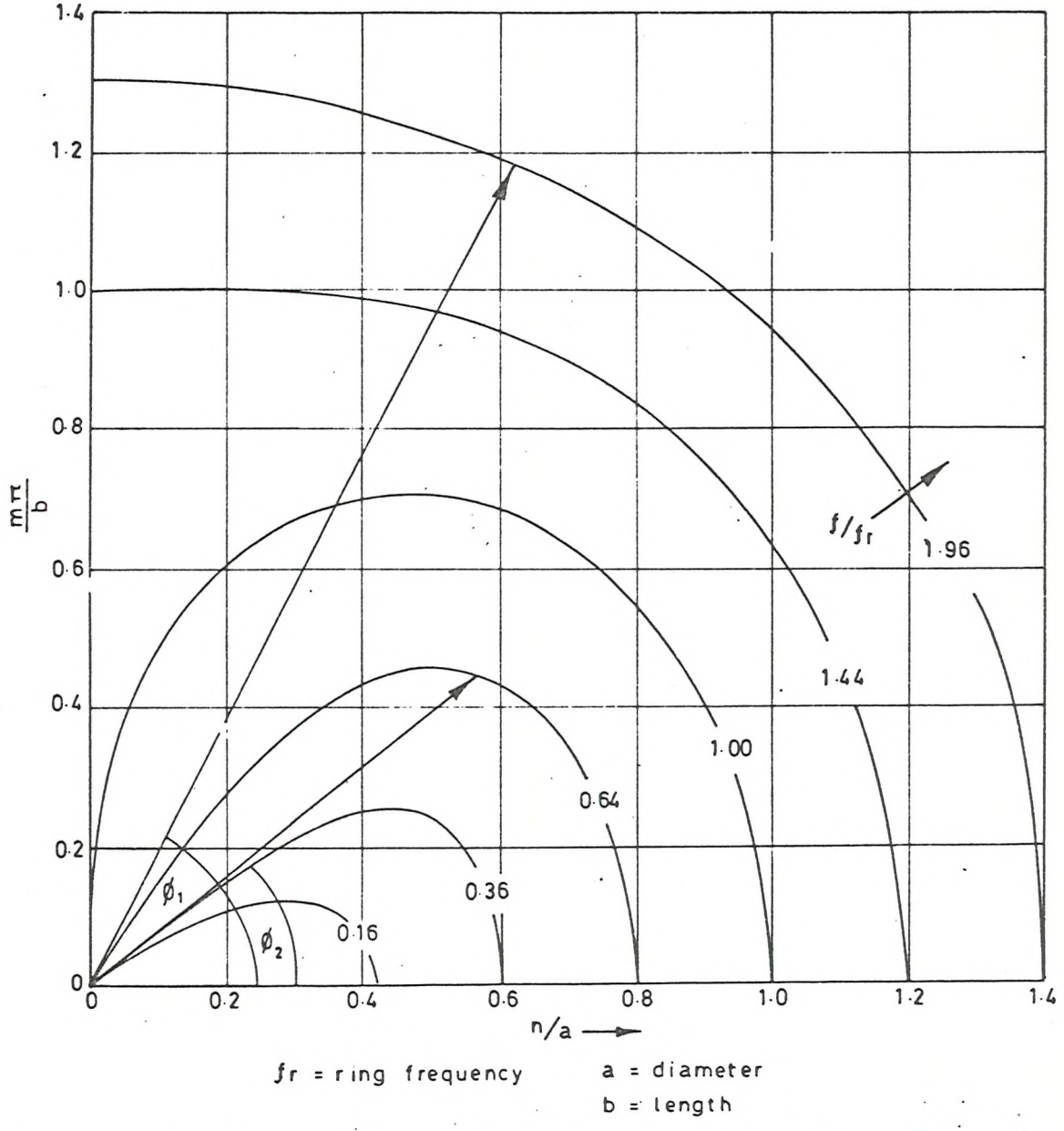

fr = ring frequency a = diameter
b = length

Figure 33 Wave Number Space for a Cylinder (Reference 34)

where D is the diameter of the cylinder and C_1 is the speed of longtitudinal waves. This is the inverse of the time taken for a longitudinal wave to go round the cylinder.

Thus, below the ring frequency, no matter how many modes are included in the analysis, the field is not diffuse, as there are always some directions from which waves may not be incident. This agrees with results obtained, as the ring frequency of this cylinder was 2000 Hz, the dividing point of the results. Above the ring frequency, the cylinder may be treated as a flat plate because bending waves may propagate in every direction.

4.1.4.3. The Effect of Heavy Damping : the Mechanically Excited Plate

Turning to the results for the mechanically excited plate, we see that they do not agree at all well with the theoretical results. This was true for all other frequencies. This suggests that the field was not diffuse.

The $\frac{1}{4}$ in. plate was very highly damped, as shown from the work of Abell[35] in Figure 34. Now the A.S.A. Standards[36] suggest that for good "reverberance" in a room, the level of the directly radiated acoustic field must be 10 db below the level of the reverberant field. Figure 35 shows the results of calculations detailed in appendix V to find the radius from the point of excitation at which, in the $\frac{1}{4}$ in. plate, the radiated component of the bending wave field would have dropped to 10 db and 3 db below the reverberant level. The calculations

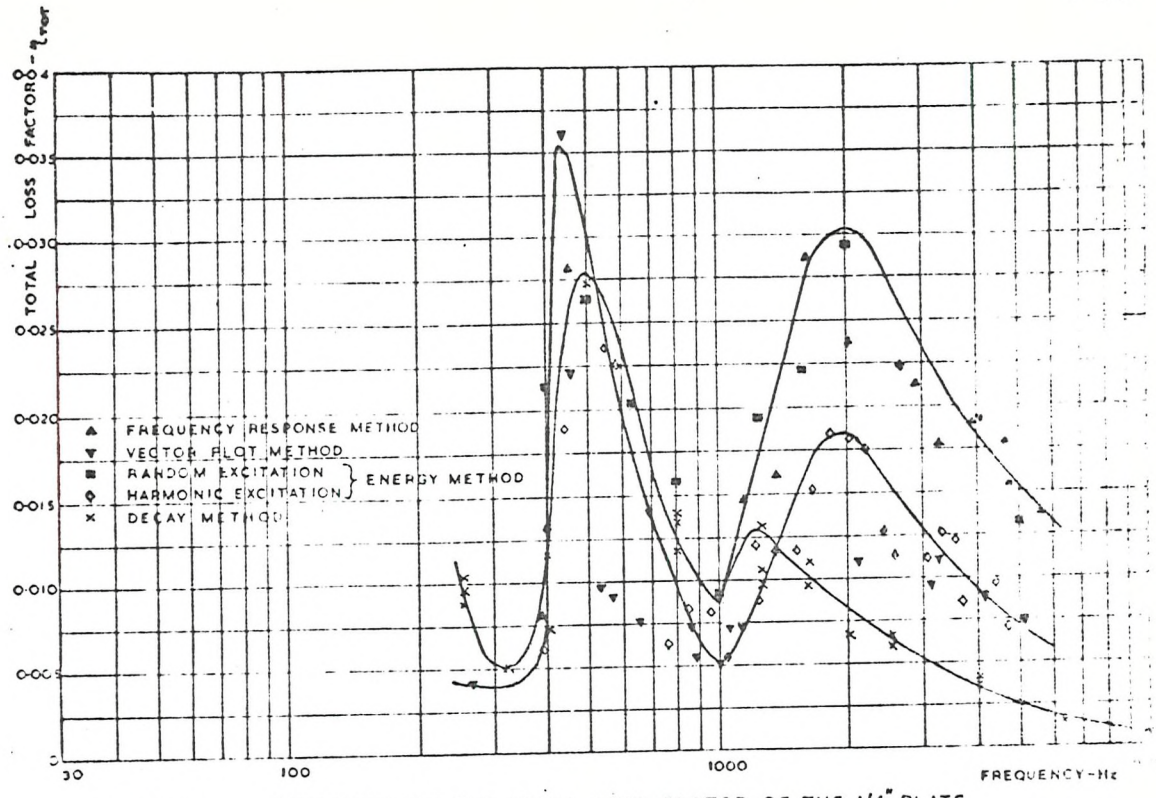

Figure 34 VARIATION OF THE TOTAL LOSS FACTOR OF THE 1/4" PLATE

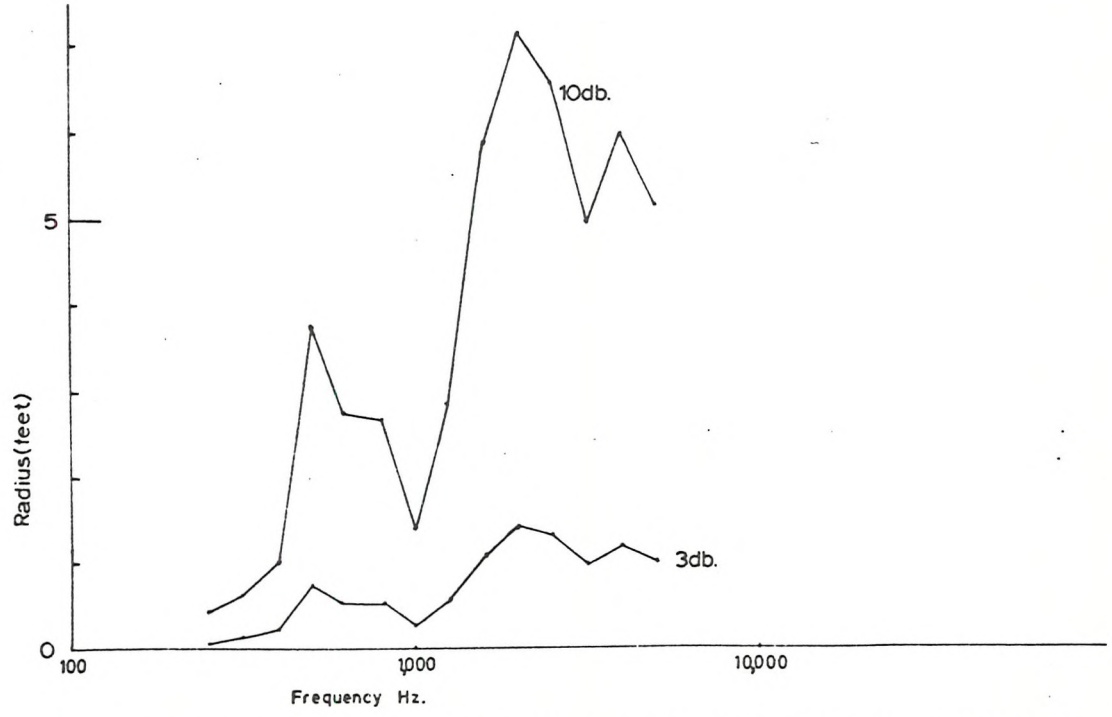

Figure 35 Radius from Shaker on 1/4 in Plate at which Reverberant Field is 10/3db. above Radiated Field.

are similar to those outlined by Morse[26]. The lines along which correlation was measured lay within 1 foot of the shaker position for much of their length. Therefore, if the 10 db level is critical, then the correlation would be affected under all conditions and if the 3 db level is critical, then at any frequency above 1600 Hz the correlation would have been affected. At 1250 Hz only 8 modes would have been included. It would therefore have been unlikely that any evidence of a diffuse field would have been recorded under mechanical excitation at a point at any frequency.

The radiated travelling wave model assumes that all energy is absorbed at the boundary. When damping is heavy, then this is entirely reasonable. It is well established that high dampings are associated with localised parts of the structure, like bolted boundaries. Beany et al[5] have investigated the increase of damping of suspended plates when bolted sections are added. Experiments performed by the author on a diffuser on Windscale Advanced Gas Cooled Reactor reveal that, when the structure was bolted into position, the total loss factor approximately doubled, as shown in Figure 36. As the material loss factors must have stayed the same, the extra damping must be associated with chaffing, pumping and similar phenomena at the bolted joint. Such mechanisms are also described in (37).

This raises the question of why the high damping of the $\frac{1}{4}$ in. plate did not affect the cross-correlation of acceleration measured when

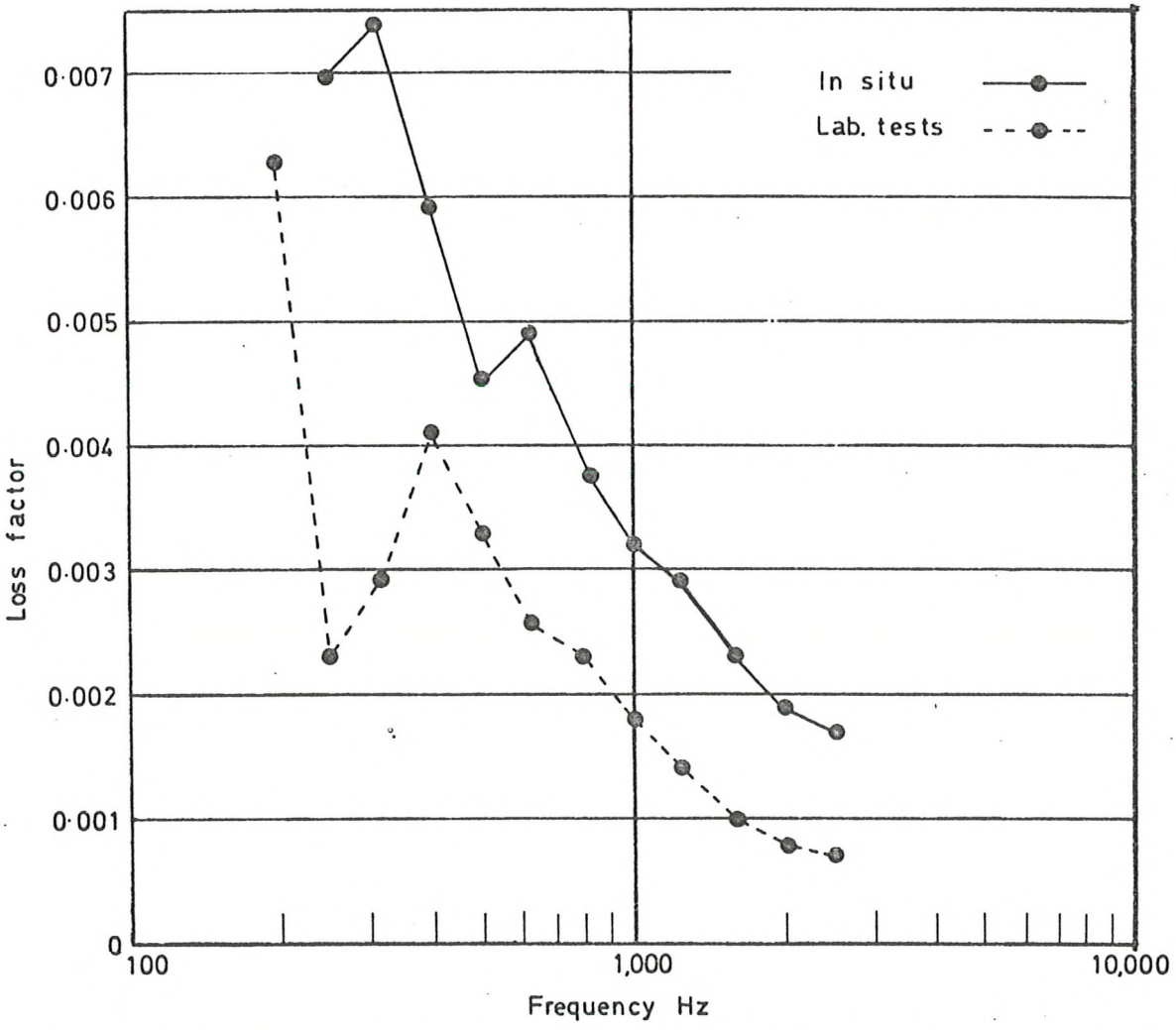

Figure 36. Loss Factor Measured on a Typical Industrial Structure

the plate was excited acoustically. The radiating component of the field would not have been so pronounced, for the excitation was all over the surface. When excited at a point the radiated field will decay with distance from the shaker; when excited all over, at any point on the plate the radiating field will be going in all directions; it will be at a constant level over all the plate, except possibly near the boundaries. Of course, the major part of the response will be governed by travelling waves that are reflected from the boundaries, for the loss factors are not extremely high. From Heckl[16] the transmission loss at a boundary to a plate in a reverberant field is given as

$$\gamma = \frac{13{\cdot}8\ \pi\ [\text{Area}]}{2\ C_B\ [\text{Boundary Length}]} \left[\frac{1}{T}\right] \qquad 4.18.$$

where T = reverberation time of the plate.

At 1000 Hz the loss factor of the $\frac{1}{4}$ in. plate was measured as 0.010. Thus the energy lost at the boundary was 6% of that incident on it. If this loss had been total, like an anechoic room, we might have been able to set up a psuedo-random field simply by exciting the plate at many points. This is currently being done at Southampton University in an anechoic room, to study the effect of altering the "reverberance" as perceived by the listener under controlled conditions. If our plate had been completely anechoic, then we could have set up a

diffuse field in this fashion without exciting any particular number of modes, for as we have discussed in Chapter 3, under very high damping the concept of normal modes breaks down. However, in the plate as tested, the number of modes excited was obviously of major importance and a sufficient number must be excited to produce a diffuse field.

4.1.4.4. The Computed Results

There is little difference between the form of the results obtained from the mechanically and acoustically excited models. There is good agreement with the results derived using the diffuse field model which starts between the limits of 12 modes and 20 modes included. The number of modes was counted during the analysis, not estimated from the theoretical model density. This compares with the agreement obtained in practice in the acoustically excited structures when more than 10 modes were excited, which is encouraging.

However, the programme completely failed to represent the practical situation under mechanical excitation, where the agreement was bad.

As discussed previously, this is a fundamental failing of the normal mode model in the analysis of highly damped structures.

These computer studies show that when enough normal modes are added together, then they behave like a diffuse field. The studies have also shown the shortcomings of the normal mode model, and also shown how expensive in computer time such calculations are. They have also revealed the assumptions that are necessary for the analysis of even

very simple situations when the frequencies are high. Even this simplified form of analysis was curtailed because of the large amount of time that the programmes were using. More accurate analysis at high frequency was not possible. The store size and time requirements would have been beyond those allowable with the available machine.

4.2. The Cross-Correlation of Strain

The correlation of acceleration is limited to narrow frequency bands of analysis. An alternative analysis, the cross-correlation of strains at 90° to each other, may be performed over very wide bandwidths, for this is not a wavelength controlled effect, like the correlation of acceleration. However, the signals are small, and difficult to handle, which makes the procedure less attractive experimentally.

4.2.1. Theoretical Value of Cross-Correlation Coefficient

Consider a bending wave approaching a strain gauge on a line $0 - x$ at an angle θ to $0 - x$.

$$y = A.\exp.i(\omega t + kx.\cos.\theta + kz.\cos.\theta) \qquad 4.19.$$

where y is the lateral displacement of the plate.

k is the bending wave number,

A is some arbitrary amplitude.

Then:

$$\xi_{ox} = -\frac{h}{2}\frac{\partial^2 y}{\partial x^2} = -\frac{h}{2}\,\overline{\overline{A}}k^2\cos^2\theta \qquad 4.20$$

where $\overline{\overline{A}}$ indicates that the two exponential terms, in time and space, have been omitted. This nomenclature is to be used later in the work.

Then the strain along the line 0 - z, at 90° to 0 - x, will be

$$\xi_{oz} = -\frac{h}{2}\frac{\partial^2 y}{\partial x^2} = -\frac{h}{2}\,\overline{\overline{A}}k^2\sin^2\theta \qquad 4.21.$$

and

$$\xi_{ox}.\xi_{oz} = \frac{h^2}{4}\overline{\overline{A}}^2 k^4\sin^2\theta\cos^2\theta \qquad 4.22.$$

Now if we assume that the bending waves arrive from all directions, uncorrelated with each other, and if they are all of the same amplitude,

then we may write:

$$\overline{\xi_{oz}\ \xi_{ox}} = \frac{k^4 h^2 A^2}{8\pi} \int_0^{2\pi} \sin^2\theta . \cos^2\theta . d\theta$$

$$= \frac{k^4 h^2 A^2}{32\pi} \qquad 4.23.$$

where the bar indicates a time average.

The mean square strain in the directions O - x and O - z will be equal in a diffuse field and given by:-

$$\overline{\xi_{ox}^2} = \overline{\xi_{oz}^2} = \frac{k^4 h^2 A^2}{8\pi} \int_0^{2\pi} \sin^4\theta . d\theta$$

$$= \frac{k^4 h^2 A^2}{32\pi}\left(3\right) \qquad 4.24.$$

Then the normalised cross-correlation coefficient is given by:-

$$\frac{\overline{\xi_{ox} \cdot \xi_{oz}}}{\sqrt{\overline{\xi_{ox}^2} \cdot \overline{\xi_{oz}^2}}} = \frac{1}{\sqrt{9}} = 0{\cdot}33 \qquad 4.25.$$

4.2.2. Experimental Procedure

The results from two structures are presented, a $\frac{1}{4}$ inch plate and a cylinder, as described in Section 4.1.2. of this Chapter.

Both structures were excited acoustically, as before. The outputs from the strain gauges were both amplified 80 dB. by a three channel strain gauge amplifier. Phase matching between the channels was tested and found to be good up to frequencies of 20,000 Hz. (See also Appendix VI.) The signals were recorded, as before, on a high quality frequency modulated tape recorder. In order to get the largest possible signals to process, semi-conductor gauges were used to measure the strain. These gauges have a gauge factor 50 times that of conventional wire strain gauges. (In Appendix X an experiment is described in which they were tested against a wire gauge to ensure that they were not sensitive to acceleration, as had been suggested. They were found satisfactory in every way, if somewhat fragile.)

The signals from the strain gauges on the cylinder were processed on an analogue correlator. On playback, they were filtered through a pair of third octave filters known to have good phase match, as before (4.1.2.). The signals from the flat plate were analysed on the digital data processor, using a digital filtering routine. Apart from the better accuracy expected, using this system, various bandwidths and centre frequencies could be chosen so that the effect of the number of modes could be seen. The results for the plate are shown on Figure 37 and on Figure 38 for the cylinder.

The positions at which strains were measured were not close to any boundaries, but were otherwise chosen at random.

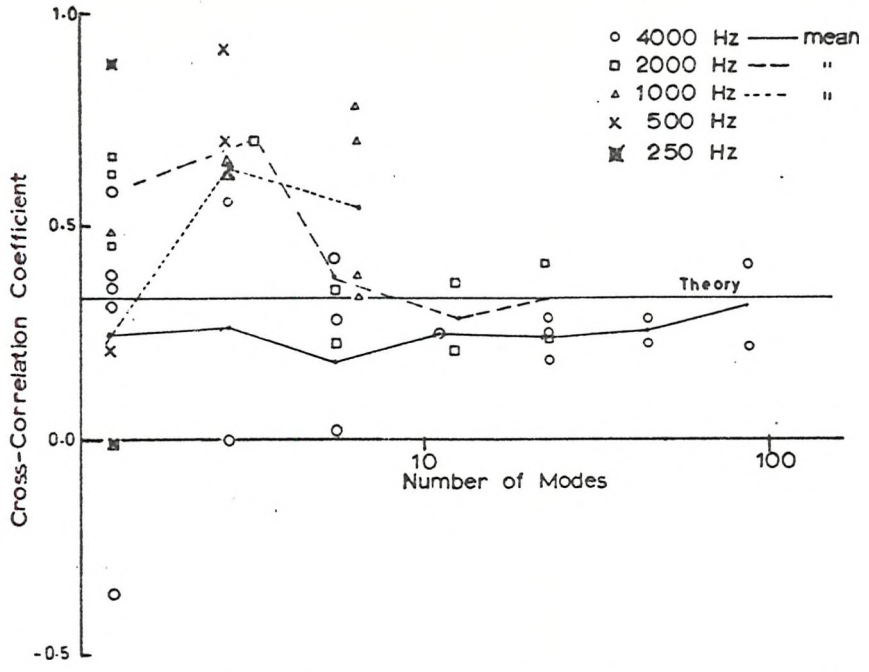

Figure 37 Cross-Correlation of Strain on Acoustically Excited 1/8 in Plate

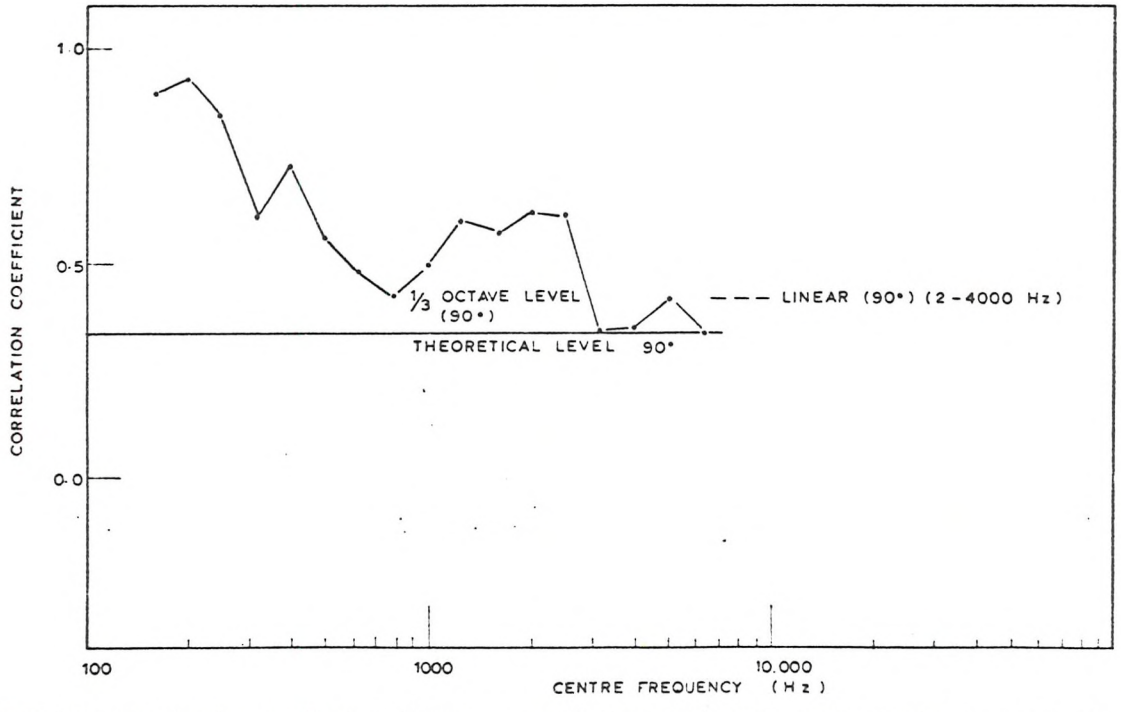

Figure 38 Acoustically excited cylinder - correlation between two strain gauges at 90° remote from boundaries.

4.2.3. Discussion of Results on Strain Correlation

The results for the plate are plotted directly in terms of the theoretical number of modes included in the band of analysis. The agreement is good provided at least ten modes are included. Below this number of modes, the scatter on the results is very great and one would deduce that the field was not diffuse.

We notice that the results for low bandwidths, whether or not at a high frequency, depart widely from the diffuse field value. However, results for high bandwidths, and therefore large numbers of included modes, lie close to the predicted value. This again shows that the number of simultaneously excited modes is the major parameter on which to judge whether or not a structure will have a diffuse bending field.

The changes in damping and in the amount that modes overlap each other in frequency which occur between high and low frequencies are less important.

The results from the cylinder suggest that at frequencies higher than 3150 Hz the bending wave field was diffuse. At lower frequencies the results fluctuate, suggesting that the field is not diffuse. At 2000 Hz, the ring frequency, some departure from the expected value might be expected, for as we have already discussed, there will be some directions along which bending waves may not propagate. However, it is surprising to record a departure from the expected value at 2500 Hz.

4.3. Conclusions

4.3.1. Conditions for Diffuse Bending Wave Field

Both sets of tests reveal that at least 10 modes must be excited in order to set up a diffuse bending wave field. In addition, a diffuse field in a cylinder can only be set up at frequencies above the ring frequency, when bending waves may propagate in all directions.

Small changes in damping, affecting the degree of modal overlap, do not seem to be important. Although the amount of modal overlapping is a function of frequency and will have changed over the frequency ranges considered in the tests, no effect was noticed.

Large values of damping can upset the diffuse field behaviour under conditions of point excitation, as we have seen.
This is exactly paralleled by the behaviour of sound in partly absorbing rooms where, unless the damping is small, the reverberant field will be swamped by the radiating field.

4.3.2. Comparison of the Two Tests

The accelerometer test was easier to perform than the strain gauge test and was susceptible to interpretation. The accelerometer signals were much bigger than those from the strain gauges, which is important. The tests involve considerable signal handling, during which phase information must be preserved carefully and electronic noise kept as low as possible in order to get reliable correlations.

The accelerometer test also offers important advantages in the interpretation of the results. It offers us two curves for comparison, theory and experiment; the strain gauge test offers us only two points, theory and experiment. Examining the accelerometer results, it is possible to examine the first zero crossing, the value and location of the first minimum and the smoothness of the curve in an objective way to decide whether or not a field is diffuse. The strain gauge's single result is much less easy to interpret. Only if its value is close to the theoretical value for a diffuse field can we interpret the result.

The only situation in which this strain gauge test is likely to be of more use than the accelerometer test is when access to the structure is very limited, when the analysis time available is limited, or when information is required over a very large bandwidth. In all other cases, the accelerometer test is more useful.

4.3.3. Sensitivity of the Tests to Diffuseness of Field

These tests both suggested than ten modes are necessary to ensure a diffuse field. We must try and establish if this is necessary or sufficient for other parts of the analysis. For example, when considering the stress at a boundary we might find that this criterion is too severe, or perhaps not severe enough. This must be borne in mind in subsequent parts of the work.

Chapter 5

The Ratio of Mean Square Stress and Strain to Velocity

The statistical energy method of vibration analysis, mentioned in Chapter 1, leads to an estimate of the level of mean square velocity, or kinetic energy, of the structure. Before we can use this information to predict the service life of a particular component we must convert this to a level of mean square stress. We can then compare this with levels of stress currently considered acceptable, to decide if the component will fail.

Yeh et al[5] have derived a value for the ratio of mean square stress to velocity for a rectangular plate, pinned at its edges, under pure tone excitation. However, using the model of bending waves, in a reverberant field, we can derive a more general result. Having shown the conditions necessary for the model to be reasonable, we may now proceed to the analysis.

5.1. Theoretical Analysis based on the Diffuse Field Model

Let us assume that a straight crested wave with a harmonic time dependance (see Chapter 2, Section 2.2.) approaches a point O on a plate at θ degrees to the line O - x, then the stress along O - x is given by:-

$$\sigma_{ox} = \frac{h}{2} \frac{E}{[1 - \upsilon^2]} \left[\frac{\partial^2 y}{\partial x^2} + \upsilon \frac{\partial^2 y}{\partial z^2} \right] \qquad 5.1.$$

where h = plate thickness

E = Young's modulus,

ν = Poisson's ratio,

y = lateral displacement $= Ae^{i(\omega t - kx\cos\theta - kx\sin\theta)}$

k = wavenumber,

ω = angular frequency.

$$\text{velocity} = V_\theta \qquad 5.2.$$

Then $$\sigma_{ox} = -\frac{Eh}{2(1-\nu^2)}\frac{k^2}{i\omega}(\cos^2\theta + \upsilon\sin^2\theta)V_\theta \qquad 5.3.$$

and the mean square stress is:-

$$\overline{\sigma_{ox}^2} = \frac{E^2h^2k^4}{4(1-\upsilon^2)\omega^2}\left(\cos^2\theta + \nu\sin^2\theta\right)\overline{V}^2 \qquad 5.4.$$

For bending waves in plates of density ρ :-

$$\frac{\omega^2}{k^4} = \frac{E h^2}{12\rho[1-\upsilon^2]} \qquad C_l^2 = \frac{E}{\rho}$$

where C_l is the velocity of longitudinal waves in the material.

If the bending wave field is diffuse, i.e., the value of is independent of θ , with the waves statistically independent of each other, then the stress will be the same at every point, in every direction and will be given by:-

$$\langle\overline{\sigma^2}\rangle = \frac{3C_l^2\rho}{(1-\upsilon^2)}\langle\overline{V^2}\rangle\int_0^{2\pi}\left(\cos^2\theta + \upsilon\sin^2\theta\right)^2\frac{d\theta}{2\pi} \qquad 5.6.$$

The pointed brackets thus:- $\langle \quad \rangle$ indicate a spatial average, the bar, $\overline{\quad}$, a time average. For most engineering materials, mild steel, light allow, etc., $\nu = 0.3$. and the ratio is then given as:-

$$\frac{\langle \overline{\sigma^2} \rangle}{\langle \overline{V^2} \rangle} = 1 \cdot 61 \, C_1^2 \rho^2 \qquad 5.7.$$

We cannot measure stress directly, we can only measure strain. Therefore we need to derive a value for the ratio of strain to mean square velocity, so that we may verify our analysis experimentally. For if this derivation proves successful, then it will be reasonable to assume that the derivation for stress will be at least as successful.

Again, we consider that a straight crested wave approaches O at an angle θ to O - x. Then the strain ξ_{ox} along O - x is:-

$$\xi_{ox} = \frac{h}{2} \frac{\partial^2 y}{\partial x^2} = - \frac{h \bar{\bar{A}}^2}{2i\omega} k^2 \cos^2 \theta \qquad 5.8.$$

Proceeding as before we obtain the relationship:-

$$\frac{\langle \bar{\xi}^2 \rangle}{\langle \bar{V}^2 \rangle} = \frac{1}{C_1^2} \qquad 5.9.$$

for a diffuse bending wave field.

These results agree with those obtained by Yeh et al[5] mentioned earlier. As we have assumed the same deflected shape in both analyses, a sinusoid, we would expect the ratios of strain energy and kinetic energy to be the same at any given frequency. This is the basis of Rayleigh's method of finding natural frequencies of beams and plates[38].

5.2. Experimental Tests

The relationship between mean square strain and velocity was investigated experimentally. Measurements of strain and acceleration were made on two different structures, both excited acoustically by the sound of air escaping from a gate valve. One structure was the cylinder, described before; the other structure was a change of section specimen, as used in the experiments to be described in Chapter 7. It was made of two aluminium plates, 4 ft. by 3 ft., slotted together along their shorter edges, (one $\frac{1}{4}$ in. thick, one $\frac{1}{8}$ in. thick).

The strain was measured using semi-conductor strain gauges. The strain gauge and accelerometer outputs were analysed in third octave bands and recorded on a paper chart level recorder. The value of the velocity was deduced by dividing the acceleration by the angular frequency corresponding to the filter centre bandwidth. This is accurate to within 10%. The results are presented on Figure 39.

The results for the cylinder were produced by Mr Fahy, of Southampton University, and are presented by his kind permission.

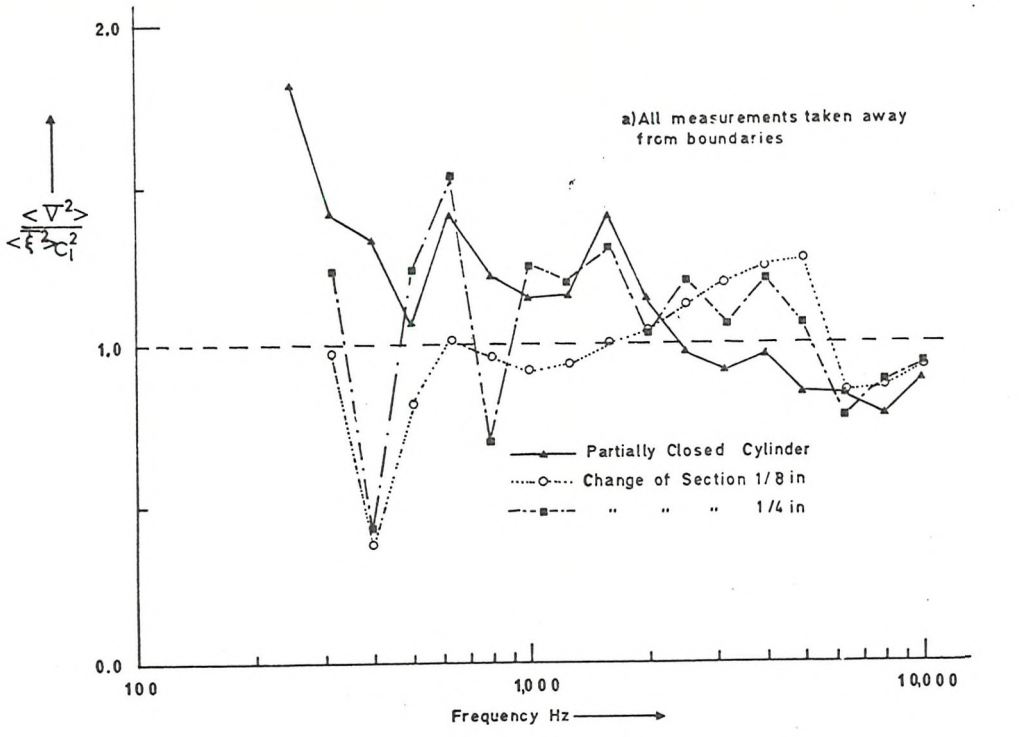

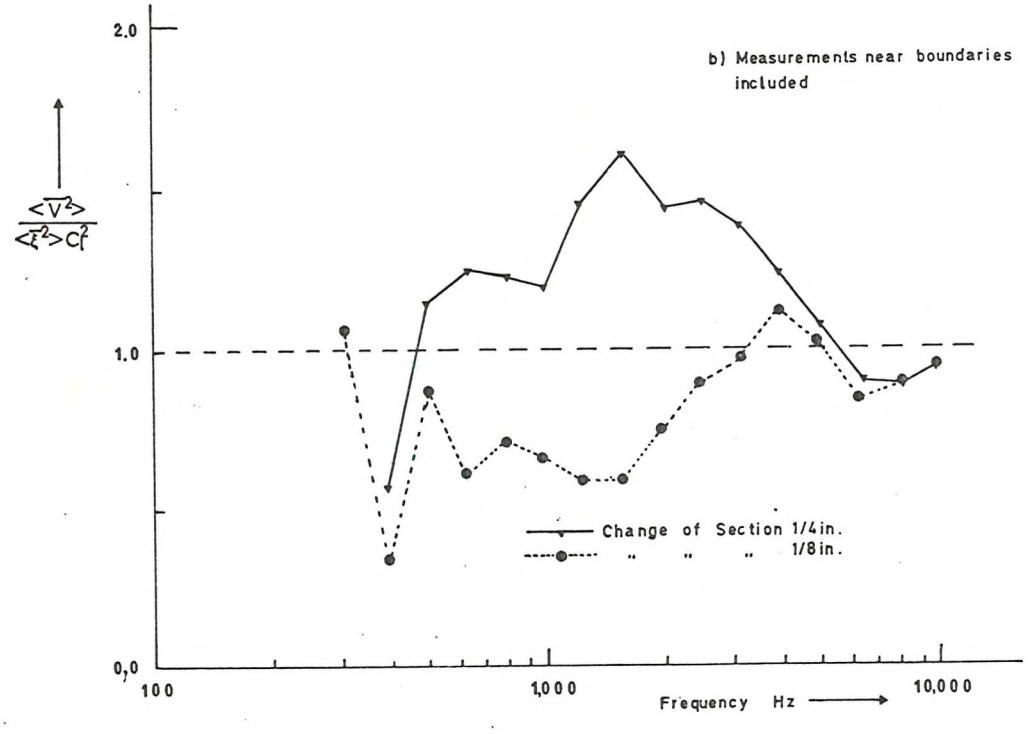

Figure 39 Ratio of Mean Square Velocity to Mean Square Strain

Four sets of results are presented for the change of section specimen; two are for the thick section of the specimen and two are for the thin section.

As we have discussed in Section 7, the deflected shape near the boundary would not be sinusoidal in space and this could upset the results. To try and judge the seriousness of this effect, for each section of the specimen, one result is presented for strain gauges and accelerometer positions chosen to be remote from the boundary, and another result is presented which includes the strain and acceleration measured near the boundary.

5.3. Comments on the Results

Turning to the results shown on Figure 39a, we see that the agreement with theory is generally good. At low frequencies, and therefore low numbers of modes, the measured ratio does vary somewhat above and below the theoretical value. This reflects on the difficulty of getting good samples of strain and acceleration when only a few modes are available. This situation gives rise to large variations of strain and acceleration about the spatial mean, as discussed later in Chapter 8. At higher frequencies the results steady up.

It seems that otherwise the measured ratio does not depend on the number of modes available. This is what we would expect, for provided the deflected shape of the structure is sinusoidal in space, the theoretical results should still hold, regardless of the number of available modes. Thus, for this result, the criterion established in

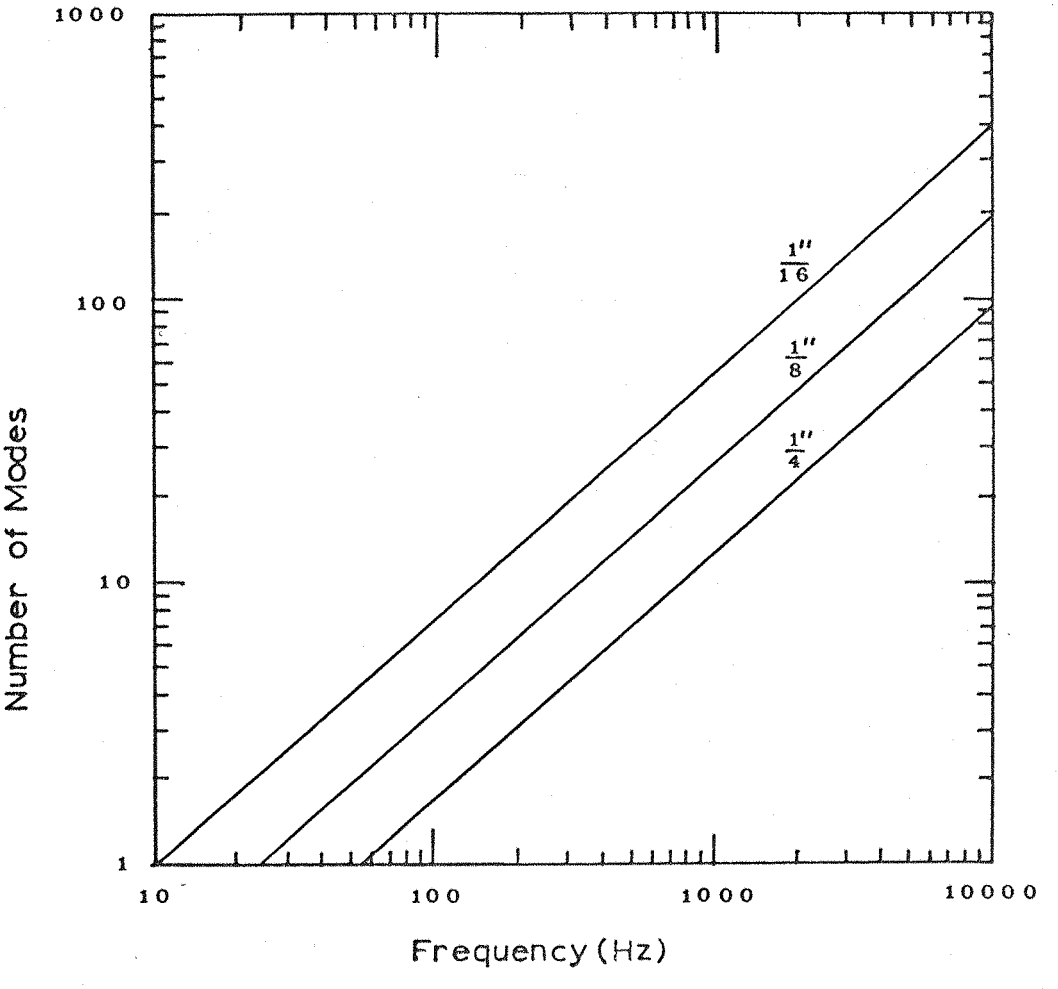

Figure 40. Modes per Third Octave Bandwidth. for the Change of Section Specimens

Chapter 4 is too severe.

The results for the cylinder show no dependence on the ring frequency, 2000 Hz. This is to be expected for the directions in which the bending waves can travel is not important here. Provided that the deflected shape is sinusoidal in space the result should still apply. Again, the criterion established in Chapter 4 is too severe.

Turning to Figure 39b, we see that the effect of the boundaries is not particularly marked. However, the ratio of velocity to strain rises for the thin section and falls for the thick section. This is in general agreement with the findings of Chapter 7, where the stresses and strain induced by a change of section are discussed in detail.

5.4. Conclusions

The diffuse field model leads to the same relationship of stress and strain to velocity as does the single mode model. This is borne out by the experimental findings. We may use the theoretical result with no particular regard to the requirements of Chapter 4, that at least 10 modes are available, and, with cylinders, only frequencies above the ring frequencies are considered.

Near the boundaries the strain must be predicted by other means.

Chapter 6

Stress and Strain Concentration at a Weld

It is necessary to be quite clear about the problem that we are to consider in this Chapter and the next.

In the first three Chapters we have considered the problems set by the complex structures of a nuclear reactor gas circuit vibrating in bending, and we have investigated some of the analytical models that we might use to solve them. We concluded that when investigating the stress and strain distribution in a localised region we should use the model of bending waves, travelling in a diffuse field. In Chapter 4, we examined various structures to see when this model was reasonable.

In Chapter 5 we have derived a value for mean square stress using this model, in terms of the mean square velocity of the structure. In Chapters 6 and 7 we will use this same model to estimate the variations from this mean value that will be induced by a discontinuity, or boundary to a particular structure.

The incidence of a bending wave on a discontinuity sets up a reflected wave which radiates energy to the far distance. Some energy may be transmitted beyond the discontinuity to the far distance. So far, this is analogous to the behaviour of light reaching the interface between a glass block and the air. But, as has been discussed

already in Chapter 2, there are four boundary conditions to match, not just two. Thus, two additional near fields are set up, which do not transmit energy to the far distance, one a reflected field and one a transmitted field. The combination of these waves, in phases determined by the impedance of the discontinuity, will govern the stresses and strains at the boundary.

In the following analysis we will assume that plane sections remain plane. Timoshenko et al[39] and Savin[40], among others, discuss the statis bending and tension of specimens of complex shape, in which initially plane sections are allowed to become non-plane. They have considered shafts of varying cross-section in bending and the stress generated round holes in a plate under tension. These effects are extremely localised, affecting the region immediately adjacent to the discontinuity.

In this analysis we confine our attention to the macroscopic changes of stress due to the interference of bending waves near the discontinuity in question, assuming that initially plane sections remain plane. A more detailed investigation is not yet possible.

It might, of course, be reasonable to use the stress concentration factors derived, for example, by Timoshenko, in addition to the factors to be derived in this section. The frequencies are low compared with the frequencies at which Rayleigh surface waves are important and away from boundaries plane sections do remain plane. However, such a discussion is beyond the scope of this present work

and is not considered further.

In the next two Chapters we consider the stress normal to a butt weld and to a sharp change of section in a plate. Both situations are met with fairly often in practice. Appendix VIII considers the stress at a rigid boundary.

The approach is as follows. First we will study the solution of the bending wave equation at a weld; then we will investigate the stress generated by a weld by a bending wave from a single direction. Then we will assume that bending waves arrive from all directions and derive a value of total stress. Finally, the derived results are tested experimentally.

6.1. The Behaviour of a Bending Wave Incident on a Butt Weld

The analysis in this section, of solutions to the bending wave equation at a rib, was first performed by Cremer[10] for a rectangular rib. It is detailed here to introduce the more complete work in Chapter 7 and also because we use the results toderive the stress.

Let the two semi-infinite plates, of identical thickness and the same material lie in the plane $x - z$, as shown in Figure 41. The weld of the same material lies along the line $x = 0$ and is assumed to have an elliptical cross-section.

We will use the following boundary conditions.

If we assume that the wavelength is large compared to the width of the weld, which is reasonable at the frequencies which are of most interest to us, then we may assume that the lateral displacement

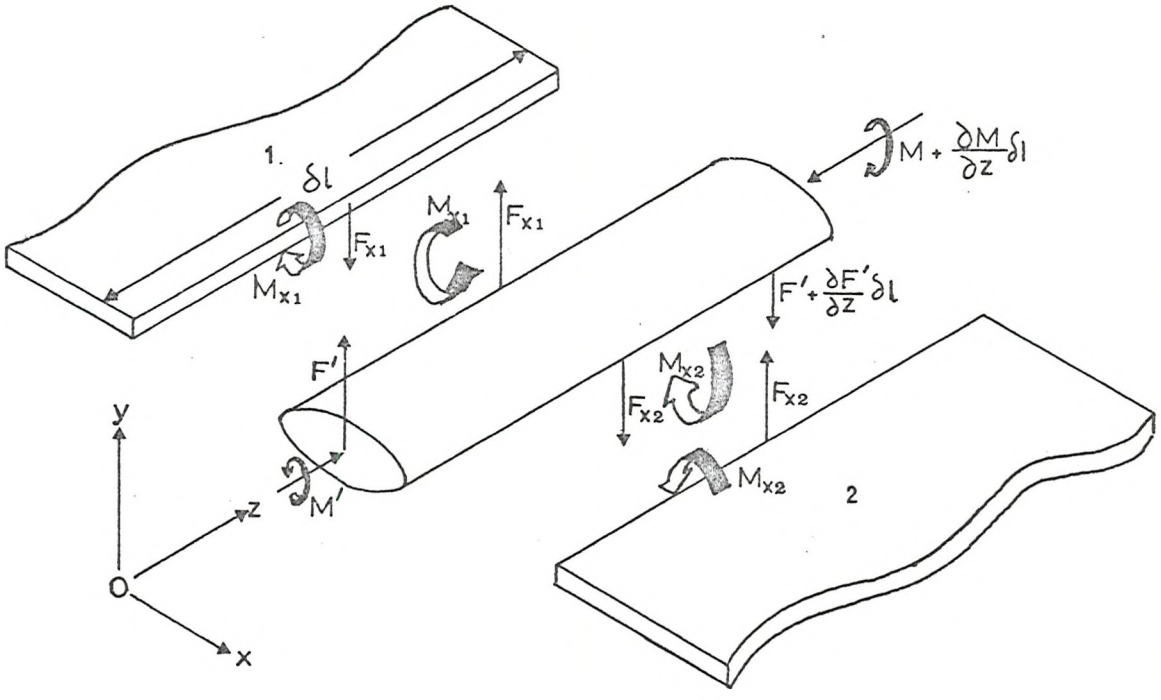

Figure 41 Forces on Weld.

and velocity of the plates are the same each side of the weld.

Further, if the weld cross-section remains undistorted, then the angular velocity will be the same each side of the weld.

For the next boundary condition we may consider the equilibrium of the bending moments each side of the weld, the torsional moment set up within the weld by the amount it twists along the line $x = 0$ and the rotary inertia of the weld.

Finally, we consider the equilibrium of the shear forces in the plate each side of the weld, the shear stresses in the weld and the d'Alembert forces due to its vertical acceleration.

6.1.1. Wave Velocities

Let us consider the velocity of the waves incident on and travelling from the weld as a first step to deriving these four boundary conditions.

Let the incident wave arrive from an angle θ to $z = 0$. We may assign to it the arbitrary amplitude of unity.

$$V_{i+} = \exp.\left[j\omega t - jkx.\cos.\theta + jkz.\sin.\theta\right] \qquad 6.1.$$

Now the trace wavelength of the incident and departing waves must be the same; their tangential wavelength must be equal, as shown in Figure 42. If not, then the relationship between the waves would be a function of their position along the Z axis; yet we are deriving this relationship at an arbitrary value of z. Thus, this relationship

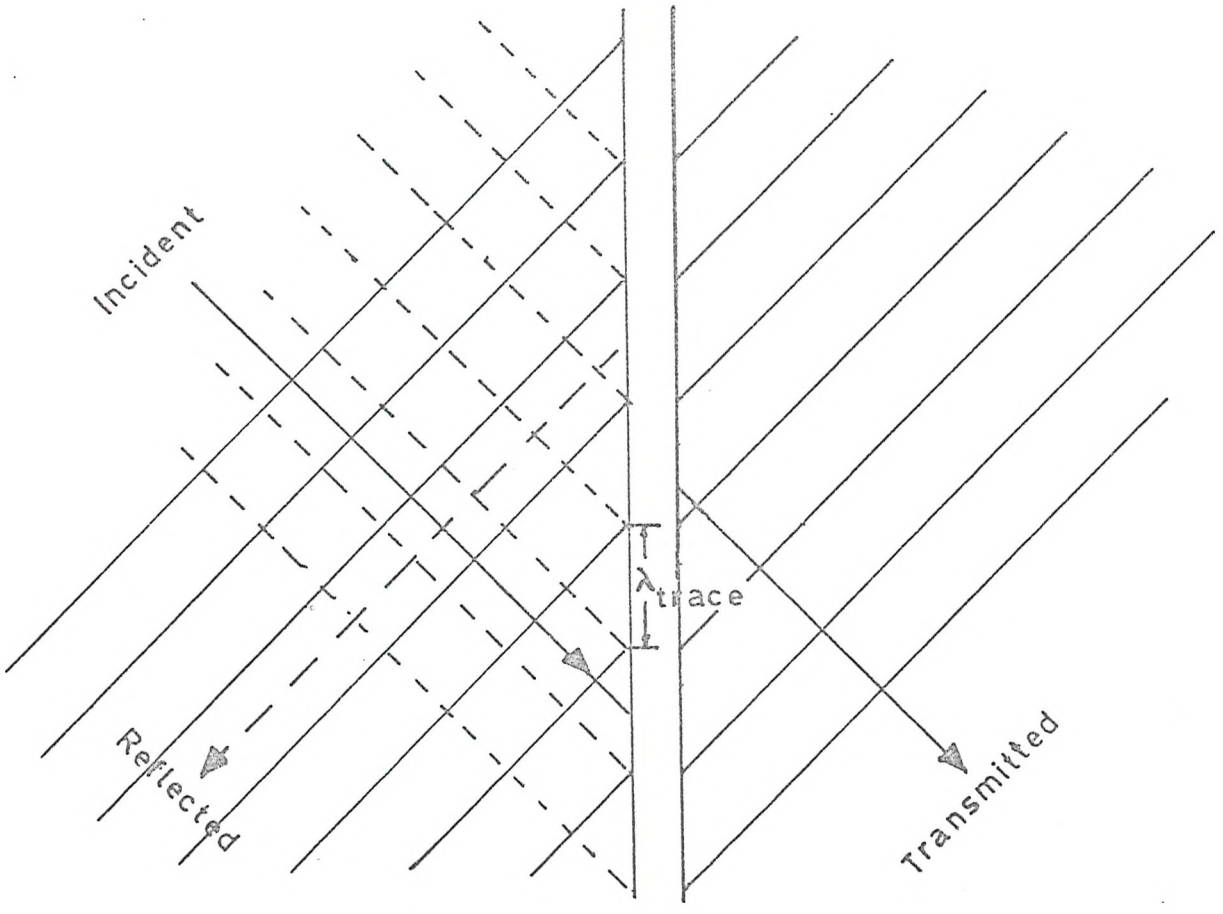

Figure 42 Trace Wavelength at Weld.

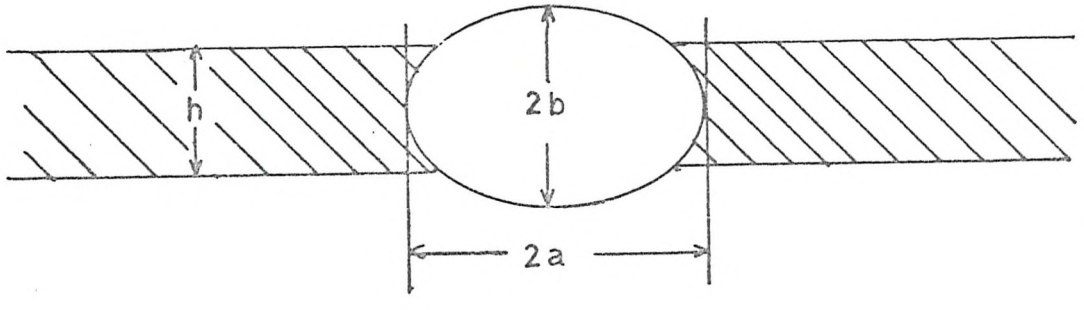

Figure 43 Dimensions of Cross Section of Weld.

must be the same at any value of z in an infinite plate.

Now to find the travelling wave we solve the equation

$$\nabla^2 V + k^2 V = 0 \quad \text{from Section [2.3]}$$

This is

$$\frac{\partial^2 V}{\partial z^2} + \frac{\partial^2 V}{\partial x^2} + k^2 V = 0$$

from which

$$\frac{\partial^2 V}{\partial x^2} + \left[-k^2 . \sin^2 \theta . + k^2 \right] = 0$$

and thus

$$\frac{\partial^2 V}{\partial x^2} + k^2 V . \cos^2 \theta = 0 \qquad 6.2.$$

Then the velocity of the reflected wave is

$$V_{-1} = R . \exp . i \left[\omega t + kx . \cos . \theta + kz . \sin . \theta \right] \qquad 6.3.$$

and the transmitted wave is

$$V_{+2} = D . \exp . i \left[\omega t - kx . \cos . \theta + kz . \sin . \theta \right] \qquad 6.4.$$

where R and D are the complex amplitudes of the reflected and travelling waves that we shall find by equating the boundary conditions.

To find the decaying near fields we consider the equation

$\nabla^2 V - k^2 V = 0$ from Section

Now the near field is steady only in the X direction. The variation in the Z direction is still given by $\exp\left[i(\omega t - kz.\sin.\theta)\right]$

and thus we have:-

$$\frac{\partial^2 V}{\partial x^2} - \left[1 + \sin^2\theta\right]k^2 V = 0 \qquad 6.5.$$

The reflected near field velocity is therefore

$$V_{-1} = R'\exp.\left[i\left[\omega t + kz.\sin.\theta\right] + kx.\sqrt{1+\sin^2\theta}\right] \qquad 6.6.$$

and the transmitted near field is:-

$$V_{+2} = D'\exp.\left[i\left[\omega t + kz.\sin.\theta\right] - kx\sqrt{1+\sin^2\theta}\right] \qquad 6.7.$$

R' and D' are complex amplitudes that we will find by equating boundary conditions.

6.1.2. The Boundary Conditions

From the four sets of boundary conditions we obtain four simultaneous equations.

Equality of Velocities

$$1 + R + R' = D + D' \qquad 6.8.$$

Equality of Angular Velocity

The angular velocity is given by $\frac{\partial V}{\partial x}$

Then at x = 0

$$-i.\cos.\theta + iR.\cos.\theta. + R'\sqrt{1+\sin^2\theta} = -i.\cos.\theta.D - \sqrt{1+\sin^2\theta}.\,D' \qquad 6.9.$$

Let $$\frac{\cos.\theta}{\sqrt{1+\sin^2\theta}} = \alpha$$

Then $$i\alpha = i\alpha R + R' + i\alpha D + D' \qquad 6.10.$$

Equilibrium of Bending Moments

At x = 0, from Figure (41)

$$M_{X_1}\delta l - M_{X_2}\delta l - \frac{\partial M'}{\partial z}\delta l = i\omega\theta W_z \delta l \qquad 6.11.$$

where M_{X_1}, M_{X_2} = bending moments about x = 0 in plate 1 and 2

M' = twisting moment along the weld

θ = inertia of the weld per unit length

W_z = angular velocity of weld.

Now the twisting moment in the weld is:-

$$M' = \frac{-T}{i\omega}\frac{\partial W_z}{\partial z} \qquad 6.12.$$

where T is the torsional rigidity of the weld

Then $$\frac{\partial M'}{\partial z} = \frac{-T}{i\omega}\frac{\partial^2 W_z}{\partial z^2} \qquad 6.13.$$

The bending moment in the plates is given by

$$M_x = B'\left[\frac{\partial^2 y}{\partial x^2} + \upsilon\frac{\partial^2 y}{\partial z^2}\right] \qquad 6.14.$$

where B' = bending stiffness/unit width.

Now since the displacement each side of the weld is the same, we may write that

$$M_{x_1}\delta l - M_{x_2}\delta l = B'\left[\left[\frac{\partial^2 y}{\partial x^2}\right]_1 - \left[\frac{\partial^2 y}{\partial x^2}\right]_2\right]\delta l. \qquad 6.15.$$

and need take no account of the variation of displacement with Z

Using the relationship:

$$\frac{\partial^2 W_z}{\partial z^2} = \left(k.\sin.\theta\right)^2 W_z \qquad 6.16.$$

the equation 6.11 may be written:-

$$\frac{i\,Bk^2}{\omega}\left[-\cos^2\theta. - R.\cos^2\theta. + \left(1+\sin^2\theta.\right)R + \cos^2\theta.\,D - \left(1+\sin^2\theta.\right)D'\right]$$

$$= i\left[\omega\theta - \frac{T(k\sin.\theta.)}{\omega}\right]^2\left[ik.\cos.\theta.D + D'\sqrt{1+\sin^2\theta.}\right] \qquad 6.17.$$

Let $$\beta = \omega\sqrt{\frac{1+\sin.\theta.}{Bk}}\left[\omega\theta - \frac{T(k.\sin.\theta.)}{\omega}\right] \qquad 6.18.$$

Then $$I = D\left[1+i\beta\alpha\right] - D'\left[1-\beta\right] - R - R' \qquad 6.19.$$

Equilibrium of Shearing Forces

Consider the equation of equilibrium of the vertical forces on the element in Figure 41 :-

$$F_{X_1} - F_{X_2} = i\omega m \overline{V_z} + \frac{\partial F'}{\partial z}$$ per unit length of weld .. 6.20

where F_{X_1} , F_{X_2} is the shear force in plates 1 and 2

m is the mass of the weld/unit length

F' is the shear force in the weld.

From the simple theory of bending beams (for example (41))

$$F' = \frac{B_o}{i\omega} \frac{\partial^3 V_y}{\partial z^3}$$ 6.21.

where Bo is the bending stiffness of the beam

where V_y is the lateral velocity.

Thus:

$$F_{X_1} - F_{X_2} = \left[i\omega m - \frac{i B_o (k.\sin.\theta.)^4}{\omega} \right] V_y$$ 6.22.

Now the shear forces in the plate are:-

$$F_x = \frac{B}{i\omega}\left[\frac{\partial^3 V}{\partial x^3} - (2-\nu)(k.\sin\theta)^2\frac{\partial V}{\partial x}\right] \qquad 6.23$$

where ν = Poisson's Ratio.

We will consider the derivation of this result in the next Chapter. For the moment, notice that the expression differs from that for the simple beam (6.21.) because of complications induced by curvatures in both directions.

However, $(2-\nu)(k.\sin.\theta)^2\frac{\partial V}{\partial x}$ is the same for both plates, and we need, therefore, only consider the terms

If we write:-

$$\gamma = \frac{\omega^2 m - B_0 k^4 \sin^4\theta.}{B k^3\sqrt{1+\sin^2\theta.}} \qquad 6.24.$$

then 6.22. reduces to:-

$$-i\alpha R + R' + \left(-i\alpha + \gamma\right)D + \left(1 + \gamma\right)D' = -i\alpha \qquad 6.25.$$

We are now able to determine the four quantities, R, R', D, D' from equations 6.8., 6.10., 6.19. and 6.25.

After extensive manipulation they are found to be:-

$$R = \frac{\gamma - \alpha^2\beta - \frac{1}{4}(\beta\gamma(1+\alpha^2))}{A + i\,C} \qquad 6.26.$$

$$D = \frac{i\alpha(4 + \gamma - \beta)}{A + iC} \qquad 6.27.$$

$$R' = \frac{\frac{\beta\gamma\alpha^2}{2} + \alpha^2\beta + i\alpha\left(\frac{\beta\gamma}{2} - \gamma\right)}{A + i\,C} \qquad 6.28.$$

$$D' = \frac{-\alpha^2\beta - i\alpha\,\gamma}{A + i\,C} \qquad 6.29.$$

$$\text{where } A = -\left[\gamma + \alpha^2\beta - \frac{\beta\gamma}{4}(1-\alpha^2)\right]$$

$$\text{and } \quad C = \alpha\left[4 + \gamma - \beta - \frac{\beta\gamma}{2}\right] \qquad \Bigg\} \quad 6.30.$$

Now we are ready to examine the stresses and strains induced at the weld.

6.2. The Stress in a Plate generated normal to a Weld

When a bending wave reaches the weld, some of it will be reflected and some transmitted. Thus it will set up stresses both sides of the weld. Conversely, the stress on one side of the weld will be caused by both reflected waves from the same side and transmitted waves from the other side. We will consider each separately.

6.2.1. Stress due to Reflected Waves.

From (11,pp45):-

$$\sigma = \frac{ihE}{2(1-\nu^2)\omega}\left[\frac{\partial^2 V}{\partial x^2} + \nu\frac{\partial^2 V}{\partial z^2}\right] \qquad 6.31.$$

where σ is the stress,

h is thickness of the plate and

E is Young's modulus of the material.

For a single wave incident from angle

$$\sigma = \frac{ihE}{2(1-\nu^2)\omega}\left\{ \begin{array}{l} (-ik.\cos.\theta.)^2 + R(i\cos.\theta.)^2 - R'(1+\sin^2\theta) \\ +\nu\left[(-ik.\sin.\theta.)^2 + R(-ik.\sin.\theta.)^2 + R'(-ik.\sin.\theta.)^2\right] \end{array} \right\} V_1 \qquad 6.32.$$

where V_1 is the velocity of the wave arriving from plate 1

$$\therefore \sigma = \frac{ihEk^2}{2(1-\nu^2)\omega}\left\{ (R+1)(\cos^2\theta. + \sin^2\theta.) - R'(1+(1-\nu)\sin^2\theta.) \right\} V_1 \qquad 6.33.$$

Then the mean square stress is given by:

$$\overline{\sigma_{r\theta}^2} = \frac{h^2E^2k^4}{4(1-\nu^2)^2\omega^2}\left| (R+1)(\cos^2\theta. + \nu\sin^2\theta) - R'(1+(1-\nu)\sin^2\theta.) \right|^2 \overline{V_1^2} \qquad 6.34.$$

where $\overline{\sigma_{r\theta}^2}$ is the time average squared stress due to the waves incident at angle θ being reflected.

Now let us assume that instead of a bending of mean square velocity $\overline{V_1^2}$ arriving from θ, bending waves arrive from all directions with a total mean square velocity $\langle \overline{V_1^2} \rangle$ The $\langle\ \rangle$ indicate a mean over space. We will also assume that they are statistically independent.

Then

$$\frac{\overline{\sigma_r^2}}{\langle \overline{V_1^2} \rangle} = \frac{h^2 E^2 k^4}{8\pi(1-\nu^2)^2\omega^2} \left| (R+1)(\cos^2\theta + \nu \sin^2\theta) - R'(1-(1-\nu)\sin^2\theta) \right|^2 d\theta$$

..... 6.35.

Now from Chapter 5, equation

$$\frac{\langle \overline{\sigma_1^2} \rangle}{\langle \overline{V_1^2} \rangle} = \frac{E^2 h^2 k^4}{4(1-\nu^2)^2\omega^2}\ 0.484 \qquad 6.36.$$

for Poisson's ratio = 0.3.

where $\langle \overline{\sigma_1^2} \rangle$ is the mean square stress in plate 1.

Then

$$\frac{\overline{\sigma_r^2}}{\langle\overline{\sigma_1^2}\rangle} = \frac{1}{2\pi 0.484}\int_{-\frac{\pi}{2}}^{\frac{\pi}{2}} \left|(R+1)(\cos^2\theta + 0.3\sin^2\theta) - R'(1+(1-\nu)\sin^2\theta)\right|^2 d\theta \qquad \ldots\ldots 6.37.$$

6.2.2. Stress due to Transmitted Waves

Again $$\sigma = \frac{ihE}{2(1-\nu^2)\omega}\left[\frac{\partial^2 v}{\partial x^2} + \nu\frac{\partial^2 v}{\partial z^2}\right] \qquad 6.38a.$$

For a single wave incident from plate 2 at angle θ, the stress in 1 is

$$\sigma = \frac{ihE}{2(1-\nu)\omega}\left[D(ik\cos\theta)^2 + D'k^2(1+\sin\theta)^2 + \nu\cdot(-ik\sin\theta)^2(D+D')\right]V_2 \qquad \ldots\ldots 6.38.$$

where V_2 is the velocity in plate 2.

Then the mean square stress normal to the weld in plate 1 is

$$\frac{\overline{\sigma_{T\theta}^2}}{\overline{V_2^2}} = \frac{h^2E^2k^4}{4(1-\nu^2)^2\omega^2}\left|D(\cos^2\theta + \nu\sin^2\theta) - D'(1+(1-\nu)\sin^2\theta)\right|^2 \qquad 6.39.$$

where $\overline{V_2^2}$ is the mean square velocity of the wave from θ in region 2 and $\overline{\sigma_{T\theta}^2}$ is the stress in 1 due to waves transmitted from an angle θ.

For a diffuse incident field, as before,

$$\frac{\overline{\sigma_T^2}}{\langle \overline{V_2^2} \rangle} = \frac{h^2 k^4 E^2}{8\pi(1-\nu^2)^2\omega^2} \int_{-\frac{\pi}{2}}^{\frac{\pi}{2}} \left| D(\cos^2\theta + \nu \sin^2\theta) - D'(1+(1-\nu)\sin^2\theta) \right|^2 . d\theta \qquad 6.40.$$

Again, for $\nu = 0.3$

$$\frac{\langle \overline{\sigma_2^2} \rangle}{\langle \overline{V_2^2} \rangle} = \frac{E^2 h^2 k^4}{4(1-\nu^2)^2\omega^2} 0.484 \qquad 6.40a.$$

Thus, for steel, aluminium, etc.

$$\frac{\overline{\sigma_T}}{\langle \overline{\sigma} \rangle} = \frac{1}{2\pi 0.484} \int_{-\frac{\pi}{2}}^{\frac{\pi}{2}} \left| D(\cos^2\theta + 0.3 \sin^2\theta) - D'(1+0.7\sin^2\theta) \right|^2 d\theta \qquad 6.41.$$

6.3. Details of Numerical Evaluation of the Integrals

Such unpleasant integrations as in equations 6.37. and 6.41. are best tackled numerically. An integration subroutine was written to integrate this expression on a computer using Simpson's Rule.

It is not necessary to detail the complete programme. However, there are three points of interest; the evaluation of the structural

parameters of weld; the limits of the integration; the modifications necessary to determine strain concentrations.

6.3.1. Structural Parameters of Weld.

In equations 6.26. to 6.30. the variables are α, β and γ.

α is determined solely by the angle of incidence.

β is given by:-

$$\beta = \frac{\omega\sqrt{1+\sin^2\theta}}{B k}\left[\omega\theta - \frac{T k^2 \sin^2\theta}{\omega}\right]$$

To evaluate this we need the angle of incidence θ, the frequency ω the bending stiffness of the plate B and the wavenumber k. These are independent of the weld parameters.

We also need to know Θ, the moment of inertia of the weld/unit length and T its torsional stiffness.

Up to this point what we have derived could apply to any rib on the plate of any cross section, providing only that it is thin compared to a wavelength.

It is reasonable to approximate the cross-section of a weld by an ellipse. From Timoshenko[42] we obtain the results that the torsional stiffness of an elliptical section is:-

$$T = \frac{\pi a^3 b^3 G}{a^2 + b^2} \qquad 6.42.$$

where the ellipse is of width 2a and height 2b (Figure 43) and where

G is the shear modulus of the material.

Likewise:-

$$\theta = \frac{\pi^2 a\ b}{4}(a^2+b^2)\rho \qquad 6.43.$$

where ρ = material density.

We are now able to evaluate β.

From equation 6.24:

$$\gamma = \frac{\omega^2 m - B_o k^4 \sin^4\theta}{B k^3 \sqrt{1+\sin^2\theta}}$$

To evaluate this we need to know the bending stiffness of the weld B_o and m its mass per unit length, in addition to the other parameters.

Again, from (42)

$$B_o = \frac{\pi a b^3 E}{4}$$

where E is Young's modulus.

$$m = \pi a b \rho$$

where ρ = material density.

We can now evaluate γ

6.3.2. The Limits of the Integration

The range of integration of 6.37. and 6.41. covers angles of incidence between $\pm 90^{\circ}$. However, there are in general two critical angles that must be considered, namely, that given when $\beta = 0$ and where $\gamma = 0$.

$\beta = 0$ when

$$\frac{\omega^2}{k^2} = \frac{T \sin^2\theta}{\theta} \qquad 6.44.$$

From table (1) we see that this corresponds to the condition that the trace velocity of bending waves equals the velocity of torsional waves in the weld. In this case the angle θ is dependent on ω, the frequency.

$\gamma = 0$ when $$\frac{\omega^2}{k^4} = \frac{B_0}{m} \sin^4\theta \qquad 6.45.$$

From table (1) this is the condition that the trace velocity of the bending waves in the plate equals the velocity of bending waves in the weld. In this case the angle θ is not dependent on ω.

For the weld considered experimentally and theoretically in Section 6.4 the angle at which $\beta = 0$ was always less than the angle giving $\gamma = 0$. Cremer's work[10] on the loss factor past a rib

on a plate shows that under these conditions the important angle is that at which $\gamma = 0$, $\theta_{\gamma=0}$. This is shown in Figure (44a) taken from his work (10). In the evaluations of stress and strain described in Section this was also true. Special routines located $\theta_{\gamma=0}$ and the integration was performed from -90° to $-\theta_{\gamma=0}$, from $-\theta_{\gamma=0}$ to $+\theta_{\gamma=0}$ and from $+\theta_{\gamma=0}$ to 90°. It was not necessary to define the angle $\theta_{\beta} = 0$.

However, if we wish to evaluate strain and stress at high frequencies we must also define $\theta_{\beta=0}$, where $\beta = 0$. For Cremer shows that at such frequencies $\theta_{\beta} = 0$ are greater than $\theta_{\gamma} = 0$, the loss factor is sharply dependent on both γ and β as shown in Figure(44b). These are also taken from Cremer's work

6.3.3. Modifications for Strain

The modifications for strain are very simple. Briefly, equations 6.31. and 6.38a. are replaced by:

$$\xi \doteq \frac{i h}{2\omega} \left(\frac{\partial^2 v}{\partial x^2} \right)_{x=0} \qquad 6.46.$$

and equations 6.36. and 6.40a. are replaced by

$$\frac{\langle \bar{\xi}^2 \rangle}{\langle \bar{v}^2 \rangle} = \frac{1}{c_l^2} \qquad 6.47.$$

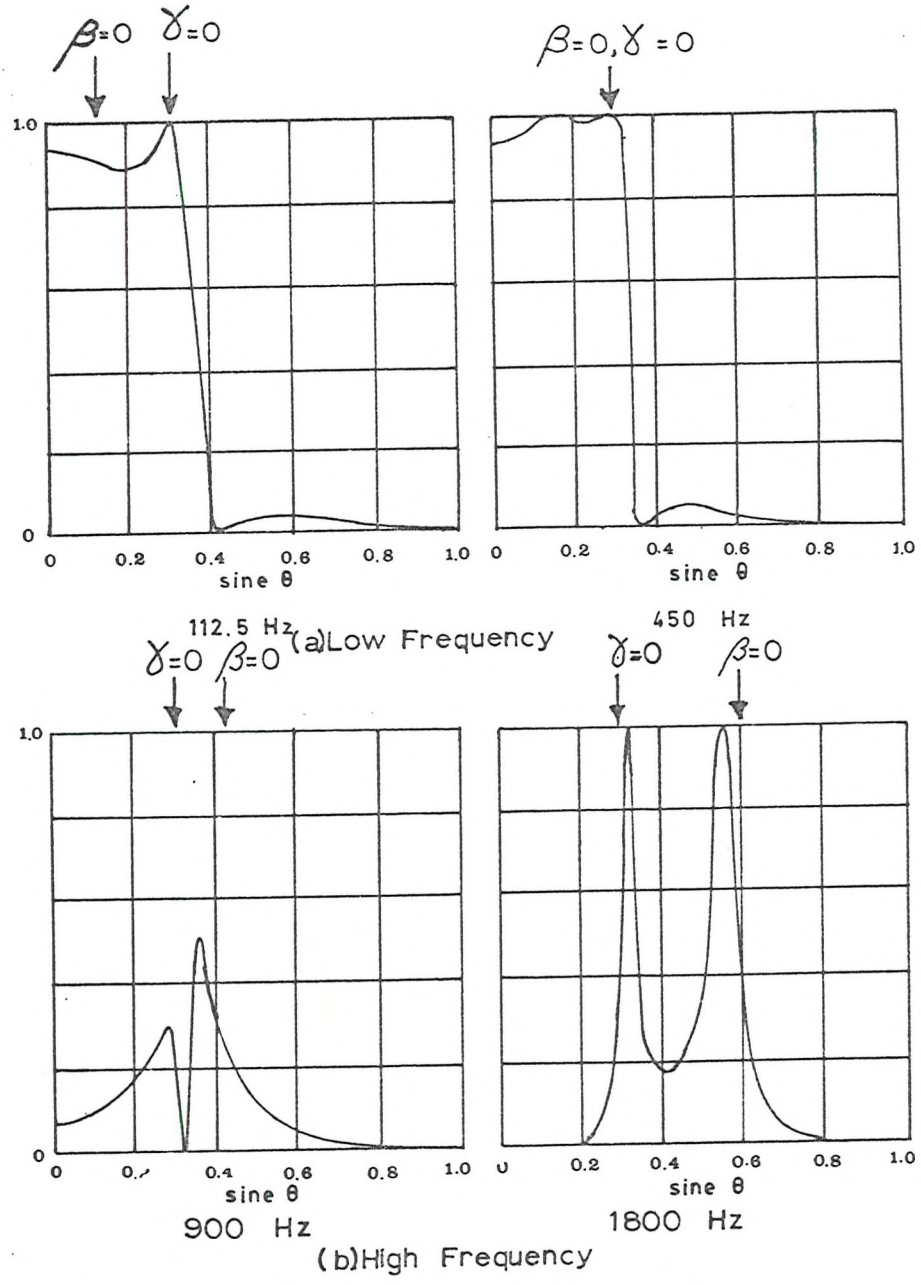

Figure 44 Transmission Past a Rectangular Rib (from 10)

where C_L is the speed of longitudinal waves, as shown in Chapter 5 Section 5.1.

Otherwise the analysis is identical.

The results are as follow

$$\frac{\overline{\xi_r^2}}{\langle \overline{\xi_1^2} \rangle} = 0.848 \int_{-\frac{\pi}{2}}^{\frac{\pi}{2}} \left| (R+1)\cos^2\theta - R'(1+\sin^2\theta) \right|^2 d\theta \qquad 6.48.$$

and

$$\frac{\overline{\xi_t^2}}{\langle \overline{\xi_2^2} \rangle} = 0.848 \int_{-\frac{\pi}{2}}^{\frac{\pi}{2}} \left| D\cos^2\theta - D'(1+\sin^2\theta) \right|^2 d\theta \qquad 6.49.$$

6.4. Experimental Tests

6.4.1. Experimental Procedure

A butt weld was prepared between two aluminium plates, as shown in Figure 45. The plates were 0.030 in. thick and the weld was on average 0.074 in. thick and 0.250 in. wide. It ran the full width of the plate. The measurements were, of course, taken at several positions, along the weld, as there was some small variation in the

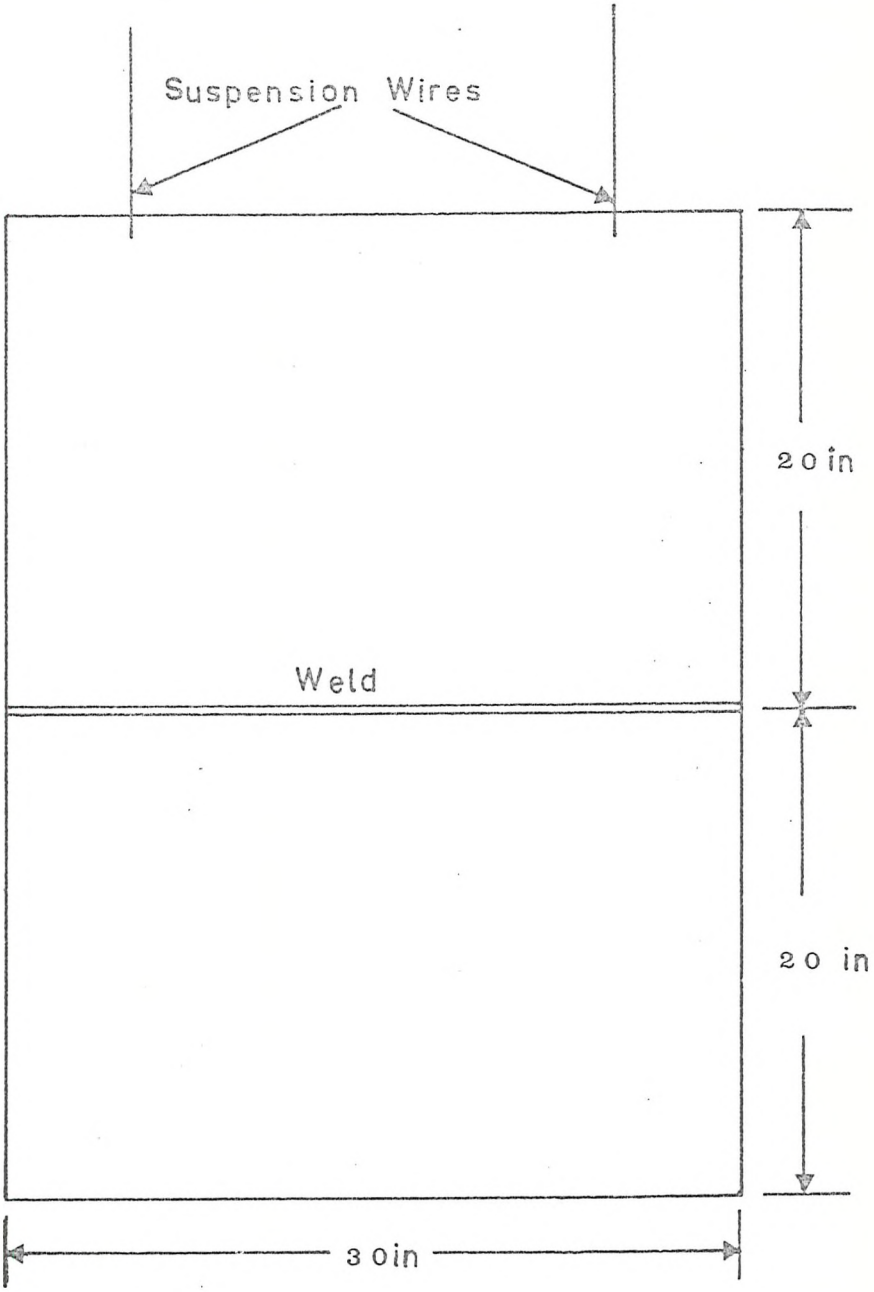

Figure 45 The Welded Aluminium Plate

dimensions of the weld with position. The plate was suspended from a light frame by thin wires from one edge. It was excited by broad frequency band noise from a loudspeaker.

The strain in the top and bottom plates was measured by semi-conductor strain gauges randomly scattered over their surfaces. Seven gauges were used on the bottom plate, but only three gauges gave good outputs from the top plate.

Semi-conductor gauges are expensive and fragile. When a number of them failed on the top plate, it was not possible to replace them within a reasonable time, so the experiment had to be continued in the knowledge that the average readings from the top plate would be less accurate than the lower plate. However, at frequencies about 500 Hz, the results from the gauges agreed within 3dB, so although less than perfect, the results from the top plate were considered adequate.

The strain at the weld was measured at three points on the lower side and two points on the upper side. At each point two or three gauges were positioned in a line normal to the weld, the first one as close as possible to the weld. Because the near field decays exponentially will distance from the boundary as described in Section 2.3, it was felt that it might be possible to extrapolate the stress from two or three gauges to give a more accurate estimate of the strain at the weld.

In fact, this proved to be impossible, as no extrapolation

was worthwhile because the readings from the strain gauges near the weld were all close, within one or two decibels. There was not enough information on which to base a satisfactory extrapolation. Instead, the reading of the gauges nearest the weld was taken and these readings averaged over each side of the weld.

All the results were analysed in third octave bands.

6.4.2. Computational Procedure

A theoretical estimate of the likely strain concentration was made on a digital computer. It would not have been reasonable to have predicted strain concentrations for a large number of welds at many frequencies. Instead, a weld of the experimental weld's proportion was studied over the range of frequencies of the experiments. As a control, the effect of a very small weld and a very large weld was considered to see that the predicted strain and stress concentration behaved as the physics would have suggested.

The programme predicted that a weld of 0.31 in. thickness that was only 0.0001 in. wide, would produce no concentrations of stress and strain on a plate 0.25 in. thick within the accuracy of the integration procedure (1%). This is wholly reasonable. A weld of circular cross-section, 0.25 in. in diameter on a 0.030 in. thick plate was calculated to produce a greater concentration of stress than the actual weld due to reflected waves and a lower stress due to transmitted waves. From Skudryk (23 pp 288-298) this is what we would have expected. Comparing the shape of the practical weld and

the circular weld, on Figures 46 and 47, we see that we have increased the angular inertia of the weld without increasing the lever arm of the bending force exerted by the plate around the centre of the weld. This Skudryk has found, decreases the transmission of bending waves. Thus, in general, one would expect the reflected waves to generate a higher stress and the transmitted waves to generate a lower stress than in a weld such as was used in practice. This is predicted by the programme. The actual predictions for strain and stress are shown on Figures 46 and 47.

The mean square stress at the side of the weld in plate 1, $\overline{\sigma}_{W1}$, is given by:

$$\overline{\sigma}_{W1}^2 = \langle \overline{\sigma}_1^2 \rangle S_A^2 + \langle \overline{\sigma}_2^2 \rangle S_B^2$$

where $\langle \overline{\sigma}_1^2 \rangle$ is the mean square stress in plate 1

$\langle \overline{\sigma}_2^2 \rangle$ is the mean square stress in plate 2

$S_{A,B}^2$ are the factors given on Figures 46 and 47.

A similar calculation gives strain.

6.4.3. Comparison of Computed and Experimental Results

The mean square strain measured at the boundary was compared with that estimated theoretically from the mean square strains measured in the plates. The ratio of the actual to theoretically predicted root

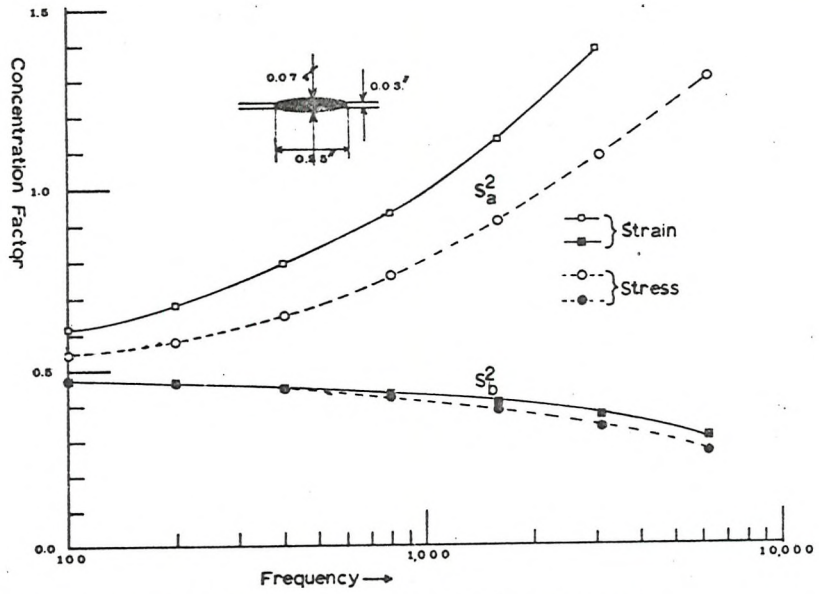

Figure 46 Theoretical Stress and Strain Concentration at a Weld.

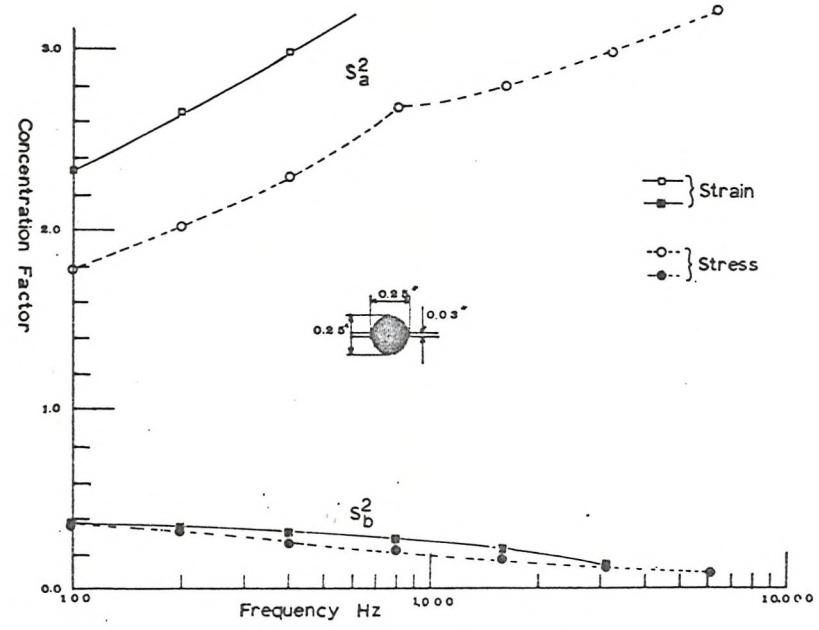

Figure 47 Theoretical Stress and Strain Concentrations at a Weld.

mean square strains at the weld is shown on Figure 48 as a function of the number of modes included in a particular measurement. Basically, the results are sound. The experimental results agree with the calculated results within, in general, 30%, though there are some larger discrepancies at low numbers of modes. When more than four or five modes are included, the results are most satisfactory. We may thus safely conclude that the theory predicts relatively low levels of stress concentration at welds of the type tested.

6.5. Conclusions

Concluding, briefly, we have used the diffuse field bending wave model to predict stress and strain concentration at a weld.

When measured, the prediction of strain was satisfactory, with even only a few modes included, less than necessary to satisfy the formal conditions of diffusivity in Chapter 4.

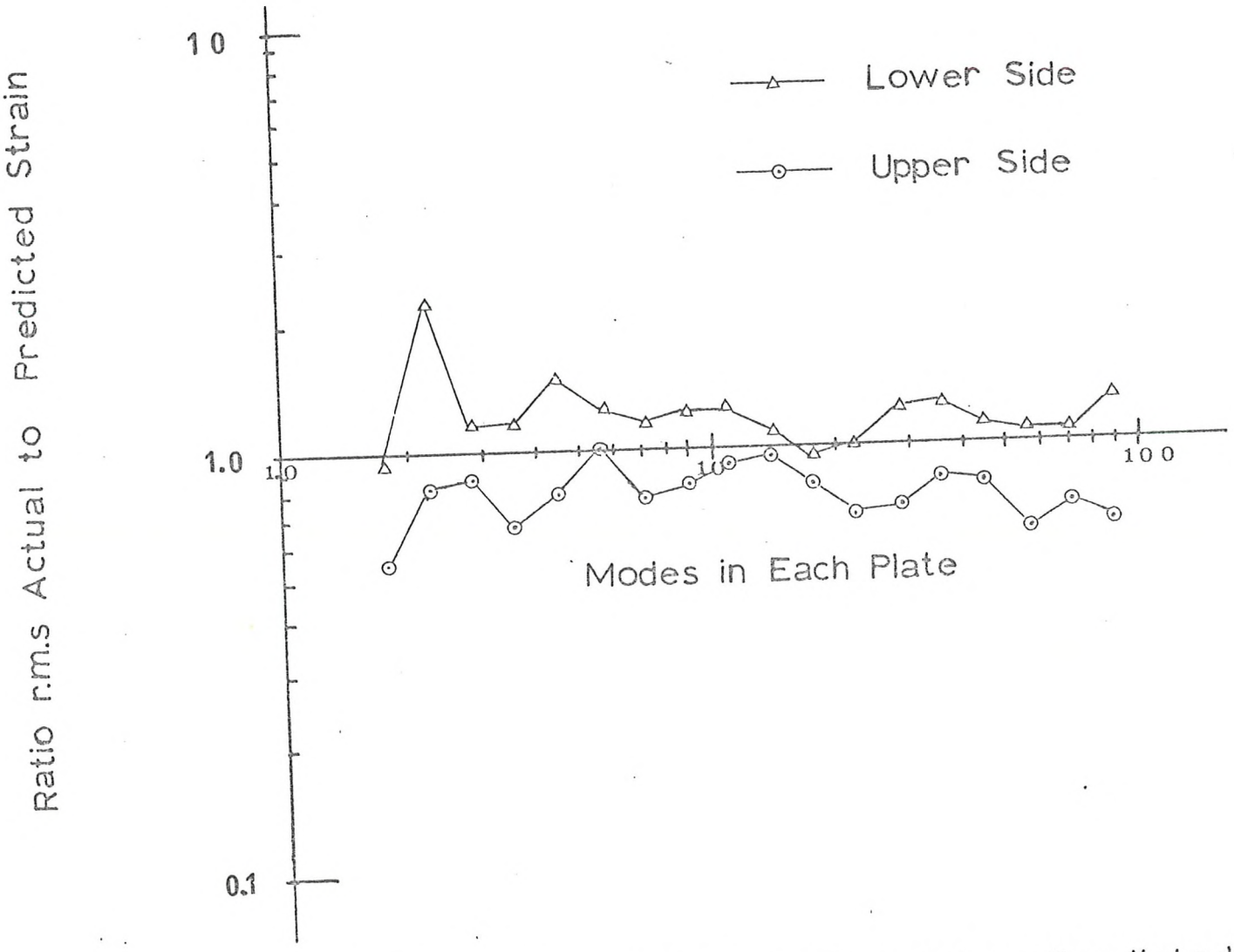

Figure 48 Strain Normal to Weld, Experimental vs. Predicted Levels.

CHAPTER 7

Stress and Strain Concentrations at a Change of Station

The problem to be solved in this chapter is similar to that solved in the previous chapter. We will use the same basic approach. First we will study the solution of the bending wave equation at a change of section, then find the stress generated by a single wave. Then, invoking the diffuse field model, we will derive a value of total stress. However, there are differences between the form of the boundary conditions to be used in this chapter and those used in Chapter 6, which we must carefully consider.

The theoretical results are tested experimentally using several different test pieces.

7.1. The Behaviour of a Bending Wave Incident on a Change of Section

Let two semi-infinite plates of the same material, but of different thickness, lie in the plane $X - Z$, joined along the line $X = O$.

The lateral and angular velocity must be the same each side of the join. The shearing forces must be equal and opposite in both plates, as must be the bending moments.

7.1.1. Wave Velocities

As before, we consider the transverse velocity incident on and

reflected from the change of section as a first step to deriving the boundary conditions.

Let an incident wave arrive from an angle θ to $Z = O$. This wave is described by:-

$$V_{1+} = \exp.i(\omega t - kx.\cos.\theta + kz.\sin.\theta) \qquad 7.1.$$

The trace wavelength of the incident. reflected and transmitted waves must be the same, as shown in Figure 49.

Now from Section 2, we find the travelling waves as a solution to

$$(\nabla^2 + k_1^2)V = O \qquad 7.2.$$

which is $$\frac{\partial^2 V}{\partial x^2} + \frac{\partial^2 V}{\partial z^2} + k_1^2 V = O \qquad 7.3.$$

For waves in region (1) :

Since $$\frac{\partial^2 V}{\partial z^2} = -k_1^2.\sin^2\theta \; V \qquad 7.4.$$

we know that the reflected travelling or propagating wave must satisfy the equation -

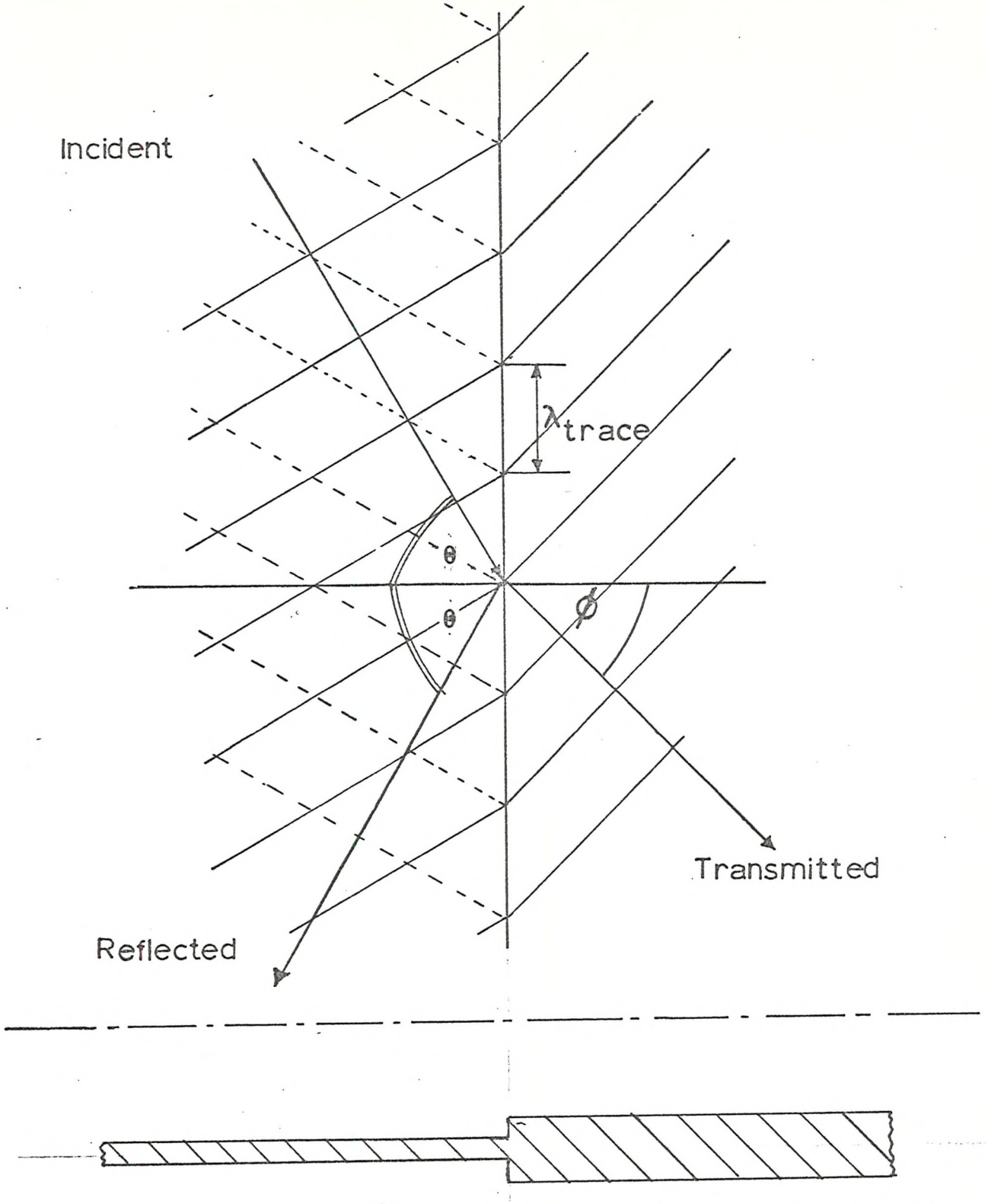

Figure 49 Equality of Trace Wavelength at a Change of Section.

$$\frac{\partial^2 V}{\partial x^2} - (1 - \sin^2\theta)k^2 V = 0 \qquad 7.5.$$

therefore -

$$V = R.\exp.i(\omega t + k_1 x.\cos.\theta + k_1 z.\sin.\theta) \qquad 7.6.$$

This is the same as for the weld.

However at a change of section, the speed of bending waves changes (table 1 p 20). To accommodate this, yet meet the requirement of equalify of trace wavelength, the angle of departure ϕ of the wave in region 2 must obey the relationship:-

$$\frac{\sin.\theta}{\lambda_1} = \frac{\sin.\phi}{\lambda_2} \qquad 7.7.$$

where λ_1 , λ_2 are the wavelengths in 1 , 2.

Under certain conditions total reflection takes place.

Clearly, when λ_1 is less than λ_2 , if sin ϕ is 1 then sin θ must be less than 1. θ will then be the critical

angle of total reflection. At angles of incidence greater than critical no energy will pass from region 1 to 2. There is an analogy with the behaviour of a ray of light leaving a glass block and passing into the air. At angles of incidence greater than the critical angle, transmission is not possible. The analogy ends there, as with bending waves four boundary conditions must be satisfied. It is important to realise that whilst no energy may be transmitted across the interface when the angle of incidence is greater than the critical angle, there is still a disturbance set up in the "receiving" plate due to the transmitted near field. We will discuss this later. Total internal reflection will occur when a wave is travelling from a thin region to a thick region.

Now the transmitted propagating wave must satisfy:-

$$(\nabla^2 + k_2^2)V = 0 \qquad 7.8.$$

or

$$\frac{\partial^2 V}{\partial x^2} - k_1^2 \sin^2\theta . V + k_2^2 V = 0 \qquad 7.9.$$

Therefore

$$\frac{\partial^2 V}{\partial x^2} - k_1^2(K^2 - \sin^2\theta)V = 0 \qquad 7.10.$$

where $K = \frac{k_2}{k_1}$

The transmitted wave is then given by

$$V_{+2} = D.\exp.i(\omega t - k_1\sqrt{K^2 - \sin^2\theta}\,.\,x + k_1 z.\sin.\theta) \qquad 7.11.$$

If there is no total reflection, then $K^2 - \sin^2\theta$ will be greater than zero and the solution for V_{+2} represents a transmitted travelling wave.

However, if there is total reflection, $K^2 - \sin^2\theta$ will be less than zero. Then we must write V_{+2} as

$$V_{+2} = D.\exp\left(i(\omega t + k_1 z.\sin.\theta) - k_1\sqrt{\sin^2\theta - K^2}\,.\,x\right) \qquad 7.12.$$

This is a wave that decays with x . It does not transmit energy and it is an additional near field.

The near fields must satisfy the equations

$$\left.\begin{aligned} (\nabla^2 - k_1^2)V = 0 \qquad & \text{in region 1} \\ (\nabla^2 - k_2^2)V = 0 \qquad & \text{in region 2} \end{aligned}\right\} \qquad 7.13.$$

From the previous reasoning, the reflected near field must satisfy:-

$$\frac{\partial^2 V}{\partial x^2} - k_1^2(1+\sin^2\theta)\,V = 0 \qquad 7.14.$$

Then:-

$$V'_{-1} = R'.\exp.\left(i\left(\omega t + k_1 z.\sin.\theta\right) + k_1\sqrt{1+\sin^2\theta}\;.x\right) \qquad 7.15$$

and since the transmitted near field satisfies

$$\frac{\partial^2 V}{\partial x^2} - k_1^2(K^2+\sin^2\theta)\,V = 0 \qquad 7.16.$$

then

$$V'_{+2} = D'.\exp.\left(i\left(\omega t + kz.\sin.\theta\right) - k_1 x\sqrt{K^2+\sin^2\theta}\right) \qquad 7.17.$$

This component is not affected by total reflection.

7.1.2. The Boundary Conditions : Transmission

7.1.2.1. Equality of Lateral Velocity

At $x = 0$, $\quad 1 + R + R' = D + D'$ 7.18.

for the velocity in each plate must be the same at the join.

7.1.2.2. Equality of Angular Velocity

At $x = 0$, the angular velocities $\dfrac{\partial V}{\partial x}$ must be the same in each plate at the join.

Therefore:

$$-i\cos\theta + iR\cos\theta + \sqrt{1+\sin^2\theta}\,.R' = -iD\sqrt{K^2-\sin^2\theta} - D'\sqrt{K^2+\sin^2\theta} \qquad 7.19.$$

7.1.2.3. Equality of Bending Moment

From (40) the bending moment in a plate is given by

$$M_x = B'\left[\frac{\partial^2 y}{\partial x^2} - \nu\frac{\partial^2 y}{\partial z^2}\right] \qquad 7.20.$$

B' = bending stiffness/unit width

ν = Poisson's Ratio.

Now we must include the terms in $\frac{\partial^2 y}{\partial z^2}$, for the bending stiffnesses are not the same in each plate.

For equilibrium:-

$$\left[\left(\frac{\partial^2 V_1}{\partial x^2}\right)_{x=0} + k_1^2 \nu . \sin^2\theta . V_1\right] = \left[\left(\frac{\partial^2 V_2}{\partial x^2}\right)_{x=0} + k_1^2 \nu . \sin^2\theta \; V_2\right] N$$

where $N = \frac{B'_2}{B'_1}$ 7.21.

Then

$$-\cos^2\theta . - R.\cos^2\theta . + R'(1+\sin^2\theta .) - \nu(1+R+R')\sin^2\theta . =$$

$$N D(K^2 - \sin^2\theta) + N D'(K^2 + \sin^2\theta) - \nu N.\sin^2\theta .(D + D')$$

7.22.

7.1.2.4. Equality of Shearing Force

First we must derive the shearing force in a plate bent in two directions; then we can equate the forces each side of the join.

The following derivation is due to Cremer[10]. It is wise for us to consider this in detail as it is not a familiar result. Consider the thin slice at the edge of each plate, as depicted in Figure 50.

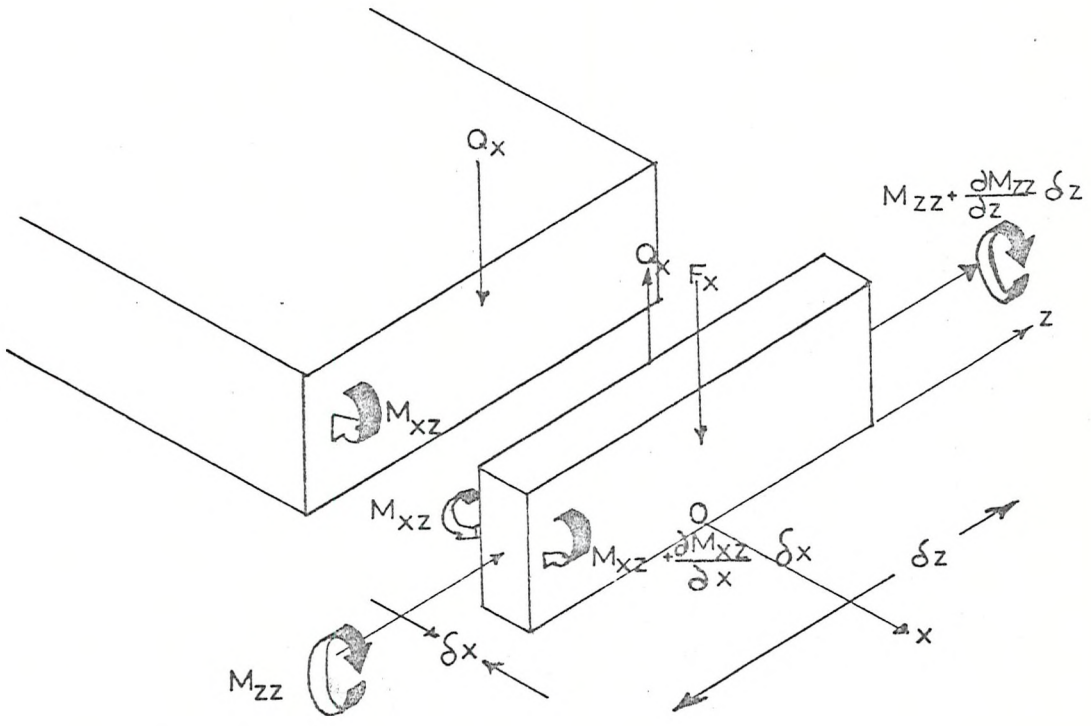

Figure 50 Shear Forces in Edge of Plate.

Q_x is the shear force generated in the material per unit width of material; Fx is the force transmitted to the other plate. Taking moments about the Z axis at $x = 0$:-

$$\delta x.\delta z.Q_x = -\frac{\partial M_{xz}}{\partial x}\delta x.\delta z - \frac{\partial M_{zz}}{\partial z}\delta z.\delta x. \qquad 7.23.$$

Therefore :-

$$Q_x = -\frac{\partial M_{xz}}{\partial x} - \frac{\partial M_{zz}}{\partial z} \qquad 7.24.$$

where M_{zz} is the torsional moment per unit width in the strip twisting about the Z axis.

Resolving forces vertically for the strip gives us:-

$$F_x.\delta x.\delta z = Q_x\delta x.\delta z + \delta x\,\frac{\partial M_{xx}}{\partial z} \qquad 7.25.$$

M_{xx} and M_{zz} are moments resulting from the shear stress τ_{zx} and τ_{xz} , which are, of course, equal. These are shown in Figure 51.

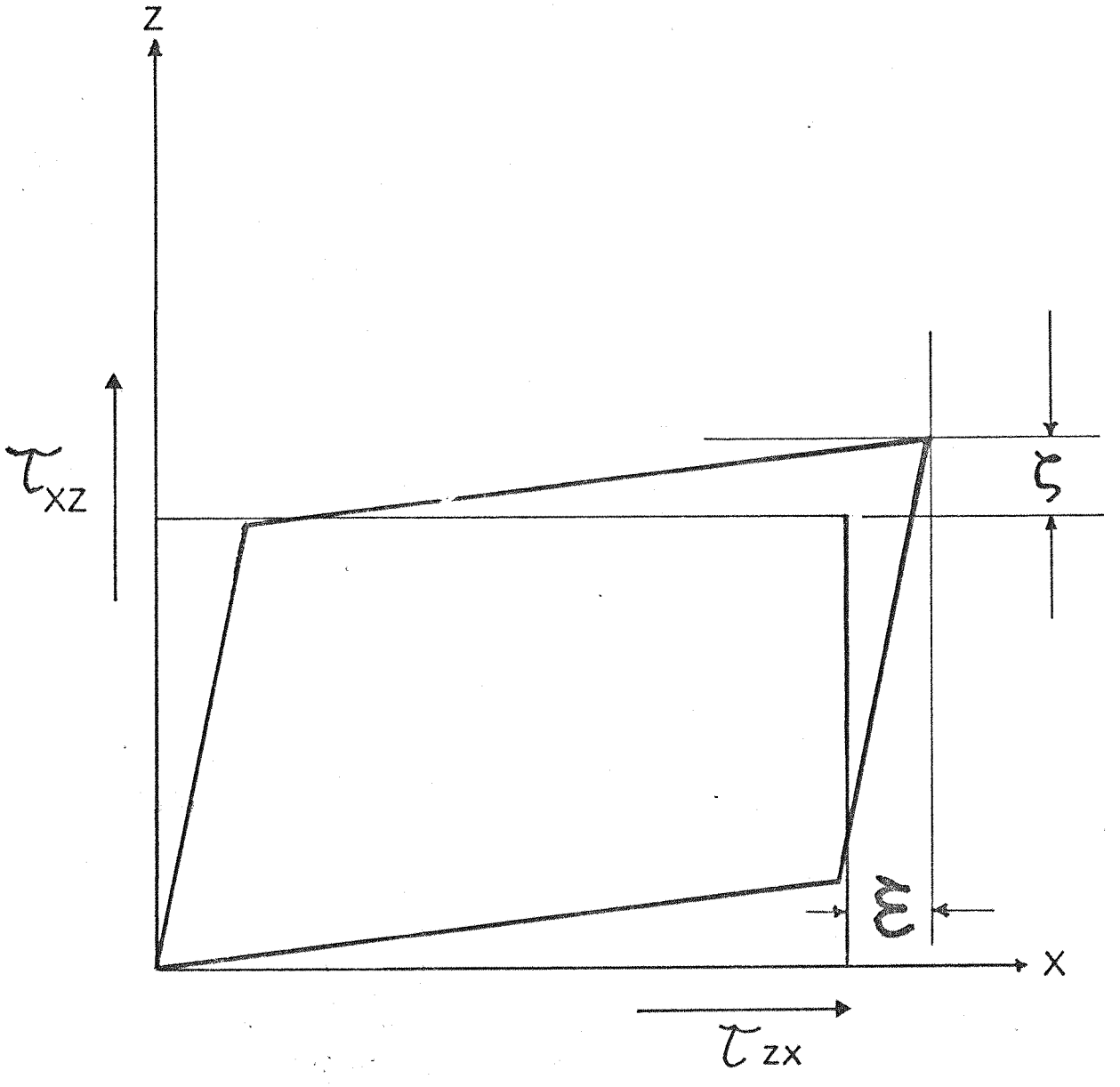

Figure 51 Shear Deformation

Then $M_{xx} = -M_{zz} = -\int_{-\frac{h}{2}}^{\frac{h}{2}} \tau_{xz}.dy$ 7.26.

where y is here the distance from the centre line of the plate.

This shear stress is due to the "lozenging" of the element shown in Figure 51 and is given by

$$\tau_{xz} = G\left(\frac{\partial \zeta}{\partial x} - \frac{\partial \xi}{\partial z}\right) \qquad 7.27.$$

where ζ and ξ are displacements defined in Figure 51 and G is the shear modulus of the material.

From the well known relationships (41 pp 205)

$$\text{Strain} = -y\frac{\partial^2 \eta}{\partial x^2} \qquad 7.28.$$

thus $$\frac{\partial \xi}{\partial x} = -y\frac{\partial^2 \eta}{\partial x^2} \qquad 7.29.$$

and $$\frac{\partial \zeta}{\partial z} = -y\frac{\partial^2 \eta}{\partial z^2} \qquad 7.30$$

where η is the lateral displacement of the centre line of the unstressed plate.

Thus $$\frac{\partial \xi}{\partial z} = \frac{\partial \gamma}{\partial x} = -\frac{\partial^2 \eta}{\partial x \partial z} \cdot y \qquad 7.31.$$

and thus $$-\tau_{xz} = 2G.y\left(\frac{\partial^2 \eta}{\partial x . \partial z}\right) \qquad 7.32.$$

$\frac{\partial^2 \eta}{\partial x . \partial z}$ is the rate at which the angle of twist varies along the edge of the plate.

$$M_{xx} = -2G \int_{-\frac{h}{2}}^{\frac{h}{2}} y^2 . \frac{\partial^2 \eta}{\partial x \partial z} . dy \qquad 7.33.$$

Now $$\int_{-\frac{h}{2}}^{\frac{h}{2}} y^2 . dy = I$$ the second moment of area of the strip per unit width

and $$\frac{2G}{(1-\nu)} = E' \qquad 7.34.$$

where E' is Young's modulus per unit width.

$$\therefore \quad M_{xx} = E' I \frac{\partial^2 \eta}{\partial x \partial z} = B' \frac{\partial^2 \eta}{\partial x \partial z} \qquad 7.35.$$

From 7.24.

$$Q_x = \frac{B}{i\omega}\left[\frac{\partial^3 V}{\partial x^3} - (k_1 \sin.\theta)^2 \frac{\partial V}{\partial x}\right] \qquad 7.36.$$

From 7.35.

$$M_{xx} = \frac{B}{i\omega}\left[\frac{\partial^2 V}{\partial x \partial z}\right]$$

$$= \frac{B}{i\omega} \frac{\partial V}{\partial x}(i k_1 \sin.\theta) \qquad 7.37.$$

Thus from 7.25.

$$F_x = \frac{B}{i\omega}\left[\frac{\partial^3 V}{\partial x^3} - (2-\nu)(k_1 \sin.\theta)^2 \frac{\partial V}{\partial x}\right] \qquad 7.38.$$

In this derivation we have assumed that the distribution of stress is linear in the y direction across the plate. This is not strictly true. From the principle of St. Venant we would deduce that

this is so only at a distance from the boundary comparable to the thickness of the plate. However, as we are considering only wavelengths greater than six times the thickness or more, then we should still be able to deduce the levels of stress caused by interference of the bending waves near the boundary, if not quite at it. This is a fundamental limitation of the theory that we have already discussed. It becomes serious at very short wavelengths and high frequencies. We have, however, already excluded these conditions.

Now we must equate the shearing forces both sides of join. Thus we obtain our fourth equation

$$i\cos^3\theta - Ri\cos^3\theta + RS^3 - (2-\nu)\sin^2\theta\,(iR\cos\theta - i\cos\theta + SR')$$
$$= iNDP^3 - DNT^3 - N(2-\nu)\sin^2\theta\,(-iDP - D'T)$$

where $S^2 = 1 + \sin^2\theta$

$P^2 = K^2 - \sin^2\theta$

$T^2 = K^2 + \sin^2\theta$

..... 7.39.

Attempts to reduce these four equations to simple results for R, R' , D, D' have been unsuccessful. Instead, the equations were solved numerically using a computer subroutine to solve the simultaneous equations, the numerical results being used directly to produce the strain and stress concentrations.

7.1.3. The Boundary Conditions : Total Reflection

The same four boundary conditions are used. The only differences in the resulting equation are due to the form of the transmitted wave, which under conditions of total reflection is only a decaying near field.

Without deriving them formally, which may be done by analogy with Section 7.1.2., we may write down the four equations as follows:

Equality of Velocity

$$1 + R + R' = D + D' \qquad 7.40.$$

Equality of Angular Velocity

$$R.i.\cos\theta - i.\cos\theta + R'S = -DP - D'T \qquad 7.41.$$

Equality of Bending Moment

$$-\cos^2\theta - R.\cos^2\theta + R'S^2 - \nu(1 + R + R')\sin^2\theta = NDP^2 + ND'T^2 - \nu N(D + D')\sin^2\theta \qquad 7.42.$$

Equality of Shear Force

$$+i\cos.^3\theta - iR.\cos.^3\theta + R'S^3 - (2-\nu)\sin.^2\theta(iR.\cos.\theta - i\cos.\theta + SR') =$$

$$-NDP^3 - D'NT^3 + (2-\nu)\sin^2\theta(DP + D'T)$$

7.43.

where N = ratio of bending stiffness

$$S^2 = 1 + \sin^2\theta$$

$$P^2 = \sin^2\theta - K^2$$

$$T^2 = K + \sin^2\theta$$

where K = ratio of wave numbers

7.2. The Stress Generated Normal to a Change of Section

The basic approach is the same as that used in Chapter 6, Section 2. We determine the stress set up by the curvature due to a wave incident from angle θ ; then the total stress is found by assuming that a diffuse field is incident on the change of section. Finally this is compared with the level of mean square stress in the region from which the bending waves arrive.

The stress in plate (1) is now due to four types of bending wave:-

1. Partial Reflection in plate (1) σ_a
2. Total Reflection in plate (1) σ_c
3. Partial Transmission from plate (2) σ_b
4. Total Non Transmission from plate (2) σ_d

7.2.1. Stress due to Partial Reflection

The stress in plate (1) normal to the join due to partial reflection at $x = 0$ is given by (40).

$$\sigma_a = \frac{ih_1 E}{2(1-\nu^2)\omega}\left[\frac{\partial^2 V}{\partial x^2} - \nu\frac{\partial^2 V}{\partial z^2}\right]_{x=0} \qquad 7.44.$$

where V = lateral velocity,

h_1 = thickness.

$$\left(\frac{\partial^2 V}{\partial x^2}\right)_{x=0} = \left[(1+\sin^2\theta)R' + (1+R)(i\cos.\theta)^2\right] V_1 k_1^2 \exp(i(\omega t + k_1 z \sin\theta)) \qquad 7.45.$$

where k_1 is the wave number in region 1

and:-

$$\left(\frac{\partial^2 V}{\partial z^2}\right)_{x=0} = (1+R+R')(i.\sin\theta)^2 V_1 k_1^2 \exp.i(\omega t + k_1 z . \sin.\theta) \qquad 7.46.$$

where V_1 is the velocity of waves incident from region 1

i.e. $V_1 = V_1 . \exp.i(\omega t + kz.\sin\theta - kx.\cos.\theta)$

$$\sigma_a = \frac{i h_1 E}{2(1-\nu^2)\omega^2}\left\{(R+1)(\cos^2\theta + \nu.\sin^2\theta) - R'(1+(1-\nu)\sin^2\theta)\right\} * V_1 \exp.i(\omega t + kz.\sin.\theta) \qquad 7.47$$

Then the mean square stress is

$$\overline{\sigma_a^2} = \frac{h_1^2 E^2 k_1^4}{4(1-\nu^2)^2\omega^4}\left|(R+1)(\cos^2\theta + \nu\sin^2\theta) - R(1+(1-\nu)\sin^2\theta)\right|^2 \overline{V_1^2} \qquad 7.48.$$

If the bending wave field is diffuse and reverberent then instead of all the energy arriving from angle θ it will arrive from all angles. From the result of Chapter 5, as in Chapter 6, we may write

$$\frac{\langle\overline{\sigma_1^2}\rangle}{\langle\overline{V_1^2}\rangle} = \frac{h_1^2 E^2 k_1^4}{4(1-\nu^2)^2\omega^4}\int_{-\frac{\pi}{2}}^{\frac{\pi}{2}} \cos^2\theta + \nu\sin^2\theta . d\theta \qquad 7.49.$$

Then

$$\frac{\overline{\sigma_a}^2}{\langle \overline{\sigma_i}^2 \rangle} = \int_{-T_c}^{T_c} \left| \frac{(R+1)(\cos^2\theta + 0.3.\sin^2\theta) - R'(1+0.7.\sin^2\theta)}{2\pi \times 0.484} \right|^2 d\theta \qquad 7.50.$$

for $\nu = 0.3$

T_c is $\frac{\pi}{2}$ when the incident wave and reflected wave lie in the thicker of the two sections. But when total reflection can take place, going from a thin to a thick section, T_c is the critical angle.

7.2.2. Stress due to Total Reflection

Now if a bending wave arrives from the thin section at an angle greater than the critical angle it will be reflected with no loss of energy at the change of section. We will find the stress generated in the thin section.

Again

$$\sigma_c = \frac{i h_1 E}{2(1-\nu^2)\omega^2} \left[\frac{\partial^2 V}{\partial x^2} + \nu \frac{\partial^2 V}{\partial z^2} \right]_{x=0} \qquad 7.51.$$

$$\sigma_c = \frac{i\, h_1 E k_1^2}{2(1-\nu^2)\omega^2}\left[(1+R)(i\cos)^2 + R'(1+\sin^2\theta)\right.$$

$$\left. + \nu(i\sin\theta)^2(1+R+R')\right] V_1 \exp.i(\omega t + kz.\sin.\theta) \qquad 7.52.$$

This may be directly compared with equation 7.47: they are identical. Thus by the same reasoning we obtain the same expression for stress concentration, except that the bending waves that contribute to this stress arrive from angles between 90° and T_c the critical angle. i.e.,

$$\frac{\overline{\sigma_c}^2}{\langle\overline{\sigma_1}^2\rangle} = \int_{-\frac{\pi}{2}}^{-T_c} \left| \frac{(R+1)(\cos^2\theta + 0.3\sin^2\theta) - R'(1+0.7\sin^2\theta)}{0.484\pi} \right|^2 d\theta \qquad 7.53.$$

7.2.3. Stress due to Partially Transmitted Bending Waves

Let a bending wave approach the change of section from plate 1, of thickness h_1, from angle θ and let the wavenumber be k_1. Let this wave be partially transmitted and depart into plate 2, of

thickness h_2 , at an angle ϕ with a wavenumber k_2.

Now the stress in 2 will be

$$\sigma_b = \frac{i h_2 E}{2(1-\nu^2)\omega^2}\left[\frac{\partial^2 V}{\partial x^2} + \nu\frac{\partial^2 V}{\partial z^2}\right]_{x=0} \qquad 7.54.$$

$$= \frac{i h_2 E k_2^2}{2(1-\nu^2)\omega^2}\left[-D\cos^2\phi + D'(1+\sin^2\phi) - \nu.\sin^2\phi(D+D')\right] V_1$$

. . . . . 7.55.

where D and D′ are the transmission coefficients from plate 1 to plate 2.

Now

$$\frac{\sin\theta}{\sin\phi} = \frac{\lambda_1}{\lambda_2} = \sqrt{\frac{h_1}{h_2}} = \frac{k_2}{k_1} = K \qquad 7.56.$$

Then 7.5.5. may be written in terms of the angle of incidence θ as

$$\sigma_b = \frac{i h_2 E}{2(1-\nu^2)}\left[\frac{k_1}{k_2}\right]^2\left[\frac{k_2}{\omega^2}\right]\left[D'(K+(1-\nu)\sin^2\theta) - D(K-(1-\nu)\sin^2\theta)\right] V_1 \qquad 7.57$$

This is a necessary operation: if we intend to use the diffuse field model we can only assume a uniform distribution of $\overline{V_1^2}$ with θ the angle of incidence, not ϕ .

Then the mean square stress in Section 2 due to one wave is given as:

$$\overline{\sigma_b^2} = \frac{E^2 h_2^2 k_2^4}{2(1-\nu^2)^2\omega^4}\left[\frac{k_1}{k_2}\right]^4\left|D'(K^2+(1-\nu)\sin^2\theta) - D(K^2-(1-\nu)\sin^2\theta)\right|^2 \overline{V_1^2} \qquad 7.58.$$

Now if the incident field is diffuse, then

$$\frac{\overline{\sigma_b^2}}{\langle\overline{V_1^2}\rangle} = \frac{E^2 h_2^2 k_2^4}{2(1-\nu^2)^2\omega^4}\frac{k_1}{k_2}\int_{-T_c}^{T_c}\left|D'(K^2+(1-\nu)\sin^2\theta) - D(K^2-(1-\nu)\sin^2\theta)\right|^2 d\theta \qquad 7.59.$$

where T_c is the critical angle from 1 to 2, or 90°.

Now from Chapter 5

$$\frac{\langle \bar{\sigma}_1^2 \rangle}{\langle \bar{V}_1^2 \rangle} = \frac{h_1^2 E^2 k_1^4}{4(1-\nu^2)^2 \omega^4} \int_{-\frac{\pi}{2}}^{\frac{\pi}{2}} \cos^2\theta + \nu \sin^2\theta \, . \, d\theta \qquad 7.60$$

Then

$$\frac{\langle \bar{\sigma}_b^2 \rangle}{\langle \bar{\sigma}_1^2 \rangle} = \left[\frac{h_2}{h_1}\right]^2 \int_{-T_c}^{T_c} \left| \frac{D(K^2 + 0.7\sin^2\theta) - D'(K^2 - 0.7\sin^2\theta)}{2\pi \times 0.484} \right|^2 d\theta \qquad 7.61.$$

$$(\nu = 0.3)$$

7.61 tells us the stress to expect in section 2, normal to and at the change of section compared to the mean square stress over section 1.

7.2.4. Stress due to Totally Non-Transmitted Bending Waves

Using the same notation as in 7.2.3. we are trying to find stress normal to and at the change of section, in section 2, presumed thicker than in 1, due to a bending wave incident from 1 at an angle greater than the critical angle.

Again

$$\sigma_d = \frac{i\, h_2 E}{2(1-\nu^2)^2\omega^2}\left[\frac{\partial^2 V}{\partial x^2} + \nu\,\frac{\partial^2 V}{\partial z^2}\right]_{x=0} \qquad 7.62$$

$$= \frac{i\, h_2 E\, k_1^2}{2(1-\nu^2)\omega^2}\left[(K^2+\sin^2\theta)D' + (\sin^2\theta - K^2)D - \nu\sin^2\theta(D+D')\right] V_1$$

. . . . . 7.63.

This is identical to 7.57.

Proceeding the same way we end with the result that

$$\frac{\langle \bar{\sigma}_d^2 \rangle}{\langle \bar{\sigma}_1^2 \rangle} = \left[\frac{h_2^2}{h_1^2}\right] \int_{-\frac{\pi}{2}}^{-T_c} \left| \frac{D'(0.7\sin^2\theta + K^2) + D(0.7\sin^2\theta - K^2)}{0.484\,\pi} \right|^2 d\theta \qquad 7.64$$

where T_c is the critical angle from 1 to 2.

We have now found the stress in plate 2 and normal to the change of section in terms of the mean square stress in plate 1.

7.3. Evaluation of the Results

7.3.1. Computation

Such complex integrations as are involved in expressions 7.50, 7.53, 7.61 and 7.64 are best solved numerically. As mentioned in section 7.1., from a given value of $\frac{h_2}{h_1}$ the values of R, R', D, D', are deduced as from equations of sections 7.1.2 and 7.1.3. From these are determined the stresses generated due to waves from various angles. Then, by integration using Simpson's rule, was calculated the effect of waves coming from every direction. The results of this calculation are presented in Figure 52. There are no particular complications that need mention and the structure is completely defined by the ratio of the change of section. The results are discussed later.

In practice we may only measure strain not stress and the results are derived also for the expected strain.concentrations. The modifications are the same as those described in section 6.3.2. for the weld. Expressions 7.44, 7.51, 7.54 and 7.62 are replaced by

$$\xi = \frac{i\,h}{2\,\omega}\left(\frac{\partial^2 V}{\partial x^2}\right)_{x=0} \qquad 7.65$$

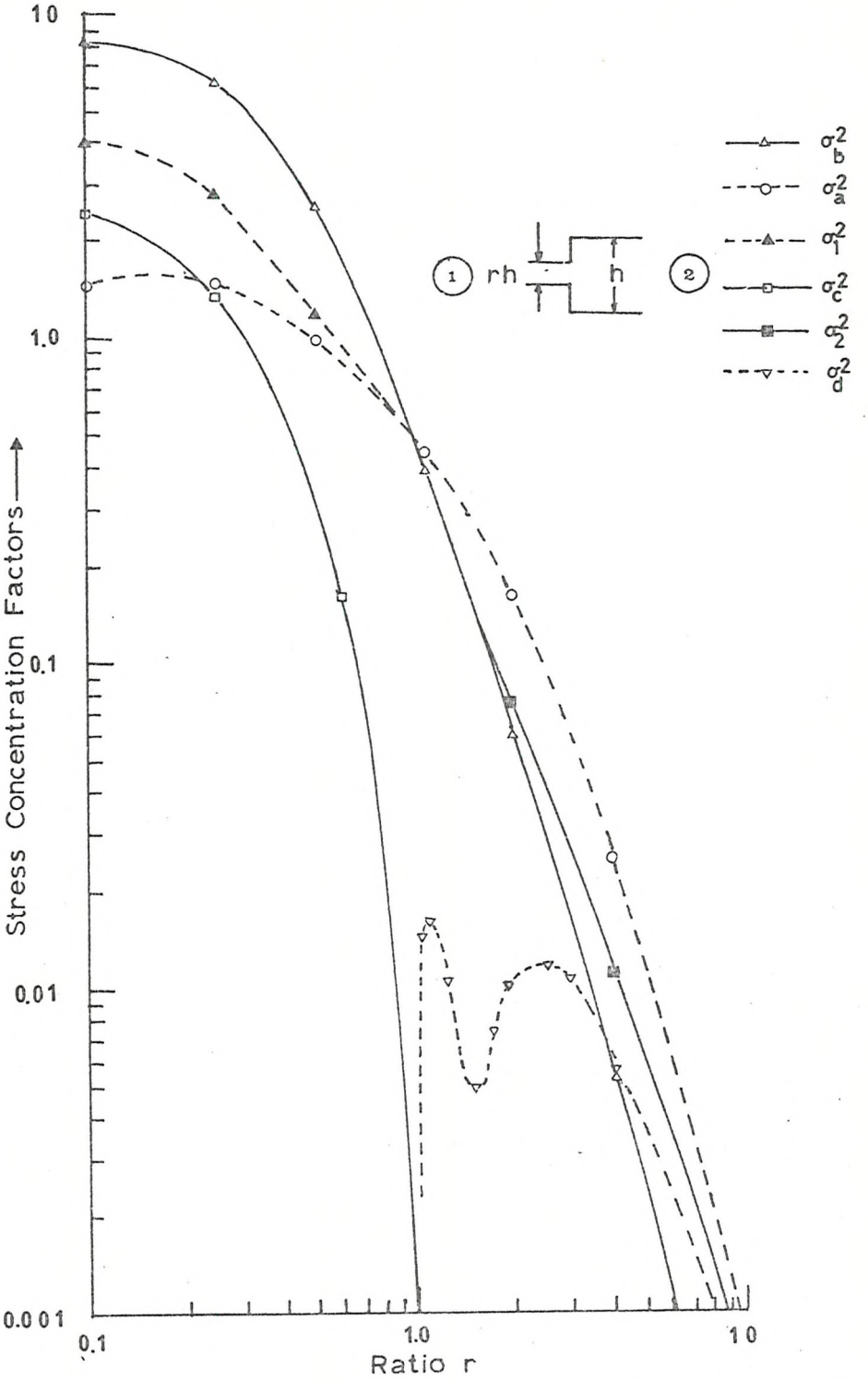

Figure 52 Stress Concentration at a Change of Section

and expressions for stress versus velocity are replaced by

$$\frac{\langle \bar{\xi}^2 \rangle}{\langle \bar{v}^2 \rangle} = \frac{1}{c_1^2} \qquad 7.66$$

(See also section 6.3.2.)

The results for strain are presented in Figure 53. The only structural parameter is the ratio of one section's thickness to the other.

7.3.2. Discussion of Computed Results

Let us first consider how to use Figures 52 and 53.

If we want to calculate the stress concentration at a change of section of 4 to 1 (say) and we estimate the mean square stress in 1 to be 100 lbf/in^2 and in 2, the thicker, to be 10 lbf/in^2 then the mean square stress on the thin side of the join will be

$$\bar{\sigma}^2 = 100^2 \sigma_{1\,(0.25)}^2 + 10^2 \sigma_{2\,(0.25)}^2 \qquad 7.67$$

$$\sigma_1^2 = \sigma_a^2 + \sigma_c^2$$

where σ_a^2 is the stress due to partial reflection

σ_c^2 is the stress due to total reflection

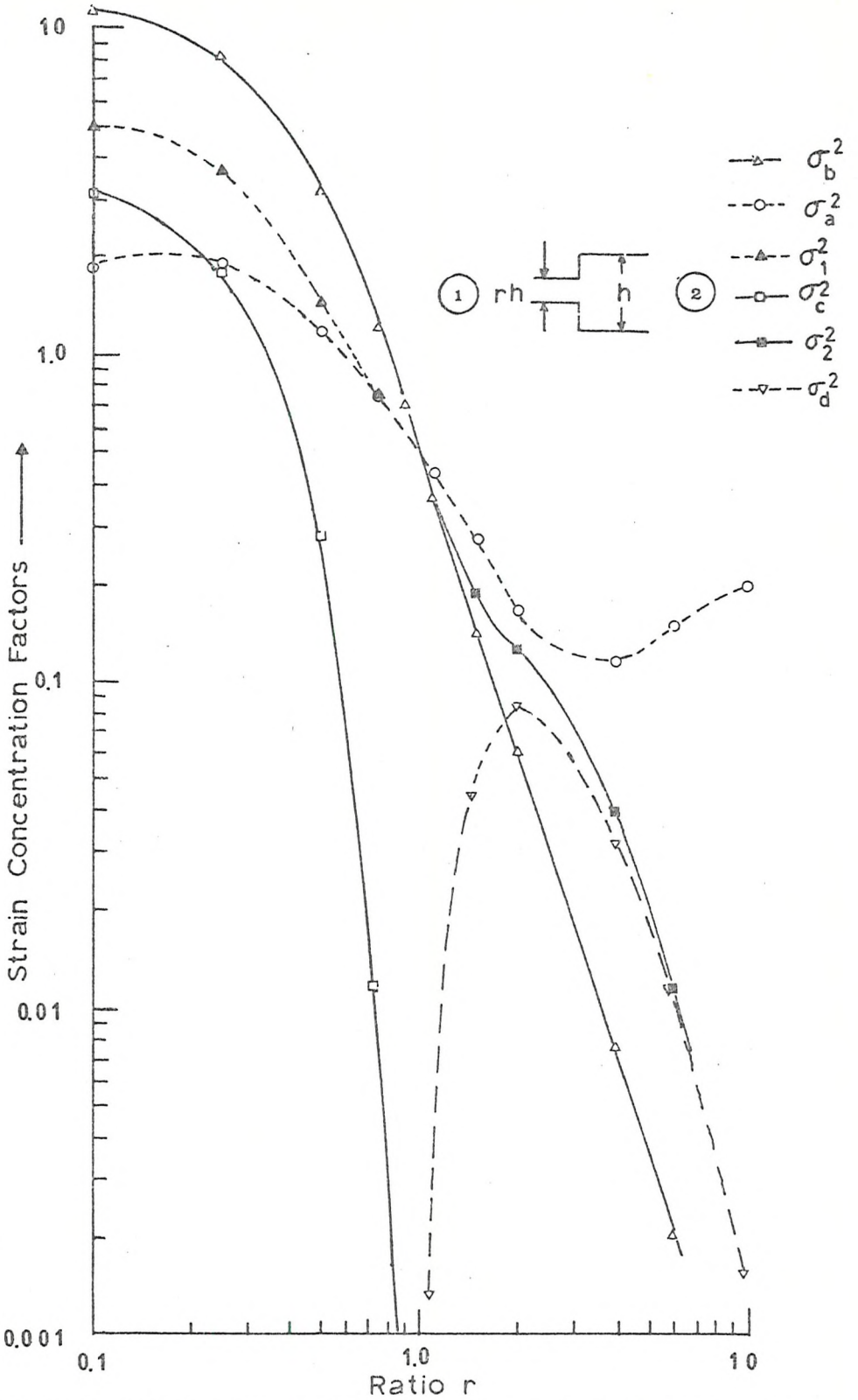

Figure 53 Strain Concentrations at a Change of Section

$\sigma_2^2 = \sigma_b^2$ = stress due to partially transmitted energy at values of $\frac{h_1}{h_2}$

Then the stress would be given by:-

$$\bar{\sigma}^2 = 100^2 \times 2.84 + 10^2 \times 6.46 \qquad 7.68$$

$$= 28640$$

$$\therefore \sigma_{r.m.s.} = 169 \text{ lbf/in}^2$$

On the thick side of the join the mean square stress will be:-

$$\bar{\sigma}^2 = 10\,\sigma_{1(4)}^2 + 100\,\sigma_{2(4)}^2 \qquad 7.69$$

where $\sigma_1^2 = \sigma_a^2$ = stress due to partially reflected energy

and where $\sigma_2^2 = \sigma_b^2 + \sigma_d^2$

and where σ_b^2 = stress due to partially transmitted waves.

σ_d^2 = stress due to totally reflected waves in the thin section.

$$\sigma^2 = 10^2 \times 0.025 + 100^2 \times 0.011 = 112.5 \quad \therefore \sigma = 10.6 \text{ lbf/in}^2 \qquad \ldots\ 7.70$$

Figure 53 is considered in exactly the same way.

We must next consider if these results are basically sensible. Do they seem reasonable in the light of our experience?

First we examine the result at a change of section of unity, i.e., no change. The stress concentration, and strain concentrations are 0.5 for both transmitted and reflected waves, i.e. there is no total stress or strain concentration. This is correct. Small departures from the uniform thickness condition introduce progressive rather than step changes in concentration factor. At very low values of r, where thin sections join very thick sections, the results suggest that high stresses and strains will be developed. This seems reasonable for the ultimate condition, the solid edge, generates high stresses (appendix VII).

At very high values of r, where thick sections are joined by very thin sections, the plate will behave as if free and the stresses near the edge will fall to zero. This is the trend indicated by Figure 52. The strain due to reflected waves is not shown as falling towards zero. At first sight this seems wrong, but this is not so.

The stress normal to the edge approaches zero if the edge becomes approximately free. Let ξ_{r_1} be the surface strain normal to edge, ξ_{r_2} along the edge. Then the stress normal to the edge

$$\sigma = \xi_{r_1} + \nu \xi_{r_2} \qquad 7.71$$

If there is curvature along the edge, which is so for any wave not normally incident and if the stress normal to the edge is to be zero,

then as $\xi_2 \neq 0$ then $\xi_1 \neq 0$. Thus one would expect that the strain normal to the edge would not approach zero. This is shown on Figure 53, at high values of r .

Figures 54 and 55 show the theoretical variation of mean square stress with angle of incidence. From this we may deduce likely variations from the diffuse field results if the incident field is not diffuse. In fact, as we see, the likely excursions above the diffuse field valve are small. From this we may deduce that even large departures from the diffuse field are unlikely to cause serious increases in stress above the average value.

At a few angles of incidence the stress is extremely low. However, from a design point of view this does not concern us.

From the magnitude of the transmitted or reflected travelling wave we can find the loss factor across the change of section; the energy loss per unit length over the energy incident. This is done in appendix XII. Whether we calculate the energy loss by measuring the reflected energy and subtracting it from the incident or by measuring the transmitted energy the results should be the same. It is, in fact, a further boundary condition, that of conservation of energy. This is also a useful check of the calculation of R and D and revealed no errors.

7.4. Experimental Tests

We have made assumptions about plane sections remaining plane and about the diffusiveness of given fields. We must now put them

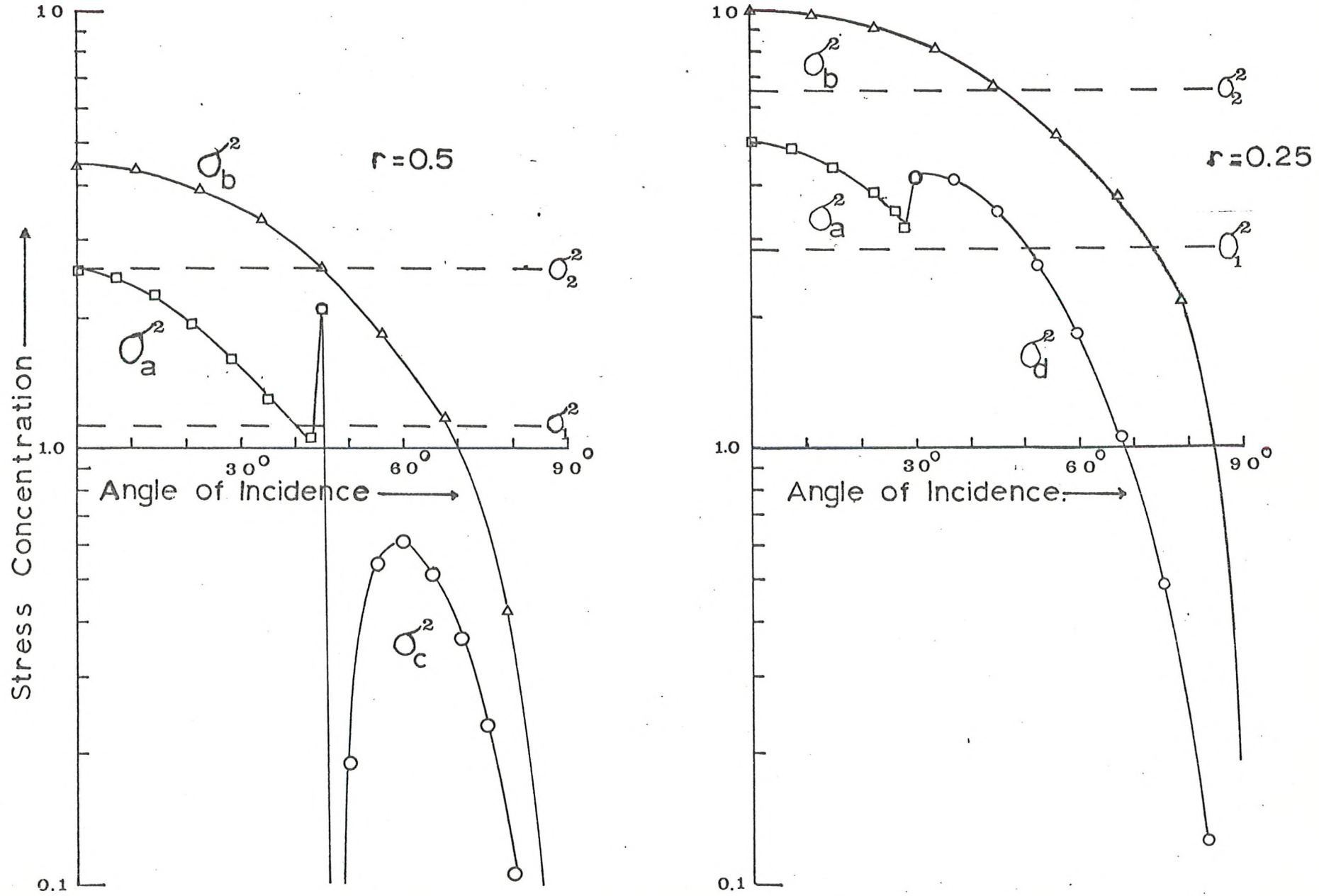

Figure 54 Stress Concentration vs. Angle of Incidence

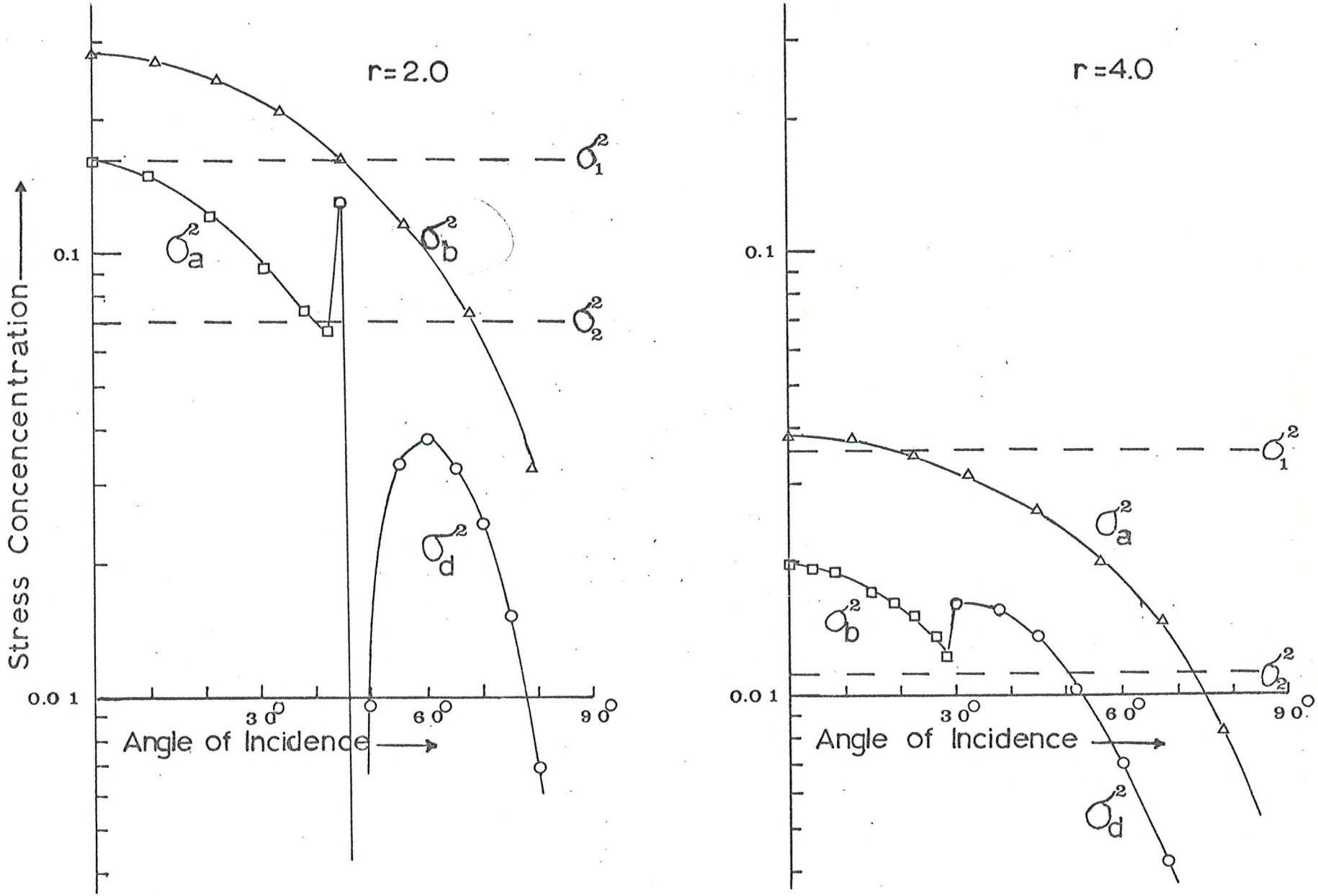

Figure 55 Stress Concentration vs Angle of Incidence

to the test to see if the theory agrees with practice and if our assumptions are justified.

7.4.1. Experimental Procedure

Three specimens were used; two incorporated a 4:1 change of section and the other a 2:1 change. Two specimens consisted of two aluminium plates 4 feet by 3 feet joined to make a specimen 8 feet by 3 feet. The thick section was $\frac{1}{4}$ inch and the thin sections either $\frac{1}{8}$ inch and $\frac{1}{4}$ inch. Of these, the 4:1 specimen is shown in position hung in a reverberant room in Figure 56. The 2:1 specimen was similarly mounted. The other was a small steel specimen made up of two plates $\frac{1}{4}$ inch and $\frac{1}{16}$ inch thick is shown in Figure 57. This was supported by wires from a light frame.

The plates were joined by milling a slot in the edge of the thick plate and fixing the thin plate into the slot with epoxy resin. The slot and thin plate were a good fit and the resulting join was considered very satisfactory. All the joins were inspected visually and the small specimen was also tested experimentally. We would call a join good if there was no relative movement between the two plates. Since the layer of epoxy resin was very thin between the two surfaces any relative movement between them must represent a failure in the band, a rubbing would occur. This rubbing would be associated with a higher loss of energy. To test this the reverberation time of the plates was measured, the rate of decay of the response to a loudspeaker after it was turned off. This was then

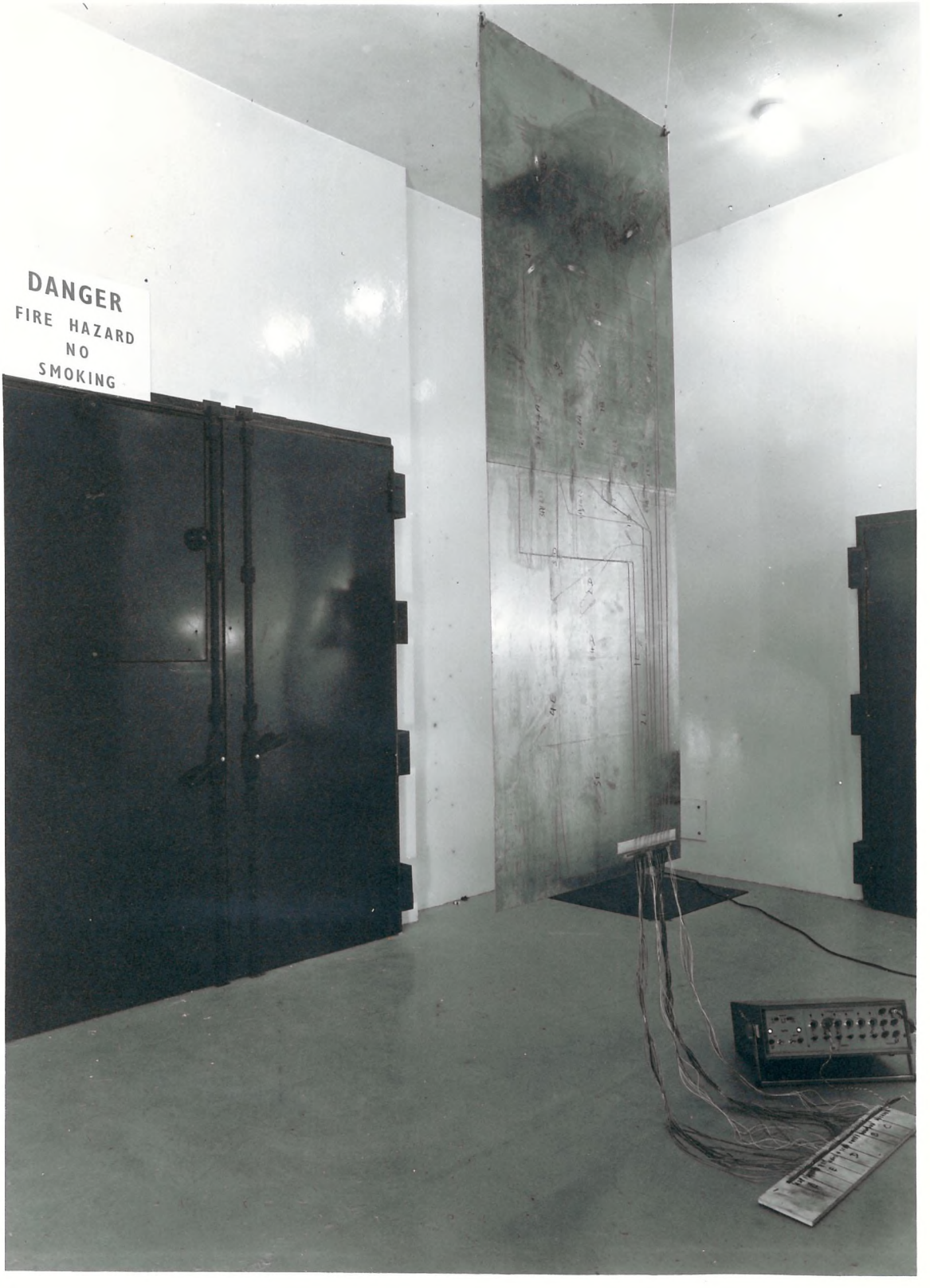

Figure 56 Large 4:1 Change of Section Specimen.

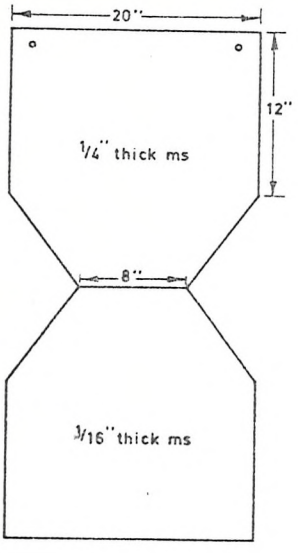

Fig.57 The small 4:1 change of section specimen

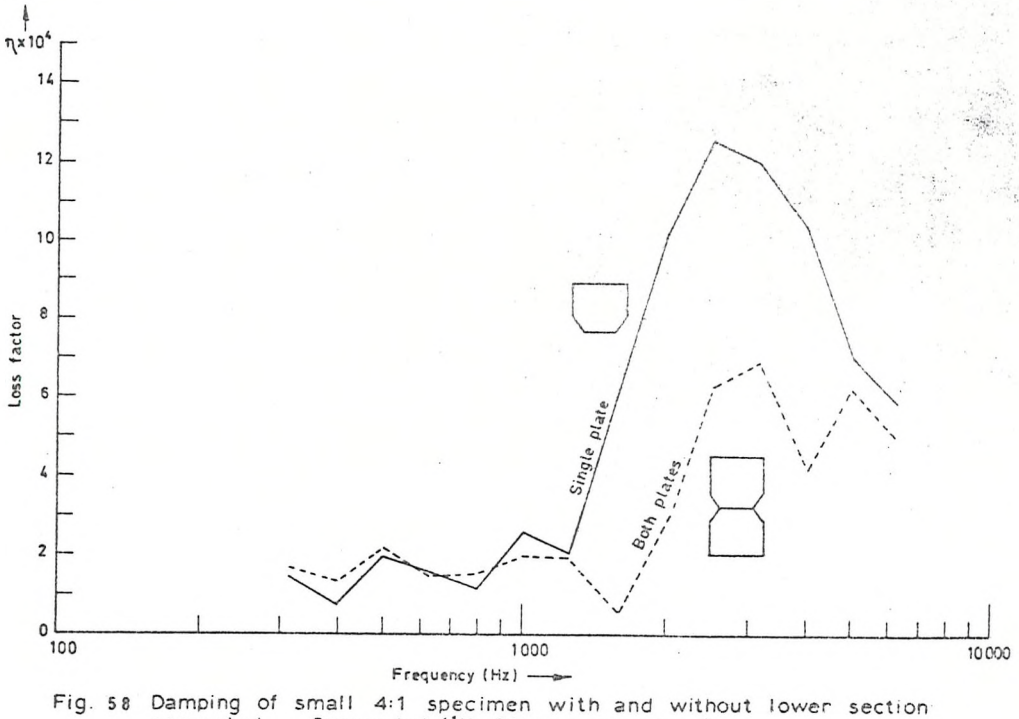

Fig. 58 Damping of small 4:1 specimen with and without lower section connected. Suspended (1/3 OB measurements)

interpreted as a loss factor. Figure 58 shows the total loss factor of both the single $\frac{1}{4}$ inch plate and the two joined plates as a function of frequency. Notice that there is no increase of damping of any significance on joining. Even the slightest loss due to chaffing would have produced a very large increase. The reduction in loss factor at high frequency, when the thinner plate is added on, is doubtless due to the reduced radiation from the thinner panel[9].

When measuring the strain concentration the specimens were all excited acoustically. The small specimen was excited by a loudspeaker driven by white noise from a power amplifier. Both the large specimens were excited by the sound generated by high pressure air escaping from a gate valve in a reverberant room. The large 4:1 specimen was also separately excited by white noise from a loudspeaker.

The strains were measured by semi-conductor gauges distributed as shown in Table 2 below. The gauges measuring the main stresses in each plate were scattered at random over the surface. The strain at the edge was estimated by fixing three gauges in line perpendicular to the change of section. The strain at the edge was then joined by fitting an exponential curve to the results by a least square fit routine and extrapolating this curve to the boundary. Sometimes this was not reasonable and then the result from the nearest gauge to the edge was taken as the strain at the edge.

The outputs were analysed in third octave frequency bands.

TABLE 2

Distribution of Strain Gauges on Change of Section Specimens

Specimen	Number of Gauges			
	Mean Thick	Mean Thin	Thick Edge	Thin Edge
Small 4:1	10	6	3 x 3	3 x 3
Large 4:1	8	8	4 x 3	4 x 3
Large 2:1	8	8	4 x 3	4 x 3

7.4.2. Experimental Results

When examining the stresses at the 4:1 change of section extrapolation technique was much more successful than it had been when applied to the welded joint (6.4.1). The strain concentrations were much greater and it was in general easier to separate them from the background level. Figure 59 shows two typically good fits. The extrapolation seems entirely reasonable. There were, however, some occasions where the technique failed, as shown in Figure 60. This was a far less frequent occasion.

The strain concentrations are presented in Figures 61 and 62 as the ratio of the actual r.m.s. strain and the predicted r.m.s. strain plotted against the theoretical number of modes available in the thinner plate in each frequency band.

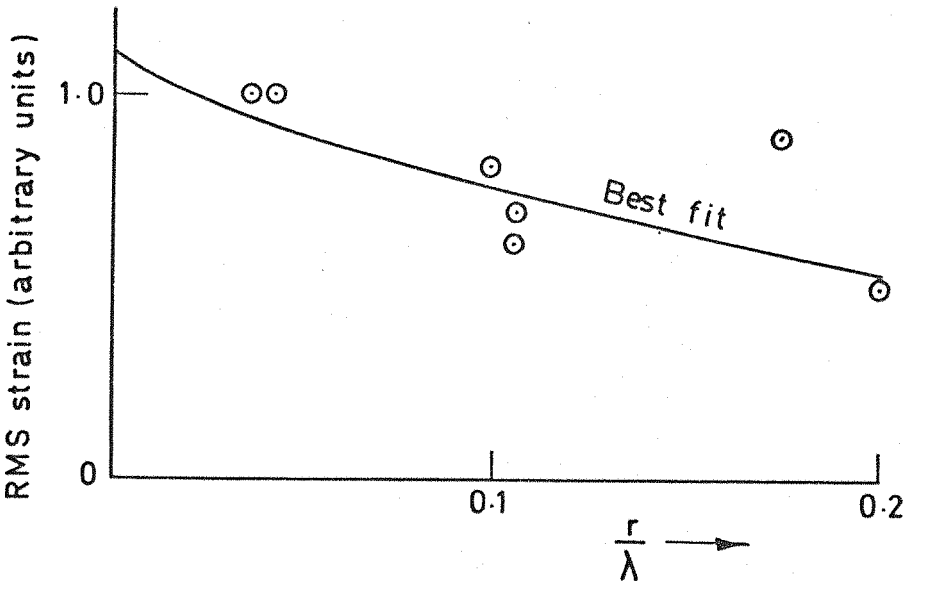

Fig. 59a Small specimen. 4:1 change of section. 2500 Hz 1/3 OB. Thick edge. Good fit by least square method of exponential curve.

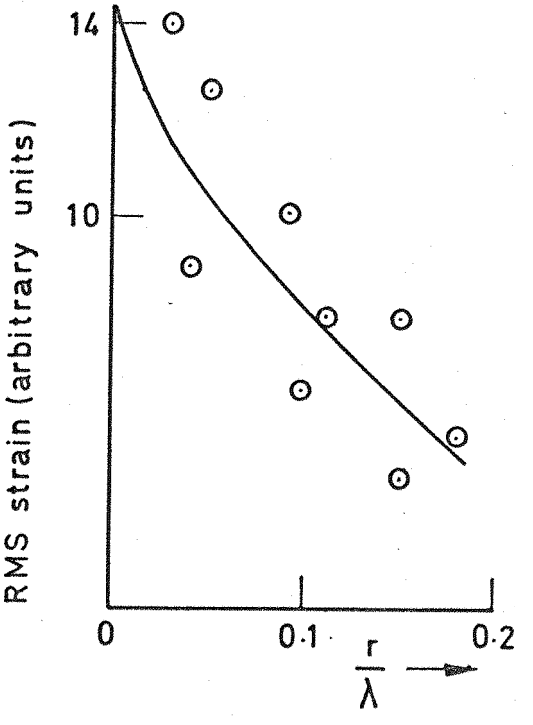

Fig. 59b Small specimen. 4:1 change of section. 400 Hz 1/3 OB. Thin edge. Good fit by least square method of exponential curve.

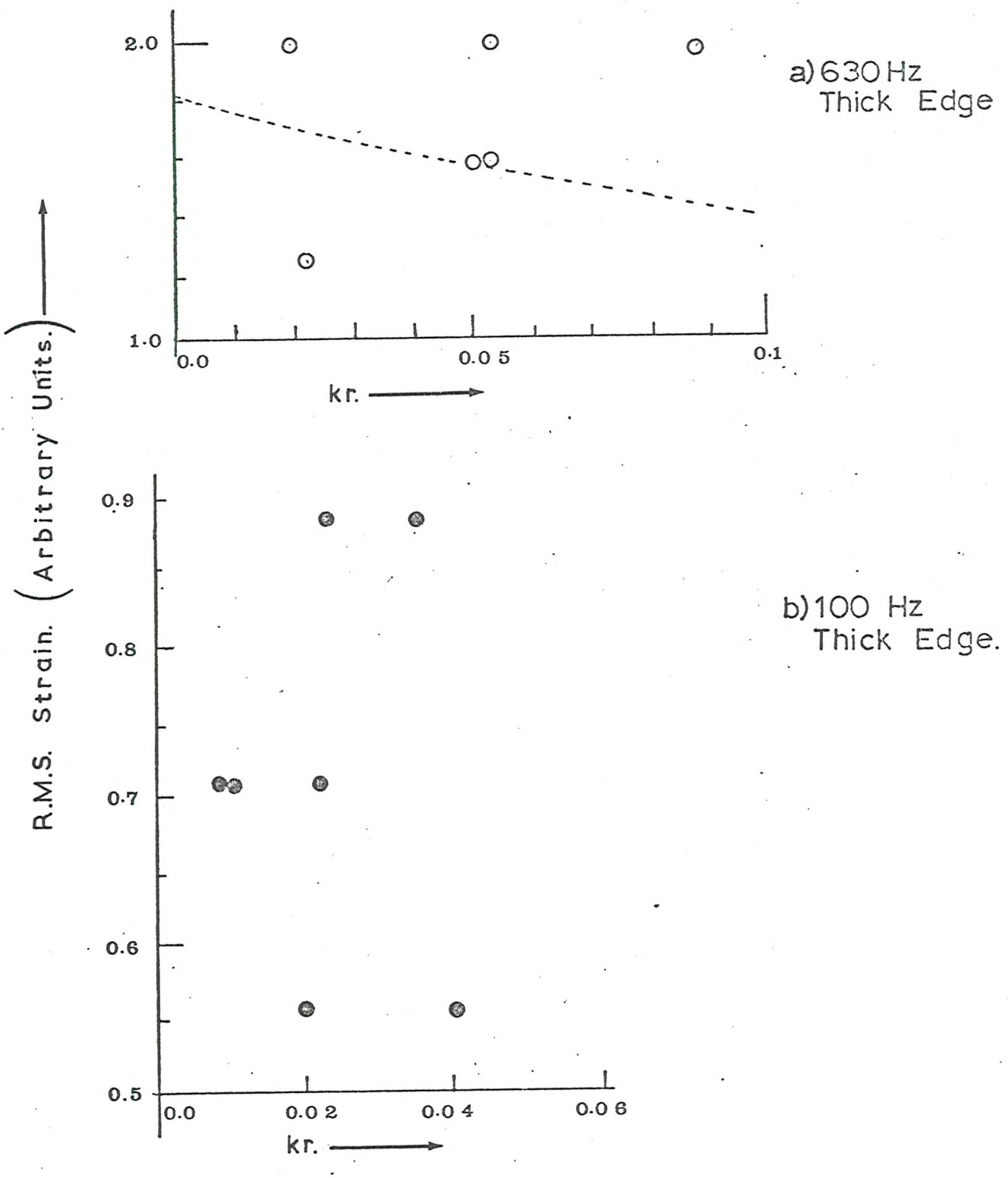

Figure 60 4:1 Change of Section Small Specimen
Good Extrapolation Not Possible

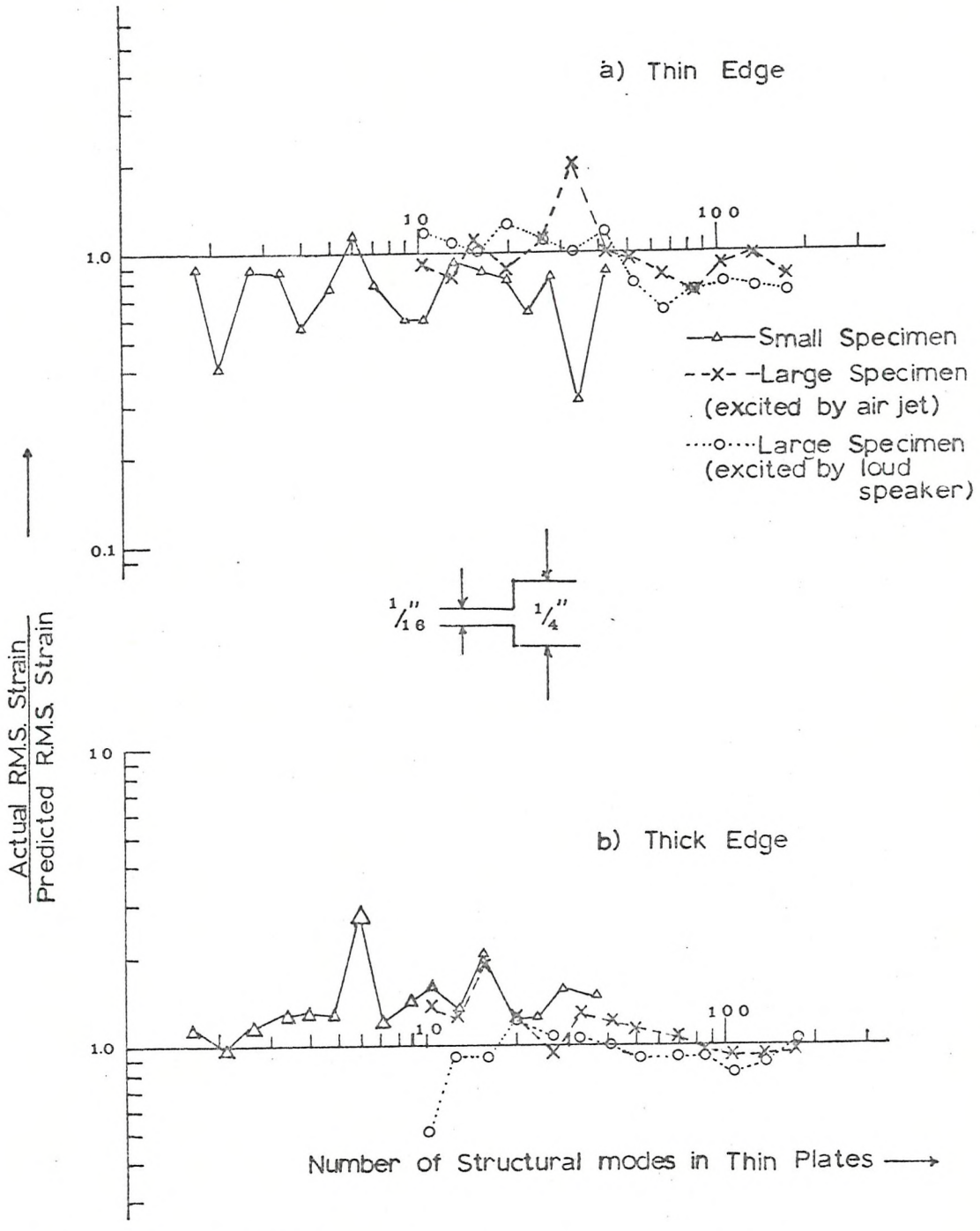

Figure 61 Strain Measured at a 4:1 Change of Section.

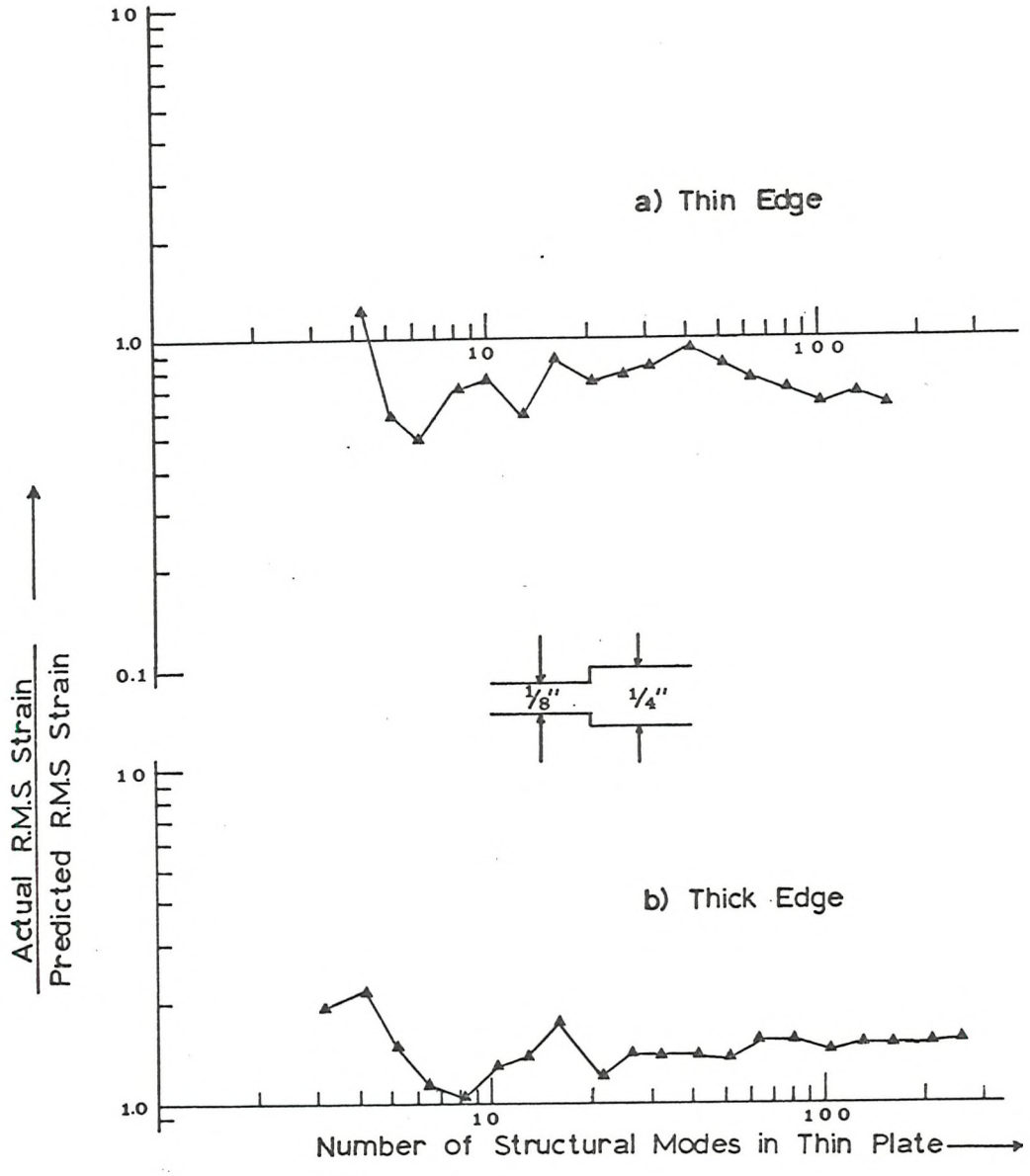

Figure 62 Strain Measured at a 2:1 Change of Section.

7.4.3. Discussion of Results

The results for the 4:1 concentration are uniformly good. There are a few digressions but none of these is very marked. Even with very few modes available, the results are close to the predicted values.

At first sight it might seem strange to quote the results along the thick edge in terms of the modes available in the thin section. However, in these experiments, the thick panels had much lower mean square strains than the thin panels and, as calculated from Figure 53, the strain in the thick edge was controlled by the strain in the thin panel rather than in the thick. The calculation in section 7.3.2. of this chapter was fairly typical.

The results for the 2:1 change of section are at first sight less satisfactory. The expected fall and rise in strain towards the thick and thin section edges were not found. In fact, this is hardly surprising for the strain concentrations expected are much less than those of the 4:1 change of section. This was not discernable above the mean level in the plate and certainly the extrapolations were not very satisfactory. No change of strain was detected near the change of section. We will discuss this at greater length in the last chapter.

7.5. Conclusions on Chapters 6 and 7

These chapters consider two very similar problems in the same

way by using the diffuse field model. However, it has been a rather long business and it is useful to summarise what we have achieved.

By studying the behaviour of a bending wave reaching a weld and a change of section we have been able to find the magnitude of the resulting reflected and transmitted travelling and decaying waves. From this we have deduced the mean square stress caused by a wave from one given direction. Then by invoking the diffuse field model, of bending of random phase travelling from every direction, we have deduced the stress likely at the join compared to the mean square stress elsewhere in the structure.

We have also deduced similar results for strain and have tested these results experimentally. We have found that in theory a typical butt weld is unlikely to cause a large strain concentration and have proved this experimentally. We have also predicted that small changes of section, i.e. 2:1, are also unlikely to produce large strain concentrations and we have shown this in practice. However, the strain concentration rises sharply as the change of section increases, and at 4:1 can be large. We have shown this experimentally.

Looking at the experimental results (Figures 61 and 62), there seems to be no dependence on the number of available modes, or wave directions. However, as more modes are available departures from the predicted diffuse field values are less common. In any case, there are no serious excursions upwards from the

predicted values. A factor of 2 would include almost all of them, however small the theoretical number of available modes.

Thus we may reasonably conclude that the diffuse field model adequately predicts stress and strain concentrations even if very few modes are available. We do not require the more stringent conditions suggested by the formal tests of the diffuse field model described in Chapter 4.

CHAPTER 8

Stress Distribution in the Mid-Structure Regions

Let us assume that we are able to make an estimate of the time and space averaged mean square velocity of a structure in response to a particular excitation by use of the statistical energy method[3]. From Chapter 5 we may then estimate the resulting time and space averaged mean square strains and stresses, noting that this result applies whether many modes are excited or only one[5]. From the criterion suggested in Chapter 4 we can decide whether or not the resulting bending wave field is diffuse. If so, then from Chapters 6 and 7, we can deduce the strain and stress concentrations likely at any butt welds or changes of section.

Now we must decide whether or not such concentrations of stress are significant compared to the variations in stress to be expected in the mid-structure regions, away from any such discontinuities. To do this we need some estimate of the distribution of local time averaged mean square stress about the structure's time and space averaged mean square stress.

From the discussion in Chapter 3 we conclude that the travelling wave model is less likely to be satisfactory than the normal mode model because we are now dealing with a property that affects the whole plate, not just localised areas. We will try to determine the variation in stress over the structure from the statistics of the sum of many normal modes.

8.1. Derivation of Mean Square Stress in a Flat Plate with Arbitrary Boundary Conditions

Starting generally we may write the response of our system as:

$$z(x,y,t)=\sum_{\alpha}^{N}\psi_{\alpha}(x,y)\,\zeta_{\alpha}(t) \qquad 8.1.$$

where $z(x,y,t)$ = displacement at x, y at time t.

$\zeta_{\alpha}(t)$ is the generalised displacement of mode α

$\psi_{\alpha}(x,y)$ is the normalised mode shape of mode α

Bolotin[28] shows that at frequencies high compared with the fundamental frequency, flat structures behave like simply supported plates away from their boundaries. The nodal lines are displaced by amounts which depend on the wave number of a particular mode and the end fixity of the boundaries of the plate. Considering first the response of a simply supported plate, we may write:-

$$z(x,y,t)=\sum_{\alpha}^{N}\sin\left(\frac{m\pi x}{a}\right)\sin\left(\frac{n\pi y}{b}\right)\zeta_{\alpha}(t) \qquad 8.2.$$

a and b are the plate dimensions in the x and y directions. $\frac{m\pi}{a}$ and $\frac{n\pi}{b}$ are the wave numbers given by:-

$$\left(\frac{m\pi}{a}\right)^2+\left(\frac{n\pi}{b}\right)^2=\left(\frac{\omega_{\alpha}}{C_B}\right)^2 \qquad 8.3.$$

where ω_{α} is the natural frequency of mode α and C_B is the speed of bending

waves at this frequency.

For these simple mode shapes the principal stresses lie along the x and y axes and the stress σ at x, y at angle θ to the x axis is given by

$$\sigma(x,y,t,\theta) = \frac{-Eh}{4(1-\nu^2)}\frac{\partial^2 z}{\partial x^2}(1+\cos.2\theta+\nu(1-\cos 2\theta))$$

$$+\frac{\partial^2 z}{\partial x^2}(1-\cos.2\theta+\nu(1+\cos.2\theta))$$

$$= \frac{-Eh}{4(1-\nu^2)}\sum \sin.\left(\frac{m\pi x}{a}\right)\sin\left(\frac{n\pi y}{b}\right)\left\{(1+\nu)\left[\left(\frac{m\pi}{a}\right)^2+\left(\frac{n\pi}{b}\right)^2\right]\right.$$

$$\left.+(1-\nu)\cos.2\theta.\left[\left(\frac{m\pi}{a}\right)^2-\left(\frac{n\pi}{b}\right)^2\right]\right\}\zeta_\alpha(t)$$

----------8.4.

From Figure 63 the wavenumber diagram for a simply supported plate, we may deduce that

$$\left(\frac{m\pi}{a}\right)^2-\left(\frac{n\pi}{b}\right)^2 = k_\alpha^2\cos 2\phi_\alpha \qquad 8.5.$$

where ϕ_α is the argument of the wavenumber vector of mode α.

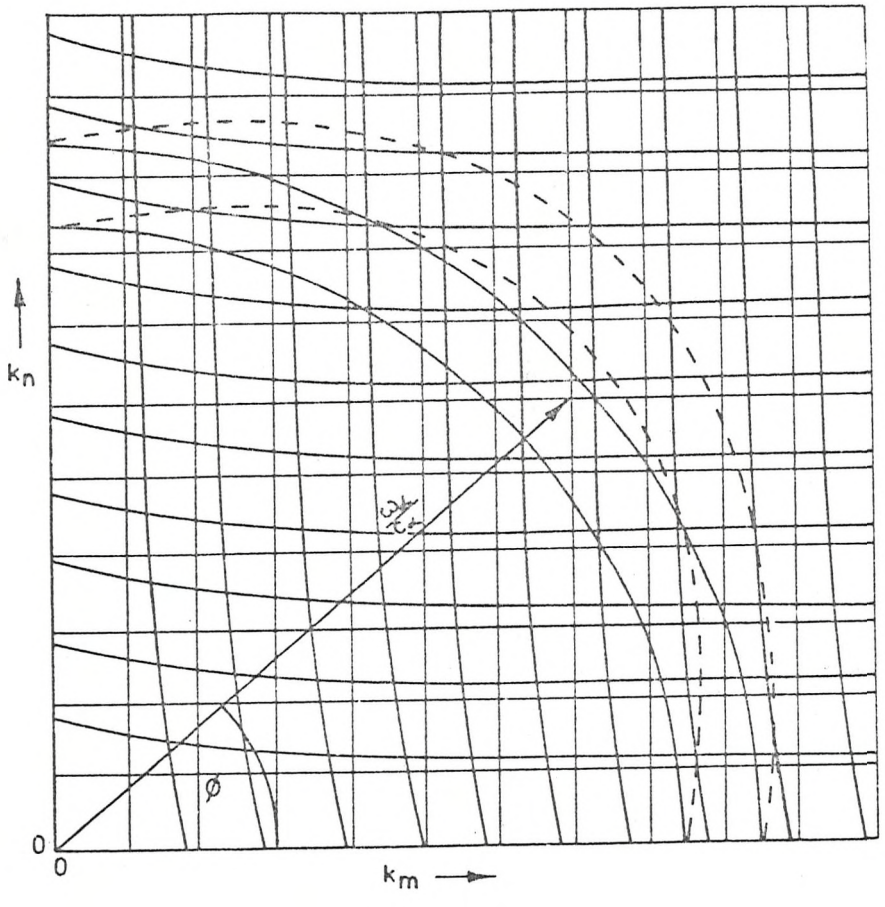

$$k_m^2 + k_n^2 = \left(\frac{\omega_\alpha}{c_\alpha}\right)^2$$

$$k_m = \frac{\omega_\alpha}{c_\alpha} \cos\phi \qquad k_n = \frac{\omega_\alpha}{c_\alpha} \sin\phi$$

$$k_m^2 - k_n^2 = \left(\frac{\omega_\alpha}{c_\alpha}\right)^2 \left[\cos^2\phi - \sin^2\phi\right]$$

$$= \left(\frac{\omega_\alpha}{c_\alpha}\right)^2 \left[\cos 2\phi\right]$$

The circle and rectangular grid correspond to the simple supports, the dashed line and offset grid to the clamped plate.

Fig.63 Wave number space for a simply supported plate showing possible shift due to boundary.

If we restrict the analysis to third octave, (23%), frequency bands, since k_α is proportional to $1/\sqrt{\omega_\alpha}$, k will vary by no more than 6% from its mean value. Thus, we may replace k_α by a constant k .

To proceed with this analysis we must also assume that the response of each mode within a given frequency band is approximately the same. Without experimental evidence it is not possible to judge the effect of the accuracy of this assumption on the results of the analysis. However, from the experimental tests, described later, we may conclude that the accuracy of the assumption is not critical.

If we assume that the modal responses are statistically independent, (i.e. that their time averaged cross products at a point are small compared with their mean squares), then we may write:-

$$\overline{\sigma^2}(x,y,\theta) = \left[\frac{E\,h\,k^2}{4(1-\nu^2)}\right] \zeta(t) \sum \sin\left(\frac{m\pi x}{a}\right) \sin\left(\frac{n\pi y}{b}\right) * \left[(1+\nu)+(1-\nu)\cos.2\theta\cos.2\phi\right] \qquad 8.6.$$

The bar indicates a time average.

This further assumption implies that modes are separated in frequency by frequency bands greater than their half-power bandwidths.

In the experimental tests this condition was not always fulfilled, but it had little effect on the results obtained. This is discussed in more detail in section 5.

For a rigidly clamped boundary, we may deduce from (28) that a more accurate description of the variation in the direction is given by:-

$$\sin\left[k_1 x + 2\tan^{-1}\left\{\frac{k_1}{\sqrt{k_1^2 + 2k_2^2}}\right\}\right] \qquad 8.7.$$

k is the wavenumber in the x direction and k in the y direction.

In practice no boundary is either rigid, or a simple support. It lies, in stiffness, at some indeterminable value between these two extremes. So instead of trying to preserve a degree of accuracy in our analysis quite out of keeping with the data available to us, we assume that the displacement of the nodal lines induced by a set of practical boundary conditions is a random function depending on the modal wavenumber. This then implies that $\frac{m\pi x}{a}$ and $\frac{n\pi y}{b}$, in the expression for $\overline{\sigma}^2$, should be treated as random variables.

For such systems the form of the wavenumber diagram will be changed as described by Bolotin[17] and as depicted in Figure 64. Although individual modes will have slightly differing eigenvectors,

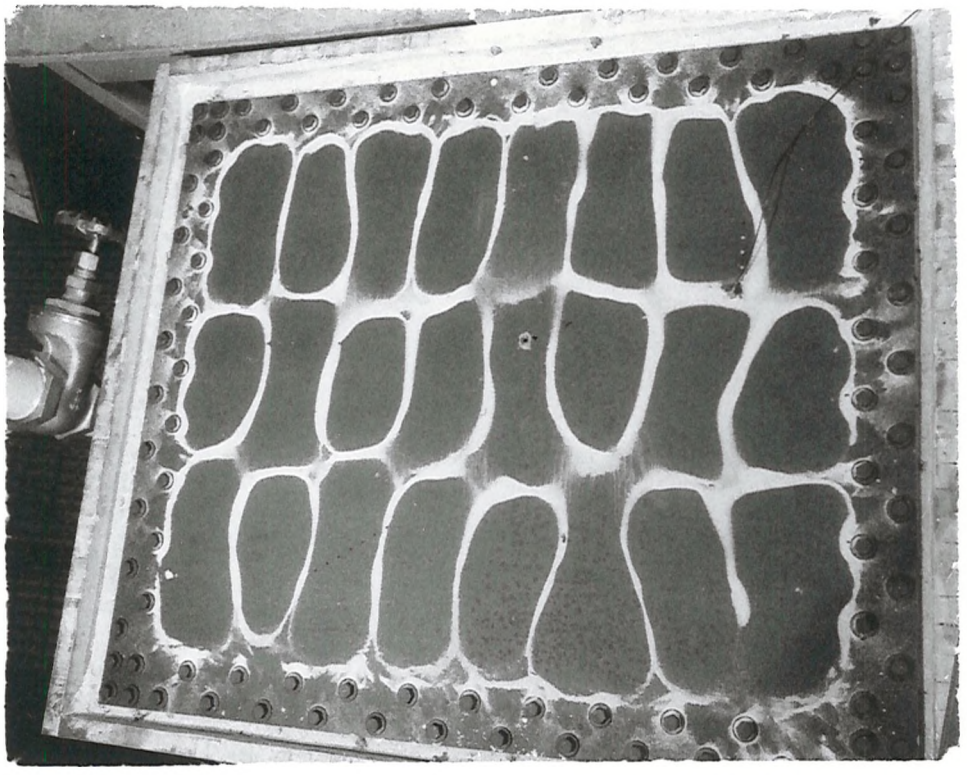

a) 945 Hz

b) 1330 Hz

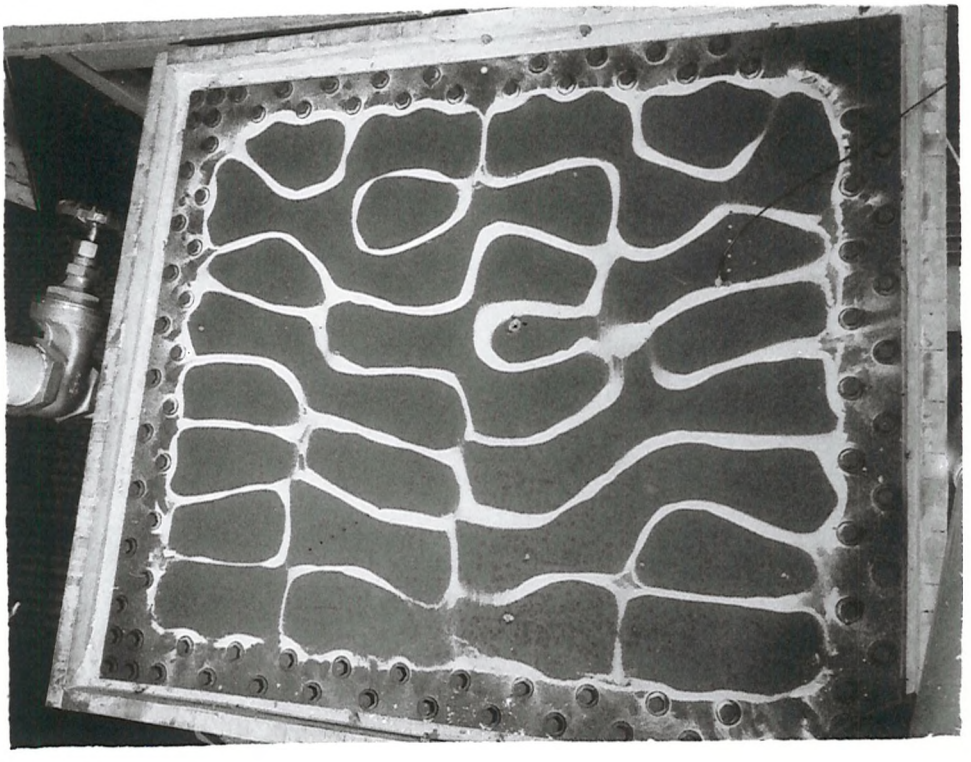

Figure 64 High Order Modes of 1/8 in Plate.

the total number of modes in a frequency band is likely to stay the same. However, the value of ϕ_α is not, in practice, determinable in advance for any particular mode and it is reasonable to consider that ϕ_α is a random function of mode number.

If we examine the behaviour of actual panels excited in their individual normal modes, we find that the principal axes of stress are not necessarily along the x, y axes due to small irregularities of shape and boundary stiffness.

Figure 64 shows two higher order modes of the $\frac{1}{8}$ inch plate used in the experiments described in section 8.3. The plate was excited at a resonance and sand was distributed over its surface. The position of the sand indicates the nodal lines of the structural mode. As can be seen, at 945 Hz, the nodal pattern is fairly regular, and the principal axis of stress would lie, in general, parallel to the edges of the plate. However, at 1330 Hz this is not so. The pattern is irregular, as is more often the case, and the direction of the principal axes of stress no longer lie parallel to the edges of the plate.

It is thus more realistic to replace θ by $\theta + \gamma_\alpha$ where γ_α represents the angle between the x axis and one of the principal axes of stress for mode α. As we are unable to predict individual values of γ_α at the design stage, we must treat $\theta + \gamma_\alpha$ as a random variable depending on the mode number.

8.2. Statistics of Mean Square Stress

First we will determine the mean square stress in a flat plate, averaged over space, and then deduce its likely variation over the structure.

8.2.1. Determination of Spatial Mean Square Stress

From expression (4)

$$\bar{\sigma}^2(x,y,\theta) = \left(\frac{Ehk^2}{4(1-\nu^2)}\right)^2 \overline{\zeta(t)}^2 \sum_{\alpha}^{N} \sin^2\frac{m\pi x}{a} \sin^2\frac{n\pi y}{b} (1+\nu)^2 + \qquad 8.8.$$

$$2(1-\nu^2)\cos 2\theta \cos 2\phi_\alpha + (1-\nu)^2 \cos^2 2\theta \cos^2 2\phi_\alpha$$

Let

$$\frac{Ehk^2}{4(1-\nu^2)} \overline{\zeta(t)}^2 = K \qquad 8.9.$$

Suppose that N modes are excited then

$$\langle \bar{\sigma}^2 \rangle = \int_0^a \int_0^b \int_0^{2\pi} \bar{\sigma}^2(x, y, \theta)\, dx.\, dy.\, d\theta \qquad 8.10a.$$

$$= K \sum_{\alpha=1}^{N} \left[(1+\nu)^2 + \tfrac{1}{2}(1-\nu)^2 \cos^2 2\phi_\alpha \right] \qquad 8.10b.$$

$$= K \sum_{\alpha=1}^{N} \left[(1+\nu)^2 + \tfrac{1}{4}(1-\nu)^2 (1 + \cos.4\phi_\alpha) \right] \qquad 8.10c.$$

where the pointed brackets, $\langle \ \rangle$, indicate a space average.

Assuming that all values of 4 are equally likely, from 0 to 2, then taking the average value for all the modes :-

$$\langle \bar{\sigma}^2 \rangle = N K \left((1+\nu)^2 + \tfrac{1}{4}(1-\nu)^2 \right) \qquad 8.11.$$

8.2.2. Probability Distribution of Mean Square Stress in Space

M. Slack[43] has shown that if ten or more cosines of equal amplitude, but random phase, are added together, then the instantaneous sum is a Gaussion variable. The standard deviation is given by $\zeta \frac{N}{2}$, where ζ is the amplitude of each cosine term and there are N such terms. In order to use this result we must

expand $\overline{\sigma^2}$ to the form of sines and cosines.

Thus we write:-

$$\overline{\sigma^2} = K\Big\{\sum(1+\nu)^2 - \sum\cos 2A\left[(1+\nu)^2 + \frac{(1-\nu)^2}{4}\right] - \sum\cos 2B \left[(1+\nu)^2 + \frac{(1-\nu)^2}{4}\right] + (1-\nu)^2\left[\sum\cos 2F + \sum\cos 2G\right]$$

$$+\left[\frac{(1+\nu)^{\frac{1}{2}}}{2} + \frac{(1-\nu)^2}{8}\right]\left[\sum\cos 2(A+B) + \sum\cos 2(A-B)\right]$$

$$-\frac{(1-\nu^2)}{2}\left[\sum\cos 2(A+F) + \sum\cos 2(B+F) + \sum\cos 2(A+G)\right.$$

$$\left. + \sum\cos 2(B+G) + \sum\cos 2(A-F) + \sum\cos 2(B-F) + \sum\cos 2(A-G)\right.$$

$$\left. + \sum\cos 2(B-G)\right] + \frac{(1-\nu^2)}{4}\left[\sum\cos 2(A+B+F) + \sum\cos 2(A+B-F)\right.$$

$$\left. + \sum\cos 2(A-B+F) + \sum\cos 2(A-B-F) + \sum\cos 2(A+B+G)\right.$$

$$\left. + \sum\cos 2(A+B-G) + \sum\cos 2(A+B+G) + \sum\cos 2(A-B-G)\right]$$

$$+\frac{(1-\nu)^2}{4}\left[1 + \sum\cos 4(F+G) + \sum\cos 4(F-G) + \sum\cos 4G + \sum\cos 4F\right.$$

$$+\tfrac{1}{2}\sum\cos\left[4(F+G) + 2(A+B)\right] - \tfrac{1}{2}\sum\cos\left[4(F+G) - 2(A+B)\right]$$
$$-\tfrac{1}{2}\sum\cos\left[4(F+G) + 2(A-B)\right] - \tfrac{1}{2}\sum\cos\left[4(F+G) - 2(A-B)\right]$$
$$+\tfrac{1}{4}\sum\cos\left[4(F+G) + 2A\right] + \tfrac{1}{4}\sum\cos\left[4(F+G) - 2A\right]$$
$$+\tfrac{1}{4}\sum\cos\left[4(F+G) + 2B\right] + \tfrac{1}{4}\sum\cos\left[4(F+G) - 2B\right]$$
$$+\tfrac{1}{2}\sum\cos\left[4(F-G) + 2(A+B)\right] + \tfrac{1}{2}\sum\cos\left[4(F-G) - 2(A+B)\right]$$
$$+\tfrac{1}{2}\sum\cos\left[4(F-G) + 2(A-B)\right] + \tfrac{1}{2}\sum\cos\left[4(F-G) - 2(A-B)\right]$$
$$+\tfrac{1}{4}\sum\cos\left[4(F-G) + 2B\right] + \tfrac{1}{4}\sum\cos\left[4(F-G) - 2B\right]$$

$$
\begin{aligned}
&+\tfrac{1}{4}\sum\cos\left[4(F-G)+2A\right]+\tfrac{1}{4}\sum\cos\left[4(F-G)-2A\right]\\
&-\tfrac{1}{4}\sum\cos\left(2A+4F\right)-\tfrac{1}{4}\sum\cos\left(2A-4F\right)\\
&-\tfrac{1}{4}\sum\cos\left(2A+4G\right)-\tfrac{1}{4}\sum\cos\left(2A-4G\right)\\
&-\tfrac{1}{4}\sum\cos\left(2B+4F\right)-\tfrac{1}{4}\sum\cos\left(2B-4F\right)\\
&-\tfrac{1}{4}\sum\cos\left(2B+4G\right)-\tfrac{1}{4}\sum\cos\left(2B-4G\right)\\
&+\tfrac{1}{8}\left\{\left[\begin{array}{ll}\sum\cos\left(4G+2(A+B)\right) & +\sum\cos\left(4G-2(A+B)\right)\\ \sum\cos\left(4G+2(A-B)\right) & +\sum\cos\left(4G-2(A-B)\right)\\ \sum\cos\left(4F+2(A+B)\right) & +\sum\cos\left(4F-2(A+B)\right)\\ \sum\cos\left(4F+2(A-B)\right) & +\sum\cos\left(4G-2(A-B)\right)\end{array}\right]\right\}
\end{aligned}
\qquad 8.12
$$

where $A=\frac{m\pi x}{a}$, $B=\frac{n\pi y}{b}$, $F=(\theta+\gamma_\alpha)+\phi_\alpha$, $G=(\theta+\gamma_\alpha)-\phi_\alpha$

Expression 8.7 contains 58 summations of cosines, but we have only four independent variables. No amount of manipulation will reduce the 58 terms to 4 sums of cosines, and the best we can do is to estimate the extreme values of standard deviation. We find the highest estimate by assuming that all the terms act as if they were independent, and the lowest reasonable estimate by assuming that only the four largest terms contribute significantly to the total. Let the variation of mean square stress be the standard deviation divided by the mean. We denote the variation by V. Then the maximum value of V is obtained by considering only the terms cos 2A, cos 2B, cos aF and cos 2C, and is:-

$$\frac{3(1+\nu)^2 + 8(1-\nu^2) + \frac{15}{4}(1-\nu)^2}{\sqrt{2N\left[(1+\nu)^2 + \frac{1}{4}(1-\nu)^2\right]}} \qquad 8.13a.$$

The minimum value is:-

$$\sqrt{\frac{2}{N}}\left[\frac{(1+\nu)^2 + (1-\nu^2) + \frac{1}{4}(1-\nu)^2}{(1+\nu)^2 + \frac{1}{4}(1-\nu)^2}\right] \qquad 8.13b.$$

Putting $\nu = 0.3$, a typical value for many engineering materials, we obtain the simple result that

$$\frac{2.11}{\sqrt{N}} < V < \frac{5.51}{\sqrt{N}} \qquad 8.14.$$

We have deduced that values of mean square stress, measured over the plate, will have a Gaussion distribution; but we may not deduce that very large values are likely. Analysis of the extreme values of stress is only possible, as yet, when one mode is excited (5), or when many modes may be excited at one frequency (6).

We now briefly consider the effect of curvature on the results, since many engineering structures are curved. The effect of plate curvature on the wavenumber diagram is shown in Figure 33, for a

circular cylinder (34) ϕ is restricted below the ring frequency, $C_L/\pi D$, where C_L is the longitudinal wave speed and D the cylinder diameter. Above that frequency ϕ can have any value, and the previously derived results should hold. Below the ring frequency, despite the fact that ϕ is restricted in range, the results should still hold. In expression 8.7 the variables are $\theta + \phi$ and $\theta - \phi$ and if θ is unrestricted and ϕ is permitted some variation (i.e. not sensibly constant) then there are still four independent variables. Of course if the range of ϕ becomes very restricted at frequencies well below the ring frequency, then $\theta + \phi$ approaches $\theta - \phi$ for all conditions and there will only be three independent variables. The expression will become invalid. For the cylinder described in section 8.3. at 300 Hz, ϕ may lie from $+35^\circ$ to 0° and $\theta + \phi$ may thus be very different from $\theta - \phi$. At this frequency the cylinder's response to acoustic noise was very low as this frequency is well below the critical frequency of the cylinder, where the bending wave speed equals the acoustic compressive wave speed. The ability of the cylinder to receive acoustic energy under these conditions is low. A fuller description of this phenomena, which is beyond the scope of the present work, is given in (4). Suffice it to say that at all frequencies of interest to us, for this cylinder, the results of this chapter are applicable.

A similar analysis for strain and acceleration gives the following results in terms of numbers of modes involved

TABLE 3

Standard Deviation/Average Mean Square

	Upper Bound	Lower Bound
Strain	$\frac{8.35}{\sqrt{N}}$	$\frac{2.54}{\sqrt{N}}$
Acceleration	$\frac{3}{2}\sqrt{\frac{2}{N}}$	$\sqrt{\frac{2}{N}}$

The results for strain may be simply obtained by putting Poisson's ratio equal to zero. Strictly, equation 8.3 should be replaced by

$$\xi(x\,y\,\theta\,t) = \frac{h}{2}\left[\frac{\partial^2 z}{\partial x^2}(1+\cos.2\theta) + \frac{\partial^2 z}{\partial y^2}(1-\cos.2\theta)\right] \qquad 8.15$$

and the analysis repeated.

The derivation for acceleration is briefly described in appendix XII

The variation in strain is predicted as being greater than that for acceleration. This would agree with the physics of the

the situation, for whilst a strain gauge is sensitive to the direction of a given bending wave, an accelerometer is not. One would therefore expect more variation from a strain gauge for a finite number of wave directions.

8.3. Experimental Tests

To verify the analysis and investigate the relative importance of some of the assumptions made in the theory, the spatial variation, V, of mean square acceleration and strain was measured on some laboratory structures, excited in broad frequency bands, either acoustically or mechanically at a point.

The results shown in Figures 65, 66 and 67 were obtained from a cylinder 6 feet long and 3 feet in diameter of $3/16$ inch mild steel and three mild steel plates, clamped at their edges, of dimensions 2.2 feet x 2.7 feet and 0.25 inches, 0.125 inches and .064 inches thick respectively. 20 gauges were used to measure the strain. The acceleration was measured at 20 positions on the plates and 13 positions on the cylinder. All measurements were taken away from boundaries or shaker positions. The transducer outputs were analysed in third octave bands and the variation, V, plotted against the theoretical number of modes available in each band, as calculated from references 3 and 33. In Figure 67 the weight referred to was a magnet of 0.8 lb. mass attached to the $\frac{1}{8}$ inch plate 4 inches from the mechanical shaker connection.

Table 2 shows the variation of strain in 3.33 feet x 1.66 feet x 0.03 inches acoustically excited with white noise.

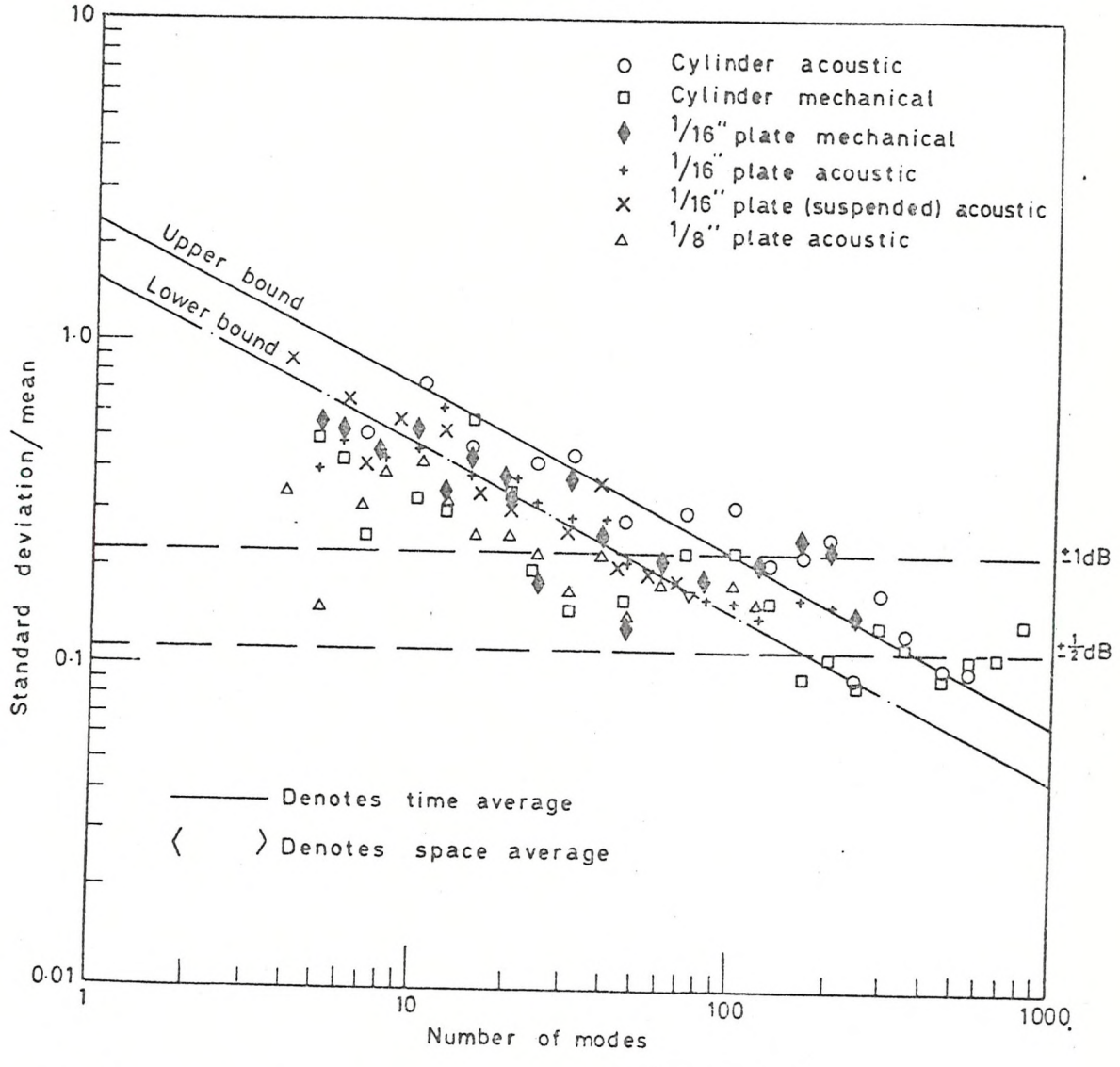

Fig.65 Standard deviation of $\overline{\text{acceleration}^2}$ / $\langle\overline{\text{acceleration}^2}\rangle$ over a series of structures

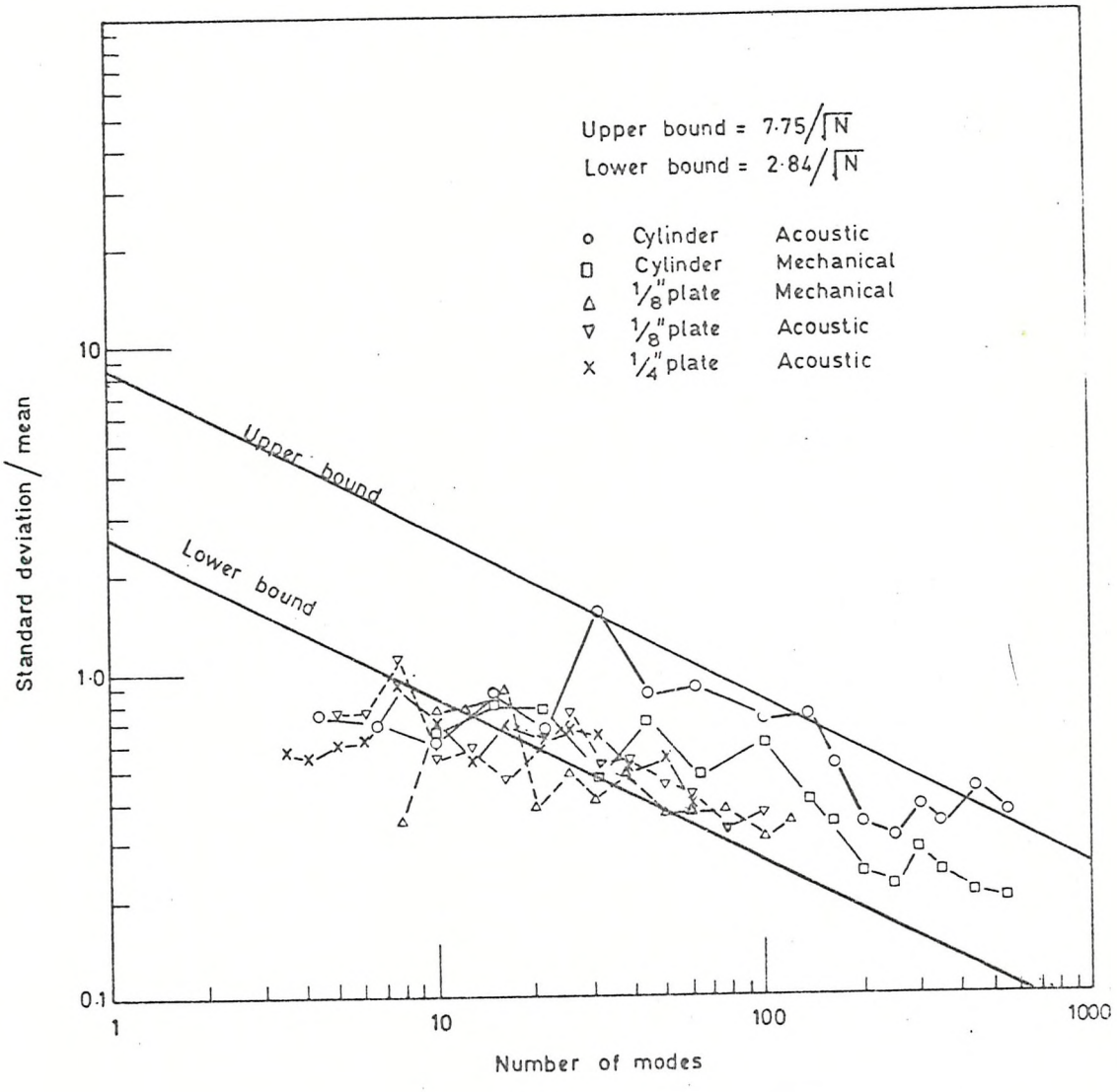

Fig. 66 Standard deviation of $\overline{\text{strain}^2} \;/\; \langle \overline{\text{strain}^2} \rangle$ over a series of structures.

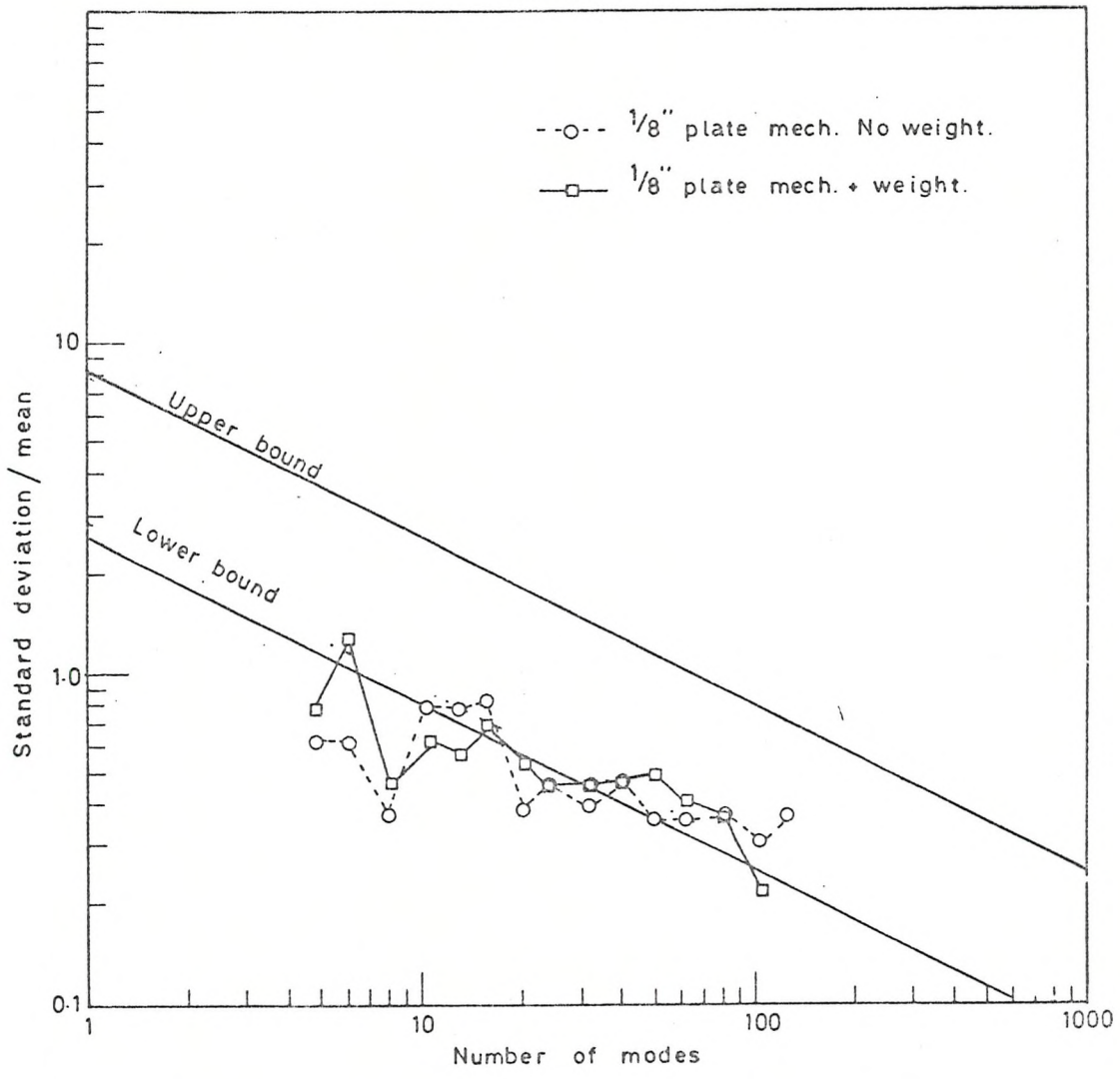

Fig. 67 Standard deviation of $\overline{\text{strain}^2}$ / $\langle\overline{\text{strain}^2}\rangle$ for a plate with and without an added lump mass. (see text)

The outputs from 10 gauges were analysed at a constant bandwidth of 50 Hz, corresponding to about 11 modes per band, as calculated from ref. 3.

8.4. Discussion of Results

The measured spatial variation of mean square acceleration, shown on Figure 65, agrees well with the theoretical prediction when over 10 modes are available. When less than 10 modes are available the agreement is only fair for under these conditions the central result quoted from 43 does not hold.

The variation of acceleration seldom falls below 0.1 and the low values predicted whe, say, 800 modes are available, are not observed. Readings were taken from a level recorder to the nearest decibel, which implies an accuracy of $\pm\frac{1}{2}$ dB. which affects the recorded variation as discussed in appendix X. The level at which the observed variation is controlled by this accuracy of measurement is shown in Figure 6 5

The experimental results for strain (Figures 66 and 67) are well described by the theoretical results when over 30 modes are available. When less than 10 modes are available the analysis fails. Both bands seem well justified and the individual curves show a strong dependance on $1/\sqrt{N}$.

We have deduced that the analysis would describe the behaviour of a cylinder above and below the ring frequency f_r. The variations in strain measured over the mechanically driven

cylinder coalesce well with the measurements from the various plates. There is no change in trend or level of results between the variations measured below and above the ring frequency, which here corresponds to 200 modes available. The variations measured over the acoustically excited cylinder group round the upper band both above and below the ring frequency.

Figures 68 and 69 show the distribution of mean square strain over the acoustically excited $\frac{1}{8}$ inch plate at 400 Hz and 1600 Hz, plotted as a cumulative total. The individual points plotted approximate to a straight line which indicates, on the distorted scale of probability, that the distribution is Gaussion, as predicted.

In deriving the theoretical predictions of variation the assumption was made that the response of the modes was uniform in each band. In Figure 3, the variation of mean square acceleration is shown for both the $1/16$ inch plate and the cylinder mechanically and acoustically excited. The distributions of the response of each mode would surely be different for the two methods of excitation, yet the differences in the variations observed was small. This shows that the effect of the assumption is small and that we were justified in making it. Figure 4 shows that the variation of mean square strain over the $\frac{1}{8}$ inch plate again was unaffected by the method of excitation.

The variation of mean square strain measured over the cylinder (Figure 66) was greater under acoustic excitation than

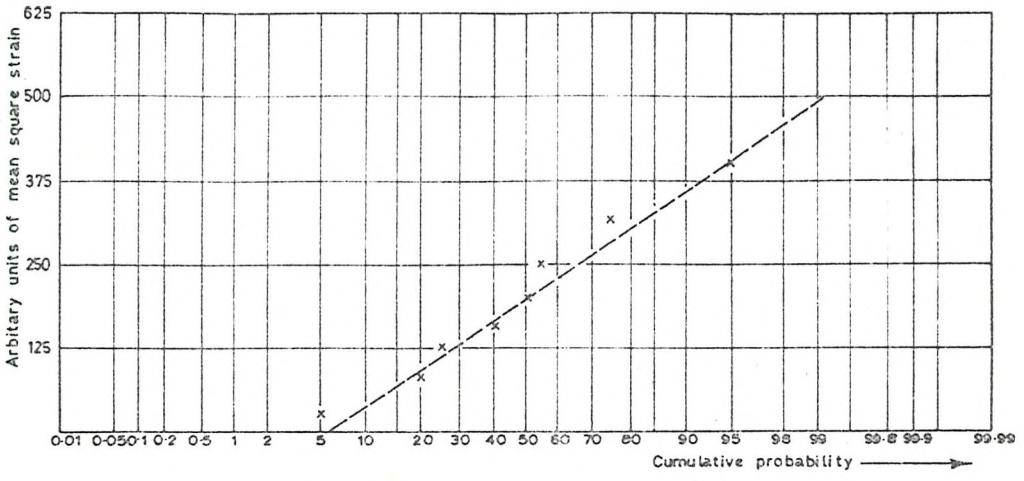

Fig. 68 Probability distribution of mean square strain in $\frac{1}{8}$ in thick plate acoustically excited by $\frac{1}{3}$ octave random-noise centred on 400 Hz.

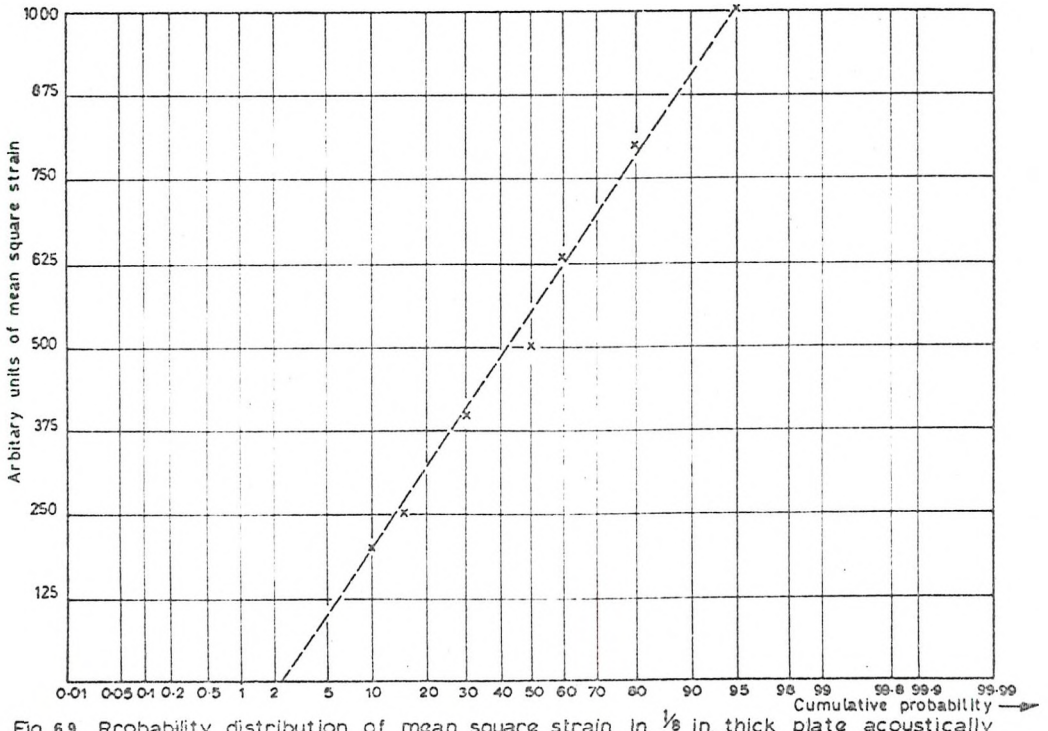

Fig. 69 Probability distribution of mean square strain in $\frac{1}{8}$ in. thick plate acoustically excited by $\frac{1}{3}$ octave random noise centred on 1600 Hz.

mechanical excitation. This suggests that consistently fewer modes were excited than predicted, under acoustic excitation. The acoustic field was set up inside the cylinder; the effect of selective coupling between acoustic and structural mode is to reduce the number of structural modes contributing significantly to the response. However, the results still lie within the suggested band and the assumption of uniform modal response still seems to be adequate.

In the analysis we assumed that the structural modal responses were statistically independent. The amount by which the modal half power bandwidths overlap is a measure of the accuracy of this assumption. If the modal overlap factor (the half power bandwidth multiplied by the modal density) is greater than 1, then the half power bands of some modes must overlap, and modal independence is no longer certain. In Table 2 is shown the variation of strain measured over the suspended aluminium panel, at various frequencies, at a constant bandwidth. With only 11 modes included, the agreement with the theoretical variation is not good. However, despite a very large change in modal overlap factor, the variation measured was reasonably constant. Thus, we may deduce that the overlapping of adjacent modes is unlikely to affect the results seriously and our assumption is reasonable.

This latter experiment also provides evidence for considering the number of available modes as the major parameter in estimating the variation of strain. As the modal density of a flat plate is

independent of frequency, the number of modes included in each analysis in Table 4 was the same (11 modes), and the variations measured should have been constant. Despite the fact that very different modes were considered, the variation measured was indeed constant as predicted.

Further strong evidence is presented in Figure 5, showing the variation of strain over the $\frac{1}{8}$ inch plate, with and without added weight. Whilst the weight altered individual modes very much indeed, the total number of modes in each frequency band was approximately the same, with and without the weight (3). Thus, we would predict no difference in the variation of strain over the surface, between the two systems. In Figure 5 we see this to be so. When more than 10 modes were available there were no significant differences in the variations measured, despite the addition of a lumped mass of 30% of the mass of the plate.

This evidence strongly endorses the theoretical findings of section 8.2.

TABLE 4

Variation V of Strain from Suspended Aluminium Plate Analysed at Constant Bandwidth (50 Hz)

Centre Frequency Hz	v	Modal Overlap
200	0.53	0.24
400	0.27	0.43
800	0.46	0.48
1600	0.49	0.83
3150	0.55	1.85
6300	0.45	2.50

50 Hz bandwidth corresponds to ~11 modes.

Modal overlap is taken as $f \eta M$

where f = centre frequency

η = total loss factor

M = modal density

8.5. Conclusions : Extension to Existing Estimates : Effect of Assumptions

By making a number of sweeping assumptions we have achieved some simple results which well describe the variation of stress, strain and acceleration with position over a variety of structures under various excitations. The only parameter required is the number of modes available. This is no more information than is required by the statistical energy analysis of vibrating structures (3) and thus having estimated the mean square stress, a designer can work

out the likely variation about this mean over a given bandwidth very simply. This result does not, of course, refer to the region near a boundary (see Chapters 6 and 7).

The assumptions made do not seem to be very critical. The assumption concerning uniformity of mode response has not caused trouble despite different types of excitation. The effects of changing damping and modal overlap are small. Damping could become important if the modal bandwidths became comparable or greater than the analysis bandwidths. Then more modes would be included than those with their centre frequency in the analysis bandwidth. Beany Yen and Smith[5] noted that under modest pressures of CO_2 a suspended structure under acoustic excitation failed to exhibit peaks in its frequency response curve. This implies extremely high radiation loss factors from the structure to the acoustic field such that the effective damping is high. Under these conditions the modal bandwidths were high and thus a narrow band of noise would excite many modes and would produce little variation of response over the structure.

It is interesting to compare the findings of this chapter with those of Chapter 4, where formal tests were applied to the structure to test the "diffuseness" of the bending wave field. About the same number of modes are required to produce satisfactory answers, i.e. at least 10. However, the dependance on point excitation vs. acoustic excitation seems to have vanished for both accelerometers and strain gauge. This seems reasonable.

We are only measuring variation in magnitude, whereas the correlation measurements are sensitive to phase as well, as discussed in section (4.1.4.1) and appendix IV.

The assumptions seem well justified and allow us to present designers with usable expressions which may easily be applied to improve estimates of the service life of components.

Chapter 9

C O N C L U S I O N S

9.1. A review of the Main Results

The problem that we set out to solve in Chapter 1 was that of predicting the stress distribution in complex plate-like structures vibrating at high frequency. We sought an approach that would be easy to apply, but sufficiently accurate for design purposes, starting from the mean square velocity. This can be estimated by the statistical energy analysis of sets of coupled oscillators. In Chapter 2 we concluded that at the frequencies of interest to this study, the structures will vibrate in bending, and we discussed the behaviour of bending waves.

Two alternative models were discussed in Chapter 3, the normal mode and the bending wave models. We concluded that the normal mode model is convenient when studying properties affecting the whole structure. We also concluded that the travelling bending wave model, coupled with the concept of the diffuse field as used in architectural acoustics, is convenient when studying local effects around boundaries, for this model enables us to make use of the fact that these effects do not propagate far from the boundary. We discussed the wavenumber diagram and its importance to the diffuse field model.

Two formal tests of the diffuse field model were developed in Chapter 4 and experiments on two plates and a cylinder were described. It was concluded that at least ten modes are necessary for a diffuse field. Further, for a cylinder, this will only apply at frequencies above the ring frequency. It was also concluded that although high dampings would not affect diffuseness by increasing the overlapping of adjacent modes, it can affect it by producing a radiating, rather than diffuse field under point excitation.

The diffuse field model was used in Chapter 5 to predict the ratio of mean square stress and strain to mean square velocity. This turned out to be the same as predicted by a single mode model, as expected. The result was tested experimentally and it was concluded that the criteria suggested in Chapter 4 were, in fact, too severe. It was found that even with only a few modes available, the result still held. With cylinders, the ring frequency had no effect on the results.

In Chapters 6 and 7 the diffuse field model was used to predict the concentration of stress and strain likely near a weld and a change of section. It was found that, at the particular weld investigated, little strain concentration was to be expected and this was proved experimentally. However, it was concluded that thicker welds and ribs could cause significant concentrations. A change of section of 2 : 1 was found experimentally not to introduce high concentrations of strain either, but significant strains

were introduced by a 4 : 1 change. This agreed with the theoretical predictions. Again, the number of modes, or bending wave directions available, was not found to be very significant. From the theoretical work the stress and strain induced was seen not to be strongly dependent on wave direction, in the sense that values much above the mean diffuse field value will not occur, even with one bending wave only in the most unfavourable direction. This is important when considering the incorporation of these results into a design method.

The variation of stress, strain and acceleration over the surface of a plate was investigated in Chapter 8 and simple theoretical results were derived, involving only the number of available modes. The normal mode model was used here, as these are properties of the whole structure. The theory breaks down when less than 10 modes are available and experiments suggested that between 10 and 30 modes are necessary for good agreement with the theory. The ring frequency of a cylinder does not seem to be important, as discussed, and the effects of damping, causing overlapping of adjacent modes, was also shown to be unimportant, unless it affected the number of modes responding within a given frequency band. The effect of differing boundaries to the structure, and different methods of exciting it is also seen as unimportant. Only the number of modes available is of importance. We can now combine these results into a design method.

9.2. Design Criteria

Let us suppose that we have estimated the mean square velocity of response for a plate to broad band noise in; say, third octave bands. Let us also suppose that we have fatigue data available. First, from Chapter 5 we work out the mean square stress. Then, from Chapters 6 and 7 we can find out stress concentrations likely at a weld or change of section and from Chapter 8 and the number of available modes(27), the standard deviation of mean square stress. Now this last result will enable us to set the level of stress which will not be exceeded over 95% of the surface of the plate. This proportion is at our choice, but 95% is convenient. It is the level greater than 2.5 times the standard deviation above the estimated mean.

This gives us two levels of stress to compare, a level at a number of boundaries and a level that we might expect to occur occasionally elsewhere in the plate. As yet, we cannot set a maximum value to this except in special cases (8.2.2) and the figure of 95% would probably be modified by experience. However, comparing these two figures will enable us to decide where the stress concentrations are highest, and, in the light of the fatigue data, most likely to cause premature failure.

As an example, let us consider the 4 : 1 and 2 : 1 change of section specimens and try to decide whether the strains where the thin section joins to the thick section are significant.

Let us consider the third octave frequency band at 2000 Hz. For simplicity we will ignore the small strains in the thicker section

Change of Section	2 : 1	4 : 1
Modes Available in Thinner Section	50	100
Standard Deviation / Mean	1.18	0.835 (Upper Band)
95% Level / Mean	3.96	3.09
Change of Section Strain Concentration (Figure 54)	1.45	3.69

Thus we would deduce that the 4 : 1 change of section would induce significant strains and the 2 : 1 change of section not so. This was what we found in practice.

Having decided that a given stress is significant, we then compare this with the fatigue data and decide whether or not any redesign is necessary. It may be that local redesign might serve the purpose, if a local stress is high, but if the mean level of stress in the plate is high, it may be necessary to redesign the whole structure, perhaps increasing its thickness. Whatever the decision, information is now available for the designer to act on.

9.3. Limitations on Design Method

Whether or not we can use this approach is chiefly a function of the number of available modes within a given bandwidth of analysis. The calculation of stress at a boundary seems relatively undemanding, needing only one or two modes for good answers. However, the prediction of the standard deviation demands about 10 to 30 modes. The formal tests of diffuseness (Chapter 4) seems rather severe, but if a given structure satisfies these tests, then this analysis may be successfully applied to it.

The effect of other parameters is small. Damping and modal overlap have little or no effect on the accuracy of the prediction, although high damping could upset the formal tests of Chapter 4 under mechanical excitation.

9.4. Future Extensions

In this work we have only considered two boundaries, the weld and the change of section. The solid edge is treated in appendix VII. Clearly, there are a vast array of details that we could consider, e.g. the right angle join, the mass, the slender rib and so on. However, the establishment of the conditions under which a diffuse field model is usable has put all such calculations into the category of routine, if complex, design calculation.

Another facet of the work could be to try and predict what will happen under narrow band random noise loading. At high modal

densities the results found here are applicable directly. However, as mentioned in Chapter 8, the controlling influence would be the bandwidth of the individual modes rather than of the exciting force, especially when the damping of the system is high. This might, perhaps, apply when the acoustic medium is of high density, as in a nuclear reactor.

Which of these points to be next tackled will depend on the needs of the nuclear engineering industry. Whatever may be decided, the method forms a basis of a simple way of tackling the otherwise intractable problem of predicting acoustically induced stresses in the plate structures of nuclear reactors

The author hopes to extend and develop this approach over the next few years.

ACKNOWLEDGMENTS

--oOo--

In the first plate, may I acknowledge gratefully the financial support given to me by the Central Electricity Generating Board for my work.

Also, I wish to thank my Supervisor, Mr Fahy, for his encouragement, help and occasional scepticism, all of which have been invaluable. My thanks, too, to the laboratory technicians who have, at various times, taken so much trouble to help the work along. In particular, I would mention Mr H. Dankin, who fixed all the strain gauges on the change of section plates, as shown in Figure 56, and Mr G. Marshall, who assisted with the experiments described in Section 8.3.

My thanks are also due to Mr Swamy of the Data Analysis Centre for writing a digital filtering programme for me, and to most of the staff of the Institute of Sound and Vibration Research, Southampton, for the help they have given me at various times.

Finally, I would like to thank my wife, Ann, for the encouragement that she has given me.

REFERENCES

1. An appraisal of the Technical and Economic Aspects of Dungeness B Nuclear Power Station. Central Electricity Generating Board Publication July 1965

2. W. Rizk and D.F. Seymour, "Investigation into the Failure of Gas Circulators and Circuit Components at Hinkley Point Nuclear Power Station" Proc. Inst. Mech. Engrs. 1965 179, part 1 (No. 21)

3. E. E. Ungar, "Fundamentals of Statistical Energy Analysis of Vibrating Systems" Bolt Beranek & Newman Inc. Teac. Report No. AFFDL-TR-66-52. April 1966

4. F. J. Fahy. "Vibration of Containing Structures by Sound in the Contained Fluid. "Institute of Sound and Vibration Research. Tech. Report No. 11. Nov. 1968

5. L. Yeh, E. M. Beany and B. Smith. "Acoustically Induced Stresses in Nuclear Structures "Proc. Inst. Mech. Engrs. 1967. 181 Part 31.2A

6. R. H. Lyon. "Spatial Response Concentrations in Extended Structures" Trans. A.S.M.E.Eng. for Industry. Paper 67-Vibr-22.

7. E. E. Ungar. "Transmission of Plate Flexural Waves Through Reinforcing Beams; Dynamic Stress Concentrations" J.A.S.A. 33 No.5. pp 633-639.

8. S. L. Chang & A. Jaharshahiia. "On Dynamic Stress Concentration Around a Discontinuity." J.Appl.Mech.Series E.VOL.34 No.2 pp 385-391

9. G. Maidanik. "Response of Ribbed Panels to Reverberant Accustic Fields" J.A.S.A. Vol.34 No.6. pp 809-826. June 1962

10. L. Cremer. "The Propagation of Structure Bourne Sound" Dept. of Scientific and Industrial Research. Sponsored Research (Germany) Report No. 1, series B.1948

11. S. P. Timoshenko & S. Woinowsky-Kreiger. "Theory of Plates and Shells" McGraw Hill. 2nd Ed. pp 40

12. L. A. Pipes. "Applied Mathematics for Engineers and Physicists" McGraw Hill. 2nd Ed. pp 217-220.

13. R. E. D. Bishop and D. C. Johnson, "The Mechanics of Vibration" Cambridge University Press. pp 438-442. 1960

14. P.E. Doak. "Fluctuations of Sound Pressure Level in Rooms when the Receiver Position is Varied." Acoustica. Vol. 9 ppl-9 1959

15. D. J. Mead and Sen Gupta. "Propagation of Flexural Waves in Infinite Rib-Skin Structures." Southampton University. I.S.C.R. Memo. 303. Contract F. 61052-68-C-0027, June 1969

16. M. Heckl. "Measurement of Absorption Coefficients on Plates" J.A.S.A. Vol.34. No. 6. pp 803-808. June 1962

17. V. V. Bolotin. "Broadband Random Vibration of Elastic Systems" Int. J. Solid Structures Vol.2 pp 105-124, 1966

18. J. D. Robson. "An Introduction to Random Vibration" Edinburgh University Press. p 91.

19. M. K. Bull, J.F. Wilby and D. R. Blackman. "Wall Pressure Fluctuations in Boundary Layer Flow and Response of Simple Structures to Random Pressure Fields" Southampton University A.S.S.U. Report 243. Contract AF.61(052)-358. Part II pp 8-11 July 1963

20. E. Ermutlu. "Dynamic Analysis of Arch Dams Subjected to Seismic Disturbances." Ph.D. Thesis Southampton University Dec. 1968

21. J. M. Deb Nath and M. Petyt. "Application of the Method of Kantovovich to the Solution of Problems of Free Vibration of Singly Curved Rectangular Plates in the Presence of Membrane Stresses." University of Southampton. I.S.V.R. Tech. Report No.19. June 1969

22. V. Mason. "Rectangular Finite Elements for Analysis of Plate Vibrations." J.S.V. Vol. 7. No. 3. pp 437-449. May 1968

23. E. Skudrzyk "Simple and Complex Vibratory Systems" Pennsylvania State University Press. Chapter IX pp 267-279 1968

24. R. V. Waterhouse. "Statistical Properties of Reverberant Sound Fields." J.A.S.A. Vo. 43.No. 6. June 1968. pp 1436

25. D. Lubman. "Fluctuations of Sound Pressure with Position in a Reverberation Room." J.A.S.A. Vol. 44. No. 6. Dec. 1968

26. P. M. Morse. "Vibration and Sound." McGraw-Hill. Chapter 8 pp 414-415.

27. E. E. Ungar and T. D. Scharton. "Analysis of Vibration Distribution in Complex Structures. "Shock and Vibration" Bulletin 36. Part 5. p 47.

28. V. V. Bolotin. "The Edge Effect in the Oscillations of Elastic Shells." Journal of Applied Mathematics & Mechanics. 24(5) pp 1257-1272. 1960

29 R. Cook, R. Waterhouse, R. Berendt, S. Edelman and M. Thompson "Measurement of Correlation Coefficients in Reveration Sound Fields." J.S.V. (1969) 9(1) pp. 21-27.

31. C. A. Mercer. "Use and Application of Digital Data Analysis Systems." Recent Advances in Stress Analysis. Royal Aero Soc. 28 March 1968.

32. C. Morrows. "Point to Point Correlation of Sound Pressure in Reverberation Chamber." LTV Research Centre, Western Division Anaheim, California, U.S.A.

33. J. Manning, G. Maidanik. "Radiation Properties of Cylindrical Shells." J.A.S.A. 36(9). pp 1691-1698. 1964.

34. K. L. Chandiramani, S.E. Widnall, R. H. Lyon, P. A. Franken, 1966. BBM Contract No. NAS 8-20026. Report No. 1417, Structural Response to Inflight Acoustic and Aerodynamic Environments.

35. A. Abell, "Comparison and Use of Transducer Designed to Measure Mechanical Power Transmission at High Frequencies." M.Sc. Thesis Southampton University March 1968.

36. U.S.A. Standards. Method for the Physical Measurement of Sound. Aug. 20. 1962

* 30 - see end of list

37. E. E. Ungar and J. R. Carbonnell. 1966 A.I.A.A. J. 4. 1385. On Panel Vibration Damping due to Structural Joints.

38. Den Hartog. "Mechanical Vibrations" pp 141. McGraw-Hill 4th Ed. 1956.

39. Timoshenko & Young. "Strength of Material." D. Van Norstrand & Co. Inc. 1947 p 334.

40. Savin. "Stress Concentrations round Holes" International Series of Monographs in Aeronautics and Astronautics.

41. Case & Chilver. "Strength of Materials." Edward Arnold. 1961 p 101.

42. Timoshenko. "Theory of Elasticity." McGraw-Hill. p 234.

43. Margaret Slack, 1946. Proc. Inst. Elect. Engrs. Pt. 3. 93. "The Probability Distributions of Sinusoidal Oscillations Combined in Random Phase."

44. Schloss. "Inherent Limitations of Accelerometers for High Frequency Vibration Measurement." J.A.S.A. 33. p 539.

30. S. M. Stearn. 1969. J. Sound Vib. 1969 9, (1), 21-27. Measurement of Correlation Coefficients on a Randomly Excited Structure.

APPENDIX I

Effect of Accelerometer on Measured Response of an Infinite Plate

For an infinite plate of thickness h vibrating at a frequency f Schloss (44) gives:-

$$V_1 = V_2\left[\frac{Z_t + Z_s}{Z_s}\right] \qquad \text{Al.1.}$$

V_1 = local velocity of the plate alone

V_2 = local velocity of the plate + accelerometer

Z_t = impedance of accelerometer = $i2\pi fM$

where M = Mass of accelerometer

Z_s = impedance of plate = $4h\sqrt{\frac{E\rho}{3}}$

ρ = density

E = Young's Modulus

} of material of plate.

$\therefore$ the velocity measured will be accurate to within 1 db.

if $$\left|\frac{Z_t}{Z_s}\right| \leq 0.51 \qquad \text{Al.2.}$$

Now $$\frac{V_1}{V_2} = 1 + \frac{Z_t}{Z_s} \qquad \text{A1.3.}$$

Z_t is imaginary.

Thus the phase error in measuring V_1 will be

$$\tan^{-1}\left[\frac{Z_t}{Z_s}\right] \qquad \text{A1.4.}$$

The effects of the accelerometer mass on amplitude and phase are plotted on Figure 70 for two accelerometer masses and for different plate thicknesses as a function of frequency.

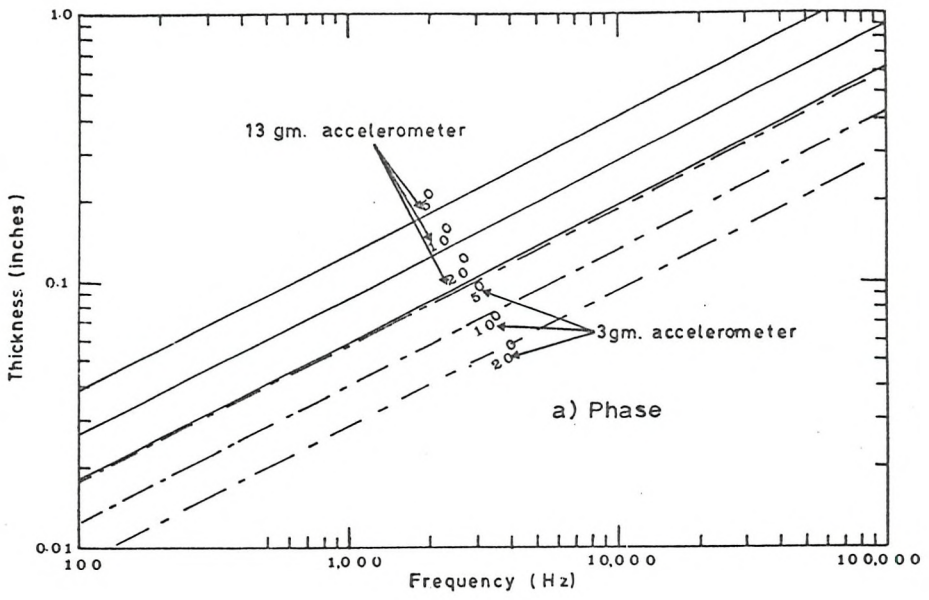

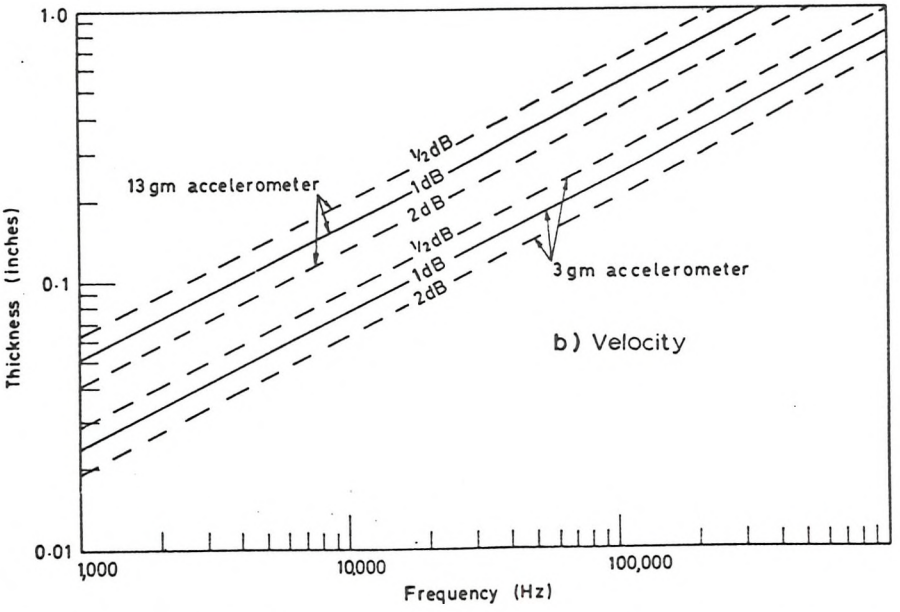

Fig.70 Effect of loading impedance of accelerometers on estimation of mean square velocity and Phase.

APPENDIX II

Phase Match of Analogue Filter

The two filters used in the analogue correlation were $\frac{1}{3}$ O.B. Spectometers made by Bruel and Kjaer.

A simple experiment was devised to test their phase match. White noise from a white noise generator was recorded on a multi-channel tape recorder and then played back to both filters. The output from these filters was correlated on the analogue correlator. The signals should have given a correlation coefficient of unity. The results are shown on Figure 71. As can be seen, the filter was adequately phase matched from 500 to 5000 Hz.

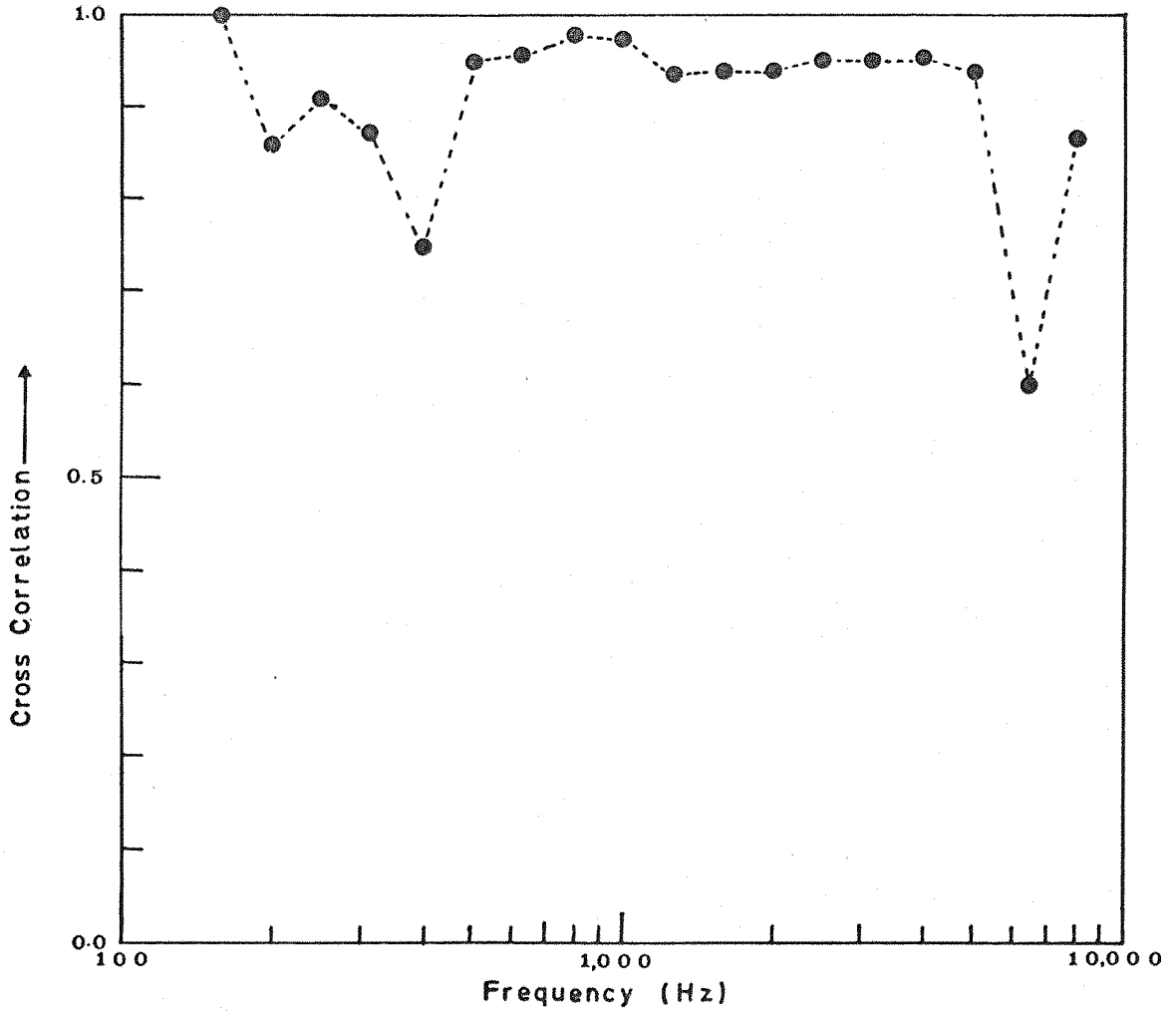

Figure 71 Phase Match of 1/3 O.B. Filters.

APPENDIX III

Use of Powell's Equation to compute Cross-Correlation of Acceleration on a Plate

From (18, 19) :-

$$W(\underline{r},\underline{r}';\omega) = \iint_{A\,A} H(\underline{r},\underline{r}_o;\omega)\; H^*(\underline{r}',\underline{r}_o';\omega)\, P(\underline{r}_o,\underline{r}_o';\omega)\; d\underline{r}_o\, d\underline{r}_o' \qquad \text{A3.1.}$$

If $R(r,r';\tau)$ is the cross correlation of response at r and r' at a time delay of τ, then

$$R(\underline{r},\underline{r}';O) = \int_{-\infty}^{\infty}\iint_{A\,A} H(\underline{r},\underline{r}_o;\omega)\; H^*(\underline{r}',\underline{r}_o';\omega)\, P(\underline{r}_o,\underline{r}_o';\omega)\, \exp(iO)\; d\underline{r}_o\, d\underline{r}_o'\, d\omega. \qquad \text{A3.2.}$$

From (19 pp30)

$$P(\underline{r}_o, \underline{r}_o'; \omega) = A + iB \qquad \text{A3.3.}$$

Where $$A = R\left(\underline{r}_o, \underline{r}_o', \tau = 0, //\omega\right) \frac{Sp(\omega)}{2} \qquad \text{A3.4.}$$

$$B = R\left(\underline{r}_o, \underline{r}_o', \tau = \frac{\pi}{2\omega}, //\omega\right) \frac{Sp(\omega)}{2} \qquad \text{A3.5.}$$

where $//\omega$ indicates a narrow frequency band and $Sp(\omega)$ is the power spectral density over that narrow band.

From the theoretical and experimental work of Cook et al[29] we may assume that if the acoustic field is diffuse, then

$$A = R\left(\underline{r}_o, \underline{r}_o', \tau = 0, //\omega\right) \cdot \frac{Sp(\omega)}{2} = \frac{\sin(kr)}{kr} \frac{Sp(\omega)}{2} \qquad \text{A3.6.}$$

where $r = \left| \underline{r}_o - \underline{r}_o' \right|$ and k = acoustic wavenumber.

Unfortunately, no such information exists about the forms of B. We will return to this awkward point in a moment.

Let us now examine the form of the cross acceptance terms.

$$\int_{-\infty}^{\infty} \iint_{A}\iint_{A} H(\underline{r}, \underline{r}_o; \omega)\, H^*(\underline{r}', \underline{r}_o'; \omega)\, P(\underline{r}_o, \underline{r}_o'; \omega)\, d\underline{r}_o\, d\underline{r}_o' d\omega =$$

$$\int_{-\infty}^{\infty} \left\{ \sum_{\alpha} \frac{\psi_\alpha(\underline{r})\psi_\alpha(\underline{r}')}{|Y_\alpha(\omega)|^2} \iint \psi_\alpha(\underline{r}_o)\psi_\alpha(\underline{r}_o')\, P(\underline{r}_o, \underline{r}_o'; \omega)\, d\underline{r}_o\, d\underline{r}_o' \; + \right.$$

$$\left. \sum_{\alpha}\sum_{\beta} \frac{\psi_\alpha(\underline{r})\psi_\beta(\underline{r}')}{Y_\alpha(\omega)\, Y_\beta^*(\omega)} \iint_{A\,A} \psi_\alpha(\underline{r}_o)\psi_\beta(\underline{r}_o')\, P(\underline{r}_o, \underline{r}_o'; \omega)\, d\underline{r}_o\, d\underline{r}_o' \right\} d\omega$$

---------- A3.7.

At this point we make the assumption about the value of the second term A3.6. compared to the first. We assume that we may neglect the cross mode terms in comparison to the direct as:-

(a) The cross mode terms contain the integral of a produce of modal functions over the panel area which is , in general, less than the integral of the square of either of the modal functions over the same area.

(b) If the modes are well separated in frequency and lightly damped, then:

$$|Y_\alpha(\omega)|^2 \ll Y_\alpha(\omega)\, Y_\beta^*(\omega) \qquad \text{A3.8.}$$

We make these assumptions with some reservations, for we are now strictly limited to lightly damped modes. However, these assumptions enable us to reduce the computation time required by a factor of N, where N is the number of modes to be examined, because while there are N direct terms, there are N^2 cross terms. Without making this assumption we could not reasonably proceed.

Now the direct terms of A3.7. will produce wholly real numbers and we could simply represent A3.2 as

$$R(r, r'; 0) = \int_{-\infty}^{\infty} C(\omega)\, \frac{Sp(\omega)}{2} \left[D(\omega) + iE(\omega) \right] d\omega \qquad \text{A3.9.}$$

where

$$D(\omega)\frac{Sp(\omega)}{2} = A$$

$$E(\omega)\frac{Sp(\omega)}{2} = B$$

Now whatever the form of $C(\omega)\frac{Sp(\omega)}{2}$, $R(r,r';0)$ must be wholly real. This can only be so if $C(\omega)\frac{Sp(\omega)}{2}E(\omega)$ is an odd function, or if $E(\omega)$ is always zero. This seems the more reasonable assumption.

Having decided to ignore the cross terms in equation A3.7., in order to reduce the computational requirements of store and time to a reasonable level, we are also obliged to make this assumption. As we have no information about the form of $E(\omega)$ this assumption is as reasonable as any we could make.

Our final expression now reduces to

$$R(\underline{r},\underline{r}';0) = \int_{-\infty}^{\infty} \sum_{\alpha} \frac{\psi_\alpha(\underline{r})\,\psi_\alpha(\underline{r}')}{|Y_\alpha(\omega)|^2} \iint_{A\,A} \psi_\alpha(\underline{r}_0)\,\psi_\alpha(\underline{r}_0')\,\frac{\sin(kr)}{kr}\,\frac{Sp(\omega)}{2}$$

$$* \; d\underline{r}_0\, d\underline{r}_0'\, d\omega \qquad \text{A3.10.}$$

APPENDIX IV

The Correlation Coefficients of Acceleration of a Diffuse Bending Wave Field with a Superimposed Uni-directional Travelling Bending Wave

Let us consider a plate in which there is both a diffuse bending wave field and a travelling bending wave and examine the acceleration at two positions x and x' along the direction of the travelling wave. We restrict the analysis to third octave frequency bands.

Let the acceleration at time t due to the travelling wave field be $A(x,t)$ at x and that due to the diffuse field be $B(x,t)$. Let us assume that at any point x the two fields are statistically independent. This is fair if we consider a frequency band of response, with a travelling wave of only one frequency within that band.

Then the zero time delay correlation coefficient of displacement or acceleration for a narrow band of frequencies, $R(x,x',0)$, will be:-

$$R(x,x',0) = \frac{\overline{[A(x,t) + B(x,t)]\,[A(x',t) + B(x',t)]}}{\sqrt{\overline{[A(x,t) + B(x,t)]^2}\,\overline{[A(x',t) + B(x',t)]^2}}}$$

.... A4.1.

$$R(x,x',0) = \frac{\overline{A(x,t)\,A(x',t)}}{\sqrt{\left[\overline{T(x,t)^2}\;\overline{T(x',t)^2}\right]}} + \frac{\overline{B(x,t)\,B(x',t)}}{\sqrt{\left[\overline{T(x,t)^2}\;\overline{T(x',t)^2}\right]}} \qquad \text{A4.2.}$$

where $\overline{\qquad}$ indicates a time average

and $T(x,t) = A(x,t) + B(x,t)$

The product $\overline{A(x,t)\,B(x',t)}$ is zero for uncorrelated fields.

The first term in A4.2. is due to the travelling wave and the second term to the diffuse field.

Let us briefly derive the correlation coefficient for a travelling wave on its own. If two points be a distance r apart and lie on a line normal to the direction of the travelling wave, then the displacement at x and x' will be identical

$$\left[A(x,t)\right] = \left[A(x',t)\right] = \left[\cos(\omega t)\right] \qquad \text{A4.3.}$$

Then the cross correlation will be 1.

Now, if the two points lie on a line parallel to the direction of a travelling wave, the displacement at x is

$$A(x,t) = \cos(\omega t) \qquad \text{A4.4.}$$

and at x' is

$$A(x,t) = \cos(\omega t + kr) \qquad \text{A4.5.}$$

where k is the wavenumber.

Then the cross correlation will be

$$\frac{\overline{\cos(\omega t)\cos(\omega t + kr)}}{\sqrt{\cos^2(\omega t)\cos^2(\omega t + kr)}} \qquad \text{A4.6.}$$

$$= \cos(kr)$$

Now, returning to A4.2., if the diffuse field is given the arbitrary mean square response of 1 and the travelling wave then

the measured cross correlation coefficient will be:-

$$= J_o(kr) + n \qquad \text{for } x - x' \text{ normal to the travelling wave direction,} \qquad A4.7.$$

$$= \frac{J_o(kr) + n.\cos(kr)}{1+n} \qquad \text{for } x - x' \text{ along the travelling wave direction.} \qquad A4.8.$$

On figure 72 these expressions are plotted as a function of kr.

Of course, the situation was observed in the mechanically excited plate, and was rather more complex. The travelling wave is more properly a radiating field of varying magnitude and the accelerometers were not in either position relative to the radiating field. However, one may judge the possible effect of a combined radiating and diffuse field. A small travelling wave ($n = 0.1$) might not be detected, but if the component was a third of the total response ($n = 0.5$) then the effect on the correlogram would be severe.

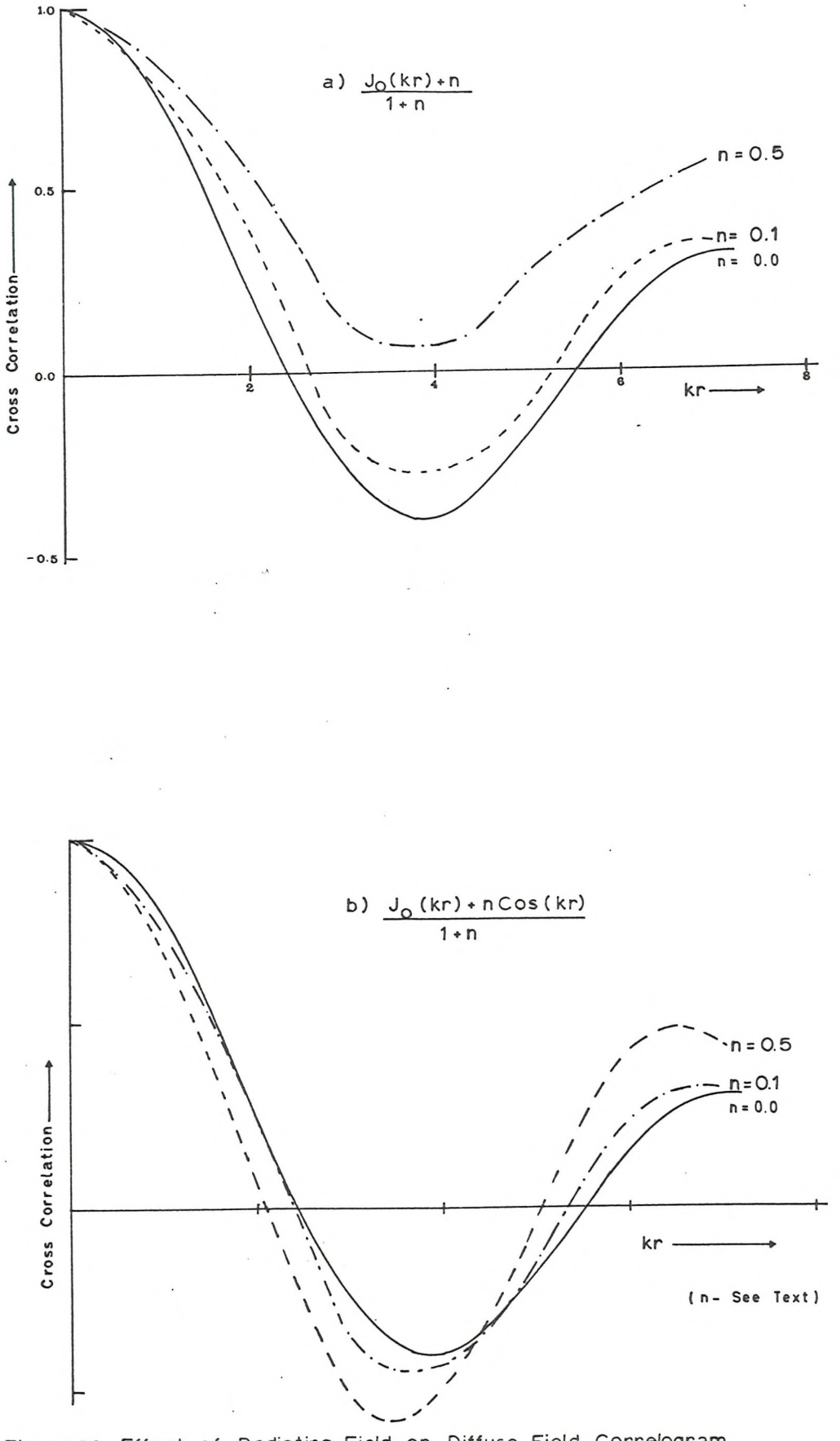

Figure 72 Effect of Radiating Field on Diffuse Field Correlogram.

APPENDIX V

The Ratio of the Reverberant Field to the Radiating Field in the $\frac{1}{4}$" Plate Mechanically Excited

The basis of this calculation is outlined in Morse (26).

Suppose we set up a point source on a plate that absorbs all energy at its boundary, then the intensity I_R will be:-

$$I_R = \frac{P}{2\pi r} \qquad \text{A5.1.}$$

where P = Power input at source

r = Radius

However, if the boundaries reflect some energy, then far away from the source the reverberant intensity I_∞ is given as:-

$$I_\infty \gamma = P \qquad \text{A5.2.}$$

where

$$\gamma = \alpha_s l_s \qquad \text{A5.3.}$$

where α_s = absorption coefficient and

l_s = length of boundary s .

Now from Heckl (16) we may deduce that

$$\gamma = \frac{13.8\pi S}{C_B T} \qquad \text{A5.4.}$$

where S = surface area of plate;

C_B = bending wave speed;

T = reverberation time.

$$\therefore \quad I_\infty = \frac{P C_B T}{13.8\pi S} \qquad \text{A5.5.}$$

$$I_R = \frac{P}{2\pi r} \qquad \text{A5.6.}$$

Then $$\frac{I_R}{I_\infty} = \frac{13.8\pi S}{C_B T 2\pi r} \qquad \text{A5.7.}$$

This result is used to predict the radii from the shaker at which I_R is 10dB and 3dB below I_∞ on the $\frac{1}{4}$" plate. The results are shown on Figure 35.

APPENDIX VI

Tests of Three Channel Strain Gauge Amplifier

To measure the signal from the semi-conductor strain gauges a combined amplifier and voltage source was built. The voltage source was to supply a potentiometer bridge including the active gauge and a dummy resistance. The signals from the strain gauges were passed through three parallel high gain amplifiers.

There were three channels to allow the examination of stress through a strain gauge rosette. However, in this project only two channels were used simultaneously in the strain correlation tests.

The service requirements were:-

(a) low noise at inputs ($< 5 \mu V$), even when in a loud sound field, as the strain signals were so small;

(b) good phase match between channels, for correlation measurements, 4 to 10 K H_z;

(c) gain of 10^4 up to 10 K H_z.

The amplifier fulfilled all these requirements.

1. Noise Test

The input to the amplifier was taken as the signal from a gauge fixed to a massive block of metal. A loud sound (>90dB) was made locally to the amplifier by allowing air to escape from a gate valve under pressure. The output signal from the amplifier

was measured on a third octave spectrometer and the level was expressed as a level at the input. The test was repeated with no local sound.

The results are plotted on Figure 73. On all channels the noise was very low. No increase of noise was observed with the local sound on.

2. Phase Match Test

A sine wave from an oscillator was fed to two channels at once and the output signals were correlated on the analogue correlator. The frequency of the input was altered and the test repeated. The test was then repeated on two other channels.

No phase shift was observed up to 20 K H_z, when the test was stopped.

3. Gain Test

A small signal, 100 μV, was set up by feeding the signal from an oscillator through a potentiometer. This voltage was deduced by Ohms Law. This voltage was passed to the amplifier and the output voltage measured. The frequency of the oscillator was varied.

The gains of the three channels are presented on Figure 73. They were flat from 80 H_z to 10 K H_z and approximately 10^4.

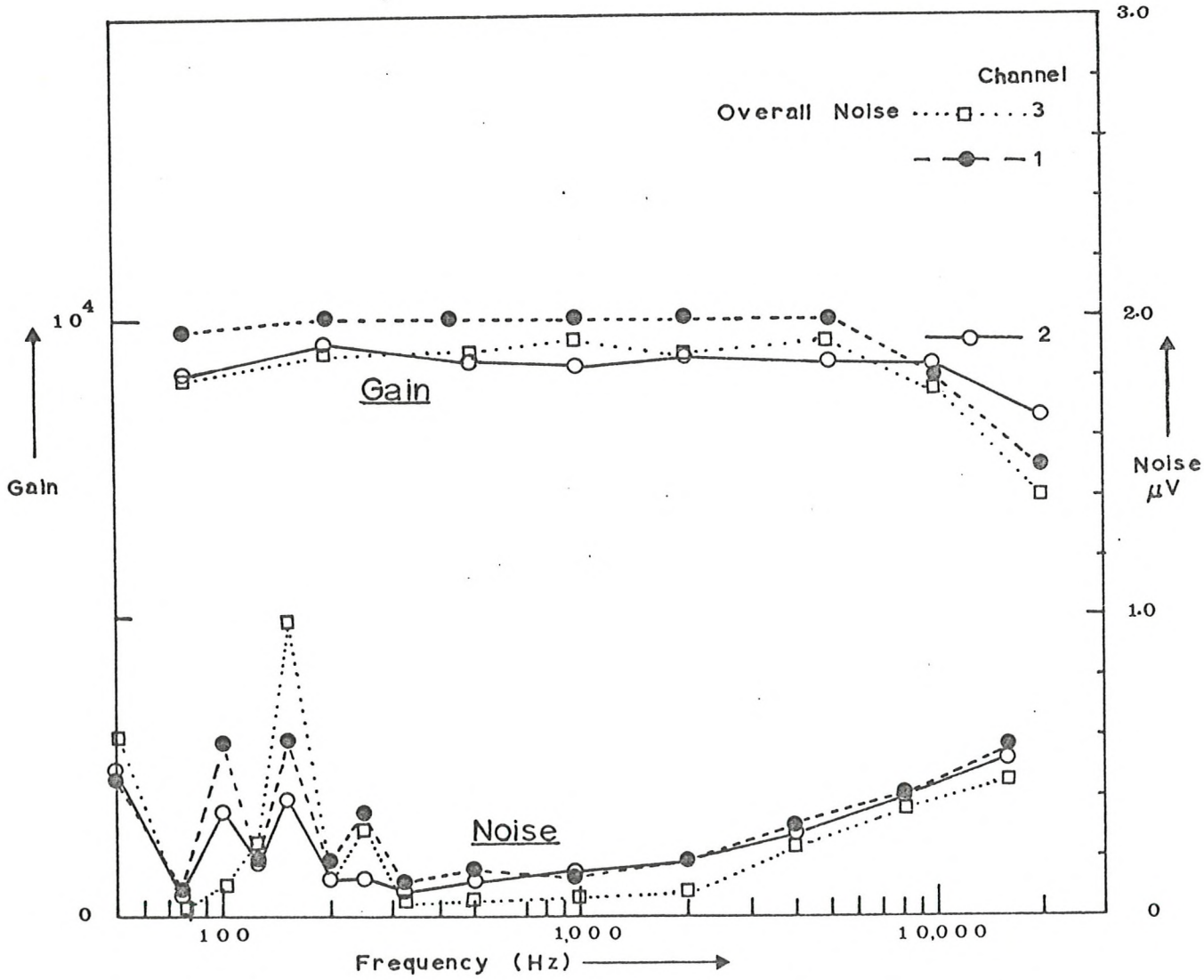

Figure 73 Callbration and Noise of Strain Gauge Amplifier.

APPENDIX VII

Stress Concentration in a Plate, Normal to a Solid Boundary

Consider a plate lying in the plane $x\,z$ and a solid boundary lying along the axis $O\,y$. Let a bending wave propagate towards the boundary at an angle θ to $O\,x$.

The boundary conditions are as follows:-

The magnitudes of both the transmitted travelling and near fields are zero, and the vertical velocity and angular velocity is zero at all points on the boundary.

The incident wave may be represented as:-

$$V_I = \bar{V}.\exp.(-ik.x.\cos.\theta + ikz.\sin.\theta) \qquad \text{A7.1.}$$

where the bar $\bar{\ }$ indicates the time variable omitted.

The reflected wave, the solution to $(\nabla^2 + k^2)x = 0$

is $$V_R = R\,\bar{V}.\exp.(ik.x.\cos.\theta) \qquad \text{A7.2.}$$

The reflected near field, the solution to $(\nabla^2 - k^2)\, x = 0$

is $$V_r = R' \bar{\bar{V}} \exp(xk\sqrt{1+\sin^2\theta}) \qquad \text{A7.3.}$$

The double $\bar{\bar{}}$ indicates the omission of the variation in the Z direction.

Now if the velocity is zero at $x = 0$ then

$$\bar{\bar{V}}(1 + R + R') = 0 \qquad \text{A7.4.}$$

and if the angular velocity is zero at $x = 0$ then

$$\bar{\bar{V}}(-ik.\cos.\theta + ikR.\cos.\theta + R'k\sqrt{1+\sin^2\theta}) = 0 \qquad \text{A7.5.}$$

$$\therefore \quad R = -\sin^2\theta + i\cos.\theta\sqrt{1+\sin^2\theta} \qquad \text{A7.6.}$$

and $$R' = -\cos^2\theta - i\cos.\theta\sqrt{1+\sin^2\theta} \qquad \text{A7.7.}$$

We may check this calculation: all the energy must be reflected at the boundary. Thus:

$$1 - |R|^2 = 0 \qquad \text{A7.8.}$$

This is the condition fulfilled by A7.6. above.

Now the stress normal to the boundary will be:-

$$\sigma_B = \frac{ihE}{2(1-\nu^2)\omega}\left[\frac{\partial^2 V}{\partial x^2} + \nu\frac{\partial^2 V}{\partial z^2}\right]_{x=0} \qquad \text{A7.9.}$$

Now $\dfrac{\partial^2 V}{\partial z^2} = 0$ for the boundary is solid

and

$$\frac{\partial^2 V}{\partial x^2} = k^2(-2\cos^2\theta - 2i\cos\theta.\sqrt{1+\sin^2\theta}\,)\bar{V} \qquad \text{A7.10.}$$

Thus the mean square stress at the boundary may be written:-

$$\bar{\sigma}_B^2 = \frac{h^2E^2k^4\bar{V}^2}{4(1-\nu^2)^2\omega^2}\,8\cos^2\theta \qquad \text{A7.11.}$$

Now let us assume that the incident field is diffuse, i.e. waves arrive from all angles with mean square velocity

Then

$$\bar{\sigma}_b^2 = \frac{2h^2E^2k^4\langle\bar{V}^2\rangle}{2\pi(1-\nu^2)^2\omega^2} \cos^2\theta.d\theta \qquad \text{A7.12a.}$$

$$= \frac{h^2E^2k^4}{2(1-\nu^2)^2\omega^2} \qquad \text{A7.12b.}$$

Now

$$\frac{h^2E^2k^4}{4(1-\nu^2)^2\omega^2} = \frac{3C_L^2\rho^2}{1-\nu^2} \qquad \text{A7.13.}$$

$$\therefore \quad \bar{\sigma}_b^2 = \frac{6C_L^2\rho^2\langle\bar{V}^2\rangle}{1-\nu^2} \qquad \text{A7.14.}$$

and thus for a Poisson ratio of 0.3

$$\bar{\sigma}_b^2 = 6.67\,C_L^2\rho^2\langle\bar{V}^2\rangle \qquad \text{A7.15.}$$

Now from section 5.1 the mean square stress in the plate will be:-

$$\langle \bar{\sigma}^2 \rangle = 1.61\, C_l^2 \rho^2 \langle \bar{V}^2 \rangle \qquad \text{A7.16.}$$

$$\bar{\sigma}_s^2 = 4.14\, \langle \bar{\sigma}^2 \rangle \qquad \text{A7.17.}$$

$$\therefore \quad \frac{\sigma_{\text{r.m.s. boundary}}}{\sigma_{\text{r.m.s. midplate}}} = 2.1 \qquad \text{A7.18.}$$

APPENDIX VIII

Loss Factor at a Change of Section

From the equations for the amplitudes of the transmitted and reflected waves derived from Chapter 7 we may calculate the loss at a change of section as follows:-

$$\frac{\text{Energy Transmitted}}{\text{Energy Incident}} = 1 - |R|^2 \qquad \text{A 8.1.}$$

$$= |D| \left(\frac{k_2}{k_1}\right)^3 \frac{B_2}{B_1} \qquad \text{A 8.2.}$$

where $\frac{k_2}{k_1}$ = ratio of wavenumbers in receiving and transmitting plates,

and $\frac{B_2}{B_1}$ = ratio of bending stiffness.

The energy loss may be calculated for a given angle of incidence θ. Then, if we assume that all values of θ are equally likely, then we may derive a value for diffuse incidence by integration of the loss factor from $\theta = -90^\circ$ to $+90^\circ$ or from one critical angle to the other, when total internal reflection takes place.

The calculation was carried out on a digital computer using the programmes to find the strain and stress concentration. The computation was performed both ways, by calculation R and D, as a check on these values.

The calculation gave identical results, whether calculated using 48.1. or 48.2., confirming our results for R and D in Section 7. The results of the computation appear in Figure 74.

The results for normal incidence and diffuse incidence are scarcely different when the transmission is to the thin plate.

When the transmission is from the thin plate, the effect of total internal reflection becomes marked and much less energy is transmitted under diffuse than normal incidence.

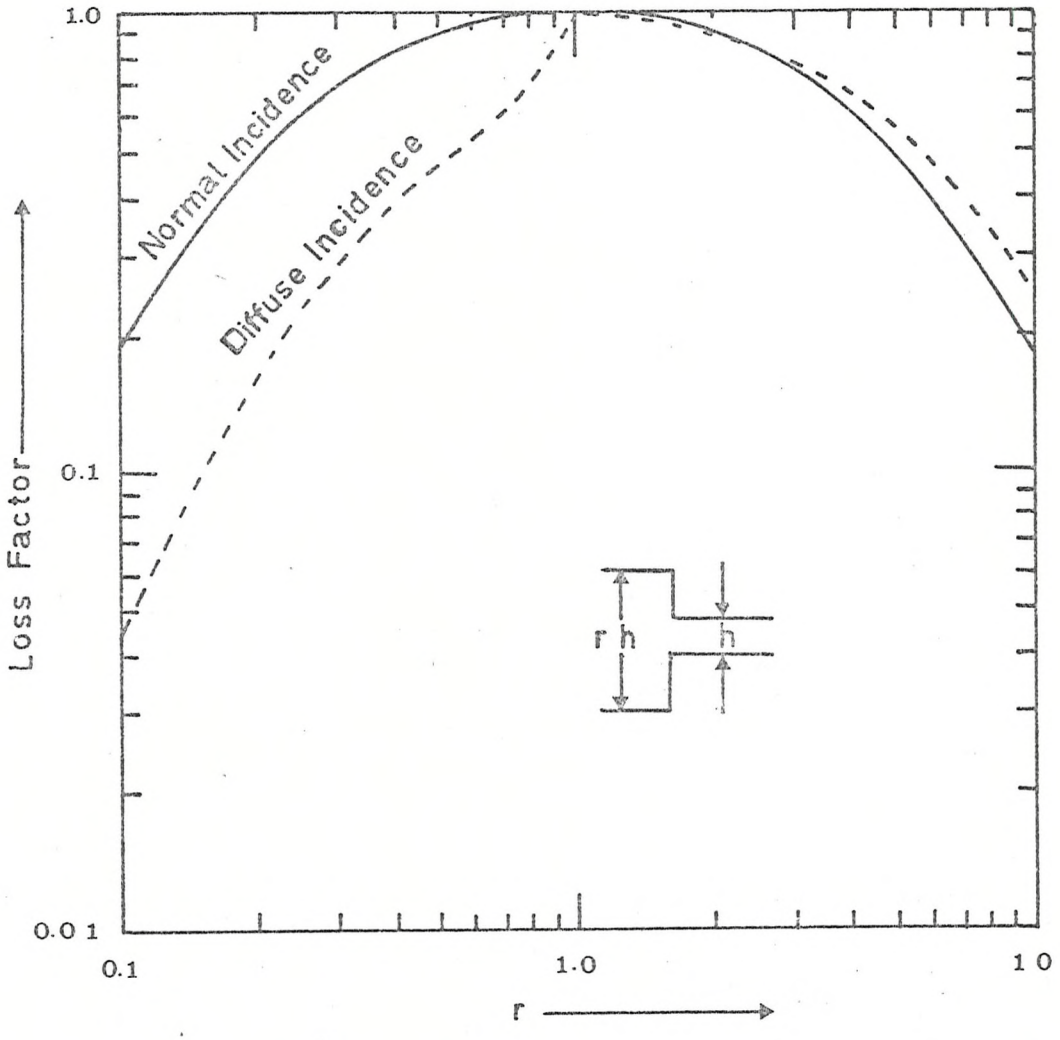

Figure 74 Loss Factor at a Change of Section

APPENDIX IX

Variation of Mean Square Acceleration

From expression 8.1 we may write

$$\ddot{z}(x,y,t) = \sum_{\alpha} A_{\alpha}(t)\,\omega_{\alpha}^2 \sin\left(\frac{m\pi x}{a}\right) \sin\left(\frac{n\pi y}{b}\right) \qquad \text{A9.1.}$$

If we restrict the analysis to a narrow band in which
may be assumed constant and assume that the modes are orthogonal,
the mean square acceleration is given by:-

$$\ddot{z}^2(x,y) = A^2(t)\,\omega^4 \sin^2\left(\frac{m\pi x}{a}\right) \sin^2\left(\frac{n\pi y}{b}\right) \qquad \text{A9.2.}$$

Then the space average mean square acceleration is

$$\langle \ddot{z}^2 \rangle = \frac{A^2(t)\,\omega^4}{ab} \int_0^a \int_0^b \sin^2\left(\frac{m\pi x}{a}\right) \sin^2\left(\frac{n\pi y}{b}\right) dx.dy \qquad \text{A9.3.}$$

$$= \frac{A(t)^2 \omega^4 N}{4} \qquad \text{A9.4.}$$

Expanding the terms in A9.2. so that we may apply Slack's result (43) we find:-

$$\overline{z''^2}(x,y) = \frac{\overline{A^2(t)}\omega^4}{4}\left[\left[1-\cos 2\left(\frac{m\pi x}{a}\right)-\cos 2\left(\frac{n\pi y}{b}\right)\right]\right.$$
$$\left.+\frac{1}{2}\left[\cos 2\left(\frac{m\pi x}{a}-\frac{n\pi y}{b}\right)\cos 2\left(\frac{m\pi x}{a}+\frac{n\pi y}{b}\right)\right]\right] \qquad \text{A9.5.}$$

Taking only the two most significant variables (as we have only two independent variables) to get the lowest estimate of standard deviation:-

$$\frac{A^2(t)\omega^4}{4}\,2\sqrt{\frac{N}{2}} \qquad \text{A9.6.}$$

Taking all variables as independent, to get the upper bound of standard deviation:-

$$\frac{A^2(t)\omega^4}{4}\,3\sqrt{\frac{N}{2}} \qquad \text{A9.7.}$$

Then the variation v is given as $\sqrt{\frac{2}{N}} \le v \le \frac{3}{2}\sqrt{\frac{2}{N}}$ A9.8.

APPENDIX X

Effect of Measurement Error on Variation

Assume that all readings lie within 1 dB and are measured within $\pm \frac{1}{2}$ dB to the nearest dB. Then the readings will be, with even probability, the next dB up or down from the actual results. Thus the mean of the readings will be at the $\frac{1}{2}$ dB point and the standard deviation will be $\frac{1}{2}$ dB. Then the variation will be 0.12.

For readings lying within 2 dB, measured to the nearest dB, a similar calculation gives a variation of 0.22.